Polymeric nanoparticles as original theranostic approach for alzheimer s disease

Davide Brambilla

UNIVERSITÉ PARIS-SUD 11

FACULTÉ DE PHARMACIE DE CHÂTENAY-MALABRY

ECOLE DOCTORALE :

INNOVATION THÉRAPEUTIQUE : DU FONDAMENTAL A L'APPLIQUÉ
PÔLE : PHARMACOTECHNIE ET PHYSICO-CHIMIE

ANNÉE 2011-2012 SÉRIE DOCTORAT N° 1149

THÈSE

Présentée

À L'UNITÉ DE FORMATION ET DE RECHERCHE
FACULTE DE PHARMACIE DE CHÂTENAY-MALABRY
UNIVERSITÉ PARIS-SUD 11

pour l'obtention du grade de

DOCTEUR DE L'UNIVERSITÉ PARIS-SUD 11

par

M. Davide BRAMBILLA

POLYMERIC NANOPARTICLES AS ORIGINAL THERANOSTIC APPROACH FOR ALZHEIMER'S DISEASE

soutenue le : 11 Janvier 2012

JURY :	Prof. Seyed Moein Moghimi	*Rapporteur*
	Prof. Claus Michael Lehr	*Rapporteur*
	Prof. Charles Duyckaerts	*Examinateur*
	Prof. Patrick Couvreur	*Co-directeur de Thèse*
	Dr. Julien Nicolas	*Co-directeur de Thèse*
	Dr. Karine Andrieux	*Co-directeur de Thèse*

Sommaire / Table of contents

Introduction générale

General introduction

Recent statistics indicate that 35 million people worldwide are affected by dementia with 4.6 million new cases per year (one new case every 7 seconds). In Europe there are 5 million cases of dementia, 3 million of which are classified as Alzheimer's disease (AD). Given the continuing increase in life expectancy, these numbers are expected to rise dramatically. In 2040, cases are expected to double in Western Europe and to triple in Eastern Europe. Despite great progresses in research, Alzheimer's disease etiology remains a big question and its treatment an important challenge of modern medicine.

A major limitation to the development of active drug against Central Nervous System (CNS)-related diseases is represented by the Blood-Brain Barrier (BBB), a formidable gatekeeper in the body towards exogenous substances. Generally, pharmaceuticals including most small molecules do not cross the BBB. Therefore, an ideal device for treatment of AD should provide two main properties: (*i*) be able to cross the BBB and (*ii*) to exert a beneficial effect by inhibiting the AD pathogenesis.

In this view, an original solution could arise from nanotechnologies. Indeed, during the last decades, nanotechnology applied to medicine, refereed as nanomedicine, showed interesting results for the treatment of numerous severe diseases leading to the development and commercialization of more efficient drugs.

This PhD thesis has been performed in the framework of the NAD (Nanoparticles for therapy and diagnosis of Alzheimer's disease) European research project aiming to develop nanoparticulate systems for the diagnosis and the therapy of Alzheimer's disease. The research is founded by the European Union's 7^{th} Framework Program and includes 19 European research centers (Grant agreement no: CP-IP 212043-2 NAD). Prof. M. Masserini from University of Milano-Bicocca is the scientific coordinator of the project.

The goal of this study was to create nanoparticlate systems able to cross the BBB in order to reach the brain, the main site of AD, and to capture the Amyloid peptide, especially $A\beta_{1-42}$ species, the aggregates of which are known to play a pivotal role in the etiology of the disease.

In particular, the PhD was oriented toward the design of polymeric nanoparticles and the study of their crossing of a novel *in vitro* BBB model (provided by P.O. Couraud, Institut Cochin) and to study the interaction between the polymeric nanoparticles and the $A\beta_{1-42}$ peptide. Different kinds of nanoparticles have been designed during the project, mainly based on poly(alkyl cyanoacrylate) (PACA) and presenting various surface properties, in order to increase their affinity towards the peptide. All the obtained particles have been screened *in vitro* for their ability to capture the peptide.

This thesis is divided in two main parts:

The first introducing part is a published bibliographic review on the recent advances of nanotechnology-based approaches for the diagnosis and therapy of Alzheimer's disease, with a particular focus on the most striking reports and developments in the field.

The second part concerned the experimental work and is divided into two chapters:

- The first chapter describes, in three sections in the form of articles (two were published and one is in preparation), the design of fluorescently-tagged PACA nanoparticles for cell imaging and the fine evaluation of their endocytosis and trancytosis across a novel human *in vitro* BBB model.
- The second chapter depicts, in four sections in the form of articles (three were published and one is about to be submitted), the design and application of a novel technique to study *in vitro* the interaction between nanoparticles and the Aβ peptide, and the development of polymeric nanoparticles with affinity for the peptide that gave interesting results as Aβ kidnapper.

Partie 1: Etude bibliographique

Part 1: Bibliographic study

Nanotechnologies for Alzheimer's disease: diagnosis, therapy and safety issues

Nanomedicine: Nanotechnology, Biology and Medicine, **2011**, 7(*5*), 521.

Davide Brambilla,[1] Benjamin Le Droumaguet,[1] Julien Nicolas,[1] S. Hossein Hashemi,[2] Lin-Ping Wu,[2] S. Moein Moghimi,[2] Patrick Couvreur,[1] and Karine Andrieux[1]

[1]Laboratoire de Physico-Chimie, Pharmacotechnie et Biopharmacie, Univ Paris-Sud, UMR CNRS 8612, Faculté de Pharmacie, 5 rue Jean-Baptiste Clément, F-92296 Châtenay-Malabry, France.

[2]Centre for Pharmaceutical Nanotechnology and Nanotoxicology, Department of Pharmaceutics and Analytical Chemistry, University of Copenhagen, Universitetsparken 2, DK-2100 Copenhagen, Denmark.

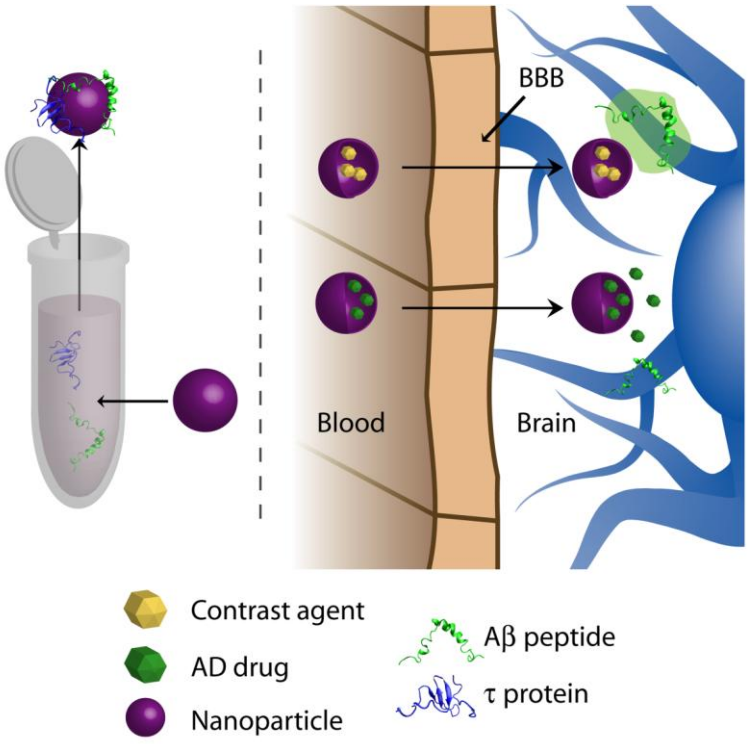

Résumé

La Maladie d'Alzheimer (MA) représente la forme la plus commune de démence et affecte 35 million de personnes. L'avancée que connait le domaine des nanotechnologies commence à avoir un impact en neurologie. Les approches résultantes, souvent basées sur la conception et l'ingénierie de nanoparticules ayant une grande spécificité pour les cellules endothéliales des capillaires cérébraux, sont actuellement étudiées pour le diagnostic précoce et le traitement de la maladie d'Alzheimer. De plus, des nanoparticules avec une grande affinité pour le peptide amyloïde β pourrait induire un « *effet sink* » et ainsi diminuer les effets de la maladie. Il y a aussi des développements pour le diagnostic *in vitro* qui utilise aussi bien des nanoparticules « code barre » ultrasensibles, des immunosenseurs ou encore de la microscopie à effet tunnel pour détecter les peptides $A\beta_{1-40}$ et $A\beta_{1-42}$. Cependant, des effets indésirables peuvent apparaitre dus à l'utilisation de nanoparticules et cela demande par conséquent de travailler avec des nanoobjets assemblés à partir de matériaux biocompatibles. Les avancées clés et les aspects toxicologiques sont aussi présentés et discutés.

Abstract

Alzheimer's disease (AD) represents the most common form of dementia worldwide, affecting more than 35 million people. Advances in nanotechnology are beginning to exert a significant impact in neurology. These approaches, which are often based on the design and engineering of a plethora of nanoparticulate entities with high specificity for brain capillary endothelial cells, are currently being applied to early AD diagnosis and treatment. In addition, nanoparticles with high affinity for the circulating amyloid-β forms may induce "*sink-effect*" and improve AD condition. There are also developments in relation to *in vitro* diagnostics for AD, which includes ultrasensitive nanoparticle-based bio-barcode, immunosensors as well as scanning tunneling microscopy procedures capable of detecting $A\beta_{1-40}$ and $A\beta_{1-42}$. However, there are concerns regarding the initiation of possible nanoparticle-mediated adverse events in AD, thus demanding the use of precisely assembled nanoconstructs from biocompatible materials. Key advances and safety issues are reviewed and discussed.

Keywords

Alzheimer's disease, nanotechnology, nanoparticles, Aβ peptide, drug delivery.

1. Introduction

Alzheimer's disease (AD) is a devastating neurodegenerative disorder and the most common form of dementia among people over the age of 65 years. This neuropathological condition is characterized by a progressive loss of cognitive function with two established pathophysiological hallmarks in the brain. These include extracellular accumulations mainly composed of amyloid-β (Aβ) peptide (also referred to as senile plaques) and intracellular neurofibrillar tangles of hyperphosphorylated τ protein.[1] Today, millions of people are affected by this neuropathology, posing a heavy economic and social burden. It is predicted that in the next few decades, AD will exert a huge societal and economical impact if no efficient therapeutic and/or early diagnosis approaches become available. Moreover, considering the increase in population aging and survival, the impact of AD on the health care systems will be even more pronounced. Therefore, strategies for early detection as well as treatment of AD are among the most challenging and timely areas in modern medicine.

The blood-brain barrier (BBB) is a formidable gatekeeper in the body towards exogenous substances that maintains the chemical composition of the neuronal "milieu" for proper functioning of neuronal circuits and synaptic transmission. This barrier is formed at the level of the endothelial cells of the cerebral capillaries and essentially composes the major interface between the blood and the brain. The most important factor limiting the development of new drugs and biologics for the central nervous system (CNS) is the BBB. Generally, pharmaceuticals including most small molecules do not cross the BBB.[2] During the past decade numerous attempts have focused on this pivotal problem by designing different strategies that aids drug passage across the BBB. Among these, nanotechnology-based strategies have gained tremendous importance as some of them are capable of overcoming the limitations inherent to BBB passage. These include various types of lipidic, polymeric, inorganic and other types of nanoparticles (NPs) for controlled drug delivery and release pertinent to various CNS conditions.[3-4]

A crucial challenge that is receiving increasing attention is to develop nanotechnology-based approaches for early diagnosis of AD. Early diagnosis could provide opportunities to treat patients at risk of AD development, thereby preventing the onset of irreversible neuronal damages. With respect to AD treatment, some strategies have been directed towards encapsulation of several types of biologically active molecules into NPs for their (targeted) delivery to the brain, whereas others have focused on the use of nanoconstructs to combat the toxicity of amyloid clusters by promoting their clearance or by altering their aggregation kinetics both in the brain and in the blood. Indeed, peripheral treatment with molecules that have high affinity for Aβ can reduce the level of Aβ in the brain through the "*sink effect*". This approach can further benefit with engineered NPs exhibiting high affinity for

Aβ, where sequestered plasma Aβ will be routed to hepatic and splenic macrophages for destruction. This approach could potentially reduce or prevent brain amyloidosis. It should also be emphasized that nanoparticles can be introduced into the body through different routes of administration. Notably, some efforts suggest that orally delivered NPs can improve bioavailability of certain drugs used in AD. Accordingly, this article discusses current state-of-the-art nanotechnology-based approaches for AD diagnosis and therapy with a particular focus on the most significant recent reports and developments in the field.

2. Imaging-based nanotechnologies for AD diagnosis

Early diagnosis in AD (*i.e.*, before clinical symptoms manifest) is crucial in preventing irreversible neuronal damages leading to dementia. Because the examination of living human brain is limited and invasive, the development of strategies to detect AD in its earlier stages is therefore essential. Since it was commonly accepted by the scientific community that the formation of senile plaques precedes the neurofibrillar degeneration, the majority of efforts are concentrated either towards detection and identification of amyloid plaques by magnetic resonance imaging (MRI) using NPs doped with contrast agents or, alternatively, by NPs tagged with fluorescent probes.

2.1. Iron oxide NPs

Magnetic iron oxide NPs have gained much interest because of their high surface area, magnetic properties and limited toxicity. They have already been approved by the U.S. Food and Drug Administration (FDA) as MRI contrast agents in liver imaging.[5]

The synthesis of monocrystalline iron oxide NPs (MION) covalently tethered to the *N*-terminus of $A\beta_{1-40}$ peptide through amide coupling and their development for the concomitant targeting and imaging of senile plaques has been reported.[6] These MRI agents, by means of longitudinal μMRI, were able to recognize with high affinity Aβ plaques in the brain of amyloid precursor protein (APP) and APP/PS1 transgenic mice when co-injected with mannitol (used to transiently open the BBB) (Figure 1). Although this study is very encouraging and demonstrates the proof of concept, manipulation of BBB remains questionable for human testing.

A novel method for the selective labeling of $A\beta_{1-40}$ fibrils has been reported with either non-fluorescent, fluorescent rhodamine-tagged or Congo red-encapsulated magnetic γ-Fe_2O_3 NPs, even under competitive conditions (*e.g.*, in the presence of human serum albumin). Moreover, these studies

described the ability of iron oxide NPs to readily remove fibrils from solubilized Aβ aqueous sample by the simple use of an external magnetic field.[7-8]

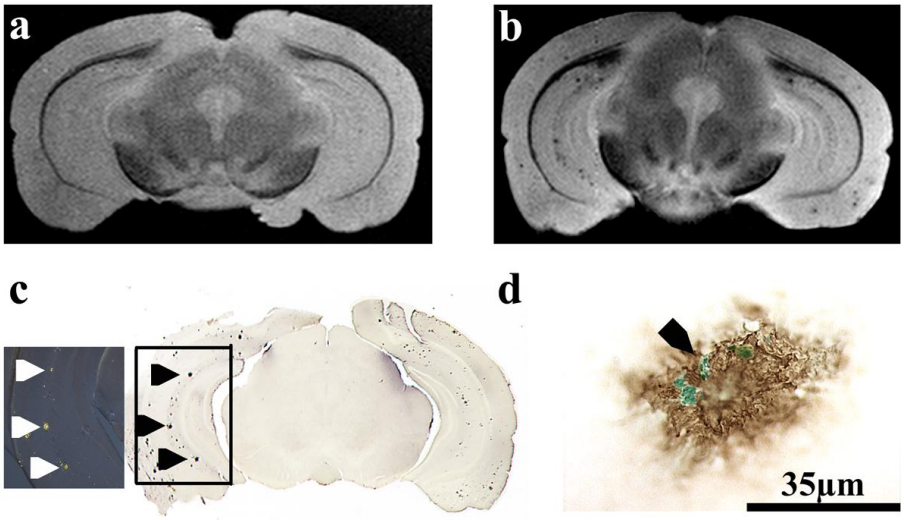

Figure 1. *(A) Aβ plaques detected with ex-vivo µMRI after injection of MION-$A\beta_{1-40}$ with mannitol. Ex vivo T_2-weighted SE coronal µMRI images show six-month old control and (b) APP-transgenic mouse brain. (c) Many µMRI lesions matched to Aβ plaques (arrows) as revealed by immunohistochemistry. (d) High-power microscopic visualization of the amiloyd plaques, double stained with an Aβ (6E10) antibody (brown color) and a Mallory stain for iron (azure color, black arrow), demonstrated the colocalization of MION with Aβ plaques. Adapted from Wadghiri et al.,[6] with permission of John Wiley and Sons.*

2.2. PE154 (heterodimeric acetylcholinesterase inhibitor)

Beyond the well-known beneficial effects of acetylcholinesterase (AChE) for the treatment of AD symptoms (see section 3.1), recent studies have conferred to this enzyme additional, non-classical functions, including interactions with the Aβ peptide.[9] Moreover, its structurally-related inhibitor PE154 was also shown to act as a fluorescent probe for Aβ plaques present in tissues brain samples from both AD mimicking triple transgenic mice and humans with AD.[10] This molecule, however, could not penetrate the BBB. To overcome this limitation, Härtig et al., developed carboxylated poly(glycidyl methacrylate) (PGMA) and core-shell polystyrene-*block*-poly(*n*-butyl cyanoacrylate) (PS-*b*-P*n*BCA) NPs both loaded with PE154-and demonstrated their ability to target Aβ deposits *in vivo* (Figure 2). Although NPs were injected in the hippocampus, this study provided the proof-of-principle regarding the Aβ targeting by using a fluorescent AChE inhibitor after its release from NPs

in vivo.[11] The authors even considered the possibility of developping the so-called theranostic approach for AD (*i.e.*, a strategy combining both therapeutic and diagnostic approaches within a single nanodevice).

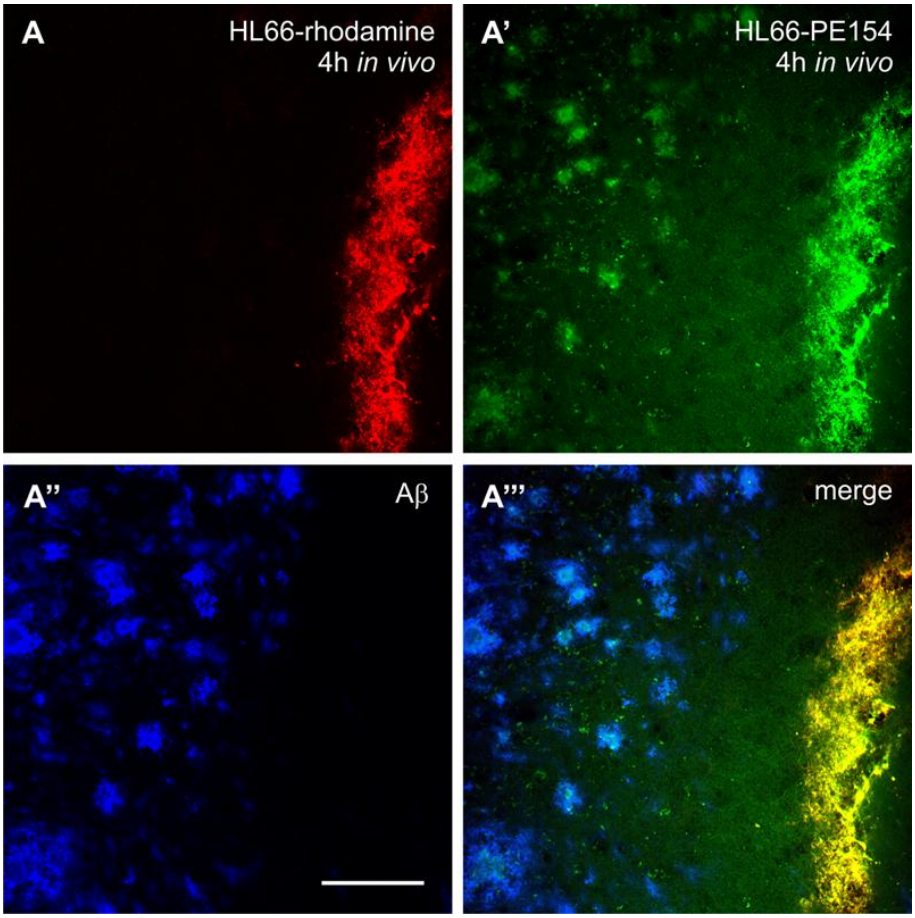

Figure 2. *Concomitantly visualized injection site of fluorescent nanoparticles and β-amyloid (Aβ)-containing deposits as the quickly reached target for PE154 released by the nanocarriers in the hippocampus of a 19-month-old triple transgenic mouse. (A) Red fluorescence of rhodamine encapsulated in PGMA nanoparticles (HL66) 4 h post injection. PE154 is visible both nanoparticle-associated at the injection site and attached to plaque-like structures (A'). Such deposits are shown in (A'') to be Aβ-immunopositive by Cy5-staining, colour-coded in blue. By merging the pictures (A'''), plaques labeled both by PE154 and Cy5 appear white, and the injection site is marked in yellow color resulting from the allocated red and green fluorescent labels of HL66. Scale bar, 100 µm. Reprinted from Hartig et al.,[11] with permission of John Wiley and Sons.*

2.3. Thioflavin T

Thioflavin T (ThT) is a molecule capable of recognizing *β*-sheet structures related to Aβ aggregates both *in vitro* and *in vivo*. A recent attempt described the encapsulation of ThT into PS-*b*-P*n*BCA NPs, its release into the brain after intracerebral injection and its interaction with Aβ species, thereby showing clear visualization of amyloid aggregates.[12]

2.4. Quantum dots-Aβ complex

Fluorescent semiconductor nanocrystals (quantum dots, QDs) have evolved over the past decade as highly useful fluorescent probes for biological labeling and diagnostics. QD features include long-term photostability and physico-chemical stability, nano-scale size, size-dependent emission λ.[13]

Tokuraku et al., designed poly(ethylene glycol) (PEG)-QD-crosslinked Aβ peptide as a tool to monitor and to quantitatively describe the formation of fibrils and oligomers in solution and in a cellular system. This approach allowed the study of the Aβ peptide aggregation kinetics but could also be used to follow the *in vivo* peptide aggregation.[14] Regarding the latter task, the authors have considered the functionalization of these nanoassemblies with appropriate ligands such as transferrin for BBB crossing purposes.[15]

2.5. Gold NPs

Gold NPs (Au NPs) also represent an interesting tool for studying Aβ peptide aggregation kinetics. Choi et al., described the synthesis of heterodimeric NPs consisting of a cobalt(II) magnetic core and a platinum shell directly fused onto Au NPs, and stabilized by lipoic acid-PEG coating.[16] The terminal carboxyl groups of the PEG chains enabled covalent binding with lysine residues of neutravidin at the surface of the NPs. The Co@Pt-Au nanoasemblies presented a high magnetization value [63 emu.g^{-1} (Co) at 3 T], making them appropriate for *T*2-weighted spin echo magnetic resonance measurements. The MRI measurements of Co@Pt-Au-Neutravidin NPs samples mixed with an increasing amount of biotinylated $A\beta_{1-40}$ peptides showed contrast changes governed by the peptide concentration. The results clearly showed that these NPs can be used in MRI imaging to monitor key structural stages of Aβ self-assembly. In particular, a significant change in MRI signals during Aβ self-aggregation that corresponds to the detection of Aβ protofibrillar species in the early reversible stages of aggregation was observed. This methodology might also be important for the screening of Aβ anti-aggregating or disaggregating molecules.[16]

However, several important parameters should be considered before a viable application is foreseen. Indeed, the intrinsic *in vitro*/*in vivo* cytotoxicity of the employed materials used to prepare the NPs should be thoroughly evaluated before further investigations. The feasibility of these approaches will further depend on developments that do not depend on invasive procedures.

3. Nanotechnologies for detection of AD biomarkers in biological fluids

The development of future effective treatments for neuronal degeneration will depend on early diagnosis methods based on the detection and quantification of soluble AD biomarkers. In practice, two approaches are available: (i) the measurement of total τ-protein and Aβ concentrations in cerebrospinal fluid (CSF) or plasma,[17-18] and (ii) the detection of suspected pathogenic biomarkers, such as the hyperphosphorylated τ-protein and the Aβ -derived diffusible ligands (ADDLs, which are soluble oligomers). The first strategy is hampered by the significant crossing of τ-protein and Aβ markers in biological fluids of healthy and AD subjects, and lead to inconclusive results,[19] whereas the second, though more reliable, is strongly limited by the extremely low concentrations of the biomarkers that cannot be identified with enough accuracy by conventional ELISA assays.

Remarkable results towards the development of new approaches for biomarker detection have been proposed by Georganopoulou et al., who developed an ultrasensitive NPs-based bio-barcode capable of detecting AD soluble biomarkers in CSF. The key feature of the system relied on the isolation of antigens (Ag) by means of a "sandwich process" involving oligonucleotide (DNA-barcode) modified Au NPs and magnetic microparticles (MMPs), both functionalized with monoclonal or polyclonal antibodies specific to the ADDLs. Practically, an excess of Au NPs and MMPs (when compared to the ADDLs concentration) were mixed in a CSF sample; the recognition of the Ag from both particles lead to the formation of the sandwiches that were then purified by magnetic separation (Figure 3a). The strands of a dehybridized double-stranded DNA were isolated and easily quantified by a scanometric method using DNA microarray (Figure 3b). The efficient Ag sequestration in solution and the amplification process resulting from the large number of DNA strands released for each Ag recognition, allowed the system to identify ADDLs at sub-femtomolar concentrations, thus improving the ELISA test sensitivity by 6 orders of magnitude.[20-21]

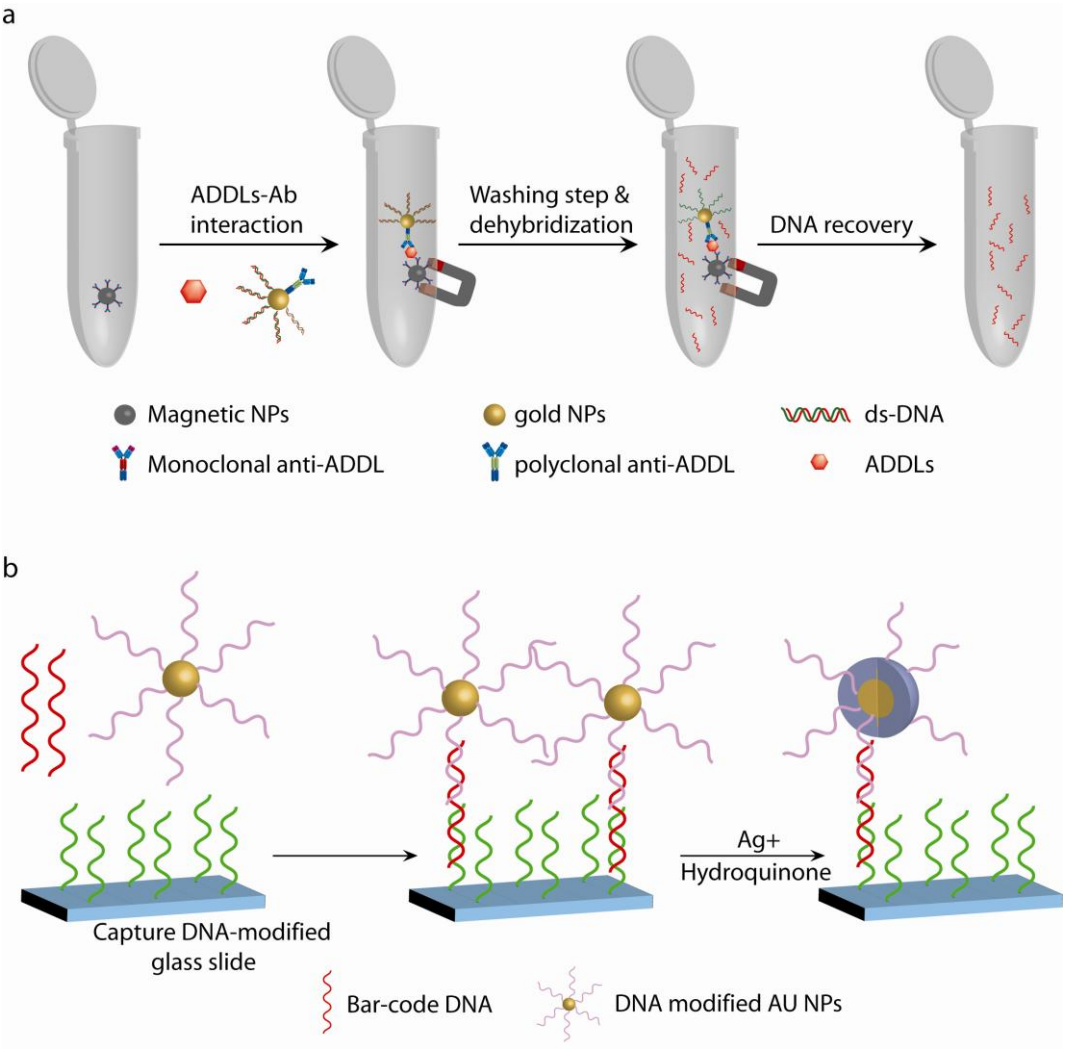

Figure 3. *(A)MMPs functionalized with mAbs recognize and bind ADDLs. The ADDLs are then sandwiched with an NP probe, modified with double-stranded DNA and an anti-ADDL pAb. After repeated washing while using a magnet to immobilize the MMPs, a dehybridization step releases hundreds of barcode DNA strands for each antigen-binding event. (B) Schematic representation of scanometric detection. The method is based on capturing the barcode DNA on a microarray with spots of oligonucleotides that are complementary to half of the barcode DNA sequence. NPs with oligonucleotides that are complementary to the other half of the barcode DNA are hybridized to the captured barcode strands. The signal is enhanced by using silver amplification.*

Another interesting procedure for Aβ detection was proposed by Chikae et al., who developed an electrochemical sensing protocol based on saccharide-protein interactions. Alkyne-terminated self-assembled monolayers (SAM) were formed at the surface of Au NPs electrodeposited on screen-printed carbon strips and subsequently reacted with azido-functionalized sialic acid by "click" chemistry.[22] The densely packed sialic acid domains were able to capture the Aβ peptide as a result of

specific interactions and the method enabled the detection of non-labeled Aβ down to sub-micromolar concentration. Importantly, the detection threshold of this technique was significantly lowered as compared with other techniques and thus represents an interesting step towards the development of a novel biomarker screening methodology.[23]

The development of ultrasensitive immunosensors based on surface plasmon resonance (SPR) for $A\beta_{1-40}$ peptide detection has also been reported. The procedure exploited the use of Au NPs-antibody fragment (fAb) complexes able to recognize Aβ peptide *via* the enhancement of the SPR signal. fAb able to specifically recognize the β-amyloid was anchored at the surface of Au NPs and the Aβ-containing sample was flowed onto the chip. This was followed by a suspension of Au NPs-fAb leading to plasmon signal generation. The procedure presented a linear correlation with the peptide concentration in a 9 orders of magnitude and increased the detection limit from 10 $ngmL^{-1}$ to 1 $fgmL^{-1}$, when compared to a system on a bare gold substrate.[24]

A parallel approach has recently been proposed by Kang et al., who developed an ultrasensitive electrical detection method for $A\beta_{1-42}$ using scanning tunneling microscopy (STM). Experimentally, a monoclonal antibody (mAb) fragment with high affinity for $A\beta_{1-42}$ was immobilized onto a gold surface. Then, the sample containing the target biomolecule was deposited onto the mAb-functionalized surface, leading to its capture. Subsequently, Au NPs-fAb complex (also immunoreactive against the target) was reacted and conducted to the formation of "sandwich-like" structures. The resulting chip was finally analyzed by STM. It was shown that the surface density of the Au NPs correlated with the number of Ab-Ag binding events and that a successful Aβ detection was achievable down 10 $fg.mL^{-1}$ (Figure 4).[25]

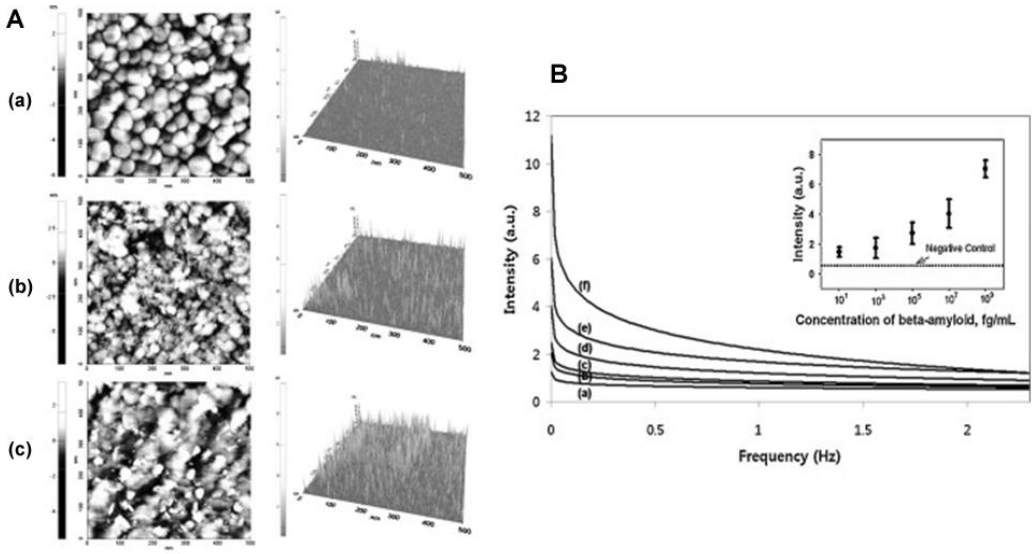

Figure 4. *STM topography and current profile of biosurface (A): bare Au (a), 100 pg.mL^{-1} A$\beta_{1–42}$ (b) and 1 μg.mL^{-1} A$\beta_{1–42}$ (c). (B) Power spectra of the current profiles acquired in STM images: bare Au (a), 10 fg.mL^{-1} (b), 1 pg.mL^{-1} (c), 100 pg.mL^{-1} (d), 10 ng.mL^{-1} (e) and 1 μg.mL^{-1} (f) of A$\beta_{1–42}$ (inset: calibration curve from the power spectra of the current profiles). Reprinted from Kang et al.,*[25] *with permission of Elsevier.*

Haes et al., designed a llocalized LSPR nanosensor to detect ADDLs as a potential biomarker for AD.[26-27] The signal transduction mechanism of the LSPR nanosensor was based on its sensitivity to local refractive index changes near the surfaces of substrate confined, size- and shape-controlled, noble metals (Au, Ag) NPs.[28] Sandwich architectures were prepared by synthesis and immobilization of surface-confined Ag nanotriangles onto a mica surface using nanosphere lithography. Then, a self assembled monolayer, consisting of a mixed monolayer of 1-octanethiol for passivation of the NPs towards non specific binding and 11-mercaptoundecanoic acid for covalent attachment of Ab to ADDL, was assembled on top of these Ag nanotriangles. The first Ab to ADDL was covalently attached onto the surface of the NPs *via* amidation reaction. The resulting biosensors were incubated with samples containing ADDLs, washed and incubated with a polyclonal Ab solution specific to ADDLs to enhance the shift response for ADDLs. The LSPR nanosensor allowed analysis of biological species in a surfactant-free environment and was demonstrated to be sensitive enough for the detection of ultralow concentrations of ADDLs in biological samples.[26-27] Moreover, this technique allowed the distinction between two different ADDLs species varying from their binding constant with the Ab specific to ADDLs (7.3×10^{12} M^{-1} and 9.5×10^{8} M^{-1}, respectively).

To the best of our knowledge, only one article has been devoted to the detection of τ protein, another specific AD biomarker, through a nanotechnology-based approaches. Neely et al., designed Au NPs coated with mAb specific to τ protein employed in a two-photon Rayleigh scattering assay, which enabled the detection of τ protein at concentrations greater than about 1 $pg.mL^{-1}$. This concentration was about 2 orders of magnitude lower than typical τ protein concentration values (*i.e.*, 195 $pg.mL^{-1}$) in CSF (Figure 5). Moreover, the two-photon Rayleigh scattering assay showed a strong sensitivity for τ protein and was able to discriminate other proteins such as bovine serum albumin.[29]

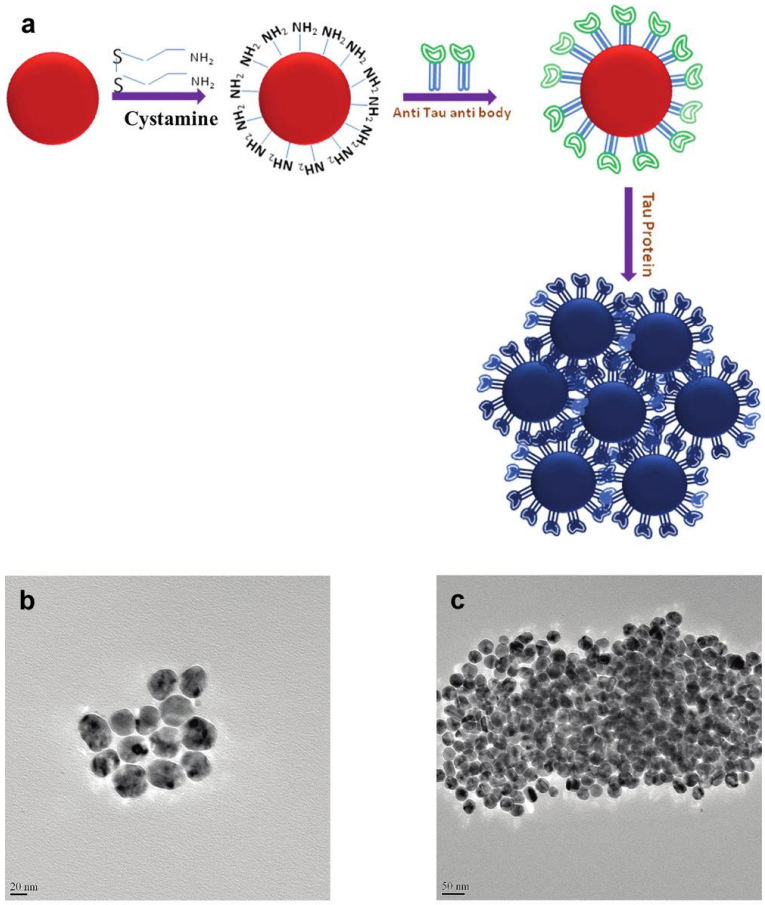

Figure 5. *(a) Schematic representation of the synthesis of monoclonal anti-τ antibody-conjugated gold nanoparticles and subsequent formation of anti-τ antibody-conjugated gold nanoparticle based sensing of τ protein. (b) TEM image of anti-τ antibod-conjugated gold nanoparticles before addition of τ protein. (c) TEM image of anti-τ antibod-conjugated gold nanoparticles after addition of 20 $ng.mL^{-1}$ τ protein. Adapted from Neely et al.,*[29] *with permission of ACS publications.*

4. Nanotechnologies for AD treatment

4.1. Delivery of bioactive molecules to the brain

Healthy BBB is a major obstacle both for the development of small and large neurotherapeutic molecules (*e.g.*, recombinant peptides, antibody fragments, anti-sense oligonucleotides, viral vectors).[4] In addition, BBB also negatively affects drug efficacy and tolerance, because large doses of drugs are needed to reach levels above the minimum effective concentration in the brain. Nanoparticulate systems offer an opportunity to overcome such problems and can be used as "Trojan" systems for transporting active molecules across the BBB (Figure 6) thus reducing toxicity and improving therapeutic efficacy (Figure 7).[30-31]

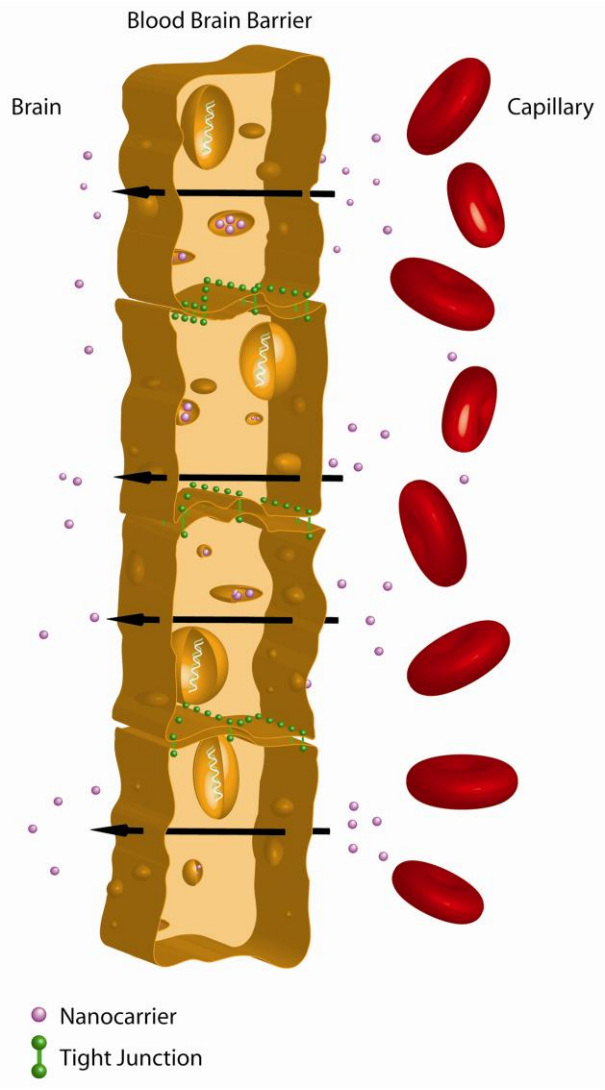

Figure 6. *Schematic representation of nanocarriers as "Trojan systems" to transport active molecules to the brain by crossing the Blood-Brain Barrier.*

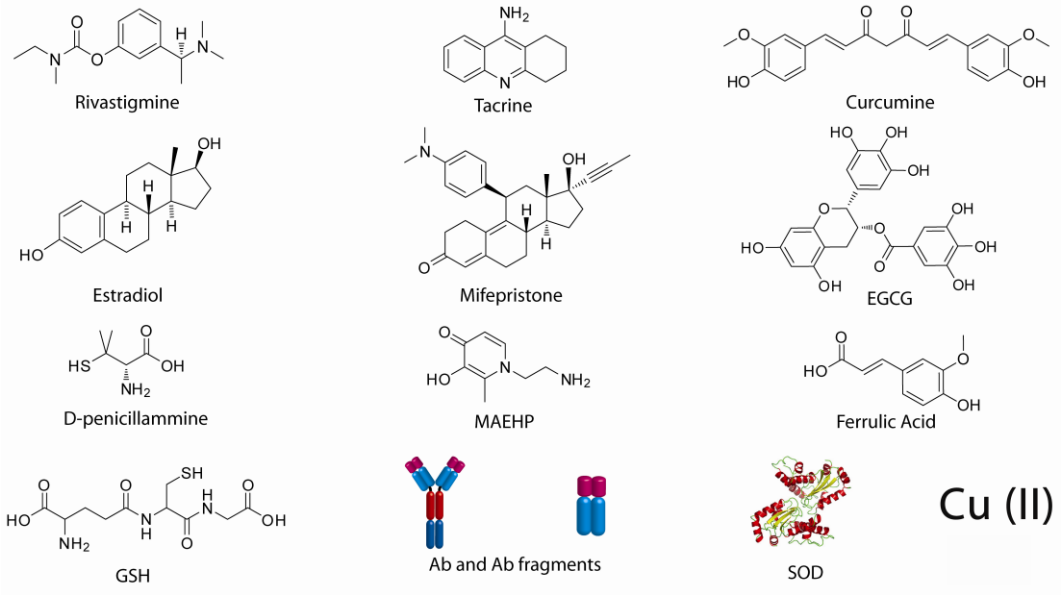

Figure 7. *Examples of bioactive molecules encapsulated into nanocarriers or covalently attached to their surface for potential AD treatement.*

4.1.1 AChE inhibitors and Acetylcholine (ACh)

The deficiency in cholinergic neurotransmission is considered to play an important role in the learning and memory impairment of AD patients.[32] So far, cholinergic neurotransmission enhancement remains the most effective therapeutic approach to treat AD. Accordingly, rivastigmine, a noncompetitive and reversible inhibitor of both AChE and butyrylcholinesterase, was approved in 2000 by the FDA for the treatment of AD. Experimentally, this drug has been shown at least to maintain if not to improve cognitive function, global function and behavior in AD patients. However, its clinical efficacy remains limited mainly due to poor brain translocation, which requires frequent injections, and its adverse cholinergic effects on peripheral organs.[33-34]

The use of nanocarriers to transport rivastigmine to the brain might represent a promising alternative to circumvent these limitations. To this end, Wilson et al., have encapsulated rivastigmine in polysorbate 80-coated polymeric P*n*BCA NPs with the aim of increasing the brain delivery of this compound and in order to reduce the side effects observed when the free drug is injected.[4, 35] The authors obtained a 3.8 fold rivastigmine uptake increase within the brain compartment compared to free rivastigmine after intravenous injection into the rats. The mechanism(s) of NP translocation to the brain is related to polysorbate 80-mediated affinity for apolipoproteins E and A-I and subsequent NP internalization through low density lipoprotein-receptors (LDL-r) of the BBB. The same group also described a similar approach to increase the brain uptake of tacrine, another AChE inhibitor, using

P*n*BCA nanocarriers. In this case, the use of NPs increased the tacrine brain concentration by a factor 4 when compared with the free drug.[36] Recently, Joshi et al., further reported positive therapeutic outcome in amnesic mice[37] with rivastigmine encapsulated in poly(lactide-*co*-glycolide) (PLGA) and P*n*BCA NPs.[38]

An interesting approach for the delivery of ACh to the brain for AD treatment was proposed by Yang et al., using single wall carbon nanotubes (SWNT).[39] However, SWNT are non-biodegradable material, and not much is known regarding their acute and chronic toxicity.

4.1.2. Estrogens/Androgens

There is ample preclinical evidence that gonadal steroids (estrogens and androgens) play an important role in CNS development and functions.[40] Estrogen treatment can decrease the risk of AD. Experimentally, estradiol may promote the growth and survival of cholinergic neurons and reduce significantly cerebral amyloid deposition.[41] Taking this into consideration, Mittal et al., proposed estradiol encapsulated PLGA NPs as an alternative approach.[42] By tuning the copolymer molecular weight and composition (*i.e.*, the ratio between lactide and glycolide units in the copolymer), they successfully increased the bioavailability of the drug after oral administration up to 10 times compared with the free drug. Likewise, mifepristone (11*β*-[4-dimethylamino]phenyl-17*β*-hydroxy-17[propynyl]estra-4,9-dien-3-one, more commonly known as RU 486), an active anti-progesterone compound, has been shown to slow down the progression of cognitive decline in AD patients,[43-44] most likely due to a mechanism related to P-glycoprotein (P-gp) transporter-mediated efflux of Aβ.[45] By encapsulating mifepristone within poly(ethylene glycol)-*block*-poly(lactide) (PEG-*b*-PLA) NPs, He et al., evaluated the increase in drug bioavailability after oral administration.[46] It was shown that NPs can significantly enhance the bioavailability of hormone and anti-hormone molecules. However, it should be emphasized that the biological effect of these NPs against the progression or development of AD still requires detailed evaluation.

4.1.3. Curcuminoids

Curcuminoids (Figure 7), obtained from *Curcuma longa* (turmeric), the most commonly used natural yellow photoconstituents in food industry, have been widely screened in the past decade for biological activities such as anti-inflammatory, antioxidant (see also part 3.1.7 for other antioxidant species), neuroprotective, hepato-protective, anticarcinogenic, antiviral activities and many others.[47-48] Numerous investigators have reported that curcumin can significantly reduce Aβ aggregate-related toxicity on neurons.[49-50] Unfortunately, this compound exhibits poor stability as it is easily hydrolyzed

under both acidic and alkaline conditions. It can also be oxidized or photodegraded, leading to poor bioavailability and thus negligible brain uptake.[51]

Non-functionalized nanoparticles. Two parallel studies investigated the encapsulation of curcumin into polymeric P*n*BCA NPs and it was demonstrated that the encapsulation procedure dramatically increased curcumin half-life and concentration in the brain when compared with free curcumin.[52-53] However, the therapeutic efficacy of this approach in AD models remains to be evaluated.

Targeted nanoparticles. Another approach has utilized NPs decorated with appropriate ligands for curcumin brain delivery.[54] This strategy was based on the preparation of curcumin-loaded PnBCA NPs decorated with ApoE3 ligands to exploit LDL-r-mediated trancytosis across the BBB and through SHSY5Y neuroblastoma cells (Figure 8).[54] The inhibition of $A\beta_{1-42}$-mediated toxicity by ApoE3-functionalized nanocarriers was evaluated and compared with free curcumin on SH-SY5Y cells. The results indicated a significant reduction (40% compared with free drug at 100 nM Aβ) of $A\beta_{1-42}$-related toxicity on cells treated with the functionalized nanospheres along with a reduction of reactive oxygen species formation.

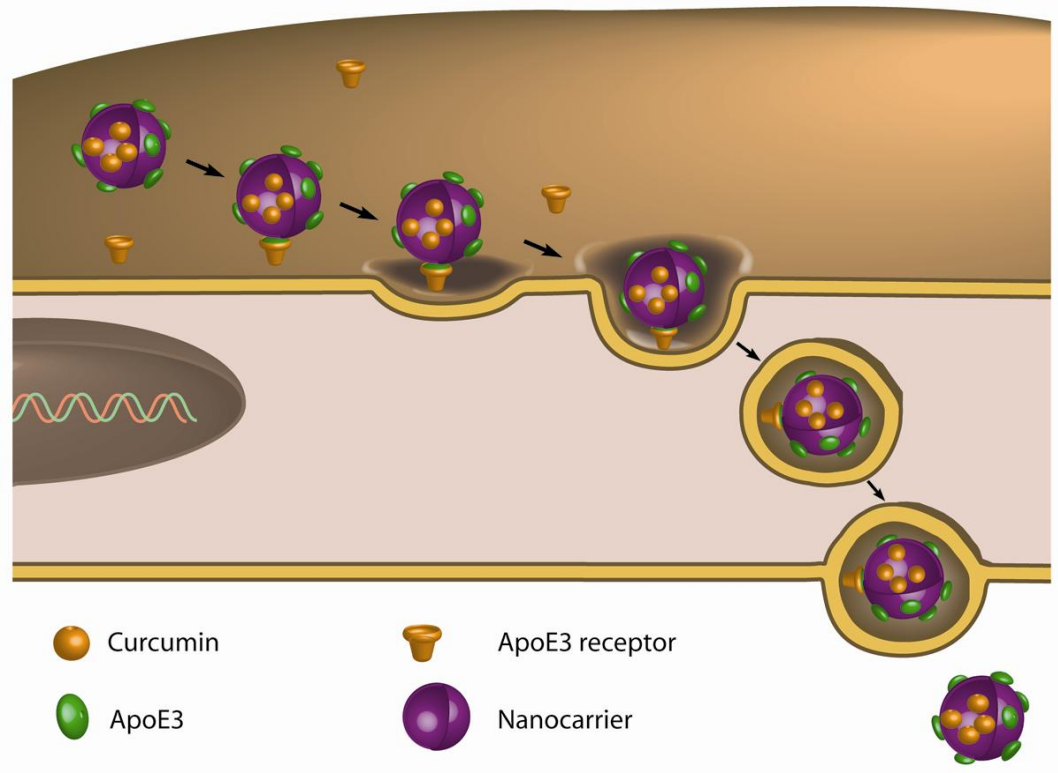

Figure 8. *Schematic representation of curcumin-loaded PnBCA nanospheres decorated with ApoE3 crossing BBB via LDL-r.*

4.1.4. Immunotherapeutics

Immunotherapy against $A\beta_{1-42}$ peptide for AD treatment was tested earlier but has encountered severe complications (meningoencephalitis) during clinical trials.[55-56] However, Agyare et al.,[57] described the preparation of chitosan-based nanocarriers functionalized with $pF(ab')_2$4.1, Ab fragment modified with putrescine and specific to Aβ, that were able to cross the BBB and to target the brain amyloid deposits. These nanoparticles could also be loaded with contrast agents for diagnosis purposes or with drugs able to reduce the amyloid plaques-associated toxicity.[57]

4.1.5. Chelating ligands

There are suggestions that aberrant copper homeostasis has implications in AD. Accordingly, Treiber et al., have engineered hyperbranched polyethyleneimine (PEI) constructs with encapsulated Cu(II) ions, which were not only internalized by cells but also increased cytosolic concentrations of Cu(II) (by releasing the metal cations) and induced weaker Aβ turnovers.[58] Unfortunately, no *in vivo* experiments have been conducted, presumably because of PEI toxicity.

Further evidence supports the hypothesis that oxidative stress, generated by various mechanisms, may be among the major risk factors that trigger and promote AD.[59] Oxidation reactions, catalyzed by metals such as iron (Fe^{2+}), copper (Cu^{2+}), aluminum (Al^{3+}) and zinc (Zn^{2+}), could take place due to an increased local concentration of transition metals.[60-64] Moreover, recent studies have shown that biometals mediate the deposition of Aβ in the CNS.[60, 65] Further confirmation arises from a study demonstrating that aggregated Aβ from post-mortem AD brains could be resolubilized by co-incubation in the presence of such ion chelators.[66]

Thus, metal-chelating compounds, such as ethylenediaminetetraacetic acid (EDTA) salts, desferrioxamine and clioquinol have been used to significantly improve the clinical conditions in AD patients.[67] However, their poor brain uptake and the toxic side-effects towards other sites have limited their systematic development as promising therapeutic agents. Because NPs represent potential carriers to transport drugs across the BBB, others have also developed synthetic strategies based on the covalent anchoring of metal chelators to NPs for CNS delivery. For instance, Cui et al., demonstrated covalent grafting of D-penicillamine (Figure 7) to lipidic NPs *via* disulfide bond allowing the solubilization of Aβ-copper aggregates *in vitro.*[68] Similarly, Liu et al., reported the synthesis of a nanoparticle-MAEHP (2-methyl-*N*-(2'-aminoethyl)-3-hydroxyl-4-pyridinone, see Figure 7) conjugate for interaction with Aβ aggregates. This study demonstrated the ability of these nanoassemblies to protect human cortical neurons from Aβ aggregate-associated toxicity and further reduced Aβ aggregate formation (Figure 9).[69]

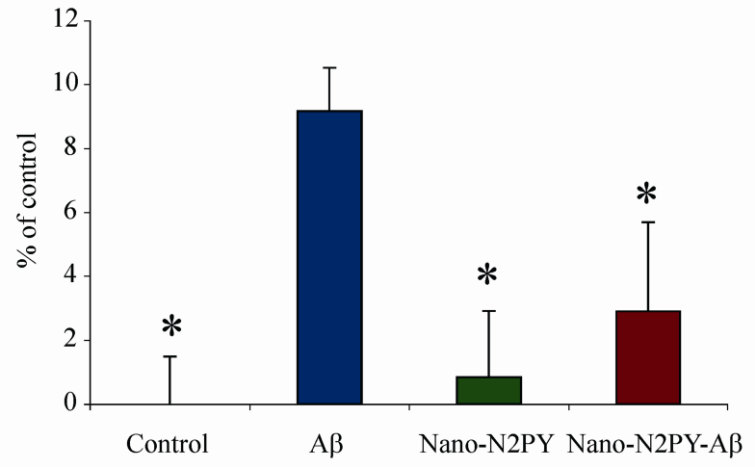

Figure 9. *Cytotoxicity of Aβ, Nano-N2PY and Aβ/Nano-N2PY (compared with control) when incubated with neuron cells as measured by LDH cytotoxicity detection assay. Absorbance wavelength measured in this experiment was 490 nm with a reference at 630 nm. Values were represented as mean ± standard errors (n = 5, significantly different from the Aβ at p < 0.05). Reprinted from Liu et al.,*[69] *with permission of Elsevier.*

4.1.6. *α*-, *β*- and *γ*-secretase inhibitors

Amyloid-β peptides originate from proteolysis of the APP by the sequential enzymatic actions of *β*-site amyloid precursor protein-cleaving enzyme 1 (BACE-1, a *β*-secretase) and *γ*-secretase, (*i.e.*, a protein complex with presenilin 1 at its catalytic core). Instead, the non-amyloidogenic pathway involves successive APP cleavages by *α*-secretase (whom cleavage precludes Aβ formation) and *γ*-secretase, leading to the formation of non-amyloidogenic fragments. The disturbance of these two pathways and the aggregative feature of Aβ could be the triggering factor in AD.[1]

Accordingly, *α*-, *β*- and *γ*-secretases can be considered as promising therapeutic targets.[70] However, due to the multiple biological functions related to *α*- and *γ*-secretases, *β*-secretase might be the most relevant and attractive target.[71] Despite several inhibitors/promoters transition-states that have been proposed so far, an important limitation is still their delivery to the CNS. Several studies have described encouraging outcomes but they were focused on intracranial injections of the inhibitors.[72] In this context, a recent study by Smith et al., suggested that the encapsulation of epigallotechin-3-gallate (EGCG, also called gallic acid, see Figure 7), a natural *α*-secretase promoter, into lipidic NPs could increase its oral bioavailability.[73] However, no additional information was provided regarding brain delivery and therapeutic efficacy of the described system.

4.1.7. Antioxidant species

Another strategy regarding the treatment of AD is directed towards the delivery of antioxidant species to the brain, because of their ability to quench the reactivity of reactive oxygen species (see also section 3.2 about antioxydant sponges).

Glutathione. The γ-glutamylcysteinylglycine (also called glutathione, GSH), a water-soluble endogenous antioxidant composed of glutamic acid, glycine and cysteine (Figure 7), is one of the most important intracellular antioxidants. It can protect cells from oxidative stress by scavenging singlet oxygen ($^1O_2$), hydroxyl radicals ($HO^\bullet$) and superoxide radicals ($O_2^{-\bullet}$).[74] Williams et al., proposed the synthesis of PEG-GSH conjugates that self-assembled into NPs with the aim of increasing GSH levels in the brain. The authors described the ability of these nanoassemblies to alleviate the oxidative stress in SH-SY5Y cells against hydrogen peroxide (H_2O_2).[75] A similar approach was proposed by Reddy et al., who investigated the encapsulation of a metalloprotein, superoxide dismutase (SOD), into PLGA NPs so as to increase its circulating half-life, cell membrane permeability and brain uptake. SOD is a free radical scavenger which plays a key role in the major endogenous cellular defense mechanism against superoxide radicals. The authors described the efficacy of these nanomaterials to deliver SOD to human neuronal cells *in vitro* and to protect them from H_2O_2-induced oxidative stress.[76]

Ferulic acid. Picone et al., recently reported the use of solid lipid NPs (SLN) as nanocarriers for ferulic acid (3-(4-hydroxy-3-methoxyphenyl)-2-propenoic acid, FA) due to their recently-demonstrated ability to cross the BBB.[77-78] Ferulic acid, an antioxidant naturally present in plant cell walls, is obtained from the alkaline hydrolysis of curcumin and consists in a phenolic nucleus conjugated to an aliphatic unsaturated side chain (see Figure 7). This conjugated structure is favorable to radical scavenging due to its resonance stabilized phenoxy radical, leading to strong antioxidant and anti-inflammatory activities.[79] The authors demonstrated that FA-loaded SLN drug delivery devices were able to enhance the inhibition of neuronal oxidative stress and thus to block the cascade reactions leading to cellular death after the treatment of LAN5 human neuroblastoma cells with $A\beta_{1-42}$ oligomers.[80] This improvement compared with free FA was claimed by the authors to be due to the ability of the SLN nanocarriers to increase drug stability within biological fluids and to target specific organelles within cells, such as mitochondria.

4.2. Antioxidant sponges

4.2.1. Fullerenes

Specific carbon-based nanostructures have shown some promising therapeutic effects in AD. For instance, radical scavenging entities, such as carboxyfullerenes (C_{60}) could trap multiple radicals and have been consequently exploited as "radical sponges".[81] In this view, Dugan et al., investigated the ability of water-soluble C_{60} carboxylic acid derivatives, containing three malonic acid groups per molecule, to reduce the apoptotic neuronal death induced by exposure to $A\beta_{1-42}$.[82] In this way, fullerenes could be an interesting alternative to reduce damages caused by Aβ toxicity.

Another widespread hypothesis about AD stipulates that calcium channels may play an important role in mediating Aβ activity on neurons. More precisely, the neurodegeneration could be mediated by an increase of Ca^{2+} influx caused by Aβ aggregates that would be able to create membrane channels permeable to Ca^{2+}.[83-84] Thus, Huangh et al., took advantage of the antioxidative effect of fullerenol-1 on the *in vitro* reduction of Aβ-related toxicity and proved the existence of a mechanism governing this activity.[85] Fullerenol-1 was found to be able to attenuate the increase of intracellular Ca^{2+} concentration promoted by Aβ aggregates, either by interacting with the membrane lipid components and thus changing the membrane permeability, or by altering the lipid peroxidation and the membrane composition.

4.2.2. Nanoceria

Nanocerias (*i.e.*, mixed-valence state cerium) were used to drastically reduce the reactive oxygen intermediates (ROI) intracellular concentration *in vitro* and *in vivo*, in order to prevent the loss of vision due to light-induced degeneration of photoreceptor cells. These results indicated that nanoceria particles were active for the inhibition of ROI-mediated cell death that is involved, among other species, in AD pathogenesis.[86]

4.3. Physical interaction with Aβ peptide

Protein/peptide conformation is often altered following adsorption onto the surface of nanoparticles and this may affect their biological functions accordingly.[87] This has been taken into advantage by designing brain-specific nanoparticles with affinity for Aβ peptides thus affecting their aggregation/nucleation.

Considering recent findings about the toxicity of Aβ aggregates,[88] an exogenous material that would be able to reduce the peptide toxicity may act following two opposite, postulated mechanisms:

(i) by decreasing monomer nucleation and hence blocking the aggregation, which would result in a reduction of the formation of oligomers, fibrils and plaques or (ii) by disaggregating amyloid plaques or fibrils (although they are currently not considered as the Aβ neurotoxic species) (Figure 10).[89-91] So far, the first mechanism has received much attention.

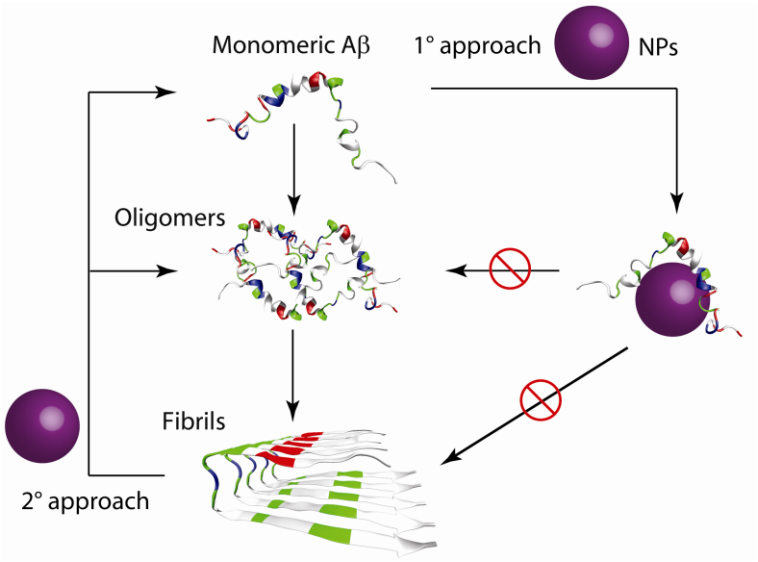

Figure 10. *Schematic representation of the two proposed physical approaches to reduce Aβ toxicity within the AD brain.*

4.3.1. Polymer nanoparticles

Cabaleiro-Lago et al., reported the use of 40 nm sized poly(*N*-isopropylacrylamide)-*co*-poly(*N*-*tert*-butylacrylamide) (PNIPAAM-*co*-P*t*BAM) NPs to hinder Aβ fibril formation. The authors demonstrated that these NPs were able to interfere with the fibrillation process by delaying, or even blocking, the nucleation step, whereas no influence on the elongation step was noticed. More importantly, it was found that the oligomerization of the peptide could be reversed sufficiently where mature fibrils start forming. These copolymeric NPs introduced a "lag phase" in between the nucleation and the elongation steps of the fibrillation. This "lag phase" was shown to be strongly dependent on the physico-chemical characteristics of the NP surface and concentration.[92] These results might help to better elucidate the aggregation process of the peptide and to design nanoparticles with optimized surface properties directed towards AD treatment.

The ability of sulfonated, sulfated and fluorinated PS nanoparticles in suppressing Aβ oligomerization and its toxicity towards cultured neurons has also been demonstrated.[93-94] In addition, it was shown

that hydrogenated NP counterparts had less efficacy, leading to *β*-sheet structures formation and aggregation. These results highlighted the crucial importance of the surface features of the NPs employed. Interestingly, Linse's[95] recently demonstrated a dual effect of cationic amino-functionalized PS NPs towards the Aβ fibrillation process. The possibility to alter the peptide aggregation simply by tuning the NP concentration was finely described, hence highlighting the pivotal role of NP dosing on the aggregation behaviour.[95] PS nanoparticles offer an interesting model for optimization of surface properties for suppressing Aβ oligomerization. However, they are nonbiodegradable and may induce adverse reactions, but these strategies may be translated to biodegradable entities.

The very first example of biodegradable NPs able to bind the Aβ peptide and to inhibit its aggregation kinetics was reported in 2010 by Brambilla et al.,[96] The authors used PEGylated poly(alkyl cyanoacrylate) NPs based on poly[methoxypoly(ethylene glycol)-*co*-(hexadecyl cyanoacrylate)] (P(MePEGCA-*co*-HDCA)) copolymer and monitored interaction with the $A\beta_{1\text{-}42}$ peptide by capillary electrophoresis coupled to laser induced fluorescence (CE-LIF) (Figure 11).

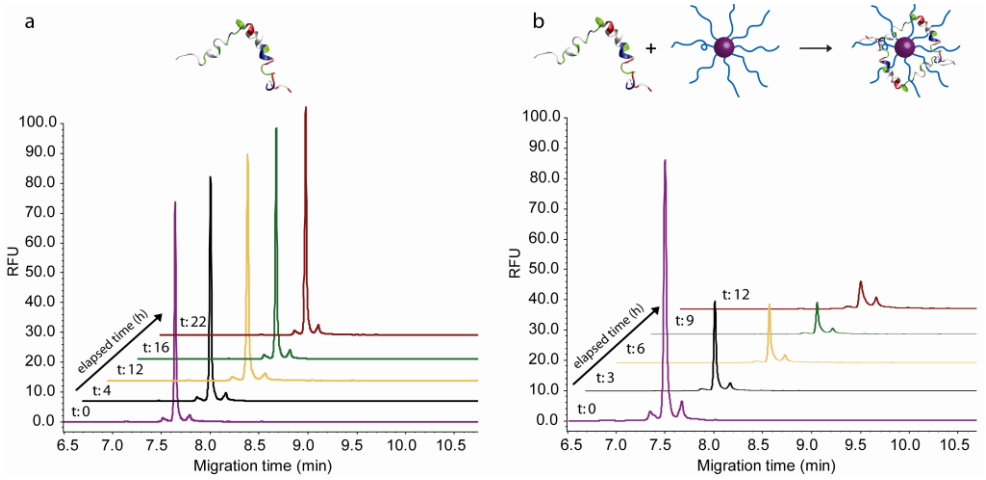

Figure 11. *CE-LIF analysis highligthing the interaction between $A\beta_{1\text{-}42}$ and PEGylated poly(alkyl cyanoacrylate) nanoparticles. Electrophoretic profile as a function of time at 37°C of a 5 µM Hilyte Fluor™ $A\beta_{1\text{-}42}$ solution alone (a) and in the presence of a 20 µM P(MePEGCA-co-HDCA) nanoparticle suspension (b). A decrease of the peak assigned to $A\beta_{1\text{-}42}$ peptide was observed in the presence of NPs suggesting its adsorption at their surface. Reprinted from Brambilla et al.,[96] with permission of ACS Publications.*

The principal advantage of this technique, when compared with other more routinely employed approaches such as ThT spectroscopy and SPR, is that NP interaction with peptide solution can be followed at nanomolar range peptide concentrations. Through this approach, not only the affinity

constant was measured, but the methodology further highlighted the crucial role of PEG chains at the surface of the NPs for peptide interaction. Experiments are currently ongoing to clarify the exact role of PEG chains as well as to develop functionalized polymeric NPs by means of click chemistry,[97] with higher affinity for the peptide. These NPs are potent candidates for suppressing Aβ aggregation as they were previously shown to cross the BBB.[98-99]

4.3.2. Liposomes

Gobbi et al., reported on preparation of liposomes and SLN incorporating either phosphatidic acid (PA) or cardiolipines (CL) as a way to target the Aβ peptide. SPR investigations demonstrated that both PA/CL-containing liposomes and SLN displayed a rather high affinity (*e.g.*, 22–60 nM) towards chip-immobilized Aβ fibrils, likely due to a multivalent interactions effect.[100]

Very recent studies from Mourtas et al.,[101] also reported the functionalization of azido-decorated liposomes with an alkyne-derivatized curcumin (see section 3.1.3) ligand by 1,3 dipolar Huisgen cycloaddition reaction (the so-called "click chemistry").[22] The authors found out by SPR experiments that the liposomes decorated with the planar curcumin had the highest affinity constant (in the 1–5 nM range) reported up-to-date for Aβ fibrils while non planar curcumin-decorated liposomes did not show any binding. As for the polymer nanoparticles, these systems could pave the way for the development of colloidal systems able to capture Aβ and to reduce its inherent toxicity.

4.3.3. Inorganic nanoparticles

Another interesting approach was proposed by Kogan et al., who demonstrated, by means of various complementary techniques, the possibility to locally and remotely heat and dissolve the $A\beta_{1-42}$ amyloid deposits *via* the combined use of weak microwave fields (100 mW, 6 times weaker than those used by conventional mobile phones) and Au NPs without any bulk effect. Although this approach was promising, it led to the formation of monomers and soluble oligomers, which are now considered as the most neurotoxic species in AD.[102-103]

4.3.4. PEGylated micelles

It was reported the ability of PEGylated phospholipidic micelles to interact with $A\beta_{1-42}$ and to moderate its *in vitro* neurotoxicity (Figure 12).[104] The authors proposed a double mechanism to explain PEGylated micelles activity. In the extracellular medium, these micelles would first interact with the peptide so as to bury its hydrophobic domains in the hydrophobic core of the micelle *via* a favored α-helical conformation that prevents its self-aggregation. Secondly, the PEGylated micelles

would shield the exposed hydrophobic domains of small $A\beta_{1-42}$ aggregates with their hydrophobic acyl chains, thus avoiding further formation of aggregate-aggregate or aggregate-monomeric $A\beta_{1-42}$.

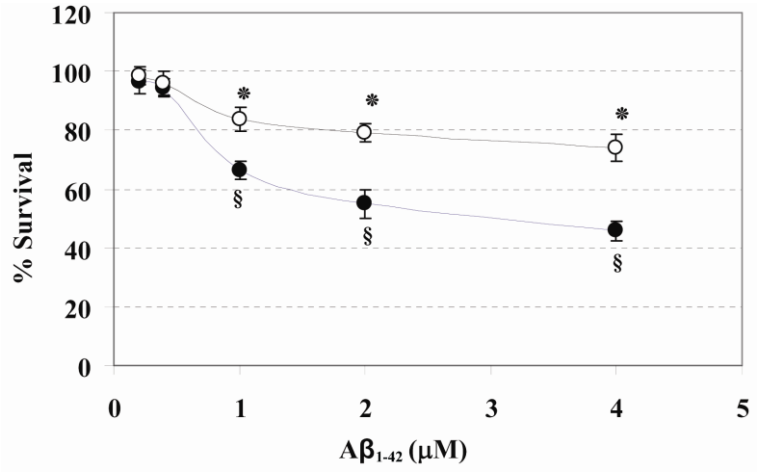

Figure 12. *Effect of PEGylated phospholipid micelles on $A\beta_{1-42}$ induced cytotoxicity. A significant reduction in $A\beta_{1-42}$ induced cytotoxicity is observed in cells treated with PEGylated lipid associated $A\beta_{1-42}$ ($n = 3$, $p < 0.05$ compared respective § without micelle treatment). Error bars represent standard deviation. Reprinted from Pai et al.,[104] with permission of Elsevier.*

4.3.5. Nanogels

Nanogels represent a promising class of drug-delivery devices because of their high loading capacity, their high stability as well as their responsiveness to environmental factors, such as ionic strength, pH, and temperature.[105]

In this view, Ikeda et al., suggested an original use of chlolesterol-bearing pullulan nanogels (CHP) with a diameter of 20–30 nm as artificial chaperone systems for controlling the aggregation and cytotoxicity of $A\beta_{1-42}$. These colloidal nanomaterials were able to efficiently incorporate the monomeric peptide and to inhibit its aggregation, thus suppressing its related toxicity against PC12 cells.[106] Recently, the same group evaluated the ability of these nanogels to interact with the $A\beta_{1-42}$ oligomeric forms and to reduce their toxicity on primary cortical and microglial cells. *In vitro* experiments indicated that CHP prevent $A\beta_{1-42}$ oligomers toxicity (Figure 13) and did not accumulate into lysosomes within the first 30 min.[107] Further experiments on transgenic animals mimicking conditions of the AD neurological disorder are ongoing, even if the ability of these nanostructures to overpass the BBB is still unproved. The concept developed with these CHP nanogels is very interesting if one considers the internalization of more specific Aβ-targeted ligands within the gel network.

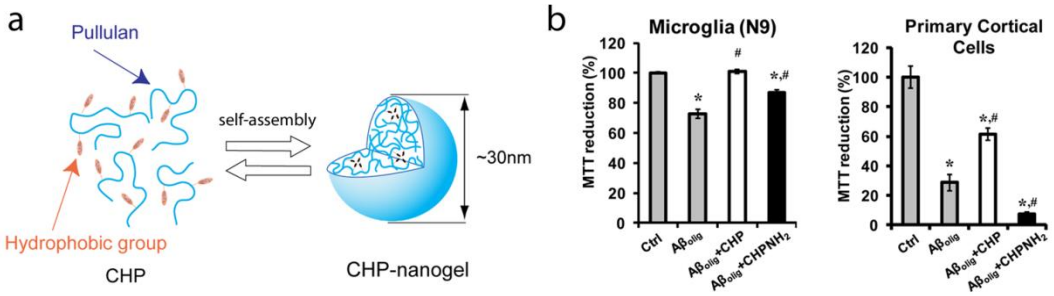

Figure 13. *Self-assembly of cholesterol-bearing pullulan (CHP) by hydrophobic interactions into nanogels (a). Rescue from Aβ-mediated diminution of MTT reduction in N9 microglial cells (left) and in primary cortical cells in the presence of nanogels (right). Cells were treated for 24 h with either 12 nM CHP or $CHPNH_2$ followed by oligomeric $A\beta_{1-42}$ (1 µM; $A\beta_{olig}$). Mean values and standard error of the means for triplicate measurements from 3 independent experiments (n = 9) are shown. Comparisons were made to control using ANOVA followed by Dunnett's test ($^{*}p < 0.01$) and to $A\beta_{olig}$ using Student's t-test ($^{\#}p < 0.01$). Adapted from Boridy et al.,*[107] *with permission of Elsevier.*

4.3.6. Dendrimers

Dendrimers, to distinguish from hyperbranched polymers, are commonly considered as nearly monodispersed macromolecules constituted by a regular and highly branched three-dimensional architecture displaying a well-defined number of spatially arranged peripheral functional groups. They are generally produced through an iterative sequence of reaction steps, in which each additional iteration affords higher generation materials. Regarding these properties, dendrimers have gained an increasing interest in pharmaceutical science as drug carriers and as constrast agents.[108] Especially, the possibility of functionalizing the peripheral groups with ligands of interest is an attractive strategy to study the physical interactions of these macromolecules with the Aβ peptide.

Several studies on the aggregation process of Aβ identified the critical peptidic sequence involved in amyloid aggregates formation. The hydrophobic core from residues 16 to 20 of Aβ, the so-called KLVFF sequence, is crucial for the formation of *β*-sheet structures.[109-110] It was also demonstrated that this peptidic region binds to its homologous sequence in Aβ and prevents its aggregation into amyloid fibrils.[111-112] This sequence has been employed as a key compound for the development of inhibiting agents for preventing Aβ aggregation *in vivo*.[109, 113] By exploiting the above-mentioned properties of this peptidic sequence, Chafekar et al., reported the synthesis of KLVFF-functionalized dendrimeric scaffolds and their marked inhibitory effect on $A\beta_{1-42}$ aggregation, as well

as their ability to disassemble pre-existing amyloid aggregates. The same authors clearly demonstrated that these nanodevices exploited the multivalency feature of dendrimers to drastically enhance the affinity and specificity of KLVFF sequence towards Aβ.[114]

Several independent studies also suggested that Aβ was able to bind cells *via* an interaction with glycolipids and/or glycoproteins present at the external surface of the cellular membrane. It was also shown that the interaction affinity increased when gangliosides or sialic acid molecules were clustered on the cell surface.[115-121] Based on these evidences, Patel et al., synthesized sialic acid-conjugated polyamidoamine (PAMAM) dendrimers as membrane clusters mimetics to create Aβ binding competiting agents. The authors investigated the affinity constant between sialic acid-functionalized PAMAM dendrimers and Aβ. They demonstrated the ability of these dendrimers to significantly reduce the Aβ-induced toxicity compared to non-treated control cells and cells treated with free sialic acid.[122] Further experiments from the same group also reported that the positioning of the covalent bond between the dendrimer and the sialic acid was crucial regarding the modulation of the biological activity of the resulting conjugates. The addition of a spacer between the anomeric hydroxyl position of sialic acid and the dendrimer shell end-groups resulted in an attenuation of the Aβ toxicity at lower concentrations compared to other binding strategies, thus highlighting a better match with the physiological attachment of sialic acid to cell membranes.[123]

Proteinaceous fibrils are normally associated to other cell substructures or biological compounds, such as cell membranes or glycosaminoglycans (GAGs) respectively. GAGs entities, such as heparin, which consists in linear arrangements of polysaccharides, have been shown to be particularly important in promoting Aβ aggregation process.[124] Thus, Klajnert et al., identified that the heparin-induced aggregation of $A\beta_{1-28}$ could be modulated by the presence of G3 generation PAMAM dendrimers. In particular the authors demonstrated that low concentrations of dendrimers reduced peptide aggregation whereas higher concentrations had the opposite effect.[125] Further experiments from the same group showed that the ionization state of acidic and basic residues of $A\beta_{1-28}$ fragment played an important role regarding the interactions between the dendrimer shell and the $A\beta_{1-28}$ amino-acids, which can result in an enhancement or a decrease of the peptide amyloidogenicity.[126] Despite experimental conditions far from physiological environment, these studies showed that dendrimers can be exploited as a powerful tool for investigating the formation mechanism of amyloid-like structures.

5. Nanotechnologies for *in vitro* evaluation of drugs activity

Although *in vivo* pharmacological assays remain the best way to evaluate drug activity and toxicity before clinical studies, they are time-consuming and rather expensive. Thus, a great deal of effort has been focused to establish efficient procedures for *in vitro* drug screening prior to *in vivo* preclinical experiments. Accordingly, a new drug sensitivity method based on the electrochemical behavior of AChE biosensor has been reported by Du et al.,[127] based on Au NPs encapsulating a sol-gel silicate matrix. This system provides a stable and biocompatible environment for AChE biosensor immobilization onto an electrode surface and appropriate conductivity properties to the network that favors interfacial enzymatic hydrolysis reaction. Two different AChE inhibitors (*i.e.*, neostigmine and galantamine) were used to verify the proof-of-principle of this methodology. Here, electroactive substances formed after reaction of substrate with the encapsulated AChE amplifies the biosensor sensitivity.

A method for ACh analysis based on its electrocatalytic oxidation on carbon paste electrodes modified with copper nanoparticles has also been proposed. Experimentally, the electro-oxidation of ACh is mediated by Cu(II) active species and the oxidized forms are detected and quantified using amperometric procedures. This technique was successfully applied for the quantification of ACh with high sensitivities in the µM range.[128]

Interestingly, the method developed by Haes et al.,[26-27] based on LSPR (see section 2), could also represent a very useful tool for the study of interactions between pharmaceutics and ADDLs.

6. Safety issues

Advances in nanotechnology and its applications in medicine have promoted serious issues in relation to nanoparticle-mediated toxicity and adverse reactions.[129-130] This is of particular concern for intravenously injected AD nanomedicines, whether they are used for the induction of the "sink-effect" or for reaching the brain for diagnostic imaging and/or therapeutic purposes. Noteworthy, nanoparticle size, shape and surface characteristics can modulate pharmacokinetics and biodistribution.[129, 131] Investigation in this area of research is still scant and particularly in relation to the brain. However, from the therapeutic point of view attention must be focused on the benefit-to-risk ratio and this is further dependent on nanoparticle dose and on the frequency of dosing. From the cytotoxicity angle, some constituents of polymeric nanoparticles and nanoconstructs may inhibit the function of P-glycoprotein efflux pumps expressed at the luminal side of the brain capillary endothelial cells.[132-133] This could potentially modulate or interfere with transport of haemostatic mediators in the central

nervous system.[134] Moreover, internalized nanoparticles, depending on their nature and intracellular trafficking could induce necrotic and/or apoptotic cell death through different pathways; a feature that is most prominent with polycationic constructs.[129, 135-137] Polymers also seem to be able to modulate gene expression[138] and this could pose serious problems in terms of nucleic acid delivery to the brain capillary endothelial cells with polyplexes and polycationic nanoconstructs. Indeed, this phenomenon has been correlated with low expression of ATP binding cassette genes after polymer treatment in some cells.[139] In cytoplasm, polymers and partially degraded nanoparticle constituents may bind to endogenous nucleic acids such as dsRNA and microRNA resulting in interference with normal cellular regulatory processes and triggering off-target effects. This possibility may account for the reported polycation-specific induced 'gene-signature'.[137] A recent report has also raised concern over potential nanoparticle-mediated DNA and chromosome damage to tissues located behind cellular barriers through complex intercellular signaling processes.[140] Therefore, some nanoparticles may induce cell damage across an intact biological barrier without having to cross the barrier.

Recent evidence with clinically approved intravenous nanomedicines attests to initiation of hypersensitivity reactions in certain individuals and these have often been correlated with activation of the complement system, which is the most ancient component of innate human immunity.[141] The reactions are non-IgE mediated and usually associated with flushing and cardiovascular disturbances. Neuro-psychomastic and vegetative responses have also been noted in animals following polymeric and lipid-based nanomedicines.[141] A wide range of polymers and nanoentities such as certain classes of liposomes, polymeric nanospheres, carbon nanotubes and metallic nanoparticles, whether stealth or not, can trigger complement activation *via* one or more of the three established initiation pathways (classical, alternative and lectin pathways) that all converge at the step where the central complement protein C3 is cleaved.[141-145] These pathways use different recognition molecules to sense a foreign particle, but use similar activation mechanisms to generate enzymes that cleave C3 (known as C3 convertases). The prime consequence of nanoparticle-mediated complement activation is surface opsonization by the opsonic fragments of C3 cleavage such as C3b and iC3b.[131, 141] This aids material recognition and rapid clearance by macrophages of the reticuloendothelial system bearing complement receptors (*e.g.*, hepatic Kupffer cells, splenic marginal zone and red-pulp macrophages, blood monocytes, etc.) and therefore may be beneficial for intravenous nanomedicines that are intended to induce "sink-effect" in AD.

Activation of the complement cascade further generates potent anaphylatoxins (C4a, C3a and C5a), and these can trigger the release of secondary mediators from a wide range of immune cells that subsequently initiate anaphylaxis in sensitive individuals.[131] Additionally, C5a is a potent chemotactic

agent for monocytes, neutrophils and a subset of T cells. It is also a powerful neutrophil activator increasing adhesiveness, stimulating the respiratory burst and degranulation. Such modulation of immune cell activities may further contribute to anaphylaxis and further complicate AD. Once C5 has been cleaved the lytic membrane attack complex (C5b-9 or MAC) is assembled from the terminal complement components C5, C6, C7, C8 and C9. Remarkably, this complex also has the capacity to elicit non-lytic stimulatory responses from vascular endothelial cells and modulate endothelial regulation of haemostasis and inflammatory cell recruitment.[131]

The complement system is strongly activated in AD brain, and particularly at the site of the senile plaque, and works in conjugation with activated microglia, which express high levels of complement receptors.[146] Most attempts have detected MAC on dystrophic neurites and neurofibrillary tangles adjacent to the senile plauqes, indicating autloytic attack and neurite loss.[146] Complement proteins and activation products have also been found to be associated with cerebrovascular Aβ.[147] However, only the earliest steps of complement activation appear in diffuse plaques containing non-filamentous Aβ in many regions of the brain, including those generally not affected by the disease (*e.g.*, cerebellum). Complement activation therefore exacerbates the patology of AD. Recent evidence also attest that the classical pathway components (*e.g.*, C1q) may be greatly upregulated in AD and particularly in the cortex.[148] The binding interaction between Aβ and C1q is mainly ionic and occurs between the first 11 predominantly ionic residues of Aβ and residues 14−26 of the A chain of the collagen-like tail of C1q, which are mostly cationic.[149] Aβ interactions with C1q also leads to increased amyloid aggregation. Therefore, it remains essential that nanoengineering strategies that allows particle delivery into the brain do not induce further complement activation (notably activation of the terminal pathway) and particularly through C1q-dependent triggering mechanism. Future efforts may further concentrate in design of brain-specific nanoparticles that can also release complement inhibitors and particularly those that can block binding to the collagen tail of C1q as this will not disturb antibody attack against an infectious agent.[150] The complement system, therefore, plays a central role in nanomaterial and nanomedicine performance and better understanding of material properties in relation to complement activation remains pivotal for precision engineering of highly effective nanomedicines for long-term management as well as treatment of AD.

Finally, with respect to the nanoparticle-mediated initiation of the “sink-effect” particular attention must be paid to the frequency and intervals between injections. Adverse responses may arise from excessive dose-dumping in macrophages (which may be selective and based on aggregate sizes) and initiation of immunogenic responses following repeated administration, resulting in altered nanoparticle pharmacokinetics and diminished efficacy.

7. Conclusions

During the past few years, we have witnessed promising developments in relation to passive and active drug delivery to the brain using nanoparticles. In parallel, remarkable nanotechnologies have emerged that can manipulate Aβ aggregation both in the brain and in the peripheral circulation thus aiding experimental AD therapy.

However, three important open questions remain to be answered before engaging further research towards clinical investigations: (i) the efficiency of symptom alleviation by these nanoparticulate systems needs to be validated in representative AD *in vivo* models, (ii) FDA-approved macromolecules for nanoconstructs have to be employed and (iii) non-invasive administrations of nanoparticles have to be considered for repeated and prolonged therapeutical purposes. These needs are also required if one considers the development of a strategy based on the production of NPs for physical interactions with Aβ peptide and/or τ protein. Moreover, in this case, the majority of the above-discussed studies were performed in buffer environments, a strong simplification of physiological conditions.

Recent achievements also described the design and the use of imaging agents and drugs based on nanoparticulate systems. However, the most prominent limitation relies on the fact that plaques are no more considered as the toxic species in AD, although the majority of described methods are based on their detection. The incredible effort devoted to the development of highly sensitive detection methods able to finely detect biomarkers from bio-samples with high specificity, may pave the way to routinely employed diagnosis kits against AD for clinical use.

Although nanotechnology is expected to have a huge impact on the development of "smart" drug delivery and theranostic devices against AD, a crucial gap to fill-in concerns the elucidation of its etiology, in which a great deal of effort is still required.

8. Acknowledgements

We are grateful to the European Community's Seventh Framework Programme (FP7/2007-2013) under grant agreement n^{o} 212043 for financial support. The French ministry of research and CNRS are also warmly acknowledged for the financial support. SMM further acknowledges financial support from Danish Agency for Science, Technology and Innovation (Det Strategiske Forskningsråd, reference 09-065746/DSF) and Lundbeck S/A.

9. References

1. Querfurth HW,LaFerla FM. Alzheimer's disease. N Engl J Med 2010; 362: 329-44.

2. Potschka H. Targeting the brain--surmounting or bypassing the blood-brain barrier. Handb Exp Pharmacol 2010; 411-31.

3. Silva GA. Nanotechnology applications and approaches for neuroregeneration and drug delivery to the central nervous system. Ann N Y Acad Sci 2010; 1199: 221-30.

4. Kreuter J. Nanoparticulate systems for brain delivery of drugs. Adv Drug Deliv Rev 2001; 47: 65-81.

5. de Vries IJ, Lesterhuis WJ, Barentsz JO, Verdijk P, van Krieken JH, Boerman OC, et al. Magnetic resonance tracking of dendritic cells in melanoma patients for monitoring of cellular therapy. Nat Biotechnol 2005; 23: 1407-13.

6. Wadghiri YZ, Sigurdsson EM, Sadowski M, Elliott JI, Li Y, Scholtzova H, et al. Detection of alzheimer's amyloid in transgenic mice using magnetic resonance microimaging. Magn Reson Med 2003; 50: 293-302.

7. Skaat H,Margel S. Synthesis of fluorescent-maghemite nanoparticles as multimodal imaging agents for amyloid-beta fibrils detection and removal by a magnetic field. Biochem Biophys Res Commun 2009; 386: 645-9.

8. Skaat H, Sorci M, Belfort G,Margel S. Effect of maghemite nanoparticles on insulin amyloid fibril formation: Selective labeling, kinetics, and fibril removal by a magnetic field. J Biomed Mater Res A 2009; 91: 342-51.

9. Soreq H,Seidman S. Acetylcholinesterase--new roles for an old actor. Nat Rev Neurosci 2001; 2: 294-302.

10. Elsinghorst PW, Hartig W, Goldhammer S, Grosche J,Gutschow M. A gorge-spanning, high-affinity cholinesterase inhibitor to explore beta-amyloid plaques. Org Biomol Chem 2009; 7: 3940-6.

11. Hartig W, Kacza J, Paulke B, Grosche J, Bauer U, Hoffmann A, et al. In vivo labelling of hippocampal-amyloid in triple-transgenic mice with a fluorescent acetylcholinesterase inhibitor released from nanoparticles. Eur J Neurosci 2010; 31: 99-109.

12. Siegemund T, Paulke BR, Schmiedel H, Bordag N, Hoffmann A, Harkany T, et al. Thioflavins released from nanoparticles target fibrillar amyloid beta in the hippocampus of app/ps1 transgenic mice. Int J Dev Neurosci 2006; 24: 195-201.

13. Dubertret B, Skourides P, Norris DJ, Noireaux V, Brivanlou AH,Libchaber A. In vivo imaging of quantum dots encapsulated in phospholipid micelles. Science 2002; 298: 1759-62.

14. Tokuraku K, Marquardt M,Ikezu T. Real-time imaging and quantification of amyloid-beta peptide aggregates by novel quantum-dot nanoprobes. PLoS One 2009; 4: e8492.

15. Xu G, Yong KT, Roy I, Mahajan SD, Ding H, Schwartz SA, et al. Bioconjugated quantum rods as targeted probes for efficient transmigration across an in vitro blood-brain barrier. Bioconjug Chem 2008; 19: 1179-85.

16. Choi JS, Choi HJ, Jung DC, Lee JH,Cheon J. Nanoparticle assisted magnetic resonance imaging of the early reversible stages of amyloid beta self-assembly. Chem Commun 2008; 2197-9.

17. Clark CM, Xie S, Chittams J, Ewbank D, Peskind E, Galasko D, et al. Cerebrospinal fluid tau and beta-amyloid: How well do these biomarkers reflect autopsy-confirmed dementia diagnoses? Arch Neurol 2003; 60: 1696-702.

18. Blennow K,Hampel H. Csf markers for incipient alzheimer's disease. Lancet Neurol 2003; 2: 605-13.

19. Teunissen CE, de Vente J, Steinbusch HW,De Bruijn C. Biochemical markers related to alzheimer's dementia in serum and cerebrospinal fluid. Neurobiol Aging 2002; 23: 485-508.

20. Keating CD. Nanoscience enables ultrasensitive detection of alzheimer's biomarker. Proc Natl Acad Sci U S A 2005; 102: 2263-4.

21. Georganopoulou DG, Chang L, Nam JM, Thaxton CS, Mufson EJ, Klein WL, et al. Nanoparticle-based detection in cerebral spinal fluid of a soluble pathogenic biomarker for alzheimer's disease. Proc Natl Acad Sci U S A 2005; 102: 2273-6.

22. Kolb HC, Finn MG,Sharpless KB. Click chemistry: Diverse chemical function from a few good reactions. Angew Chem Int Ed Engl 2001; 40: 2004-21.

23. Chikae M, Fukuda T, Kerman K, Idegami K, Miura Y,Tamiya E. Amyloid-beta detection with saccharide immobilized gold nanoparticle on carbon electrode. Bioelectrochemistry 2008; 74: 118-23.

24. Lee JH, Kang DY, Lee T, Kim SU, Oh BK,Choil JW. Signal enhancement of surface plasmon resonance based immunosensor using gold nanoparticle-antibody complex for beta-amyloid (1-40) detection. J Nanosci Nanotechnol 2009; 9: 7155-60.

25. Kang DY, Lee JH, Oh BK,Choi JW. Ultra-sensitive immunosensor for beta-amyloid (1-42) using scanning tunneling microscopy-based electrical detection. Biosens Bioelectron 2009; 24: 1431-6.

26. Haes AJ, Chang L, Klein WL,Van Duyne RP. Detection of a biomarker for alzheimer's disease from synthetic and clinical samples using a nanoscale optical biosensor. J Am Chem Soc 2005; 127: 2264-71.

27. Haes AJ, Hall WP, Chang L, Klein WL,Van Duyne RP. A localized surface plasmon resonance biosensor: First steps toward an assay for alzheimer's disease. Nano letters 2004; 4: 1029-34.

28. Zhao J, Zhang X, Yonzon CR, Haes AJ,Van Duyne RP. Localized surface plasmon resonance biosensors. Nanomedicine (Lond) 2006; 1: 219-28.

29. Neely A, Perry C, Varisli B, Singh AK, Arbneshi T, Senapati D, et al. Ultrasensitive and highly selective detection of alzheimer's disease biomarker using two-photon rayleigh scattering properties of gold nanoparticle. ACS Nano 2009; 3: 2834-40.

30. Nazem A,Mansoori GA. Nanotechnology solutions for alzheimer's disease: Advances in research tools, diagnostic methods and therapeutic agents. J Alzheimers Dis 2008; 13: 199-223.

31. Modi G, Pillay V,Choonara YE. Advances in the treatment of neurodegenerative disorders employing nanotechnology. Ann N Y Acad Sci 2010; 1184: 154-72.

32. Ryan J, Scali J, Carriere I, Ritchie K,Ancelin ML. Hormonal treatment, mild cognitive impairment and alzheimer's disease. Int Psychogeriatr 2008; 20: 47-56.

33. Gauthier S, Juby A, Dalziel W, Rehel B,Schecter R. Effects of rivastigmine on common symptomatology of alzheimer's disease. Curr Med Res Opin 2010; 26: 1149-60.

34. Lockhart IA, Mitchell SA,Kelly S. Safety and tolerability of donepezil, rivastigmine and galantamine for patients with alzheimer's disease: Systematic review of the 'real-world' evidence. Dement Geriatr Cogn Disord 2009; 28: 389-403.

35. Wilson B, Samanta MK, Santhi K, Kumar KP, Paramakrishnan N,Suresh B. Poly(n-butylcyanoacrylate) nanoparticles coated with polysorbate 80 for the targeted delivery of rivastigmine into the brain to treat alzheimer's disease. Brain Res 2008; 1200: 159-68.

36. Wilson B, Samanta MK, Santhi K, Kumar KP, Paramakrishnan N,Suresh B. Targeted delivery of tacrine into the brain with polysorbate 80-coated poly(n-butylcyanoacrylate) nanoparticles. Eur J Pharm Biopharm 2008; 70: 75-84.

37. Morris R. Developments of a water-maze procedure for studying spatial learning in the rat. J Neurosci Methods 1984; 11: 47-60.

38. Joshi SA, Chavhan SS,Sawant KK. Rivastigmine-loaded plga and pbca nanoparticles: Preparation, optimization, characterization, in vitro and pharmacodynamic studies. Eur J Pharm Biopharm 2010; 76: 189-99.

39. Yang Z, Zhang Y, Yang Y, Sun L, Han D, Li H, et al. Pharmacological and toxicological target organelles and safe use of single-walled carbon nanotubes as drug carriers in treating alzheimer disease. Nanomedicine 2010; 6: 427-41.

40. Pike CJ, Carroll JC, Rosario ER,Barron AM. Protective actions of sex steroid hormones in alzheimer's disease. Front Neuroendocrinol 2009; 30: 239-58.

41. Amtul Z, Wang L, Westaway D,Rozmahel RF. Neuroprotective mechanism conferred by 17beta-estradiol on the biochemical basis of alzheimer's disease. Neuroscience 2010; 169: 781-6.

42. Mittal G, Sahana DK, Bhardwaj V,Ravi Kumar MN. Estradiol loaded plga nanoparticles for oral administration: Effect of polymer molecular weight and copolymer composition on release behavior in vitro and in vivo. J Control Release 2007; 119: 77-85.

43. Belanoff JK, Jurik J, Schatzberg LD, DeBattista C,Schatzberg AF. Slowing the progression of cognitive decline in alzheimer's disease using mifepristone. J Mol Neurosci 2002; 19: 201-6.

44. DeBattista C,Belanoff J. C-1073 (mifepristone) in the adjunctive treatment of alzheimer's disease. Curr Alzheimer Res 2005; 2: 125-9.

45. Lam FC, Liu R, Lu P, Shapiro AB, Renoir JM, Sharom FJ, et al. Beta-amyloid efflux mediated by p-glycoprotein. J Neurochem 2001; 76: 1121-8.

46. He W, Horn SW,Hussain MD. Improved bioavailability of orally administered mifepristone from plga nanoparticles. Int J Pharm 2007; 334: 173-8.

47. Sharma RA, Steward WP,Gescher AJ. Pharmacokinetics and pharmacodynamics of curcumin. Adv Exp Med Biol 2007; 595: 453-70.

48. Osawa T. Nephroprotective and hepatoprotective effects of curcuminoids. Adv Exp Med Biol 2007; 595: 407-23.

49. Ishrat T, Hoda MN, Khan MB, Yousuf S, Ahmad M, Khan MM, et al. Amelioration of cognitive deficits and neurodegeneration by curcumin in rat model of sporadic dementia of alzheimer's type (sdat). Eur Neuropsychopharmacol 2009; 19: 636-47.

50. Ringman JM, Frautschy SA, Cole GM, Masterman DL,Cummings JL. A potential role of the curry spice curcumin in alzheimer's disease. Curr Alzheimer Res 2005; 2: 131-6.

51. Anand P, Kunnumakkara AB, Newman RA,Aggarwal BB. Bioavailability of curcumin: Problems and promises. Mol Pharm 2007; 4: 807-18.

52. Sun M, Gao Y, Guo C, Cao F, Song Z, Xi Y, et al. Enhancement of transport of curcumin to brain in mice by poly(n-butylcyanoacrylate) nanoparticle. J Nanopart Res 2010; 12: 3111-22.

53. Mulik R, Mahadik K,Paradkar A. Development of curcuminoids loaded poly(butyl cyanoacrylate) nanoparticles: Physicochemical characterization and stability study. Eur J Pharm Sci 2009; 37: 395-404.

54. Mulik RS, Monkkonen J, Juvonen RO, Mahadik KR,Paradkar AR. Apoe3 mediated poly(butyl) cyanoacrylate nanoparticles containing curcumin: Study of enhanced activity of curcumin against beta amyloid induced cytotoxicity using in vitro cell culture model. Mol Pharm 2010;

55. Moretto N, Bolchi A, Rivetti C, Imbimbo BP, Villetti G, Pietrini V, et al. Conformation-sensitive antibodies against alzheimer amyloid-beta by immunization with a thioredoxin-constrained b-cell epitope peptide. J Biol Chem 2007; 282: 11436-45.

56. Gelinas DS, DaSilva K, Fenili D, St George-Hyslop P,McLaurin J. Immunotherapy for alzheimer's disease. Proc Natl Acad Sci U S A 2004; 101 Suppl 2: 14657-62.

57. Agyare EK, Curran GL, Ramakrishnan M, Yu CC, Poduslo JF,Kandimalla KK. Development of a smart nano-vehicle to target cerebrovascular amyloid deposits and brain parenchymal plaques observed in alzheimer's disease and cerebral amyloid angiopathy. Pharm Res 2008; 25: 2674-84.

58. Treiber C, Quadir MA, Voigt P, Radowski M, Xu S, Munter LM, et al. Cellular copper import by nanocarrier systems, intracellular availability, and effects on amyloid beta peptide secretion. Biochemistry 2009; 48: 4273-84.

59. Castellani RJ, Moreira PI, Liu G, Dobson J, Perry G, Smith MA, et al. Iron: The redox-active center of oxidative stress in alzheimer disease. Neurochem Res 2007; 32: 1640-5.

60. Bush AI, Pettingell WH, Multhaup G, d Paradis M, Vonsattel JP, Gusella JF, et al. Rapid induction of alzheimer abeta amyloid formation by zinc. Science 1994; 265: 1464-7.

61. Sensi SL, Paoletti P, Bush AI,Sekler I. Zinc in the physiology and pathology of the cns. Nat Rev Neurosci 2009; 10: 780-91.

62. Sayre LM, Perry G, Harris PL, Liu Y, Schubert KA,Smith MA. In situ oxidative catalysis by neurofibrillary tangles and senile plaques in alzheimer's disease: A central role for bound transition metals. J Neurochem 2000; 74: 270-9.

63. Pratico D, Uryu K, Sung S, Tang S, Trojanowski JQ,Lee VM. Aluminum modulates brain amyloidosis through oxidative stress in app transgenic mice. FASEB J 2002; 16: 1138-40.

64. Smith MA, Harris PL, Sayre LM,Perry G. Iron accumulation in alzheimer disease is a source of redox-generated free radicals. Proc Natl Acad Sci U S A 1997; 94: 9866-8.

65. Atwood CS, Scarpa RC, Huang X, Moir RD, Jones WD, Fairlie DP, et al. Characterization of copper interactions with alzheimer amyloid beta peptides: Identification of an attomolar-affinity copper binding site on amyloid beta1-42. J Neurochem 2000; 75: 1219-33.

66. Cherny RA, Barnham KJ, Lynch T, Volitakis I, Li QX, McLean CA, et al. Chelation and intercalation: Complementary properties in a compound for the treatment of alzheimer's disease. J Struct Biol 2000; 130: 209-16.

67. Crapper McLachlan DR, Dalton AJ, Kruck TP, Bell MY, Smith WL, Kalow W, et al. Intramuscular desferrioxamine in patients with alzheimer's disease. Lancet 1991; 337: 1304-8.

68. Cui Z, Lockman PR, Atwood CS, Hsu CH, Gupte A, Allen DD, et al. Novel d-penicillamine carrying nanoparticles for metal chelation therapy in alzheimer's and other cns diseases. Eur J Pharm Biopharm 2005; 59: 263-72.

69. Liu G, Men P, Kudo W, Perry G,Smith MA. Nanoparticle-chelator conjugates as inhibitors of amyloid-beta aggregation and neurotoxicity: A novel therapeutic approach for alzheimer disease. Neurosci Lett 2009; 455: 187-90.

70. Roberson ED,Mucke L. 100 years and counting: Prospects for defeating alzheimer's disease. Science 2006; 314: 781-4.

71. Vassar R. Beta-secretase (bace) as a drug target for alzheimer's disease. Adv Drug Deliv Rev 2002; 54: 1589-602.

72. Rajendran L, Schneider A, Schlechtingen G, Weidlich S, Ries J, Braxmeier T, et al. Efficient inhibition of the alzheimer's disease beta-secretase by membrane targeting. Science 2008; 320: 520-3.

73. Smith A, Giunta B, Bickford PC, Fountain M, Tan J,Shytle RD. Nanolipidic particles improve the bioavailability and alpha-secretase inducing ability of epigallocatechin-3-gallate (egcg) for the treatment of alzheimer's disease. Int J Pharm 2010; 389: 207-12.

74. Masella R, Di Benedetto R, Vari R, Filesi C,Giovannini C. Novel mechanisms of natural antioxidant compounds in biological systems: Involvement of glutathione and glutathione-related enzymes. J Nutr Biochem 2005; 16: 577-86.

75. Williams S, Lepene B, Thatcher C,Long T. Synthesis and characterization of poly(ethylene glycol)-glutathione conjugate self-assembled nanoparticles for antioxidant delivery. Biomacromolecules 2009; 10: 155-61.

76. Reddy MK, Wu L, Kou W, Ghorpade A,Labhasetwar V. Superoxide dismutase-loaded plga nanoparticles protect cultured human neurons under oxidative stress. Appl Biochem Biotechnol 2008; 151: 565-77.

77. Wissing SA, Kayser O,Muller RH. Solid lipid nanoparticles for parenteral drug delivery. Adv Drug Deliv Rev 2004; 56: 1257-72.

78. Wang JX, Sun X,Zhang ZR. Enhanced brain targeting by synthesis of 3',5'-dioctanoyl-5-fluoro-2'-deoxyuridine and incorporation into solid lipid nanoparticles. Eur J Pharm Biopharm 2002; 54: 285-90.

79. Ozaki Y. Antiinflammatory effect of tetramethylpyrazine and ferulic acid. Chem Pharm Bull 1992; 40: 954-6.

80. Picone P, Bondi ML, Montana G, Bruno A, Pitarresi G, Giammona G, et al. Ferulic acid inhibits oxidative stress and cell death induced by ab oligomers: Improved delivery by solid lipid nanoparticles. Free Radic Res 2009; 43: 1133-45.

81. Krusic PJ, Wasserman E, Keizer PN, Morton JR,Preston KF. Radical reactions of c60. Science 1991; 254: 1183-5.

82. Dugan LL, Turetsky DM, Du C, Lobner D, Wheeler M, Almli CR, et al. Carboxyfullerenes as neuroprotective agents. Proc Natl Acad Sci U S A 1997; 94: 9434-9.

83. Arispe N, Pollard HB,Rojas E. Giant multilevel cation channels formed by alzheimer disease amyloid beta-protein [a beta p-(1-40)] in bilayer membranes. Proc Natl Acad Sci U S A 1993; 90: 10573-7.

84. Arispe N, Pollard HB,Rojas E. Beta-amyloid ca(2+)-channel hypothesis for neuronal death in alzheimer disease. Mol Cell Biochem 1994; 140: 119-25.

85. Huang HM, Ou HC, Hsieh SJ,Chiang LY. Blockage of amyloid beta peptide-induced cytosolic free calcium by fullerenol-1, carboxylate c60 in pc12 cells. Life Sci 2000; 66: 1525-33.

86. Chen J, Patil S, Seal S,McGinnis JF. Rare earth nanoparticles prevent retinal degeneration induced by intracellular peroxides. Nat Nanotechnol 2006; 1: 142-50.

87. Auer S, Trovato A,Vendruscolo M. A condensation-ordering mechanism in nanoparticle-catalyzed peptide aggregation. PloS Comput Biol 2009;

88. Ono K, Condron MM,Teplow DB. Structure-neurotoxicity relationships of amyloid beta-protein oligomers. Proc Natl Acad Sci U S A 2009; 106: 14745-50.

89. Roychaudhuri R, Yang M, Hoshi MM,Teplow DB. Amyloid beta-protein assembly and alzheimer disease. J Biol Chem 2009; 284: 4749-53.

90. Cizas P, Budvytyte R, Morkuniene R, Moldovan R, Broccio M, Losche M, et al. Size-dependent neurotoxicity of beta-amyloid oligomers. Arch Biochem Biophys 2010; 496: 84-92.

91. Dahlgren KN, Manelli AM, Stine WB, Jr., Baker LK, Krafft GA,LaDu MJ. Oligomeric and fibrillar species of amyloid-beta peptides differentially affect neuronal viability. J Biol Chem 2002; 277: 32046-53.

92. Cabaleiro-Lago C, Quinlan-Pluck F, Lynch I, Lindman S, Minogue AM, Thulin E, et al. Inhibition of amyloid beta protein fibrillation by polymeric nanoparticles. J Am Chem Soc 2008; 130: 15437-43.

93. Rocha S, Thunemann AF, Pereira Mdo C, Coelho M, Mohwald H,Brezesinski G. Influence of fluorinated and hydrogenated nanoparticles on the structure and fibrillogenesis of amyloid beta-peptide. Biophys Chem 2008; 137: 35-42.

94. Saraiva AM, Cardoso I, Saraiva MJ, Tauer K, Pereira MC, Coelho MA, et al. Randomization of amyloid-beta-peptide(1-42) conformation by sulfonated and sulfated nanoparticles reduces aggregation and cytotoxicity. Macromol Biosci 2010;

95. Cabaleiro-Lago C, Quinlan-Pluck F, Lynch I, Dawson K,Linse S. Dual effect of amino modified polystyrene nanoparticles on amyloid protein fibrillation. ACS Chem Neurosci 2010; 1: 279-87.

96. Brambilla D, Verpillot R, Taverna M, De Kimpe L, Le Droumaguet B, Nicolas J, et al. New method based on capillary electrophoresis with laser-induced fluorescence detection (ce-lif) to monitor interaction between nanoparticles and the amyloid-β peptide. Anal Chem 2010; 82: 10083-89.

97. Le Droumaguet B, Souguir H, Brambilla D, Verpillot R, Nicolas J, Taverna M, et al. Selegiline-functionalized, pegylated poly(alkyl cyanoacrylate) nanoparticles: Investigation of interaction with amyloid-b peptide and surface reorganization. Int. J. Pharm. 2011; in press.

98. Kim HR, Gil S, Andrieux K, Nicolas V, Appel M, Chacun H, et al. Low-density lipoprotein receptor-mediated endocytosis of pegylated nanoparticles in rat brain endothelial cells. Cell Mol Life Sci 2007; 64: 356-64.

99. Calvo P, Gouritin B, Chacun H, Desmaele D, D'Angelo J, Noel JP, et al. Long-circulating pegylated polycyanoacrylate nanoparticles as new drug carrier for brain delivery. Pharm Res 2001; 18: 1157-66.

100. Gobbi M, Re F, Canovi M, Beeg M, Gregori M, Sesana S, et al. Lipid-based nanoparticles with high binding affinity for amyloid-beta1-42 peptide. Biomaterials 2010; 31: 6519-29.

101. Murtas C, Canovi M, Zona C, Aurilia D, Niarakis A, LaFerla B, et al. Curcumin-decorated nanoliposomes with very high affinity for amyloid-b1-42. Biomaterials 2010;

102. Bastus N, Kogan M, Amigo R, Grillo-Bosch D, Araya E, Turiel A, et al. Gold nanoparticles for selective and remote heating of [beta]-amyloid protein aggregates. Mater Sci Eng C 2007; 27: 1236-40.

103. Kogan MJ, Bastus NG, Amigo R, Grillo-Bosch D, Araya E, Turiel A, et al. Nanoparticle-mediated local and remote manipulation of protein aggregation. Nano Lett 2006; 6: 110-5.

104. Pai AS, Rubinstein I,Onyuksel H. Pegylated phospholipid nanomicelles interact with beta-amyloid(1-42) and mitigate its beta-sheet formation, aggregation and neurotoxicity in vitro. Peptides 2006; 27: 2858-66.

105. Kabanov AV,Vinogradov SV. Nanogels as pharmaceutical carriers: Finite networks of infinite capabilities. Angew Chem Int Ed Engl 2009; 48: 5418-29.

106. Ikeda K, Sawada S, Akiyoshi K,Matsuzaki K. Inhibition of amyloid beta peptide fibril formation by hydrogel nanoparticles. Pept Sci 2006; 2005: 313-16.

107. Boridy S, Takahashi H, Akiyoshi K,Maysinger D. The binding of pullulan modified cholesteryl nanogels to abeta oligomers and their suppression of cytotoxicity. Biomaterials 2009; 30: 5583-91.

108. Stiriba SE, Frey H,Haag R. Dendritic polymers in biomedical applications: From potential to clinical use in diagnostics and therapy. Angew Chem Int Ed Engl 2002; 41: 1329-34.

109. Lowe TL, Strzelec A, Kiessling LL,Murphy RM. Structure-function relationships for inhibitors of beta-amyloid toxicity containing the recognition sequence klvff. Biochemistry 2001; 40: 7882-9.

110. Hilbich C, Kisters-Woike B, Reed J, Masters CL,Beyreuther K. Substitutions of hydrophobic amino acids reduce the amyloidogenicity of alzheimer's disease beta a4 peptides. J Mol Biol 1992; 228: 460-73.

111. Tjernberg LO, Lilliehook C, Callaway DJ, Naslund J, Hahne S, Thyberg J, et al. Controlling amyloid beta-peptide fibril formation with protease-stable ligands. J Biol Chem 1997; 272: 12601-5.

112. Tjernberg LO, Naslund J, Lindqvist F, Johansson J, Karlstrom AR, Thyberg J, et al. Arrest of beta-amyloid fibril formation by a pentapeptide ligand. J Biol Chem 1996; 271: 8545-8.

113. Zhang G, Leibowitz MJ, Sinko PJ,Stein S. Multiple-peptide conjugates for binding beta-amyloid plaques of alzheimer's disease. Bioconjug Chem 2003; 14: 86-92.

114. Chafekar SM, Malda H, Merkx M, Meijer EW, Viertl D, Lashuel HA, et al. Branched klvff tetramers strongly potentiate inhibition of beta-amyloid aggregation. Chembiochem 2007; 8: 1857-64.

115. Choo-Smith LP, Garzon-Rodriguez W, Glabe CG,Surewicz WK. Acceleration of amyloid fibril formation by specific binding of abeta-(1-40) peptide to ganglioside-containing membrane vesicles. J Biol Chem 1997; 272: 22987-90.

116. Choo-Smith LP,Surewicz WK. The interaction between alzheimer amyloid beta(1-40) peptide and ganglioside gm1-containing membranes. FEBS Lett 1997; 402: 95-8.

117. Ariga T, Kobayashi K, Hasegawa A, Kiso M, Ishida H,Miyatake T. Characterization of high-affinity binding between gangliosides and amyloid beta-protein. Arch Biochem Biophys 2001; 388: 225-30.

118. Ariga T,Yu RK. Gm1 inhibits amyloid beta-protein-induced cytokine release. Neurochem Res 1999; 24: 219-26.

119. Avdulov NA, Chochina SV, Igbavboa U, Warden CS, Vassiliev AV,Wood WG. Lipid binding to amyloid beta-peptide aggregates: Preferential binding of cholesterol as compared with phosphatidylcholine and fatty acids. J Neurochem 1997; 69: 1746-52.

120. Kakio A, Nishimoto SI, Yanagisawa K, Kozutsumi Y,Matsuzaki K. Cholesterol-dependent formation of gm1 ganglioside-bound amyloid beta-protein, an endogenous seed for alzheimer amyloid. J Biol Chem 2001; 276: 24985-90.

121. Kakio A, Yano Y, Takai D, Kuroda Y, Matsumoto O, Kozutsumi Y, et al. Interaction between amyloid beta-protein aggregates and membranes. J Pept Sci 2004; 10: 612-21.

122. Patel DA, Henry JE,Good TA. Attenuation of beta-amyloid induced toxicity by sialic acid-conjugated dendrimeric polymers. Biochim Biophys Acta 2006; 1760: 1802-9.

123. Patel DA, Henry JE,Good TA. Attenuation of beta-amyloid-induced toxicity by sialic-acid-conjugated dendrimers: Role of sialic acid attachment. Brain Res 2007; 1161: 95-105.

124. McLaurin J, Franklin T, Zhang X, Deng J,Fraser PE. Interactions of alzheimer amyloid-beta peptides with glycosaminoglycans effects on fibril nucleation and growth. Eur J Biochem 1999; 266: 1101-10.

125. Klajnert B, Cortijo-Arellano M, Bryszewska M,Cladera J. Influence of heparin and dendrimers on the aggregation of two amyloid peptides related to alzheimer's and prion diseases. Biochem Biophys Res Commun 2006; 339: 577-82.

126. Klajnert B, Cladera J,Bryszewska M. Molecular interactions of dendrimers with amyloid peptides: Ph dependence. Biomacromolecules 2006; 7: 2186-91.

127. Du D, Chen S, Cai J,Song D. Comparison of drug sensitivity using acetylcholinesterase biosensor based on nanoparticles-chitosan sol-gel composite. J Electroanal Chem 2007; 611: 60-66.

128. Heli H, Hajjizadeh M, Jabbari A,Moosavi-Movahedi A. Copper nanoparticles-modified carbon paste transducer as a biosensor for determination of acetylcholine. Biosens Bioelectron 2009; 24: 2328-33.

129. Moghimi SM, Hunter AC,Murray JC. Nanomedicine: Current status and future prospects. FASEB J 2005; 19: 311-30.

130. Dobrovolskaia MA,McNeil SE. Immunological properties of engineered nanomaterials. Nat Nanotechnol 2007; 2: 469-78.

131. Moghimi SM, Hunter AC,Murray JC. Long-circulating and target-specific nanoparticles: Theory to practice. Pharmacol Rev 2001; 53: 283-318.

132. Batrakova EV, Li S, Alakhov VY, Miller DW,Kabanov AV. Optimal structure requirements for pluronic block copolymers in modifying p-glycoprotein drug efflux transporter activity in bovine brain microvessel endothelial cells. J Pharmacol Exp Ther 2003; 304: 845-54.

133. Hunter AC,Moghimi SM. Synthetic polymers in 21st century therapeutics: The way forward. Drug Discov Today 2003; 8: 154-6.

134. King M, Su W, Chang A, Zuckerman A,Pasternak GW. Transport of opioids from the brain to the periphery by p-glycoprotein: Peripheral actions of central drugs. Nat Neurosci 2001; 4: 268-74.

135. Moghimi SM, Symonds P, Murray JC, Hunter AC, Debska G,Szewczyk A. A two-stage poly(ethylenimine)-mediated cytotoxicity: Implications for gene transfer/therapy. Mol Ther 2005; 11: 990-5.

136. Symonds P, Murray JC, Hunter AC, Debska G, Szewczyk A,Moghimi SM. Low and high molecular weight poly(l-lysine)s/poly(l-lysine)-DNA complexes initiate mitochondrial-mediated apoptosis differently. FEBS Lett 2005; 579: 6191-8.

137. Parhamifar L, Larsen AK, Hunter AC, Andresen TL,Moghimi SM. Polycation cytotoxicity: A delicate matter for nucleic acid therapy-focus on polyethylenimine. Soft Matter 2010; 6: 4001-09.

138. Akhtar S,Benter IF. Nonviral delivery of synthetic sirnas in vivo. J Clin Invest 2007; 117: 3623-32.

139. Kabanov AV, Batrakova EV,Alakhov VY. An essential relationship between atp depletion and chemosensitizing activity of pluronic block copolymers. J Control Release 2003; 91: 75-83.

140. Bhabra G, Sood A, Fisher B, Cartwright L, Saunders M, Evans WH, et al. Nanoparticles can cause DNA damage across a cellular barrier. Nat Nanotechnol 2009; 4: 876-83.

141. Moghimi SM, Andersen AJ, Hashemi SH, Lettiero B, Ahmadvand D, Hunter AC, et al. Complement activation cascade triggered by peg-pl engineered nanomedicines and carbon nanotubes: The challenges ahead. J Control Release 2010; 146: 175-81.

142. Hamad I, Al-Hanbali O, Hunter AC, Rutt KJ, Andresen TL,Moghimi SM. Distinct polymer architecture mediates switching of complement activation pathways at the nanosphere-serum interface: Implications for stealth nanoparticle engineering. ACS Nano 2010; 4: 6629-38.

143. Moghimi SM, Hamad I, Andresen TL, Jorgensen K,Szebeni J. Methylation of the phosphate oxygen moiety of phospholipid-methoxy(polyethylene glycol) conjugate prevents pegylated liposome-mediated complement activation and anaphylatoxin production. FASEB J 2006; 20: 2591-3.

144. Hamad I, Hunter AC, Szebeni J,Moghimi SM. Poly(ethylene glycol)s generate complement activation products in human serum through increased alternative pathway turnover and a masp-2-dependent process. Mol Immunol 2008; 46: 225-32.

145. Hamad I, Hunter CA, Rutt KJ, Liu Z, Dai H,Moghimi SM. Complement activation by pegylated single-walled carbon nanotubes is independent of c1q and alternative pathway turnover. Mol Immunol 2008; 45: 3797-803.

146. Itagaki S, Akiyama H, Saito H,McGeer PL. Ultrastructural localization of complement membrane attack complex (mac)-like immunoreactivity in brains of patients with alzheimer's disease. Brain Res 1994; 645: 78-84.

147. Rozemuller JM, Bots GT, Roos RA,Eikelenboom P. Acute phase proteins but not activated microglial cells are present in parenchymal beta/a4 deposits in the brains of patients with hereditary cerebral hemorrhage with amyloidosis-dutch type. Neurosci Lett 1992; 140: 137-40.

148. Yasojima K, Schwab C, McGeer EG,McGeer PL. Up-regulated production and activation of the complement system in alzheimer's disease brain. Am J Pathol 1999; 154: 927-36.

149. Webster S, Bonnell B,Rogers J. Charge-based binding of complement component c1q to the alzheimer amyloid beta-peptide. Am J Pathol 1997; 150: 1531-6.

150. McGeer PL,McGeer EG. The possible role of complement activation in alzheimer disease. Trends Mol Med 2002; 8: 519-23.

Partie 2: Travail expérimental

Part 2: Experimental work

Chapitre 1: Nanoparticules polymériques et barrière hématoencéphalique

Chapter 1: Polymeric nanoparticles and blood-brain barrier

Ce premier chapitre décrit le développement de nanoparticules fluorescentes et leur internalisation dans des cellules endothéliales de capillaires cérébraux humains capables de s'organiser en formant un modèle in vitro de BHE (hCMEC/D3). Il est composé de 3 sections sous la forme d'articles:

Le premier article est dédié à la conception de polymères fluorescents de poly(cyanoacrylate d'alkyle) capables de s'auto-assembler sous la forme de nanoparticules. Ces dernières ont été finement caractérisées et utilisées dans le cadre d'une étude préliminaire d'internalisation au sein des cellules hCMEC/D3.

La deuxième section concerne l'encapsulation de Quantum Dots dans les nanoparticules mentionnées précédemment et leur visualisation *in vitro* et *in vivo*.

La dernière section décrit quant à elle une étude plus approfondie du devenir des nanoparticules dans les cellules endothéliales. Leur internalisation, leur distribution et leur transcytose à travers le modèle *in vitro* de BHE ont été étudiées en détails et les résultats obtenus à ce jour sont présentés sous la forme d'un article en préparation.

This chapter describes the development of fluorescent nanoparticles and their interplay with human brain capillary endothelial cells able to form an *in vitro* BBB model (hCMEC/D3). It is composed of 3 sections in the form of articles:

The first one is dedicated to the design of fluorescently-tagged PEGylated poly(alkyl cyanoacrylate) polymers able to self-assemble into nanoparticles. The nanoparticles have been finely characterized and employed into a preliminary internalization study within hCMEC/D3 cells.

The second section concerns the encapsulation of Quantum Dots into the above mentioned nanoparticles and their visualization *in vitro* and *in vivo*.

The last section reports a deeper investigation of the nanoparticle fate within the endothelial cells. Their cellular uptake, distribution and the transcytosis across the in vitro BBB model have been investigated in details and the results obtained so far are presented in form of an article in preparation.

Section 1

Implications dans le projet NAD

Un des objectifs du projet NAD repose sur le développement de nanoparticules capables de traverser efficacement la Barrière Hémato-Encéphalique (BHE). Le rôle de notre équipe a été de concevoir des nanoparticules rendues fluorescentes pour permettre leurs suivies lors d'études biologiques. Pour ce faire, nos premiers objectifs ont été de coupler un fluorophore (Rhodamine B ou Dansyl) de manière covalente sur un polymère de poly(MePEGCA-*co*-PHDCA) capable de s'autoassembler en nanoparticules, de caractériser ce polymère et les particules obtenues, ainsi que de confirmer la possibilité d'utiliser ces nanoparticules pour l'étude de leurs interactions avec des cellules cérébrales endothéliales cultivées *in vitro*.

Implications in the NAD project

One of the aims of the NAD project is the development of nanoparticles able to cross the Blood-Brain Barrier in an appreciable amount. The task of our team was the design of fluorescent polymeric nanoparticles in order to follow their fate during biological studies. Thus, our first aims were the covalent attachment of a fluorophore (Rhodamine B or Dansyl) to the poly(MePEGCA-*co*-PHDCA) polymer able to self-assemble into nanoparticles, to characterize the polymer and the corresponding particles, and to confirm their possible employment for *in vitro* brain endothelial cell interaction studies.

Design of fluorescently tagged poly(alkyl cyanoacrylate) nanoparticles for human brain endothelial cells imaging

Chemical Communications, **2010**, *46*, 2602.

Davide Brambilla,[1] Julien Nicolas,[1] Benjamin Le Droumaguet,[1] Karine Andrieux,[1] Véronique Marsaud,[1] Pierre-Olivier Couraud,[2,3] and Patrick Couvreur[1]

[1] Laboratoire de Physico-Chimie, Pharmacotechnie et Biopharmacie, Université Paris-Sud, UMR CNRS 8612, Faculté de Pharmacie, 5 rue Jean-Baptiste Clément, F-92296 Châtenay-Malabry cedex, France

[2] Institut Cochin, Université Paris Descartes, UMR CNRS 8104, 75014 Paris, France.

[3] Inserm, U567, Paris, France.

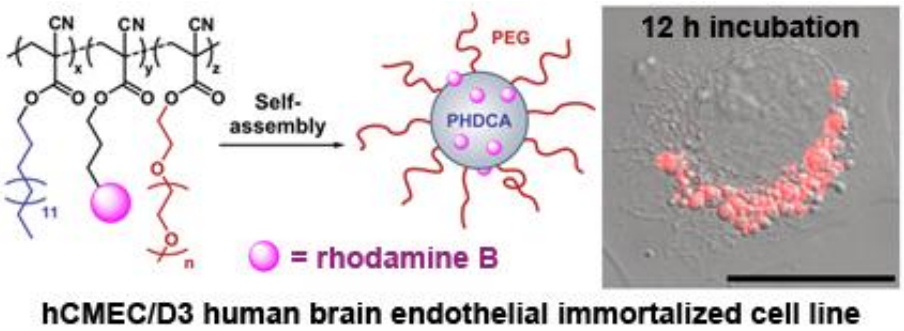

Résumé

Un copolymère amphiphile de poly(cyanoacrylate d'alkyle) a été synthétisé, caractérisé et utilisé pour préparer des nanoparticules fluorescentes pour l'imagerie de cellules endothéliales du cerveau humain. Ce marquage des nanoparticules permet d'observer finament leur internalisation et leur évolution intracellulaire.

Abstract

Rhodamine B-tagged poly(alkyl cyanoacrylate) amphiphilic copolymers have been synthesised, characterised and successfully used to prepare fluorescent nanoparticles for human brain endothelial cells imaging, allowing their uptake and intracellular trafficking to be finely observed.

1. Communication

The medical application of nanotechnologies, often termed nanomedicine, has witnessed a crucial impulse with the development of various types of drug-carrier nanodevices.[1] Among suitable nanocarriers for drug delivery purposes, nanoparticles based on biodegradable poly(alkyl cyanoacrylate) (PACA) (co)polymers have appeared as an established technology for colloidal nanomedicine.[2] Since their introduction in the field of pharmacology, PACA drug carriers have indeed demonstrated significant results in multiple pathologies, well-reviewed in the recent literature.[3]

However, one of the major drawbacks of PACA compared to other biopolymers is the very high reactivity of cyanoacrylate monomers that hampers easy access to well-defined, complex macromolecular architectures and/or functionalised materials.[2] Herein, we report a simple strategy for the synthesis of fluorescently tagged PEGylated nanoparticles and their application to *in vitro* imaging. A convenient strategy to prepare fluorescent nanoparticles is usually to encapsulate a lipophilic dye during the self-assembly process of the corresponding amphiphilic copolymer. However, potential problems may appear by using this approach: (i) as recently highlighted,[4] the fluorescent dye may leak out from the nanoparticles leading to wrong/inaccurate interpretations of confocal fluorescence images regarding the localization of the nanoparticles, due to cell membrane affinity of lipophilic dyes; (ii) the so-called burst effect, corresponding to the surface adsorbed fraction of the dye which is quickly released from the nanoparticles, may lead to an overestimation of the fluorescence intensity in a particular area whereas the nanoparticles are not yet biodegraded (iii) if a drug has to be encapsulated inside nanoparticles, the co-encapsulation of the fluorescent dye may alter the encapsulation yield of the drug. As a consequence, a fluorescent tag covalently attached to the nanoparticles is highly

preferable and would fill in a crucial GAP in the field of PACA-based nanoparticles for drug delivery and cell imaging.

In this view, our strategy was to incorporate the fluorophore during the synthesis of an amphiphilic PACA copolymer, by tandem Knoevenagel condensation-Michael addition reaction with hexadecyl cyanoacetate (HDCA), methoxypoly(ethylene glycol) cyanoacetate (MePEGCA) and a small amount of a cyanoacetate derivative based on the desired fluorescent dye (Scheme 1).

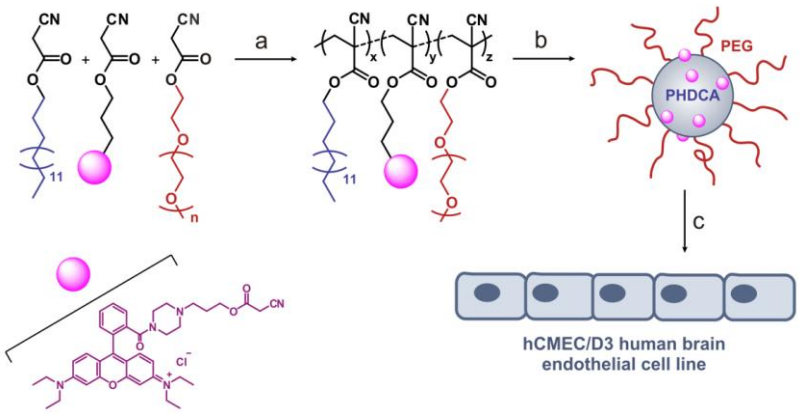

Scheme 1. *Design of fluorescent P(HDCA-co-RCA-co-MePEGCA) copolymers (Ci) and nanoparticles (Ni) for cell imaging (i = 1–3). Reagents and conditions: a) [HDCA]0/[MePEGCA]0 = 4:1, [RCA]0 = 4.1, 0.85 or 0.16 mol.%, formaldehyde, pyrrolidine, EtOH/CH2Cl2, 25 °C, 24 h; b) acetone/H2O; c) incubation with hCMEC/D3 cells.*

Among the possible fluorescent dyes available for fluorescence detection, a rhodamine B derivative was selected. Rhodamine-based fluorescent tags are indeed widely used in the field of biomedical research as they offer a combination of advantageous properties such as a rather high water-solubility, a good photostability, a high extinction coefficient and a high quantum yield. Besides, emission wavelengths of rhodamine-derived fluorescent dyes are higher than those commonly associated with autofluorescence of cells.[5] A rhodamine B tertiary amide bearing a hydroxyl group[6] was readily transformed into the corresponding cyanoacetate derivative by a DCC-assisted coupling reaction. This synthetic route was chosen because rhodamine tertiary amides avoid intramolecular cyclization (which would result in a loss of fluorescence) and fluorescence emission is retained over a broad pH range.[6] The synthesis of rhodamine B cyanoacetate (RCA) was confirmed by 1H and 13C NMR spectroscopy as well as by ESI-MS mass spectrometry. Synthesis of several fluorescent rhodamine B-containing P(HDCA-co-RCA-co-MePEGCA) copolymers was then undertaken with different RCA initial amounts. Three of these copolymers are discussed here: copolymers C1, C2 and C3, corresponding respectively to 4.10, 0.85 and 0.16 mol.% of RCA in the initial cyanoacetate feed. The fluorescent copolymers were analysed by ^{1}H NMR spectroscopy and

showed an excellent correlation with the expected structure (Figure S1). Size exclusion chromatography showed low number-average molar masses, Mn, with high polydispersity indexes (Table S1) due to the significant amount of low-molar mass amphiphilic oligomers, commonly observed for this kind of reaction.[7,8] No influence of the initial amount of RCA over the copolymerisation process was observed.

Well-defined nanoparticles were formed by self-assembly in aqueous medium and characterised by DLS and ζ-potential measurements as the function of the RCA initial amount and time (Table S1 and Figure S2). In all cases, stable nanoparticles were obtained with average diameters in the 115–125 nm range together with narrow particle size distributions. ζ-potential measurements showed negative values from -30.9 to -40.6 mV. Besides, nanoparticle diameters and surface charge remained constant over time in aqueous solution at 37 °C, thus confirming their excellent stability at a temperature relevant for biomedical assays. Therefore, all these caracteristics make them suitable candidates for drug delivery purposes and cell imaging. The presence of different amounts of RCA in the copolymers and associated nanoparticles could be readily perceived under visible light and U.V. excitation at 365 nm (Figure 1). Fluorescent properties of the materials were then thoroughly studied by fluorescence spectroscopy (Figure 1 and S3-S7). Emission and excitation wavelengths of copolymers and nanoparticles were determined. For instance for copolymer C2, λex. = 563 nm and λem. = 583 nm, with a Stokes shift of 20 nm, in good agreement with the spectral properties of rhodamine B-tertiary amide derivatives.[6] No significant change was observed upon self-assembly as λex. = 568 nm and λem. = 583 nm were recorded for nanoparticles N2. Besides, for a given copolymer (or nanoparticle) concentration, the fluorescence intensity decreased when decreasing the initial amount of RCA in the starting cyanoacetate mixture (Figure 1).

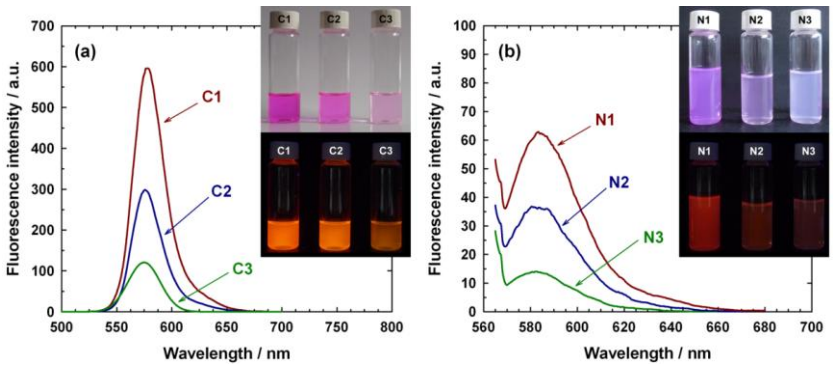

Figure 1. *Fluorescence emission spectra of P(HDCA-co-RCA-co-MePEGCA) copolymer solutions in CHCl3 at 0.1 mg.mL-1 (a) and of resulting nanoparticle suspensions in water at 0.1 mg.mL-1 (b). Insert: pictures of copolymer solutions (left) and nanoparticles suspensions (right) under visible light or under U.V. excitation at 365 nm.*

Eventually, the evolution of the fluorescence intensity of copolymer solutions and resulting nanoparticle suspensions was recorded as a function of the concentration, allowing linear and curved parts to be determined (Figure S7), which is useful for fluorescence intensity-based calculations. Whatever the nature of the copolymer and associated nanoparticles, linear evolutions of fluorescence intensity vs. concentration were observed up to rather high concentrations.

Rhodamine B-tagged PACA nanoparticles were then employed for *in vitro* imaging studies on hCMEC/D3 human brain endothelial cell line, which has been validated as a unique *in vitro* model of human blood-brain barrier (BBB).[9] Prior to imaging studies, cell viability assays were performed in order to determine the cytotoxicity of the P(HDCA-*co*-RCA-*co*-MePEGCA) nanoparticles on hCMEC/D3 cells. No statistical difference in cytotoxicity was observed between nanoparticles containing an increasing amount of rhodamine B (Figure S10). Similarly to non-fluorescent P(HDCA-*co*-MePEGCA) nanoparticles, no significant cytotoxicity was obtained until a concentration of 30 µg.mL-1.

Confocal laser scanning microscopy (CLSM) was then employed for *in vitro* imaging studies. Upon microscope observation, the fluorescent nanoparticles in water appeared as small, well-defined, fluorescent spots displaying typical Brownian motion (Figure S11). After a 12 h incubation period of hCMEC/D3 cells with fluorescent nanoparticles (N1), cells were washed with fresh cell culture medium in order to remove adsorbed nanoparticles and observed by CLSM. Nomarsky contrast images showed a typical fibroblast shape for the cells with no morphological alteration, thus supporting the absence of cytotoxicity as previously shown by cell viability assays (this observation was made on the basis of numerous images randomly taken from the cells monolayer). Fluorescence images superimposed on the Nomarski images showed intense and fine fluorescence spots accumulated within the cells and especially around the nuclei. (Figure 2a–c) This observation suggested that the mechanism by which nanoparticles entered the cells was governed by endocytosis since fluorescence was localised into vesicles. However, according to their proximity to the nuclei, those vesicles are highly supposed to be late endosomes (Figure 2d). These results confirmed previous observations with primary cultures of rat brain endothelial cells showing that P(HDCA-*co*-MePEGCA) nanoparticles were able to penetrate by endocytosis.[10]

As long as poly(alkyl cyanoacrylate) nanoparticles are known to be biodegradable by enzymatic degradation via hydrolysis of ester functions,[2] it was important to assess that the observed fluorescence intensity was coming from the fluorescent nanoparticles and not from free rhodamine B alcohol (released after hydrolysis). After 8 h incubation of fluorescent nanoparticles at different concentrations with Fischer rat plasma at 37 °C, only 11–14% of fluorescence loss was measured

(Figure S12), in very good agreement with the *in vitro* biodegradation profile of non-fluorescent P(HDCA-co-MePEGCA) nanoparticles.[11] This result also showed that the presence of rhodamine B cyanoacetate units in the macromolecular structure did not alter the degradation profile of the nanoparticles.

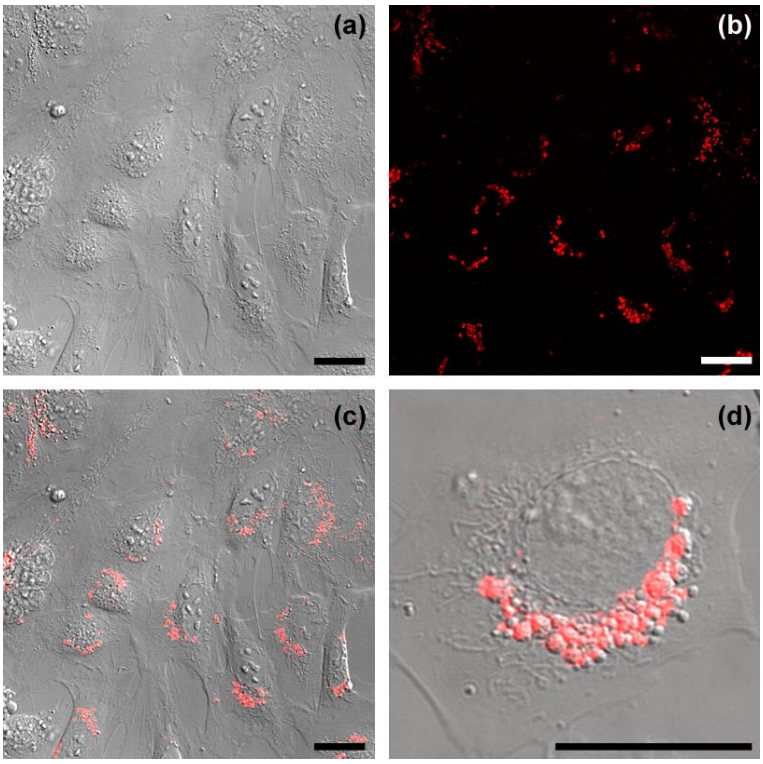

Figure 2. *hCMEC/D3 Human brain endothelial cells Nomarski image (a), confocal microscopy image (b) and fluorescence image superimposed on hCMEC/D3 human brain endothelial cell Nomarski image after incubation with fluorescent P(HDCA-co-RCA-co-MePEGCA) nanoparticles N1 for 12 h and subsequent washing of the medium (c). Enlarged picture (d). Scale bars = 20 μm.*

Under identical experimental conditions and acquisition settings (detector gain: 535, laser power: 57%), a lower amount of rhodamine dye covalently linked to the nanoparticles resulted in a decrease of fluorescence intensity. Indeed, only faint fluorescent areas were noticed for nanoparticles **N3** (Figure S13). Nevertheless, by increasing the detector gain up to 700 together with a laser power at 65%, intense fluorescence spots appeared around cell nuclei. Therefore, tuning the amount of fluorescent dye attached to the nanoparticles together with adjusting acquisition settings allowed great flexibility regarding *in vitro* imaging.

Concerning BBB crossing, important work remains to be done as long as several crucial mechanisms are still unknown such as those of intracellular trafficking and exocytosis. In order to determine whether these fluorescent nanoparticles are suitable for such investigations, real-time confocal fluorescence microscopy observations were performed. While focusing on a dividing cell, the fine fluorescence signal coming from the nanoparticles allowed their intracellular progression to be accurately followed. Indeed, we clearly observed that nanoparticles were trafficked from the polar extremity during metaphase/anaphase (Figure 3a) to the midbody area during telophase, where the fluorescence exhibited a filament-like clustered structure (Figure 3b). Thus, this new synthetic tool allows intracellular events to be finely monitored and could give new insights into intracellular mechanisms.

Finally, this approach is very versatile and can be applied to other fluorescent dyes after suitable modification to insert the cyanoacetate moiety. This was examplified by the synthesis of dansyl cyanoacetate (DCA, Scheme S2) and the preparation of the corresponding P(HDCA-*co*-DCA-*co*-MePEGCA) fluorescent nanoparticles **N4** (see Supporting Information).

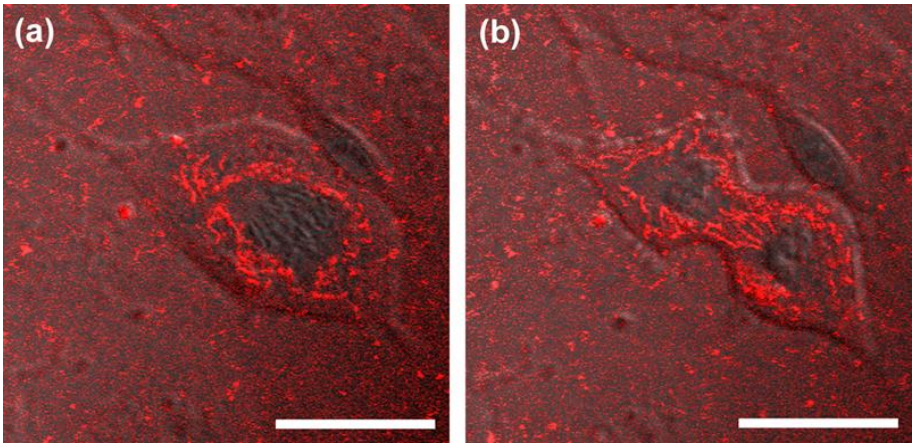

Figure 3. *Fluorescence images (red) superimposed with hCMEC/D3 human brain endothelial cells Nomarski images viewed from the top cell surface recorded at various time after incubation with fluorescent P(HDCA-co-RCA-co-MePEGCA) nanoparticles (**N1**): 8.5 min (a) and 18 min (b). Scale bars = 20 µm.*

In order to circumvent the drawbacks usually encountered with the use of encapsulated fluorescent dyes into nanoparticles, an original and versatile strategy has been developed to prepare fluorescent nanoparticles where a hydrophilic dye based on rhodamine B has been covalently linked to P(HDCA-*co*-MePEGCA) amphiphilic copolymers. The resulting fluorescently tagged nanoparticles were found suitable for *in vitro* imaging on human brain endothelial cells and their fluorescence signal was found

extremely accurate, as opposed to a diffuse signal when a lipophilic dye is encapsulated. This allowed their uptake and intracellular trafficking to be finely observed. These results also open the door to further studies related to endocytosis during mitosis which represents an important aspect of cellular biology.

2. Acknowledgments

The authors thank Valérie Nicolas (Plateforme Imagerie Cellulaire, IFR 141) for her kind help with the CLSM. The research leading to these results has received funding from the European Community's Seventh Framework Programme (FP7/2007-2013) under grant agreement n° 212043. The CNRS is also warmly acknowledged for financial support.

3. References

1. Farokhzad OC and Langer R, Impact of Nanotechnology on Drug Delivery. ACS Nano, 2009, 3, 16-20.
2. Nicolas J and Couvreur P, Synthesis of poly(alkyl cyanoacrylate)-based colloidal nanomedicines. Wiley Interdiscip. Rev.: Nanomed. Nanobiotechnol., 2009, 1, 111-27.
3. Vauthier C, Dubernet C, Fattal E, Pinto-Alphandary H and Couvreur P, Poly(alkylcyanoacrylates) as biodegradable materials for biomedical applications. Adv. Drug Delivery Rev., 2003, 55, 519-48.
4. Xu P, Gullotti E, Tong L, Highley CB, Errabelli DR, Hasan T, et al. Intracellular drug delivery by poly(lactic-co-glycolic acid) nanoparticles, revisited. Mol. Pharmaceutics, 2009, 6, 190-201.
5. Benson RC, Meyer RA, Zaruba ME and McKhann GM. Cellular autofluorescence--is it due to flavins? J. Histochem. Cytochem., 1979, 27, 44-8.
6. Nguyen T and Francis MB, Practical synthetic route to functionalized rhodamine dyes. Org. Lett., 2003, 5, 3245-8.
7. Peracchia MT, Desmaële D, Couvreur P and d'Angelo J. Synthesis of a Novel Poly(MePEG cyanoacrylate-co-alkyl cyanoacrylate) Amphiphilic Copolymer for Nanoparticle Technology Macromolecules, 1997, 30, 846-51.
8. Nicolas J, Bensaid F, Desmaele D, Grogna M, Detrembleur D, Andrieux K and Couvreur P, Synthesis of Highly Functionalized Poly(alkyl cyanoacrylate) Nanoparticles by Means of Click Chemistry. Macromolecules, 2008, 41, 8418-28.
9. Cucullo L, Couraud PO, Weksler B, Romero IA, Hossain M, Rapp E, Immortalized human brain endothelial cells and flow-based vascular modeling: a marriage of convenience for rational neurovascular studies et al. J. Cereb. Blood. Flow Metab., 2008, 28, 312-28.
10. Kim HR, Gil S, Andrieux K, Nicolas V, Appel M, Chacun H, et al. Low-density lipoprotein receptor-mediated endocytosis of PEGylated nanoparticles in rat brain endothelial cells. Cell. Mol. Life Sci., 2007, 64, 356-64.
11. Brigger I, Morizet J, Aubert G, Chacun H, Terrier-Lacombe MJ, Couvreur P et al. Poly(ethylene glycol)-coated hexadecylcyanoacrylate nanospheres display a combined effect for brain tumor targeting. J. Pharmacol. Exp. Ther., 2002, 303, 928-36.

Supporting Information

Materials

Poly(ethylene glycol) monomethyl ether (MePEG, $M_{n,\ NMR}$ = 1910 g.mol^{-1}, $DP_{n,\ NMR}$ = 43, Fluka), cyanoacetic acid (99 %, Fluka), *N*,*N'*-dicyclohexylcarbodiimide (DCC, >99 %, Fluka), 4-dimethylaminopyridine (DMAP, 99 %, Aldrich), formaldehyde (37 % in water, Aldrich), pyrrolidine (99 %, Aldrich), anhydrous magnesium sulfate ($MgSO_4$, >99 %, Aldrich), triethyl amine (TEA, Aldrich) and dimethylsulfoxide (DMSO, 99.9 %, Bio Basic Inc.) were used as received. Rhodamine B alcohol[151] and dansyl alcohol[152] were synthesized as described elsewhere. 2-Propanol (99.5 %) and Pluronic F-68 (cell culture tested) was purchased from Fluka. All other solvents (tetrahydrofuran, (THF), methanol (MeOH), dichloromethane (DCM), diethyl ether (Et_2O), chloroform ($CHCl_3$), ethanol (EtOH), ethyl acetate (EtOAc) and hexane) were purchased at the highest grade from Carlo Erba. hCMEC/D3 human brain endothelial cell line was prepared as described elsewhere.[153-155] Dulbecco's phosphate buffer saline (DPBS) without $CaCl_2$ and $MgCl_2$ and EMB-2 medium were purchased from Lonza. Penicillin 10000 units-Streptomycin 10000 μg.mL^{-1} and Trypsin/EDTA were obtained from Invitrogen, Gibco. Hydrocortisone, human basic fibroblast growth factor (bFGF) cell culture tested and 3-(4,5-dimethylthiazol-2-yl)-2,5-diphenyltetrazolium bromide (MTT, 98 %) were purchased from Sigma. HEPES 1 M was purchased from PAA – The Cell Culture Company. Fetal bovine serum was purchased from Eurobio. Rat tail collagen type I was purchased from Becton-Dickinson. Fisher rat plasma was purchased from Charles River Laboratories.

Synthesis of hexadecyl cyanoacetate (HDCA)

HDCA was synthesized as follows. In a 250 mL round bottom flask containing hexadecane-1-ol (10.65 g, 44 × 10^{-3} mol), cyanoacetic acid (7.48 g, 88 × 10^{-3} mol), EtOAc (5 mL) and DCM (50 mL) were introduced dropwise by a syringe over ca. 20 min, a solution of DCC (9.98 g, 48.4 × 10^{-3} mol) and DMAP (120 mg, 0.82 × 10^{-3} mol) in DCM (50 mL). The reaction medium was stirred during 24 h at ambient temperature under argon atmosphere. The solid was filtered off and the solvents were removed under reduced pressure. The solid was then purified by flash chromatography (SiO_2, hexane/EtOAc; 5:1; v:v) to give a fine, white powder: 12.9 g (95 %). ^{1}H NMR δ = 0.88 (t, *J* = 7.0 Hz, 3H, CH_2CH_3), 1.14–1.50 (m, 26H, CH_2), 1.67 (m, *J* = 13.6, 6.8 Hz, 2H, $COOCH_2CH_2$), 3.45 (s, 2H, $CNCH_2$), 4.20 (t, *J* = 6.8 Hz, 2H, $COOCH_2CH_2$). IR (neat): υ (cm^{-1}) = 2261 (C≡N), 1728 (C=O).

Synthesis of methoxypoly(ethylene glycol) cyanoacetate (MePEGCA)

MePEGCA was synthesized as follows. In a 100 mL round bottom flask containing poly(ethylene glycol) monomethyl ether (11.0 g, DP_n = 45, 5.5×10^{-3} mol), cyanoacetic acid (0.955 g, 11.0×10^{-3} mol) and DCM (30 mL) were introduced dropwise by a syringe over ca. 20 min, a solution of DCC (2.27 g, 11.0×10^{-3} mol) and DMAP (60 mg, 0.41×10^{-3} mol) in DCM (10 mL). The reaction medium was stirred during 24 h at room temperature under argon atmosphere. The solid was filtered off and the solvent was removed under reduced pressure. The solid was then purified by recrystallization from isopropanol, filtered and dried under vacuum overnight to give a fine, white powder: 10.7 g (94 %). ^{1}H NMR δ = 3.34 (s, 3H, OCH_3), 3.53 (s, 2H, CNCH_2), 3.25–3.92 (m, 172H, OCH_2CH_2O), 4.32 (t, 2H, J = 4.5 Hz, COOCH_2CH$_2$). IR (neat): υ (cm^{-1}) = 1745 (C=O), 2251 (C≡N). $M_{n,\,SEC}$ = 1890 g.mol^{-1}, M_w/M_n = 1.04.

Synthesis of rhodamine B cyanoacetate (RCA)

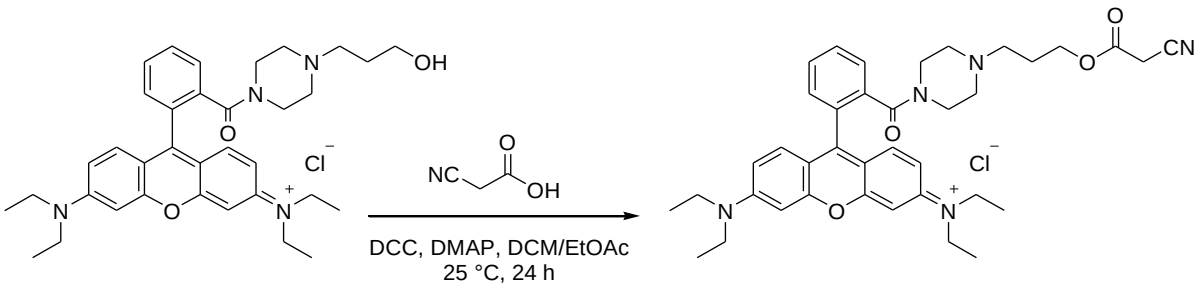

Scheme S1. *Synthesis of rhodamine B cyanoacetate (RCA).*

The rhodamine B cyanoacetate monomer was synthesized as follows. In a round bottom flask, rhodamine B alcohol[151] (450 mg, 0.74×10^{-3} mol) and cyanoacetic acid (127 mg, 1.49×10^{-3} mol) were dissolved in a mixture of DCM (10 mL) and EtOAc (1 mL). The resulting solution was bubbled for 30 min with N_2 while cooling down to 0 °C in an ice/water bath. To this solution was added dropwise over 20 min at 0 °C under N_2 a solution of DCC (169 mg, 0.82×10^{-3} mol) and DMAP (cat. amount) in DCM (10 mL). The reaction mixture was allowed to warm to room temperature and then stirred for 24 h. The resulting solution was filtered off to remove insoluble dicyclohexylurea and the precipitate was rinsed with dichloromethane until only a faint purple coloration was observed. The mother liquors were concentrated, redissolved in a minimum amount of DCM and precipitated in a large volume of cold diethyl ether. The precipitate was filtered and dried under high vacuum to give the pure product as purple crystals: 330 mg (70 % yield). ^{1}H NMR δ = 1.31 (t, 12H, J = 7.0 Hz, CH_3CH$_2$N), 2.17 (t, 2H, J = 6.2 Hz, CH$_2$CH_2CH$_2$), 3.20 (t, 2H, NCH_2(CH$_2$)$_2$O), 3.27 (bs, 4H,

$NCH_2CH_2NCH_2$), 3.61 (q, 8H, *J* = 7.0 Hz, CH_3CH_2N), 3.70 (bs, 4H, $CH_2N(C=O)$), 3.72 (s, 2H, CH_2OCO), 4.25 (t, 2H, *J* = 6.0 Hz, CH_2CN), 6.72 (s, 2H, $H_{aromatic}$), 6.98 (d, 2H, *J* = 6.98 Hz, $H_{aromatic}$), 7.18 (d, 2H, *J* = 9.2 Hz, $H_{aromatic}$), 7.29 (d, 1H, *J* = 7.6 Hz, $H_{aromatic}$), 7.60–7.78 (m, 2H, $H_{aromatic}$). ^{13}C NMR δ = 10.28, 23.44, 25.08, 26.21, 46.09, 63.51, 96.15, 106.57, 113.62, 113.65, 114.28, 116.05, 128.35, 130.12, 130.45, 130.79, 131.76, 134.15, 155.59, 155.97, 157.64, 163.39, 166.58, 167.24. MS (+ESI) calculated for $C_{34}H_{46}N_5O_4^+$: 636.35; found: 636.5 ([M]$^{\bullet}$).

Synthesis of dansyl cyanoacetate (DCA)

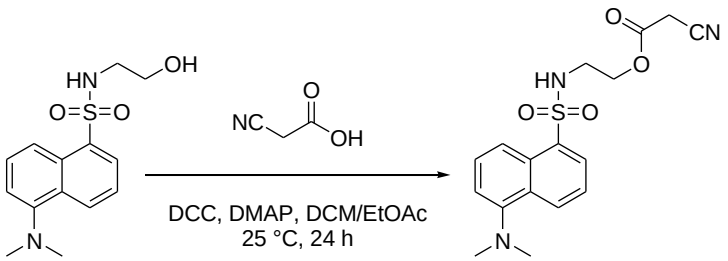

Scheme S2. *Synthesis of dansyl cyanoacetate (DCA).*

The dansyl cyanoacetate monomer was synthesized as follows. In a round bottom flask, dansyl alcohol[152] (450 mg, 1.54×10^{-3} mol) and cyanoacetic acid (261 mg, 3.07×10^{-3} mol) were dissolved in a mixture of DCM (20 mL) and EtOAc (5 mL). The resulting solution was bubbled for 30 min with N_2 while cooling down to 0 °C in an ice/water bath. To this solution was added dropwise over 20 min at 0 °C under N_2 a solution of DCC (348 mg, 1.69×10^{-3} mol) and DMAP (cat. amount) in DCM (20 mL). The reaction mixture was allowed to warm to room temperature and then stirred for 24 h. The resulting solution was filtered off to remove insoluble dicyclohexylurea and the precipitate was rinsed with dichloromethane. The mother liquors were concentrated, redissolved in EtOAc and washed three times with water. The organic phase was dried over $MgSO_4$, filtered off and concentrated under vacuum. The crude product was purified on silica gel column eluting with a mixture hexanes/AcOEt (1:1) to afford the pure product as a yellow crystalline powder (360 mg, 65 % yield). ^1H NMR (DMSO-d_6, 298 K) δ = 2.88 (s, 6H, *J* = 7.0 Hz, $(CH_3)_2N$), 3.13 (q, 2H, *J* = 5.5 Hz, $NHCH_2CH_2$), 3.81 (s, 2H, CH_2CN), 4.06 (t, 2H, *J* = 5.5 Hz, CH_2OCO), 7.31 (d, 1H, *J* = 7.5 Hz, $H_{aromatic}$), 7.67 (q, 2H, *J* = 7.3 Hz, $H_{aromatic}$), 8.17 (d, 1H, *J* = 7.3 Hz, $H_{aromatic}$), 8.23 (t, 1H, *J* = 5.6 Hz, NH), 8.32 (d, 1H, *J* = 8.7 Hz, $H_{aromatic}$), 8.52 (d, 1H, *J* = 8.5 Hz, $H_{aromatic}$). ^{13}C NMR (DMSO-d_6, 298 K) δ = 24.31, 40.87, 45.02, 64.22, 114.77, 115.16, 118.98, 114.28, 123.59, 127.87, 128.25, 128.93, 129.06, 129.54, 135.77, 151.38, 164.08. MS (+ESI) calculated for $C_{17}H_{19}N_3O_4S$: 361.11; found: 384.20 ([M+Na]$^+$).

Synthesis of poly[hexadecyl cyanoacrylate-*co*-rhodamine B cyanoacrylate-*co*-

methoxypoly(ethylene glycol) cyanoacrylate] (P(HDCA-*co*-RCA-*co*-MePEGCA)) fluorescent copolymer

A typical synthesis of P(HDCA-*co*-RCA-*co*-MePEGCA) fluorescent copolymer (expt. **1**, Table 1) was as follows. In a 50 mL round bottom flask containing MePEGCA (0.4 g, 1.9×10^{-4} mol), HDCA (0.26 g, 8.4×10^{-4} mol), RCA (29.72 mg, 4.4×10^{-5} mol, 4.10 mol.% in the initial cyanoacetate mixture), EtOH (5 mL) and DCM (10 mL) under magnetic stirring, was sequentially introduced dropwise by a syringe over ca. 20 min, formaldehyde (0.4 mL, 5.3×10^{-3} mol) and pyrrolidine (20 µL, 2.4×10^{-4} mol). The mixture was allowed to stir during 24 h at room temperature and was then concentrated under reduced pressure. The residue was taken into DCM and washed multiple times with water. The resulting organic layer was dried over $MgSO_4$, filtered and concentrated under reduced pressure and dried under vacuum to give a purple, waxy solid. The copolymer was analyzed by ^{1}H NMR and SEC. The same procedure was applied with different initial amounts of RCA (5.94 and 1.13 mg for expt **2** and **3**, respectively (see Table S1)).

Synthesis of poly[hexadecyl cyanoacrylate-*co*-dansyl cyanoacrylate-*co*-methoxypoly(ethylene glycol) cyanoacrylate] (P(HDCA-*co*-DCA-*co*-MePEGCA)) fluorescent copolymer

In a 50 mL round bottom flask containing MePEGCA (0.4 g, 1.9×10^{-4} mol), HDCA (0.26 g, 8.4×10^{-4} mol), DCA (15.97 mg, 4.4×10^{-5} mol, 4.08 mol.% in the initial cyanoacetate mixture), EtOH (4 mL) and DCM (8 mL) under magnetic stirring, was sequentially introduced dropwise by a syringe over ca. 20 min, formaldehyde (0.4 mL, 5.3×10^{-3} mol) and pyrrolidine (20 µL, 2.4×10^{-4} mol). The mixture was allowed to stir during 24 h at room temperature and was then concentrated under reduced pressure. The residue was taken into DCM and washed multiple times with water, once with 1M HCl and once with brine. The resulting organic layer was dried over $MgSO_4$, filtered, concentrated under reduced pressure and dried under vacuum to give a yellow, waxy solid. The copolymer **C4** was analyzed by ^{1}H NMR and SEC (see Table S2). ^{1}H NMR ($CDCl_3$, 298 K) δ = 0.87 (t, 16H, CH_2CH_3), 1.1–1.5 (bm, 120H, CH_2CH_3), 1.6–1.8 (bm, 10H, $COOCH_2CH_2CH_2$), 2.3–2.9 (bm, 10H, $C(CN)CH_2$), 3.37 (s, 3H, OCH_3), 3.4–3.9 (bm, 172H, CH_2CH_2O), 4.1–4.5 (bm, 10H, $COOCH_2CH_2$).

Preparation of nanoparticles

Nanoparticles were prepared by the nanoprecipitation technique.[156] In practice, the copolymer **C1** (10 mg) was dissolved in acetone (2 mL), and the copolymer solution was added dropwise to an aqueous solution 0.5 % (w/v) of Pluronic F68 (4 mL) under vigorous mechanical stirring. A milky suspension was observed almost instantaneously. Acetone was then evaporated under reduced pressure

and nanoparticles were purified by ultracentrifugation (150 000 *g*, 1 h, 4 °C, Beckman Coulter, Inc.). The supernatant was discarded and the pellet was resuspended in the appropriated volume of water to yield a stable nanoparticles suspension (**N1**) of 5 $mg.mL^{-1}$. The same procedure was applied for copolymers **C2, C3** and **C4** to yield nanoparticle suspensions **N2**, **N3** and **N4** respectively.

Cytotoxicity of nanoparticles

The cytotoxicity of rhodamine B-tagged nanoparticles was investigated by MTT viability test on hCMEC/D3 human brain endothelial cell line. Cells were cultured according to previous studies.[153-155] Briefly, cells were grown on Type I collagen-coated plates in EBM-2 basal medium supplemented with fetal bovine serum 5 %, hydrocortisone 1.4 µM, basic fibroblast growth factor 1 $ng.mL^{-1}$, pen-strep 1 % and HEPES 10 mM. Polystyrene 96 wells plates were used and cells were seeded in each well (15 000 cells per well) with the medium previously described. The day after, an aqueous suspension of nanoparticles was administrated at three different concentrations: 10, 20 and 30 $\mu g.mL^{-1}$. After 48 h incubation at 37 °C and 5 % CO_2, the MTT reagent (at a final concentration of 0.05 % in DPBS) was administered and 3 h later, the percentage of living cells was evaluated with 96 wells plate absorbance reader at 570 nm. Cells treated with the same volume of water were used as negative controls. All these results were compared with non-fluorescent P(HDCA-*co*-MePEGCA) nanoparticles.

Plasma stability of nanoparticles

The fluorescent nanoparticles (**N2**) at 0.5 $mg.mL^{-1}$ or 0.3 $mg.mL^{-1}$ were incubated *in vitro* in Fischer rat plasma at 37 °C following a previously described protocol.[157] At predetermined time intervals (5 min, 30 min, 4 h and 8 h), an aliquot of the plasma medium was withdrawn and ultrafiltrated (Nanosep Centrifugal Devices 100 kDa, Pall Corporation) at 10 000 *g* during 20 min upon which the soluble degradation products were collected in the bottom chamber. Subsequently, the fluorescence intensity of the upper chamber (containing the nanoparticles) was measured by fluorescent spectroscopy and the results were expressed as a percentage of the initial measured fluorescence in the plasma medium.

***In vitro* imaging with fluorescent nanoparticles**

In vitro imaging was performed on hCMEC/D3 human brain endothelial cell line incubated with rhodamine B-tagged nanoparticles. Cells were seeded on type-I collagen-coated glass disk (25 mm in diameter) at a concentration of 25 000 $cells.cm^{-2}$. After 2 days, an aqueous suspension of

nanoparticles (25 μg.mL^{-1}) was incubated with hCMEC/D3 cells. Following a 12 h incubation time, the cells monolayer was washed with fresh medium and then analyzed by confocal laser scanning microscopy.

Analytical techniques

^{1}H and ^{13}C NMR spectra were performed in deuterated chloroform ($CDCl_3$) or in dimethyl sulfoxide (DMSO) at ambient temperature on a Bruker Avance (300 MHz and 75 MHz, respectively). IR spectra were obtained on a Fourier Transform Bruker Vector 22 spectrometer. Size exclusion chromatography (SEC) was performed at 30 °C with two columns from Polymer Laboratories (PL-gel MIXED-D; 300 × 7.5 mm; bead diameter: 5 μm; linear part: 400 – 4 × 10^5 g.mol^{-1}) and a differential refractive index detector (Spectrasystem RI-150 from Thermo Electron Corp.). The eluent was chloroform ($CHCl_3$) at a flow rate of 1 mL.min^{-1} and toluene was used as a flow-rate marker. The calibration curve was based on poly(methyl methacrylate) (PMMA) standards (peak molar masses, M_p = 625 – 625 500 g.mol^{-1}) from Polymer Laboratories. This technique allowed M_n (the number-average molar mass), M_w (the weight-average molar mass) and M_w/M_n (the polydispersity index, PDI) to be determined. Nanoparticles diameter (D_z) was measured by dynamic light scattering (DLS) with a Nano ZS from Malvern (173° scattering angle) at a temperature of 25 °C. The particle size distribution is generally considered as narrow when below 0.10. The surface charge of nanoparticles was investigated by ζ-potential (mV) measurement at 25 °C after dilution with NaCl 1 mM and using the Smoluchowski equation. DLS and ζ-potential measurements were used to study nanoparticles stability as a function of time at 37 °C. Fluorescence spectroscopy (Perkin-Elmer LS50B) with 10 mm optical quartz cuvette (Hellma 101-QS Suprasil) was used to evaluate the fluorescence properties of RCA, DCA, P(HDCA-*co*-RCA-*co*-MePEGCA) and P(HDCA-*co*-DCA-*co*-MePEGCA) copolymers as well as associated nanoparticles. Maximum emission ($\lambda_{ex.}$) and maximum excitation ($\lambda_{em.}$) wavelengths were determined as well as the maximum intensity of fluorescence (in a.u.) at different concentrations. The same procedure was followed for nanoparticles (**N1**, **N2**, **N3** and **N4**) in aqueous solution. *In vitro* imaging experiments were performed with a confocal laser scanning microscope LSM 510 META (Zeiss, Germany) equipped with a 1 mW Helium Neon laser and a Plan-Apochromat 63X objective lens (Numerical Aperture / 1.4, oil immersion). Fluorescence was collected with long-pass 560 nm emission filter under 543 nm wavelength excitation. To specifically consider intracellular nanoparticles localization, acquisitions were made at the median plane of the cell monolayer. The pinhole size was set at 1.0 Airy unit (106 μm diameter) giving an optical section thickness of 0.8 μm. Prior to observations, it was checked that autofluorescence of hCMEC/D3 cells was negligible under

the acquisition settings and did not interfere with the fluorescence coming from the nanoparticles.

Characterization of fluorescently tagged copolymers and nanoparticles

Table S1. *Synthesis of Poly[hexadecyl cyanoacrylate-co-rhodamine B cyanoacrylate-co-methoxypoly(ethylene glycol) cyanoacrylate] (P(HDCA-co-RCA-co-MePEGCA) Copolymers (C) and Associated Nanoparticles (N).*

Expt.	RCA	M_n [b]	M_w/M_n [b]	Average particle diameter (D_z)	Particle size distribution[c]	Zeta potential (ξ)
	mol.%[a]	g.mol^{-1}		nm		mV
1 (C1, N1)	4.10	1370	1.96	115 ± 7.3	0.118	–40.6 ± 0.3
2 (C2, N2)	0.85	1330	1.94	124 ± 9.9	0.106	–35.0 ± 3.4
3 (C3, N3)	0.16	1400	1.99	123 ± 5.5	0.078	–30.9 ± 3.2

[a]molar fraction in the initial cyanoacetate mixture. [b]determined by SEC with a calibration curve based on PMMA standards. [c]given by the DLS apparatus.

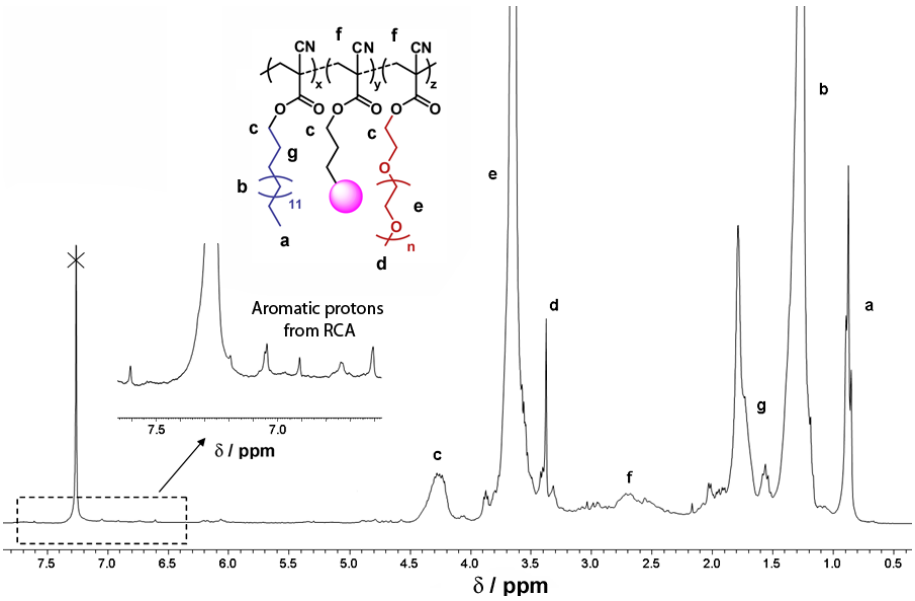

Figure S1 *300 MHz ^{1}H NMR of the fluorescent P(HDCA-co-RCA-co-MePEGCA) copolymer* ***C1*** *in $CDCl_3$. Insert: enlarged area in the 6.6–7.6 ppm region. Quantification of RCA in the copolymers was not undertaken due to its very low percentage, which would have led to strong inaccuracies.*

Table S2 *Synthesis of Poly[hexadecyl cyanoacrylate-co-dansyl cyanoacrylate-co-methoxypoly(ethylene glycol) cyanoacrylate] (P(HDCA-co-DCA-co-MePEGCA) Copolymers* ***(C4)*** *and Associated Nanoparticles* ***(N4)****.*

Expt.	RCA	M_n[b]	M_w/M_n[b]	Average particle diameter (D_z)	Particle size distribution[c]	Zeta potential (ξ)
	mol.%[a]	g.mol^{-1}		nm		mV
4 (C4, N4)	4.07	1640	2.27	89 ± 0.5	0.172	–31.6 ± 0.6

[a]*molar fraction in the initial cyanoacetate mixture.* [b]*determined by SEC with a calibration curve based on PMMA standards.* [c]*given by the DLS apparatus.*

Colloidal characteristics of fluorescently tagged poly(alkyl cyanoacrylate) nanoparticles

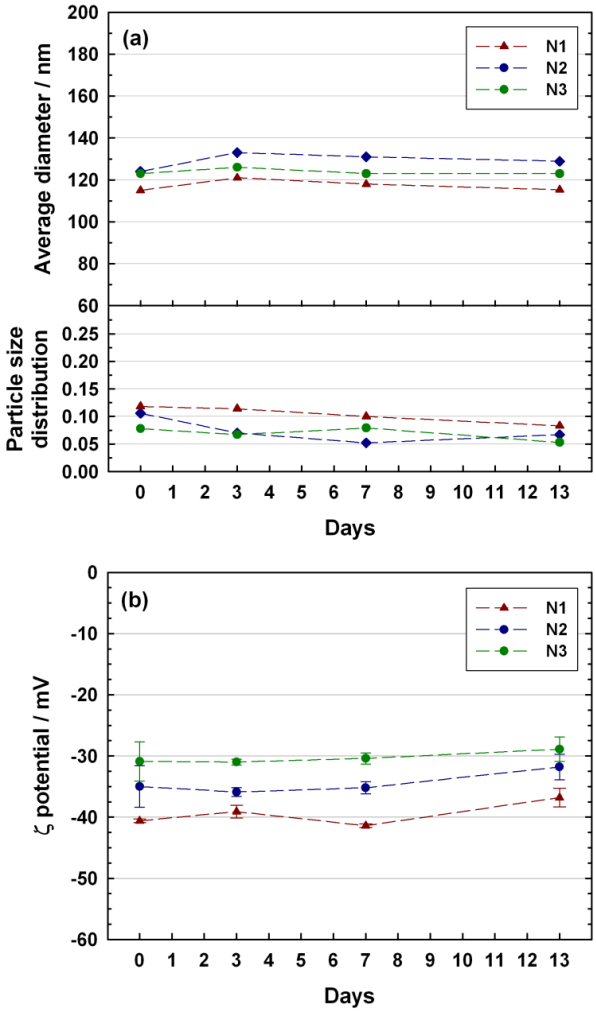

Figure S2. *Evolution of average diameters and particle size distribution (a) and ζ-potential values (b) of P(HDCA-co-RCA-co-MePEGCA) nanoparticles (****N1****,* ***N2*** *and* ***N3****) in water at 37 °C as a function of time.*

Fluorescent properties of rhodamine B-tagged poly(alkyl cyanoacrylate) copolymers and nanoparticles

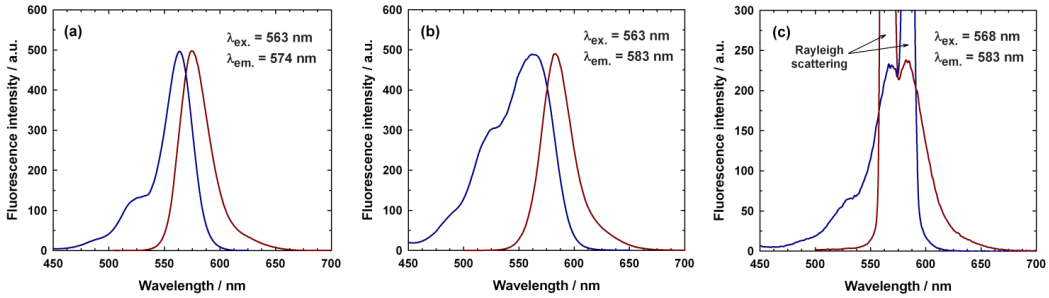

Figure S3. *Normalized excitation (blue line) and emission (red line) spectra of rhodamine B cyanoacetate (RCA) in $CHCl_3$ (a), P(HDCA-co-RCA-co-MePEGCA) copolymer* ***C2*** *in $CHCl_3$ (b) and P(HDCA-co-RCA-co-MePEGCA) nanoparticles* ***N2*** *in water (c).*

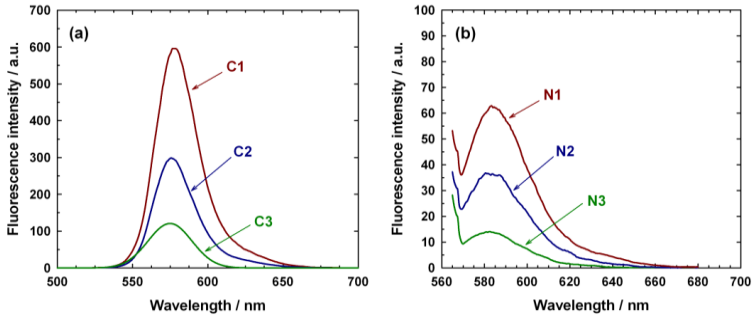

Figure S4. *Fluorescence emission spectra of P(HDCA-co-RCA-co-MePEGCA) copolymer solutions in $CHCl_3$ at 0.1 mg.mL^{-1} (a) and of P(HDCA-co-RCA-co-MePEGCA) nanoparticle suspensions in water at 0.1 mg.mL^{-1} (b).*

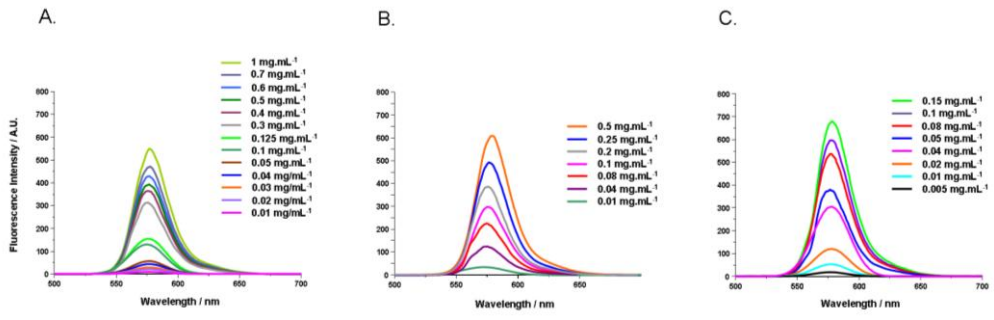

Figure S5. *Emission spectra in $CHCl_3$ of P(HDCA-co-RCA-co-MePEGCA) copolymer* ***C3*** *(a),* ***C2*** *(b) and* ***C1*** *(c) as the function of the copolymer concentration.*

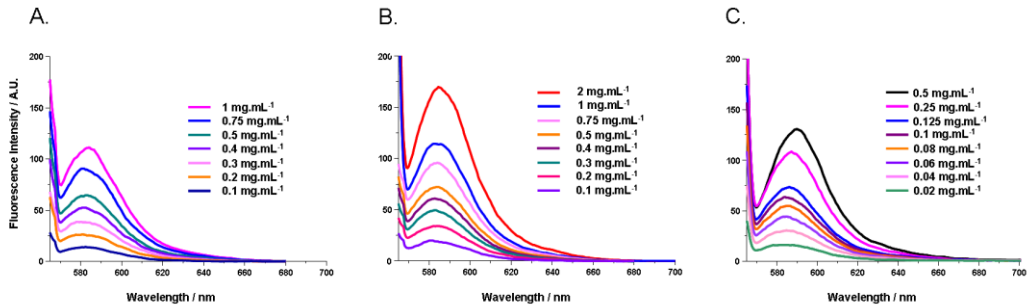

Figure S6. *Emission spectra in water of P(HDCA-co-RCA-co-MePEGCA) nanoparticle suspensions* ***N3*** *(a),* ***N2*** *(b) and* ***N1*** *(c) as the function of the nanoparticle concentration.*

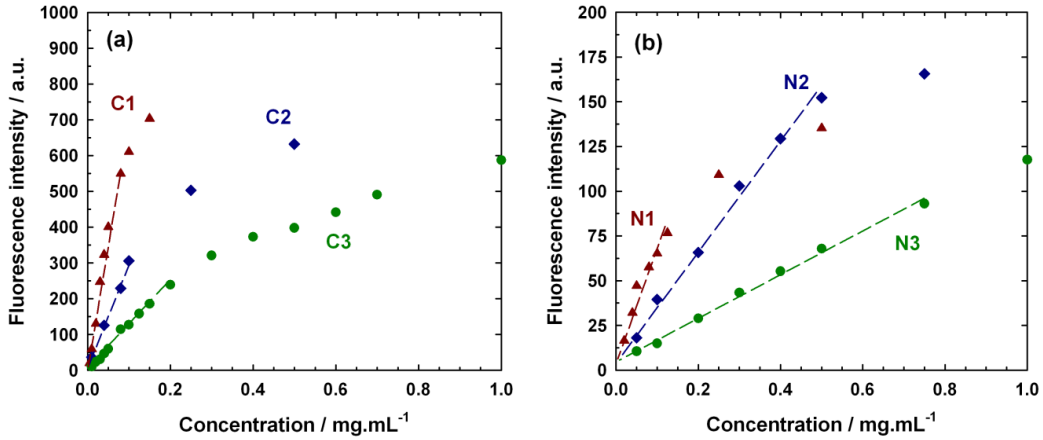

Figure S7. *Evolution of fluorescence intensity as a function of P(HDCA-co-RCA-co-MePEGCA) copolymer concentration (a) and P(HDCA-co-RCA-co-MePEGCA) nanoparticles concentration (b).*

Fluorescent properties of dansyl-tagged poly(alkyl cyanoacrylate) copolymers and nanoparticles

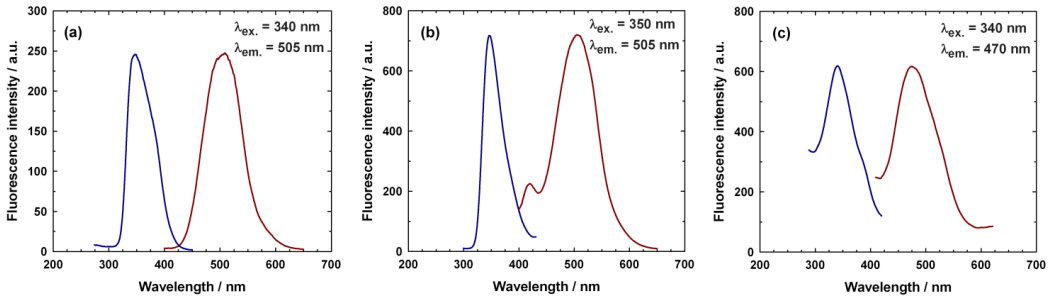

Figure S8. *Normalized excitation (blue line) and emission (red line) spectra of dansyl cyanoacetate (DCA) in acetone (a), P(HDCA-co-DCA-co-MePEGCA) copolymer* ***C4*** *in acetone (b) and P(HDCA-co-DCA-co-MePEGCA) nanoparticles* ***N4*** *in water (c).*

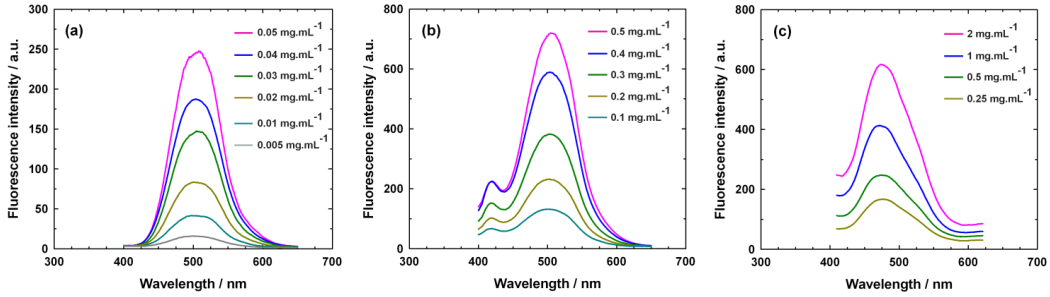

Figure S9. *Emission spectra of dansyl cyanoacetate (DCA) in acetone (a), P(HDCA-co-DCA-co-MePEGCA) copolymer* ***C4*** *in acetone (b) and P(HDCA-co-DCA-co-MePEGCA) nanoparticles* ***N4*** *in water (c) as the function of the concentration.*

Application to *in vitro* cell imaging

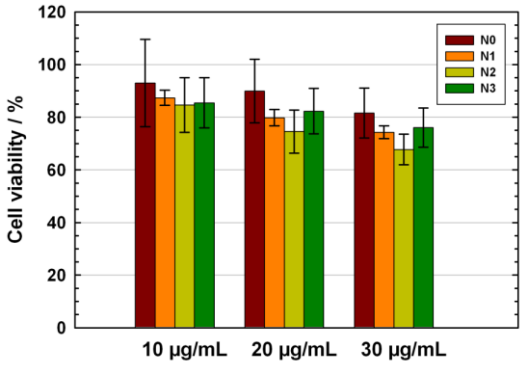

Figure S10. *Cell viability (MTT assay) after 48 h incubation of hCMEC/D3 human brain endothelial cell line with non-fluorescent P(HDCA-co-MePEGCA) (****N0****) or fluorescent P(HDCA-co-RCA-co-MePEGCA) (****N1****,* ***N2****,* ***N3****) nanoparticles as a function of nanoparticles concentration.*

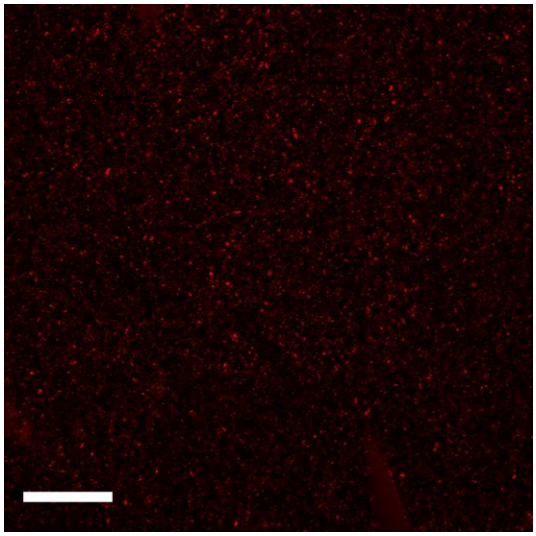

Figure S11. *Confocal microscopy images of fluorescently tagged nanoparticles (****N1****). Scale bar = 25 µm; Laser illumination: 543 nm; detection gain: 494; laser power: 100 %.*

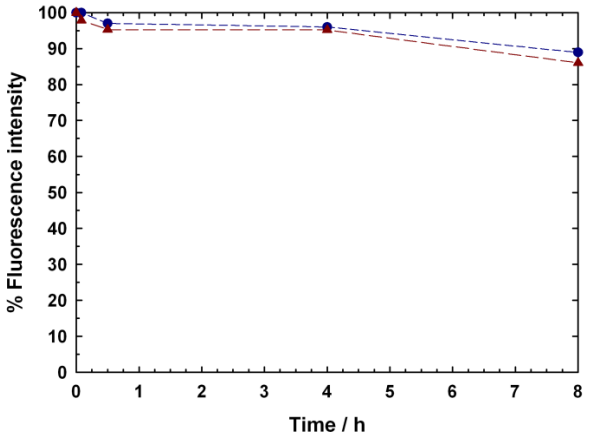

Figure S12. *In vitro biodegradation profile of fluorescent P(HDCA-co-RCA-co-MePEGCA) nanoparticles (**N2**) at 0.5 mg.mL^{-1} (●) or 0.3 mg.mL^{-1} (▲) in Fischer rat plasma at 37 °C.*

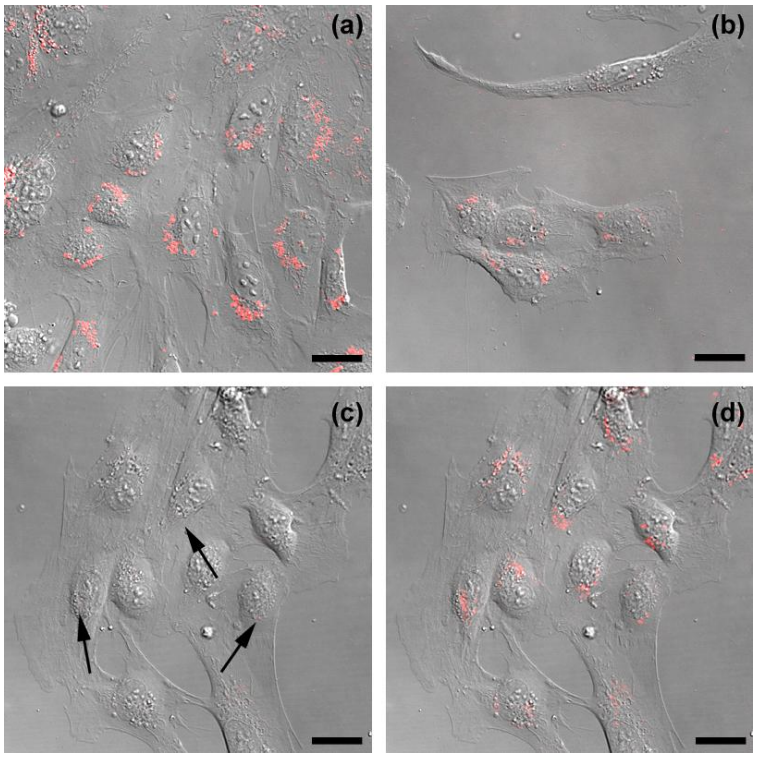

Figure S13. *Fluorescence images (red) superimposed with hCMEC/D3 human brain endothelial cells Nomarski images viewed from the top cell surface after incubation with fluorescent P(HDCA-co-RCA-co-MePEGCA) nanoparticles for 12 h and subsequent washing of the medium. (a): **N1**; (b): **N2**; (c): **N3** and (d) **N3** with increased gain and laser power. The arrows indicate faint fluorescence areas. Scale bars = 20 μm.*

References

1. Nguyen T and Francis MB. Practical synthetic route to functionalized rhodamine dyes. *Org. Lett.*, 2003, 5, 3245-8.

2. Kim TW, Park JH and Hong JI. Zn2+ fluorescent chemosensors and the influence of their spacer length on tuning Zn2+ selectivity. *J. Chem. Soc., Perkin Trans. 2*, 2002, 923.

3. Schreibelt G, Kooij G, Reijerkerk A, van Doorn R, Gringhuis SI, van der Pol S, et al. Reactive oxygen species alter brain endothelial tight junction dynamics via RhoA, PI3 kinase, and PKB signaling. *FASEB J.*, 2007, 21, 3666-76.

4. Weksler BB, Subileau EA, Perriere N, Charneau P, Holloway K, Leveque M et al. Blood-brain barrier-specific properties of a human adult brain endothelial cell line. *FASEB J.*, 2005, 19, 1872-4.

5. Cucullo L, Couraud PO, Weksler BB, Romero IA, Hossain M, Rapp E et al. Immortalized human brain endothelial cells and flow-based vascular modeling: a marriage of convenience for rational neurovascular studies et al. J. Cereb. Blood. Flow Metab., 2008, 28, 312-28.

6. Thioune O, Fessi H, Devissaguet JP and Puisieux F. Preparation of pseudolatex by nanoprecipitation: Influence of the solvent nature on intrinsic viscosity and interaction constant. *Int. J. Pharm.*, 1997, 146, 233-238.

7. Brigger I, Morizet J, Aubert G, Chacun H, Terrier-Lacombe MJ, Couvreur P et al. Poly(ethylene glycol)-coated hexadecylcyanoacrylate nanospheres display a combined effect for brain tumor targeting. J. Pharmacol. Exp. Ther., 2002, 303, 928-36.

Section 2

Implications dans le projet NAD

Une partie importante du projet NAD a été tournée vers le développement d'une méthode de diagnostic permettant d'identifier et de visualiser la présence et la formation de plaques amyloïdes, caractéristiques de la maladie d'Alzheimer, dans le cerveau. Nous avons donc proposé de développer des nanoparticules, chargées avec des sondes ou des agents de contraste, capables de traverser la BHE et de cibler les plaques amyloïdes comme une opportunité de visualiser précocement la formation des plaques cérébrales. Dans ce but, nous avons tout d'abord préparé des nanoparticules PEGylées de poly(alkyl cyanoacrylate) chargées avec des Quantum Dots (QDs) en tant qu'outil servant à l'identification du devenir des nanoparticules au cours des études biologiques. Plusieurs types de QDs ont été encapsulés dans ces nanoparticules puis visualisés *in vitro* après leur incubation avec des cellules endothéliales de BHE. De plus, l'encapsulation de QDs à l'intérieur de nanoparticules rendues fluorescentes par greffage de la Rhodamine B (cf. section 1) a permis l'obtention de nanoparticules doublement marquées. D'autre part, afin de réaliser la visualisation *in vivo* des particules, des QDs émettant dans le proche infrarouge ont également été utilisés.

Implications in the NAD project

An important part of the NAD project was directed towards to the development of a diagnosis procedure able to identify the presence of Alzheimer's disease typical plaques within the brain. The development of probes/contrast agents-charged nanoparticles able to cross the BBB and to target the amyloid plaques has been proposed as an opportunity to early visualize plaques formation within the brain. Toward this scope, we first decided to develop Quantum Dot (QD)-loaded PEGylated poly(alkyl cyanoacrylate) nanoparticles as a tool for the identification of nanoparticles fate during biological studies. Several types of QDs have been encapsulated within the nanoparticles and visualized *in vitro* after interaction with BBB endothelial cells. Moreover, the encapsulation of QDs into fluorescent Rhodamine B-tagged nanoparticles (described in section 1) allowed the double labeling of the nanoparticles. To achieve *in vivo* visualization of the particles, near infrared emitting QDs has been also employed.

Quantum dots-loaded PEGylated poly(alkyl cyanoacrylate) nanoparticles for *in vitro* and *in vivo* imaging

Soft Matter, 2011, 7, 6187-6193

Julien Nicolas,[1] Davide Brambilla,[1] Olivier Carion,[2] Thomas Pons,[3] Ivan Maksimovic,[4] Eric Larquet,[3] Benjamin Le Droumaguet,[1] Karine Andrieux,[1] Benoit Dubertret[2] and Patrick Couvreur[1]

[1] Laboratoire de Physico-Chimie, Pharmacotechnie et Biopharmacie, Univ Paris-Sud, UMR CNRS 8612, Faculté de Pharmacie, 5 rue Jean-Baptiste Clément, 92296 Châtenay-Malabry, France.

[2] Laboratoire Physique et Etude des Matériaux, ESPCI-CNRS-UPMC UMR 8213, 10 rue Vauquelin 75231 Paris, France.

[3] Institut de minéralogie et de physique des milieux condensés, Université Pierre et Marie Curie, Université Paris Diderot, CNRS UMR 7590, 4 place Jussieu, 75005 Paris.

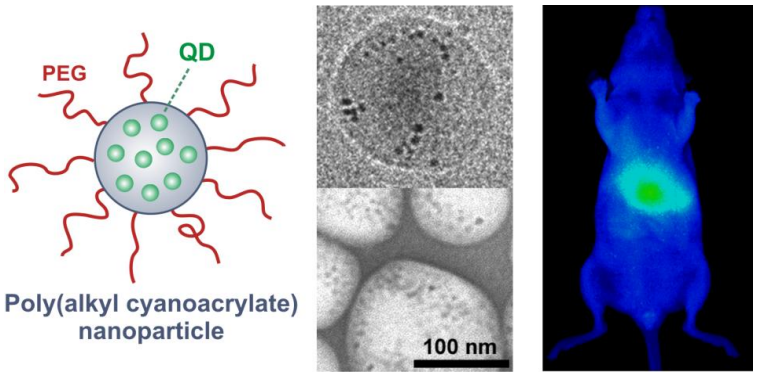

Résumé

Des Quantum Dots (QDs), émettant dans l'UV-Visible et dans le proche infrarouge, ont été encapsulés, avec des rendements élevés, à l'intérieur de nanoparticules (NPs) PEGylées de poly(cyanoacrylate d'alkyle) par auto-assemblage en solution aqueuse. Les NPs chargées en QDs ainsi obtenues ont été purifiées et caractérisées par microscopie électronique en transmission, diffusion de lumière, mesures de potentiel zêta ainsi que par des études de stabilité et des tests de viabilité cellulaire. La co-encapsulation de différents types de QDs a conduit à des NPs code-barres. Elles ont ensuite été utilisées pour l'imagerie de cellules endothéliales humaines permettant d'étudier leur capture. Enfin, le devenir *in vivo* des NPs contenant des QDs émettant dans le proche infrarouge a été visualisé de façon non invasive par imagerie optique de fluorescence.

Abstract

Visible-light and near infrared-emitting quantum-dots (QDs) were readily encapsulated with high yields into PEGylated poly(alkyl cyanoacrylate) nanoparticles (NPs) by self-assembly in aqueous solution. The resulting QDs-loaded NPs were efficiently purified and characterized by transmission electron microscopy, dynamic light scattering and zeta-potential measurements as well as by stability studies and cell viability assays. Concomitant encapsulation of different kinds of QDs led to barcode NPs. They were then used for human brain endothelial cell imaging allowing their uptake to be monitored. Finally, the *in vivo* fate of near-infrared fluorescent NPs was visualized noninvasively by fluorescence optical imaging.

1. Introduction

Nanotechnologies can be seen as a believable opportunity regarding various challenges encountered in the fields of materials science, drug delivery, supramolecular chemistry and other nanoscaled areas. The application of nanotechnologies to drug delivery,[1,2] often termed nanomedicine,[3-5] has witnessed a crucial impulse with the development of various types of drug-carrier nanodevices. Among suitable candidates for drug delivery purposes, nanoparticles (NPs) based on biodegradable poly(alkyl cyanoacrylate) (PACA) hold great promise and have appeared as a well-established technology for colloidal nanomedicine.[6] PACA drug carriers have indeed demonstrated significant results in multiple pathologies such as cancer,[7] severe infections (viral, bacteriologic, parasite)[8] as well as in several metabolic and autoimmune diseases,[9] well-reviewed in the recent literature.[10-13] Noteworthy, when PACA nanoparticles were loaded with the anticancer drug doxorubicin, they were able to overcome multidrug resistance (MDR) of cancer cells[14] and their biodegradability and safety have allowed clinical trials (currently phase II/III) for the treatment of MDR resistant hepatocarcinoma. The survival of the patients treated with this nanomedicine has been importantly increased as compared to the standard treatment (arterial chemoembolization).[15]

In the last 25 years, various types of PACA nanoparticles have been developed.[6,16-20] One of the major improvement of PACA nanotechnology is undoubtedly their coating and stabilization by poly(ethylene glycol) (PEG), a nonionic, flexible and hydrophilic polymer. This approach, usually termed PEGylation resulted in nanoparticles able to partially escape from the immune system response, thus allowing an increased blood concentration even if, similarly to most of the other PEGylated colloids, these nanoparticles finally end-up into the liver tissue.[21,22]

More recently, it has been demonstrated that after intravenous administration, a small fraction of the injected PEGylated nanoparticles composed of amphiphilic poly[hexadecyl cyanoacrylate-*co*-methoxypoly(ethylene glycol) cyanoacrylate] (P(HDCA-*co*-MePEGCA))[23] copolymer were able to cross the blood-brain-barrier (BBB),[11,24] as opposed to their non-PEGylated counterparts, thus opening the door to drug delivery into the central nervous system (CNS). In addition, it was recently discovered that these nanoparticles were able to bind the amyloid β-peptide, a biomarker for Alzheimer's disease, and to influence its aggregation kinetics.[25]

Quantum dots (QDs) are fluorescent nanocrystals that offer unique optical properties such as a wideband excitation, sharp symmetrical emission spectra, a long-term photostability, high quantum yields and size-dependant emission wavelengths. A great deal of work has focused on QD surface modification for enhanced water-solubility, (bio)conjugation and other applications in

biological areas.[26,27] Encapsulation of QDs into polymer nanoparticles or micelles was also investigated,[28,39] but to the best of our knowledge, none of them reported QD loading into poly(alkyl cyanoacrylate) nanoparticles or into other PEGylated, biodegradable NPs.

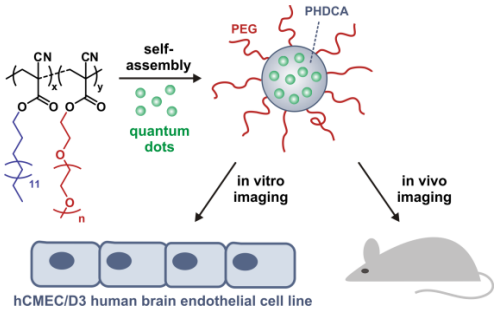

Scheme 1 *Preparation of quantum dots-loaded, fluorescent P(HDCA-co-MePEGCA) nanoparticles for in vitro and in vivo imaging.*

Herein, we reported a straightforward method to efficiently encapsulate QDs as fluorescent tags into PEGylated P(HDCA-*co*-MePEGCA) NPs (Scheme 1). Concomitant encapsulation of two kinds of QDs was also achieved as a step forward to "barcode" nanocarriers, which is of interest for multiplex detection and which is unprecedent in the field. We wished to take advantage of the BBB crossing ability of these NPs to monitor their *in vitro* uptake by hCMEC/D3 human brain endothelial cells. In addition, the *in vivo* fate of near-infrared fluorescent QDs-loaded nanoparticles was imaged noninvasively by fluorescence optical imaging.

2. Experimental part

2.1 Materials

Pluronic F-68 and poly(vinyl alcohol) (PVA, cell culture tested) were purchased from Fluka. All solvents were purchased at the highest grade from Carlo Erba. Rhodamine B cyanoacetate (RCA), rhodamine B-tagged P(MePEGCA-*co*-RCA-*co*-HDCA) and P(MePEGCA-*co*-HDCA) copolymers were synthesized as described elsewhere.[40,41] Dulbecco's phosphate buffer saline (DPBS) without $CaCl_2$ and $MgCl_2$, and EMB-2 medium were purchased from Lonza. Penicillin 10,000 units-Streptomycin 10,000 $\mu g.mL^{-1}$ and Trypsin/EDTA were obtained from Invitrogen, Gibco. Hydrocortisone, human basic fibroblast growth factor (bFGF) cell culture tested and 3-(4,5-dimethylthiazol-2-yl)-2,5-diphenyltetrazolium bromide (MTT, 98%) were purchased from Sigma. HEPES 1 M was obtained from PAA – The Cell Culture Company. Fetal bovine serum was purchased from Eurobio. hCMEC/D3 human brain endothelial cell line was prepared as described elsewhere.[42-44]

2.2 Synthesis of quantum dots (QDs)

Visible emitting CdSe/CdS/ZnS and near-infrared emitting $CuInSe_2$/ZnS quantum dots were synthesized in organic solvents using previously published protocols.[45,46] These QDs were finally precipitated in ethanol and resuspended in chloroform before use.

2.3 Preparation of QDs-loaded, PEGylated nanoparticles

QDs were encapsulated into P(MePEGCA-*co*-HDCA) or into fluorescent P(MePEGCA-*co*-RCA-*co*-HDCA) polymeric nanoparticles by the solvent emulsion/evaporation technique.[47] A typical formulation (**N1**, Table 1) is prepared as follows. 10 mg of P(MePEGCA-*co*-HDCA) copolymer and 100 µL of QD ($\lambda_{em.}$ = 590 nm, 10 µM) were dissolved in 0.9 mL of chloroform. To this organic phase was added 4 mL of an aqueous solution of PVA (0.25% w/w). The resulting emulsion was vortexed two times for 1 min at 3200 rpm and ultrasonicated on ice for 1 min at 300 W (40%) using a Vibracell sonicator. The solvent was then removed under reduced pressure to yield a stable suspension of QDs-loaded P(MePEGCA-*co*-HDCA) NPs. NPs were purified by filtration on 1 µm glass fiber membrane (Acrodisc, Pall) slide. These QD-loaded NPs were further purified by ultracentrifugation for 2 h in a 10-60% sucrose gradient at 50,000 rpm (MLS50 rotor; Optimax ultracentrifuge, Beckman-Coulter). Proportions of QDs in the different bands were measured by dosing cadmium concentration by ICP-MS (Ascal, France) after dissolution in concentrated nitric acid. The same protocol was followed for the other formulations (Table 1). When Pluronic was used, its concentration was 0.5% w/w.

3. Analytical techniques

3.1 Dynamic light scattering

The nanoparticle diameter (D_z) was measured by dynamic light scattering (DLS) with a NanoZS from Malvern (173° scattering angle) at 25°C. DLS measurements were used to monitor the nanoparticles stability as a function of time in solution. The nanoparticle surface charge was investigated by ζ-potential measurement at 25°C after dilution with 1 mM NaCl solution applying the Smoluchowski equation and using the same apparatus.

3.2 Cryo-transmission electron microscopy (Cryo-TEM)

Thin liquid films of particle were flash frozen in liquid ethane and observed at –180°C on a JEOL JEM-2100 LaB6 electron microscope (Cs = 2.0 mm) operating at 200 kV under low-dose conditions (10 electron.$Å^{-2}.s^{-1}$) at a nominal magnification of 20,000 to 40,000, with a –1.5 – –2.0

μm defocus range. For negative staining, nanoparticles were stained, using a 2% uranyl acetate solution, and observed at –1.5 μm defocus under low electron dose conditions. Digital images were directly recorded on a Gatan Ultrascan 1000 CCD camera.

3.3 Fluorescence micro-spectroscopy

Fluorescence micro-spectroscopy was performed using a slit and an N-SF11 glass prism to provide spectral dispersion on a CCD camera at the output of an inverted fluorescence microscope (IX71, Olympus).[48]

3.4 Confocal laser scanning microscopy (CLSM)

In vitro imaging was performed on hCMEC/D3 human brain endothelial cell line incubated with rhodamine B-tagged nanoparticles containing QDs. Cells were seeded on glass disk (25 mm in diameter) at a concentration of 25,000 cells.cm^{-2}. After 2 days, an aqueous suspension of nanoparticles (25 μg.mL^{-1}) was incubated with hCMEC/D3 cells. Following a 12 and 24 h incubation time, the cell monolayer was washed with fresh medium and then analyzed by confocal laser scanning microscopy equipped with a 1 mW helium-neon laser and a Plan-Apochromat 63× objective lens (numerical aperture/1.4, oil immersion). For QDs-loaded P(MePEGCA-*co*-HDCA) NPs (**N2**, Table 1), fluorescence was collected with long-pass 530 nm emission filter under 458 nm wavelength excitation. For QDs-loaded P(MePEGCA-*co*-RCA-*co*-HDCA) NPs (**N5**, Table 1), fluorescence was collected with long-pass 560 nm emission filter under 543 nm wavelength excitation (rhodamine B channel) and a band-pass 505–550 nm emission filter under 488 nm excitation (QDs channel). The pinhole size was set at 1.0 Airy unit (106 μm diameter) giving an optical section thickness of 0.8 μm.

3.5 Cytotoxicity studies

The cytotoxicity of QDs-loaded nanoparticles was investigated by MTT viability test on hCMEC/D3 human brain endothelial cell line. Cells were grown on 10 cm diameter plates in EBM-2 basal medium supplemented with fetal bovine serum 5%, hydrocortisone 1.4 μM, basic fibroblast growth factor 1 ng.mL^{-1}, penicillin:streptomycin solution 1% and HEPES 10 mM. Polystyrene 96 wells plates were used and cells were seeded in each well (15,000 cells per well) with the medium previously described. After a 1 day growth, an aqueous suspension of nanoparticles was incubated at four different concentrations: 10, 20, 30 and 500 μg.mL^{-1}. After 48 h of incubation at 37 °C in 5% CO_2, the MTT reagent (at a final concentration of 0.05% in DPBS)

was added and 3 h later, the percentage of living cells was evaluated with a 96 wells plate absorbance reader at 570 nm. Cells treated with the same volume of water were used as negative controls.

3.6 *In vivo* visualization

For *in vivo* imaging, retro-orbital injections of 200 µL QDs-loaded nanoparticles (**N0** and **N5**, Table 1) in 5% glucose were performed on female nude mice weighting approximately 23 g (injected dose of ~22 $mg.kg^{-1}$) and housed under standard conditions with food and water *ad libitum*. After 24 h, the animals were anesthetized and imaged with the Fluobeam NIR imaging system (Fluoptics, Grenoble, France). The optical system consists of a 690-nm laser (52 $\mu W.mm^{-2}$) and a pixelfly camera fitted with a high-pass RG 9 filter (Schott).

4. Results and discussion

P(HDCA-*co*-MePEGCA) nanoparticles are usually prepared by the nanoprecipitation technique.[6,49] However, we selected the solvent emulsion/evaporation method[50] as it involves chloroform (or dichloromethane) in which QDs were perfectly dispersed. Thus, the encapsulation method consisted in an organic phase, comprising the amphiphilic copolymer and the QDs, emulsified in an aqueous solution of surfactant (either Pluronic or PVA) and subsequently subjected to high shear by means of ultrasounds. The organic solvent was then removed under reduced pressure to yield a stable suspension of QDs-loaded P(HDCA-*co*-MePEGCA) nanoparticles.

A small library of QDs-loaded nanoparticles was obtained by varying the nature of the QDs, their initial amount and the nature of the surfactant (Table 1, **N1–N4**). In addition, a dual labeling was performed with the use of a rhodamine B-tagged P(HDCA-*co*-RCA-*co*-MePEGCA) copolymer (Table 1, expt. **N5**). In all cases, stable suspensions of QDs-loaded PACA nanoparticles were obtained. Average diameters were in the 150–180 nm range with narrow particle size distributions (Table 1).

Table 1. *Synthesis and Colloidal Characteristics of QDs-Loaded, PEGylated Poly(Alkyl Cyanoacrylate) Nanoparticles.*

Expt.	Copolymer	Surfactant	Quantum-dots		Average diameter (D_z) (nm)	Particle size distribution [a]	Zeta-potential (ζ) (mV)
			$\lambda_{em.}$ (nm)	Initial amount (mol)			
N0	P(HDCA-*co*-MePEGCA)	Pluronic	-	-	175 ± 4	0.158	–8.6 ± 0.1
N1	P(HDCA-*co*-MePEGCA)	PVA	590	1×10^{-9}	153 ± 4	0.117	–8.8 ± 0.2
N2	P(HDCA-*co*-MePEGCA)	PVA	600	5×10^{-9}	162 ± 3	0.102	–4.8 ± 0.4
N3	P(HDCA-*co*-MePEGCA)	PVA	590	2×10^{-9}	158 ± 4	0.129	–6.0 ± 0.6
			560	2×10^{-9}			
			540	2×10^{-9}			
N4	P(HDCA-*co*-MePEGCA)	Pluronic	840	2×10^{-9}	181 ± 3	0.098	–2.4 ± 0.4
N5	P(HDCA-*co*-RCA-*co*-MePEGCA)	PVA	540	3×10^{-9}	171 ± 2	0.119	–16.0 ± 0.8
N6	P(HDCA-*co*-MePEGCA)	PVA	620	0.6×10^{-9}	157 ± 7	0.039	–9.4 ± 3.4
			580	0.3×10^{-9}			
N7	P(HDCA-*co*-MePEGCA)	PVA	620	0.6×10^{-9}	213 ± 6	0.132	–7.3 ± 2.5
			580	0.15×10^{-9}			

[a] Determined by the DLS apparatus.

Long-term stability of the QDs-loaded NPs was then assessed over a period of 9 days at 37 °C, a relevant temperature when biological applications are foreseen. Average diameters and particle size distributions were found to remain constant (Figure 1).

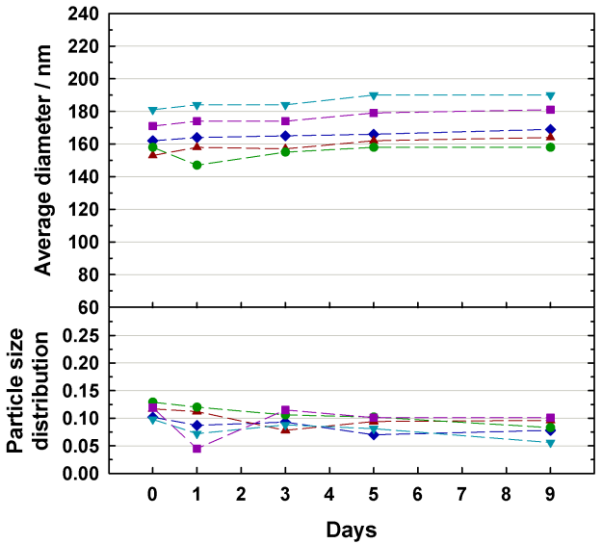

Figure 1. *Evolution of the average diameter and the particle size distribution of QDs-loaded poly(alkyl cyanoacrylate) nanoparticles in water at 37°C as a function of time.* ▲ *(N1),* ♦ *(N2),* ● *(N3),* ▼ *(N4),* ■ *(N5).*

ζ-potential measurements showed negative values from –2.4 to –8.8 mV with the P(HDCA-*co*-MePEGCA) whereas a lower value of –16.0 mV was obtained when the P(HDCA-*co*-RCA-*co*-MePEGCA) was used. This observation is in good agreement with lower ζ-potential

values of rhodamine B-tagged poly(alkyl cyanoacrylate) nanoparticles compared to unlabeled counterparts,[41] due to the positioning of rhodamine moieties at the nanoparticle surface.

Ultracentrifugation on sucrose gradient was performed and allowed QDs-loaded nanoparticles to be isolated from both empty nanoparticles and free QDs, as assessed by cryo-TEM images (Figure 2a and Figure S1). With normal contrast (**N1**), QDs were clearly seen as dark spots inside polymer nanoparticles which sizes were consistent with DLS measurements. When a negative staining specific to PEG (constituting the NP shell) was applied (**N3**), nanoparticles were surrounded by a dark coloration inside which QDs still appeared as dark spots (Figure 2b). This confirmed their successful encapsulation inside P(HDCA-*co*-MePEGCA) nanoparticles. In addition, the higher loading targeted with QDs-loaded nanoparticles **N3** compared to **N1** was visually assessed by cryo-TEM. Quantum dot encapsulation yields of **N1** and **N3** batches were as high as 35% and 11%, respectively, as assessed by ICP-MS cadmium concentration measurements.[51-53] The rest of QDswere either aggregated outside the copolymer beads or encapsulated as a single QDs in small copolymer micelles.

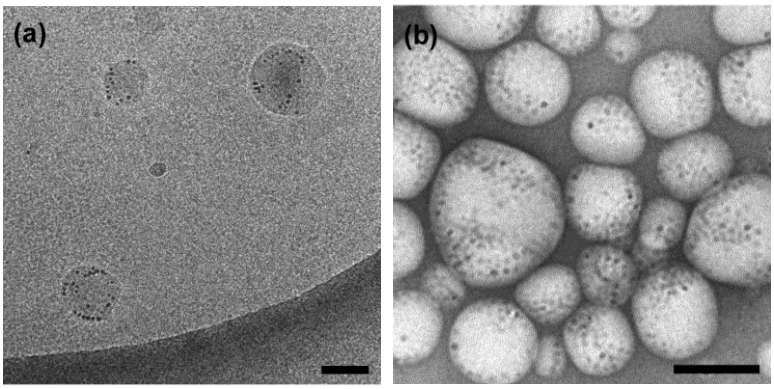

Figure 2. *Cryo-transmission electron microscopy of QD-loaded P(HDCA-co-MePEGCA) nanoparticles N1 (a) and N3 with negative staining (b). Scale bars = 100 nm.*

We then took advantage of the ease of encapsulating QDs into PACA nanocarriers by going a step further towards barcode nanoparticles. We performed a concomitant encapsulation of variable amounts of two batches of QDs emitting at 580 nm and 620 nm (**N6** and **N7**, Table 1) and we investigated whether the initial stoichiometry (i.e., the initial intensity ratio between the two populations of QDs) was maintained individually in each nanoparticle. Considering the fluorescence intensity of each kind of QDs, the initial average intensity ratios of QDs utilized for the preparation of nanoparticles **N6** and **N7** were 0.53 and 0.69, respectively. These NPs were prepared following the same protocol and their individual emission spectra were measured by fluorescence micro-spectroscopy (n = 40 beads) after purification. As shown in Figure 3, the

emission spectra of individual nanoparticles correlated well with the initial blend of the two populations of QDs. Average final ratios were 0.42 ± 0.11 for **N6** and 0.65 ± 0.07 for **N7**.

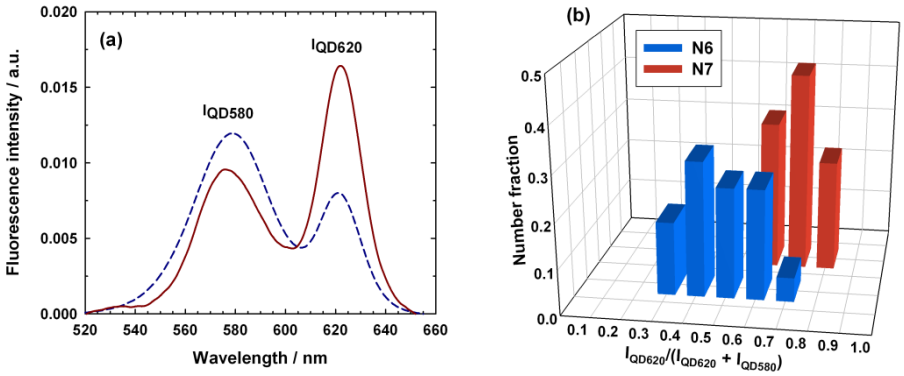

Figure 3. *Typical fluorescence emission spectra (a) and fluorescence intensity distribution, $I_{QD620}/(I_{QD620}+I_{QD580})$, of individual nanoparticles* ***N6*** *(dashed line) and* ***N7*** *(solid line) (b).*

QDs-loaded poly(alkyl cyanoacrylate) nanoparticles were then employed for *in vitro* imaging studies on hCMEC/D3 human brain endothelial cell line, which has been validated as a unique *in vitro* model of human BBB.[42] Prior to imaging studies, cell viability assays were performed by the MTT test in order to determine the cytotoxicity of QDs-loaded PACA nanoparticles on hCMEC/D3 cells. With QDs-loaded NPs N2 and N5, which exhibited among the highest QD loading, no statistical difference in cytotoxicity was observed up to a copolymer concentration of 0.1 mg.mL^{-1} (Figure 4).

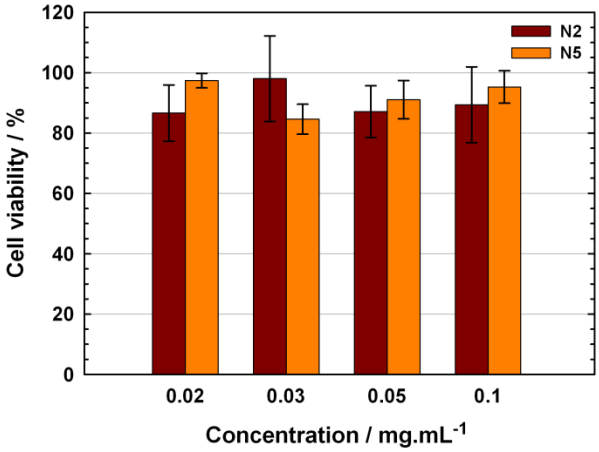

Figure 4. *Cell viability (MTT assay) after 48 h incubation of hCMEC/D3 human brain endothelial cell line with QD-loaded P(HDCA-co-MePEGCA) (**N2**) and P(HDCA-co-RCA-co-MePEGCA) (**N5**) nanoparticles as a function of the nanoparticle concentration. Each experiment was repeated 3 times from 8 independent incubation preparations. Results were expressed as percentages of absorption of treated cells (± SD) in comparison with the values obtained from untreated control cells.*

In vitro imaging studies after incubation of hCMEC/D3 cells with fluorescent QDs-loaded nanoparticles **N2** were performed by confocal laser scanning microscopy (CLSM). After a 12 h incubation period, it was shown that: (i) Nomarsky contrast image exhibited a typical fibroblast shape for the cells with no morphological alteration which was in good agreement with cell viability assays and (ii) fluorescence image superimposed with Nomarski image highlighted intense and fine fluorescence spots mainly accumulated within the cells and especially around the nuclei (Figure 5). This observation is in good agreement with a previously reported endocytosis mechanism of similar nanoparticles in primary culture of rat brain endothelial cells.[54]

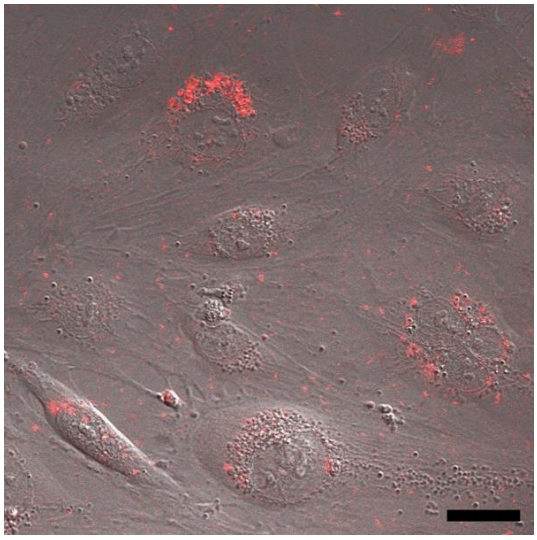

Figure 5. *Superimposed confocal fluorescence and Nomarski images of hCMEC/D3 human brain endothelial cells viewed from the top cell surface after incubation with QD-loaded fluorescent P(HDCA-co-MePEGCA) nanoparticles N2 for 12 h. Scale bar = 20 µm.*

Considering that poly(alkyl cyanoacrylate) nanoparticles are biodegraded enzymatically *via* hydrolysis of the ester functions,[6] it was important to assess that the fluorescence signal arising from CLSM images was assigned to QDs still encapsulated into PACA nanoparticles and not to free QDs that would have precociously leaked out of PACA nanocarriers. Therefore, green-emitting QDs ($\lambda_{em.}$ = 540 nm) were encapsulated into rhodamine B-tagged P(HDCA-*co*-RCA-*co*-MePEGCA) copolymer (Table 1, **N5**) in order to separately visualize fluorescent signals coming from the QDs and from the rhodamine B tag by CLSM. After a 24 h incubation period, nanoparticles **N5** were observed to be taken up by hCMEC/D3 cells and CLSM allowed fluorescence signals from QDs and from the fluorescent copolymer to be independently detected (Figure 6b–c). More importantly, it can be seen on Figure 6d that an almost perfect co-localization

of both signals was obtained which led us to conclude that CLSM fluorescence signal can be safely assigned to the presence of encapsulated QDs into poly(alkyl cyanoacrylate) nanoparticles.

This new fluorescently-labeled PEGylated nanoparticles are therefore adapted to *in vitro* imaging. Moreover, it is believed that these nanoconstructs are a suitable alternative to the usual pathway consisting in the encapsulation of organic fluorochromes which exhibit a severe tendency to leak out from nanoparticles and therefore to lead to misinterpretation of CLSM images.[55]

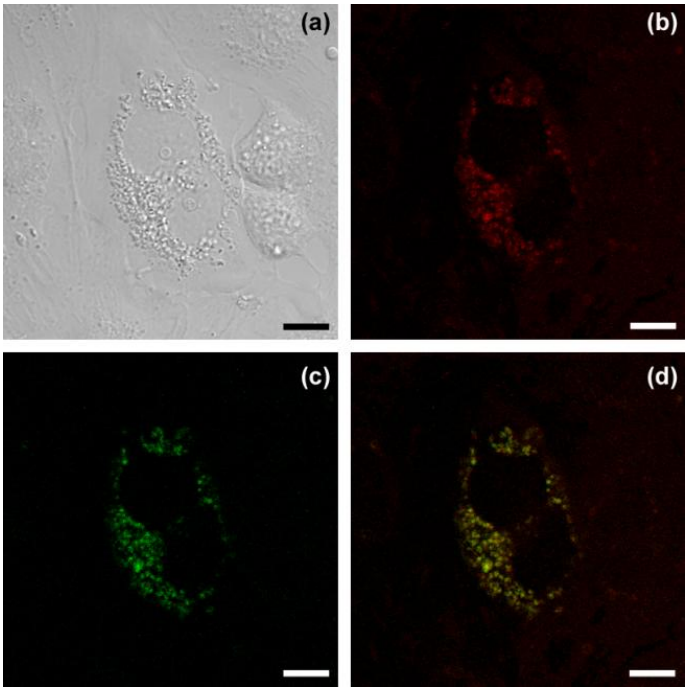

Figure 6. *hCMEC/D3 human brain endothelial cells Nomarski image (a) and confocal microscopy images [red fluorescence image (b); green fluorescence image (c); merge of red and green fluorescence images (d)] viewed from the top cell surface after incubation with QD-loaded fluorescent P(HDCA-co-RCA-co-MePEGCA) nanoparticles* ***N5*** *for 24 h. Scale bars = 10 µm.*

In addition, our approach is very versatile due to the wide range of QDs that can be encapsulated. This was illustrated with the loading of Cd-free near-infrared (NIR) emitting QDs inside P(HDCA-*co*-MePEGCA) nanoparticles (Table 1, **N4**), hence suitable for *in vivo* imaging purposes. Retro-orbital injections of nanoparticles were performed on nude mice and they were imaged non-invasively by fluorescence optical imaging after 24 h. Whereas only a faint auto-fluorescence signal was obtained with empty nanoparticles (Table 1, **N0**), used as a negative control, (Figure 7a), NIR QDs-loaded PACA nanoparticles led to a strong fluorescence signal emitted from the liver (Figure 7b). It is worth mentioning that although these nanoparticles were

PEGylated, their accumulation in the liver was not surprising, somewhat expected, at a time interval as long as 24 h post-injection.[24,56]

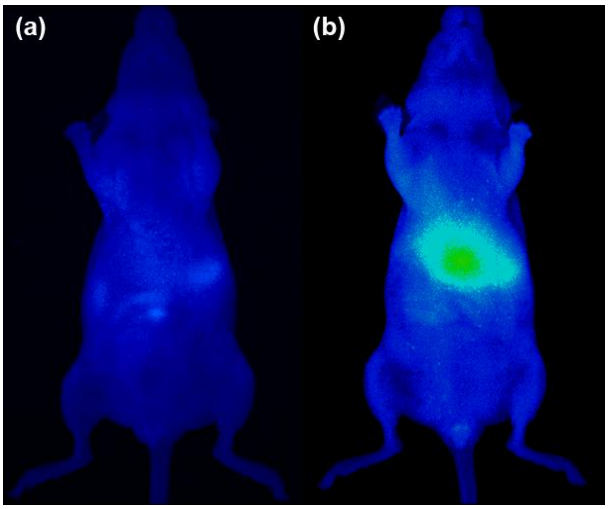

Figure 7. *2D-fluorescence optical imaging of mice performed 24 h after retro-orbital injection of (a) empty P(HDCA-co-MePEGCA) NPs (**N0**) and (b) QDs-loaded P(HDCA-co-MePEGCA) NPs (**N4**).*

5. Conclusions

For the first time, QDs were loaded into PEGylated and biodegradable nanoparticles. The strategy relied on the encapsulation of QDs upon self-assembly of amphiphilic P(HDCA-*co*-MePEGCA) copolymer. The resulting nanoparticles were very stable and were used for human brain endothelial cell *in vitro* imaging. The flexibility of this approach was then illustrated by the encapsulation of: (i) different kinds of QDs as a step towards barcode NPs for multiplex detection purposes and (ii) near-infrared QDs in order to noninvasively visualize *in vivo* nanoparticles by fluorescence optical imaging. These results are of importance as they lay down the foundations of a versatile fluorescent, nanoparticulate platform useful for biomedical applications. Since it was previously demonstrated that PACA nanoparticles are able to efficiently encapsulate a wide variety of drugs, the nanoconstructs described in the current study open the door to the so-called theranostic approach.

6. Acknowledgements

The authors thank Dr. Véronique Marsaud for *in vivo* injections, Valérie Nicolas (Plateforme Imagerie Cellulaire, IFR 141) for her help with CLSM experiments and Drs. Odile Allard and Stéphanie Guillermet from Fluoptics for use of the Fluobeam® system and for technical

assistance. We also thank Dr. Vincent Loriette for help with the design of the fluorescence micro-spectroscopy set-up. We are grateful to the European Community's Seventh Framework Programme (FP7/2007-2013) under grant agreement no 212043 for financial support. The French ministry of research and CNRS are also warmly acknowledged for the financial support.

7. References

1. Erb SE. Nanotechnology in drug delivery. Drug Deliv. Syst. 2009; 24: 63-70.

2. Farokhzad OC,Langer R. Impact of nanotechnology on drug delivery. ACS Nano 2009; 3: 16-20.

3. Park JH, Lee S, Kim J-H, Park K, Kim K,Kwon IC. Polymeric nanomedicine for cancer therapy. Prog. Polym. Sci. 2008; 33: 113-37.

4. Riehemann K, Schneider SW, Luger TA, Godin B, Ferrari M,Fuchs H. Nanomedicine-challenge and perspectives. Angew. Chem., Int. Ed. 2009; 48: 872-97.

5. Sanhai WR, Sakamoto JH, Canady R,Ferrari M. Seven challenges for nanomedicine. Nat. Nanotechnol. 2008; 3: 242-44.

6. Nicolas J,Couvreur P. Synthesis of poly(alkyl cyanoacrylate)-based colloidal nanomedicines. Wiley Interdiscip. Rev. Nanomed. Nanobiotechnol. 2009; 1: 111-27.

7. Chiannilkulchai N, Driouich Z, Benoit JP, Parodi AL,Couvreur P. Doxorubicin-loaded nanoparticles: Increased efficiency in murine hepatic metastases. Sel. Cancer Ther. 1989; 5: 1-11.

8. Fattal E, Youssef M, Couvreur P,Andremont A. Treatment of experimental salmonellosis in mice with ampicillin-bound nanoparticles. Antimicrob. Agents Chemother. 1989; 33: 1540-43.

9. de Kozak Y, Andrieux K, Villarroya H, Klein C, Thillaye-Goldenberg B, Naud M-C, et al. Intraocular injection of tamoxifen-loaded nanoparticles: A new treatment of experimental autoimmune uveoretinitis. Eur. J. Immunol. 2004; 34: 3702-12.

10. Couvreur P,Vauthier C. Nanotechnology: Intelligent design to treat complex disease. Pharm. Res. 2006; 23: 1417-50.

11. Garcia-Garcia E, Andrieux K, Gil S,Couvreur P. Colloidal carriers and blood-brain barrier (bbb) translocation: A way to deliver drugs to the brain? Int. J. Pharm. 2005; 298: 274-92.

12. Vauthier C, Dubernet C, Fattal E, Pinto-Alphandary H,Couvreur P. Poly(alkylcyanoacrylates) as biodegradable materials for biomedical applications. Adv. Drug Delivery Rev. 2003; 55: 519-48.

13. Vauthier C, Labarre D,Ponchel G. Design aspects of poly(alkylcyanoacrylate) nanoparticles for targeted drug delivery. J. Drug Targeting 2007; 15: 641-63.

14. Bennis S, Chapey C, Robert J,Couvreur P. Enhanced cytotoxicity of doxorubicin encapsulated in polyisohexylcyanoacrylate nanospheres against multidrug-resistant tumour cells in culture. European Journal of Cancer 1994; 30: 89-93.

15. Unpublished results from BioAlliance Pharma, http://www.bioalliancepharma.com/eng/.

16. Limouzin C, Caviggia A, Ganachaud F,Hémery P. Anionic polymerization of n-butyl cyanoacrylate in emulsion and miniemulsion. Macromolecules 2003; 36: 667-74.

17. Maitre C, Ganachaud F, Ferreira O, Lutz JF, Paintoux Y,Hémery P. Anionic polymerization of phenyl glycidyl ether in miniemulsion. Macromolecules 2000; 33: 7730-36.

18. Musyanovich,Landfester. Prog. Colloid Polym. Sci. 2008; 134: 120-27.

19. Weiss CK, Ziener U,Landfester K. A route to nonfunctionalized and functionalized poly(n-butylcyanoacrylate) nanoparticles: Preparation in miniemulsion. Macromolecules 2007; 40: 928-38.

20. Nicolas J, Bensaid F, Desmaele D, Grogna M, Detrembleur C, Andrieux K, et al. Synthesis of highly functionalized poly(alkyl cyanoacrylate) nanoparticles by means of click chemistry. Macromolecules 2008; 41: 8418-28.

21. Stolnik S, Illum L,Davis SS. Long circulating microparticulate drug carriers. Adv. Drug Delivery Rev. 1995; 16: 195-214.

22. Storm G, Belliot SO, Daemen T,Lasic DD. Surface modification of nanoparticles to oppose uptake by the mononuclear phagocyte system. Adv. Drug Delivery Rev. 1995; 17: 31-48.

23. Peracchia MT, Desmaële D, Couvreur P,d'Angelo J. Synthesis of a novel poly(mepeg cyanoacrylate-co-alkyl cyanoacrylate) amphiphilic copolymer for nanoparticle technology. Macromolecules 1997; 30: 846-51.

24. Calvo P, Gouritin B, Chacun H, Desmaele D, D'Angelo J, Noel JP, et al. Long-circulating pegylated polycyanoacrylate nanoparticles as new drug carrier for brain delivery. Pharm. Res. 2001; 18: 1157-66.

25. Brambilla D, Verpillot R, Taverna M, De Kimpe L, Le Droumaguet B, Nicolas J, et al. Capillary electrophoresis with laser-induced fluorescence detection (ce-lif) as a new protocol to monitor interaction between nanoparticles and the amyloid-β peptide. Anal. Chem. 2010; 82: 10083-89.

26. Medintz IL, Uyeda HT, Goldman ER,Mattoussi H. Quantum dot bioconjugates for imaging, labelling and sensing. Nat. Mater. 2005; 4: 435-46.

27. Michalet X, Pinaud FF, Bentolila LA, Tsay JM, Doose S, Li JJ, et al. Quantum dots for live cells, in vivo imaging, and diagnostics. Science 2005; 307: 538-44.

28. Kim JS, Cho KJ, Tran TH, Nurunnabi M, Moon TH, Hong SM, et al. In vivo nir imaging with cdte/cdse quantum dots entrapped in plga nanospheres. J. Colloid Interface Sci. 2011; 353: 363-71.

29. Pan J,Feng S-S. Targeting and imaging cancer cells by folate-decorated, quantum dots (qds)-loaded nanoparticles of biodegradable polymers. Biomaterials 2009; 30: 1176-83.

30. Carion O, Mahler B, Pons T,Dubertret B. Synthesis, encapsulation, purification and coupling of single quantum dots in phospholipid micelles for their use in cellular and in vivo imaging. Nat. Protoc. 2007; 2: 2383-90.

31. Dubertret B, Skourides P, Norris DJ, Noireaux V, Brivanlou AH,Libchaber A. In vivo imaging of quantum dots encapsulated in phospholipid micelles. Science 2002; 298: 1759-62.

32. Lee P-W, Hsu S-H, Tsai J-S, Chen F-R, Huang P-J, Ke C-J, et al. Multifunctional core-shell polymeric nanoparticles for transdermal DNA delivery and epidermal langerhans cells tracking. Biomaterials 2010; 31: 2425-34.

33. Lees EE, Nguyen T-L, Clayton AHA,Mulvaney P. The preparation of colloidally stable, water-soluble, biocompatible, semiconductor nanocrystals with a small hydrodynamic diameter. ACS Nano 2009; 3: 1121-28.

34. Nehilla BJ, Allen PG,Desai TA. Surfactant-free, drug-quantum-dot coloaded poly(lactide-co-glycolide) nanoparticles: Towards multifunctional nanoparticles. ACS Nano 2008; 2: 538-44.

35. Nurunnabi M, Cho KJ, Choi JS, Huh KM,Lee YK. Targeted near-ir qds-loaded micelles for cancer therapy and imaging. Biomaterials 2010; 31: 5436-44.

36. Weaver J, Zakeri R, Aouadi S,Kohli P. Synthesis and characterization of quantum dot-polymer composites. J. Mater. Chem. 2009; 19: 3198-206.

37. Wu X, Liu H, Liu J, Haley KN, Treadway JA, Larson JP, et al. Immunofluorescent labeling of cancer marker her2 and other cellular targets with semiconductor quantum dots. Nat Biotech 2003; 21: 41-46.

38. Yang X,Zhang Y. Encapsulation of quantum nanodots in polystyrene and silica micro-/nanoparticles. Langmuir 2004; 20: 6071-3.

39. Zhang P,Liu W. Zno qd@pmaa-co-pdmaema nonviral vector for plasmid DNA delivery and bioimaging. Biomaterials 2010; 31: 3087-94.

40. Bourgeois J, Pierson L-A, Nicolas J, Lalanne M, Couvreur P,Andrieux K. Application of thermal analysis to the study of lipidic prodrug incorporation into nanocarriers. J. Therm. Anal. Calorim. 2009; 98: 65-71.

41. Brambilla D, Nicolas J, Le Droumaguet B, Andrieux K, Marsaud V, Couraud P-O, et al. Design of fluorescently tagged poly(alkyl cyanoacrylate) nanoparticles for human brain endothelial cell imaging. Chem. Commun. 2010; 46: 2602-04.

42. Cucullo L, Couraud PO, Weksler B, Romero IA, Hossain M, Rapp E, et al. Immortalized human brain endothelial cells and flow-based vascular modeling: A marriage of convenience for rational neurovascular studies. J. Cereb. Blood. Flow Metab. 2008; 28: 312-28.

43. Schreibelt G, Kooij G, Reijerkerk A, van Doorn R, Gringhuis SI, van der Pol S, et al. Reactive oxygen species alter brain endothelial tight junction dynamics via rhoa, pi3 kinase, and pkb signaling. FASEB J. 2007; 21: 3666-76.

44. Weksler BB, Subileau EA, Perriere N, Charneau P, Holloway K, Leveque M, et al. Blood-brain barrier-specific properties of a human adult brain endothelial cell line. FASEB J. 2005; 19: 1872-74.

45. Cassette E, Pons T, Bouet C, Helle M, Bezdetnaya L, Marchal F, et al. Synthesis and characterization of near-infrared cu−in−se/zns core/shell quantum dots for in vivo imaging. Chem. Mater. 2010; 22: 6117-24.

46. Xie R, Kolb U, Li J, Basché T,Mews A. Synthesis and characterization of highly luminescent cdse−core cds/zn0.5cd0.5s/zns multishell nanocrystals. J. Am. Chem. Soc. 2005; 127: 7480-88.

47. Pierson L-A, Nicolas J, Lalanne M, Brambilla D, Marsaud V, Nicolas V, et al. Formulation of didanosine prodrugs into pegylated poly(alkyl cyanoacrylate) nanoparticles and uptake by brain endothelial cells. J. Nanoneurosci. 2009; 1: 174-83.

48. Allen CN, Lequeux N, Chassenieux C, Tessier G,Dubertret B. Optical analysis of beads encoded with quantum dots coated with a cationic polymer. Adv. Mater. 2007; 19: 4420-25.

49. Aubry J, Ganachaud F, Cohen Addad JP,Cabane B. Nanoprecipitation of polymethylmethacrylate by solvent shifting: 1. Boundaries. Langmuir 2009; 25: 1970-9.

50. Loxley A,Vincent B. Preparation of poly(methylmethacrylate) microcapsules with liquid cores. J Colloid Interface Sci 1998; 208: 49-62.

51. Pic E, Pons T, Bezdetnaya L, Leroux A, Guillemin F, Dubertret B, et al. Fluorescence imaging and whole-body biodistribution of near-infrared-emitting quantum dots after subcutaneous injection for regional lymph node mapping in mice. Mol Imaging Biol 2010; 12: 394-405.

52. Yang RS, Chang LW, Wu JP, Tsai MH, Wang HJ, Kuo YC, et al. Persistent tissue kinetics and redistribution of nanoparticles, quantum dot 705, in mice: Icp-ms quantitative assessment. Environ Health Perspect 2007; 115: 1339-43.

53. Gopee NV, Roberts DW, Webb P, Cozart CR, Siitonen PH, Warbritton AR, et al. Migration of intradermally injected quantum dots to sentinel organs in mice. Toxicol Sci 2007; 98: 249-57.

54. Kim HR, Gil S, Andrieux K, Nicolas V, Appel M, Chacun H, et al. Low-density lipoprotein receptor-mediated endocytosis of pegylated nanoparticles in rat brain endothelial cells. Cell. Mol. Life Sci. 2007; 64: 356-64.

55. Xu P, Gullotti E, Tong L, Highley CB, Errabelli DR, Hasan T, et al. Intracellular drug delivery by poly(lactic-co-glycolic acid) nanoparticles, revisited. Mol. Pharm. 2009; 6: 190-201.

56. Calvo P, Gouritin B, Villarroya H, Eclancher F, Giannavola C, Klein C, et al. Quantification and localization of pegylated polycyanoacrylate nanoparticles in brain and spinal cord during experimental allergic encephalomyelitis in the rat. Eur. J. Neurosci. 2002; 15: 1317-26.

Supporting Information

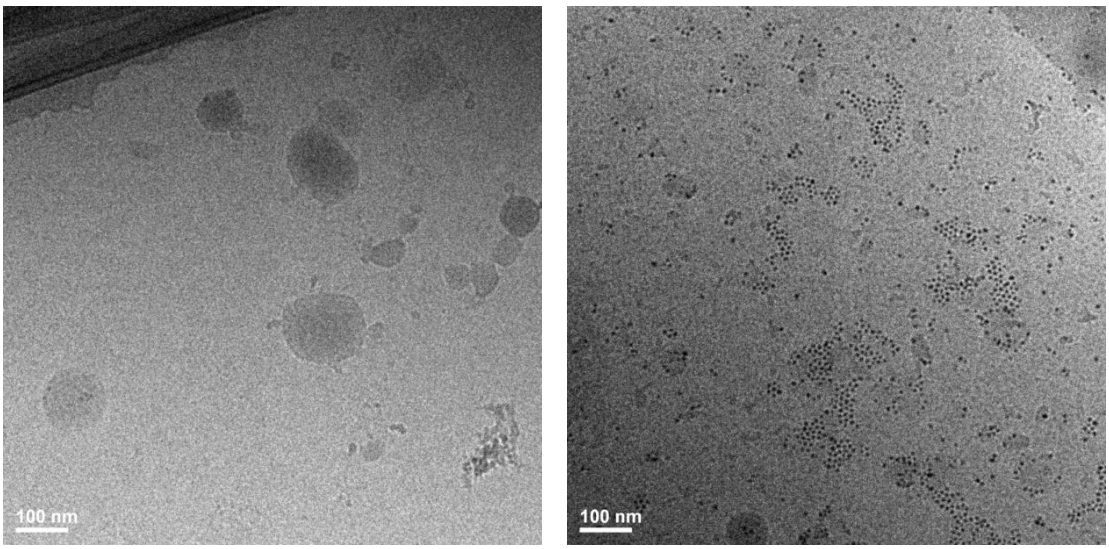

Figure S1. *Cryo-transmission electron microscopy of QD-loaded P(HDCA-co-MePEGCA) nanoparticle suspension N1 after ultracentrifugation on sucrose gradient. Left: empty P(HDCA-coMePEGCA) nanoparticles; right: free QD.*

Section 3

Implications dans le projet NAD

Un nouveau modèle de barrière hémato-encéphalique nous a été fourni par le Docteur P.-O. Couraud de l'unité UMR CNRS 8104 (Institut Cochin, Paris). Ces cellules ont été précédemment caractérisées tant sur le plan morphologique que biochimique. L'objectif de cette partie du projet était, dans un premier temps, de valider le modèle et dans un second temps, d'étudier le passage des nanoparticules fluorescentes P(MePEGCA-*co*-RCA-*co*-PHDCA) précédemment décrites, à travers ces cellules. La finalité du projet est l'évaluation de plusieurs types de fonctionnalisation de nanoparticules pour augmenter leur passage de la BHE. Les protocoles de plusieurs techniques complémentaires, comme la microscopie confocale et la cytométrie en flux, ont été mis au point pour finement explorer l'interaction entre les particules et les cellules. Certaines expériences dont celles avec des nanoparticules fonctionnalisées avec des molécules capables de promouvoir le passage à travers la BHE sont actuellement en cours.

Implications in the NAD project

A novel human BBB *in-vitro* model has been gently provided by Dr. P.-O. Couraud from the UMR CNRS 8104 unit (Institut Cochin, Paris). These cells have been previously thoroughly characterized for morphological and biochemical aspects. The aim of this part of the project was first, to validate the model and secondly, to study the trancytosis across the cells of the previously described fluorescent P(MePEGCA-*co*-RCA-*co*-PHDCA) nanoparticles. The final aim will be the evaluation of different types of nanoparticle functionalization supposed to increase their BBB permeability. Protocols of several complementary techniques, such as confocal laser scanning microscopy and flow cytometry, have been optimized to finely explore the nanoparticles interaction with these cells. Some experiments such as ones with nanoparticles functionalized with molecules able to promote BBB crossing are now running.

Fine evaluation of polymeric nanoparticles endocytosis and transcytosis across a human Blood-Brain Barrier *in vitro* model

Paper in preparation

Davide Brambilla,[1] Benjamin Le Droumaguet,[1] Julien Nicolas,[1] Valérie Nicolas,[2] Patrick Couvreur,[1] and Karine Andrieux[1]

[1] Laboratoire de Physico-Chimie, Pharmacotechnie et Biopharmacie, UMR CNRS 8612, Univ Paris-Sud 11, Faculté de Pharmacie, 5 rue Jean-Baptiste Clément, F-92296 Chatenay-Malabry, France;

[2] Institut d'Innovation Thérapeutique (IFR141 ITFM), Univ Paris-Sud, Faculté de Pharmacie, 5 rue Jean-Baptiste Clément, F-92296 Châtenay-Malabry, France;

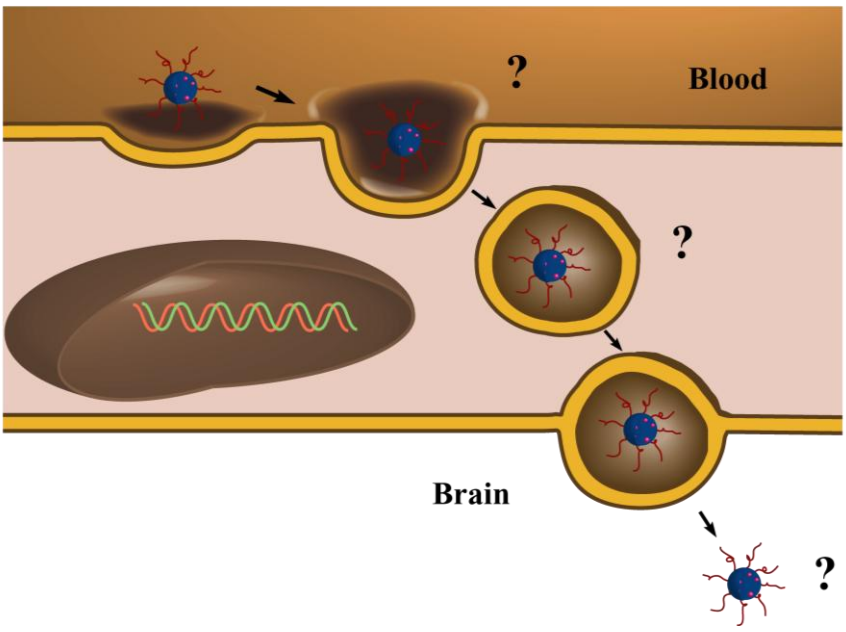

Résumé

La nanomédecine peut constituer une stratégie originale pour la déliverance cérébrale de principes actifs pour le traitement des maladies du système nerveux central. Dans ce but, les systèmes nanoparticulaires doivent démontrer leur capacité à franchir la barrière hématoencéphalique (BHE). A ce jour, peu de publications ont étudié l'intégrité des nanoparticules (NPs) après le passage de la BHE. Dans ce papier, nous proposons d'évaluer l'internalisation mais aussi la transcytose de nanoparticules polymériques à travers un modèle de BHE humaine composée de cellules hCMEC/D3 immortalisées. Des NPs fluorescentes grâce au greffage covalent de la rhodamine ont été incubées avec des cellules confluentes on non et leur internalisation, leur trafic intacellulaire et leur transcytose ont été analysées par microscopie confocale à balayage laser, cytométrie de flux et microscopie électronique à transmission. Ces résultats ont été comparés avec ceux précédemment obtenus avec un modèle de BHE de rat à partir de culture primaire soulignant les différences entre les modèles. Toutes les données conduisent à proposer un passage des NPs à travers le modèle humain de BHE grâce à un mécanisme d'endocytose médiée par un récepteur permettant d'échapper aux lysosomes, où un récepteur à l'Apo E tel que le récepteur aux LDL serait impliqué. Des expériences ultérieures permettront de confirmer ce mécanisme et l'intégrité des NPs après leur passage de la BHE.

Abstract

Nanomedicine can propose an original strategy for drug delivery to the brain for the treatment of central nervous system diseases. With this aim, nanoparticulate systems must demonstrate their ability to translocate through the Blood-Brain Barrier (BBB). Up to now, a low number of publications have studied the integrity of nanoparticles (NPs) after BBB crossing. In this paper, we propose to evaluate the internalization but also transcystosis of polymeric nanoparticles through a novel human BBB model composed of immortalized hCMEC/D3 cells. Rhodamine labelled fluorescent NPs have been incubated with confluent and non confluent cells and their internalisation, intracellular trafficking and transcytosis have been analysed by confocal laser scanning microscopy, flow cytometry and transmission electronic microscopy. The results are compared with the previously obtained with a rat BBB model from primary culture, underlying the differences between models. All the data suggest a passage of these NPs through the human BBB model thanks to a receptor mediated endocytosis pathway allowing lysosome escape where an Apo E receptor such as LDL-r could be involved. Further experiments will be performed to confirm this mechanism and the NPs integrity after their BBB passage.

Keywords

Poly(alky cyanoacrylate) nanoparticles, Blood-Brain Barrier, Transcytosis

1. Introduction

The application of nanotechnologies in medicine and biology for diagnostic or therapeutic purposes has gained great interest in the last decade leading to the birth of a new research field usually termed as Nanomedicine.[1] A consistent part of nanomedicine works are oriented toward the development of "magic bullets" able to selectively bring drugs to a damaged organ reducing their toxicity to periphery and the required dose.[2] The first application of nanomedicine concerns the treatment of cancer where the nanoparticles (NPs) allow to target and increase the drug concentration within tumor cells.[3] Among several nanoparticulate systems, NPs composed of biodegradable Poly(Alkyl Cyanoacrylate) (PACA), represent a well established technology for colloidal nanomedicine. They have been employed in several studies providing promising results against different pathological conditions such as cancer, infections etc. and leading to a phase II/III clinical trial against MDR resistant hepatocarcinoma.[4-7]

A big challenge is represented by the delivery of drugs to the brain being protected by the Blood-Brain Barrier (BBB), a physiological wall essential for brain homeostasis preservation.[8-10] Indeed, it has a tremendous impact on the ability of exogenous molecules, drugs included, to reach the Central Nervous System (CNS). Only 2% of small molecules (<400 Da) can cross the BBB except for the receptor recognized ones. Nanomedicine can propose a solution for the treatment and diagnosis of CNS diseases such as neurodegenerative disorders.[11] To this purpose, NPs must be able carry loaded drug across the BBB, meaning that the transcytosis of NPs through this barrier is essential. Numerous *in vivo* studies have investigated the passage of labeled or drug loaded NPs through the BBB by measuring the tracking agent amount or directly the drug effect in animal brain but few ones have demonstrated the localization of intact NPs inside brain parenchyma.[12-15]

The BBB is composed of 4 different cellular entities: i) astrocytes which the main role is to assure nutrition of endothelial cells, ii) pericytes playing as mechanical support for endothelial cells, iii) neurons that could be connected to the others cellular types and iv) the endothelial cells strongly connected by means of tight junctions composed of intracellular, transmembrane and extracellular proteins. The cross talk between these cells endows to the BBB a unique phenotype, comprising not only the morphological barrier of the inter-endothelial tight junctions, but also the enzymatic and metabolic barrier and the uptake and efflux transport.[9]

The development of *in vitro* reconstituted models of the BBB from different mammalian species, employed since late 1970, allowed facilitating the study of the physiology and the pathophysiology of the BBB. Even if they do not completely mimic the *in vivo* environment, several models have been proposed, characterized and employed to identify the BBB permeability of drugs.[16] At the moment these models, even if intrinsically limited and not fully comparable between them, represent an essential tool for studying NP capacity to cross the barrier.

In vivo previous experiments on rat and mice have evidenced that PEGylation of PACA based nanocarriers allowed, after intravenous injection, a drastic increase of their bloodstream half-life and an interesting ability to cross the BBB, even if in small proportions.[12-13, 17] *In vitro* experiments have been performed using a new rat BBB model based on primary culture of rat endothelial cells and astrocytes.[18] They permitted to finely elucidate the molecular mechanism governing the passage across the BBB: once in the bloodstream the PEGylated nanocarriers can adsorb, among other serum proteins, the Apolipoprotein E (Apo E) which can be recognized by Low Density Lipoprotein receptor (LDL-r) expressed from brain endothelial cells mediating the NPs endocytosis.[19-22]

In this work, in order to anticipate the application of these NPs in clinic, a human BBB model has been chosen. This stable and fully characterized BBB model based on well-differentiated human brain microendothelial cell line (hCMEC/D3) has been recently developed and applied for several permeability studies.[23-24] In order to follow NPs uptake and intracellular distribution fluorescent-labeled NPs are usually employed. A commonly strategy used to prepare fluorescent NPs is based on the encapsulation of a lipophilic dye within the solid matrix or a liquid core. However several problems may occur following this procedure: i) the fluorescent dye can leak the nanoparticles leading to inappropriate evaluations, ii) adsorption of part of fluorescent dye at the surface of the nanoparticles which release may not correspond to the nanoparticles biodegradation.[25] To prevent interference from artifacts, we recently detailed the synthesis of a fluorescent polymer based on Poly(hexadecyl cyanoacrylate-*co*-Rhodamine cyanoacetate-*co*-methoxypoly (ethylene glycol)) (P(HDCA-*co*-RCA-*co*-MePEGCA)) able to self-assemble in nanoparticles.[23, 26] Moreover the encapsulation of several types of quantum dots in these NPs (QD/P(HDCA-*co*-RCA-*co*-MePEGCA NPs) has been performed leading to a double fluorescently labeled NPs, a useful tool for studying the integrity of particles during BBB crossing process.[26]

The aims of this work are i) to finely describe the P(HDCA-*co*-RCA-*co*-MePEGCA) NPs up-take kinetic by hCMEC/D3, ii) to compare the entry mechanism of these NPs between rat and human models and iii) to quantify the NPs transcytosis across the human model. The results would help to evaluate the ability of these NPs to reach the brain parenchyma in a particulate form.

2. Experimental section

2.1 Materials and chemicals

Poly[hexadecyl cyanoacrylate-*co*-rhodamine B cyanoacrylate-*co*-methoxypoly (ethylene glycol) cyanoacrylate] P(HDCA-*co*-RCA-*co*-MePEGCA) copolymers, poly[hexadecyl cyanoacrylate-*co*-methoxypoly (ethylene glycol) cyanoacrylate] P(HDCA-*co*-MePEGCA) were obtained following previously reported procedures.[4,23] Dulbecco's phosphate buffer saline (DPBS) without $CaCl_2$ and $MgCl_2$ and EMB-2 medium were purchased from Lonza. Penicillin 10,000 units-Streptomycin 10,000 $\mu g.mL^{-1}$, Trypsin/EDTA and Chemically Defined Lipid Concentrate were obtained from Invitrogen, Gibco. Pluronic F-68, hydrocortisone, Trypsine/EDTA 1X, human basic fibroblast growth factor (bFGF) cell culture tested, glycerol, TRIS buffer, Sodium Dodecyl Sulfate (SDS), 3',3",5',5"-tetrabromophenolsulfonphthalein (bromophenol blue), 1,4-dithioerythritol (DTE), acrilammide (40%), tetramethylethylenediamine (TEMED), ammonium persulfate (APS), paraformaldehyde (PFA), CHAPS (3-[(3-Cholamidopropyl) dimethylammonio]-1-propanesulfonate), Thiourea, Urea, Glycerol, SDS, Dithiothreitol (DTT), Iodocetamide, Glycine, Tris buffer, Sypro ruby, Agarose, Bradford Reagent ammoniun persulfate (APS), and ascorbic acid were purchased from Sigma-Aldrich. Quantum Dots have been prepared as previously described.[26] Poly (vinylalcohol) (PVA, 30-70 kDa, cell culture tested) was purchased from Fluka. HEPES 1 M was obtained from PAA The Cell Culture Company. Fetal bovine serum was purchased from Eurobio. hCMEC/D3 human brain endothelial cell line was prepared as described elsewhere.[24] Sprague-Dawley rat serum was purchased from Charles-River Laboratories. Mouse anti-human Lysosomes Associated Membrane Protein 2 (LAMP-2) polyclonal antibody, mouse anti-human 58K Golgi protein (Clone, 58K-9) monoclonal antibody, mouse anti-human Protein Disulphide Isomerase of Endoplasmic Reticulum (Clone, RL90) monoclonal antibody and rabbit anti-human early-endosomes (EEA1) polyclonal antibody were purchased from Abcam. Alexa Fluor 488 anti-mouse and Alexa-Fluor 488 anti-rabbit were purchased from Molecular Probes. Goat anti-human Low Density Lipoprotein Receptor (LDL-r) monoclonal antibody, goat anti-rat ApolipoproteinE polyclonal antibody and HRP mouse anti-goat were purchased from Santa-Cruz Biotechnology. Vectashield mounting medium was purchased from Vector. 13mm diameter glass disks (0.7mm thickness) were purchased from Thermo Scientific.

Collagen pre-coated Transweell® (0.45µm porus, 24mm diameter) were purchased from Corning. Amicon centrifugation filters (0.5mL, 30KDa) were purchased from Millipore. All solvents were purchased at the highest grade from Carlo Erba. 2-D uncontinous gel 7 cm, pH 3-10 (Immobilin™ Drystrip gels) was purchased from GE-Healthcare.

2.2 Nanoparticles preparation

Nanoparticles were prepared using P(HDCA-*co*-RCA-*co*-MePEGCA) according to a protocol previously published by our group: 10 mg of copolymer was dissolved in acetone (2 mL) and added dropwise to an aqueous solution 0.5 % (w/v) of Pluronic F-68 (4 mL) under vigorous mechanical stirring. A purple suspension was observed almost instantaneously. Acetone was then evaporated under reduced pressure and nanoparticles were purified by ultracentrifugation (150,000 g, 1 h, 4°C, Beckman Coulter, Inc.). The supernatant was discarded and the pellet was resuspended in the appropriate volume of nanopure water to yield a 2.5 $mg.mL^{-1}$ nanoparticle suspension. Quantum dots loaded particles have been prepared and purified as previously described by our group.[26]

2.3 Nanoparticles characterization

The nanoparticle diameter (D_z) was measured by Dynamic Light Scattering (DLS) with a Nano ZS from Malvern (173° scattering angle) at 25 °C. The nanoparticle surface charge was investigated by ζ-potential measurement at 25°C after dilution with 1 mM NaCl solution applying the Smoluchowski equation and using the same apparatus.

2.4 Cell culture protocols for NPs internalization by confocal microscopy

hCMEC/D3 cells were seeded on 12 mm diameter glass disks at a concentration of 50,000 $cells.cm^{-2}$ using EBM-2 basal medium supplemented with fetal bovine serum 5%, hydrocortisone 1.4 µm, basic fibroblast growth factor 1 $ng.mL^{-1}$, penicillin:streptomycin solution 1%, HEPES 10 mM, ascorbic acid (5 $\mu g.mL^{-1}$) and chemically defined lipid concentrate (1/100).

For experiments with confluent cells, after 3 days, medium was replaced with fresh one and at day 7 cells were treated with an aqueous solution of fluorescent NPs (30 $\mu g.mL^{-1}$) for different times: 5 min, 20 min, 60 min, 6 h, 12 h and 24 h. Finally the cells were fixed using PFA 4% and different cellular regions were marked using the specific antibodies. Alexa Fluor 488 IgG was employed for fluorescence detection. Non treated cells were used as control. For experiments in non-confluent conditions, cells were seeded at 50,000 $cells.cm^{-2}$ and treated with nanoparticles after 3 day of culture.

Observations were made by sequential acquisition with a Zeiss LSM-510 confocal scanning laser microscope equipped with a 30 mW argon laser and 1 mW helium neon laser, using a Plan-Apochromat 63X objective lens (NA 1.40, oil immersion). Red fluorescence was observed with a long-pass 560 nm emission filter and under a 543 nm laser illumination. Green fluorescence was observed with a band-pass 505 and 550 nm emission filter and under a 488 nm laser illumination. The pinhole diameter was set at 61 µm giving an optical section thickness of 0.6 µm. Stacks of images

were collected every 0.3 µm along the z axis. 12 bit numerical images were acquired with LSM 510 software version 3.2.

2.5 NPs uptake experiments at 4°C by confocal microscopy

In order to assure that an endocytosis mechanism govern the up-take of nanoparticles within hCMEC/D3 cells, the confluent cells obtained according to the protocol described above (chap. 2.4) have been treated with fluorescent P(HDCA-*co*-RCA-*co*-MePEGCA) NPs for 20 min or 12 h at 4°C in order to block all energy-related cellular process, endocytosis included. Subsequently the cells have been fixed with PFA (4%) stored in dark at 4°C and analyzed by confocal laser scanning microscopy with a long-pass 560 nm emission filter and under a 543 nm laser illumination. Cells treated at 37°C were employed as control.

2.6 NPs uptake experiments at 4 and 37°C by flow cytometry analysis

NPs uptake at different time points was quantified using a C6 Flow Cytometry system (Accuri Cytometers). Cells were seeded in a 24 wells plate at a concentration of 50,000 cells.cm^{-2}. After 7 days (confluence reached) cells were treated with an aqueous suspension of fluorescent nanoparticles (final concentration 30 µg.mL^{-1}) for 5 min, 20 min, 60 min, 1 h, 6 h, 12 h and 24h at 37 or 4°C. Subsequently the cells were extensively washed with PBS, dispersed by tripsination and fixed with PFA (1%). Resulting sample was analyzed by Flow cytometry using CFlow™ Software (Accuri Cytometers). During the experiments cell debris were excluded by setting an appropriate gate of side-scattered light (SSC) *vs* forward-scattered light (FSC). A total of 20,000 gated cells were analyzed. The increase of fluorescence intensity in cells treated with nanoparticles was expressed as mean fluorescence increase relative to non-treated cells.

2.7 LDL-r expression from hCEMC/D3 cells

The expression of LDL-r was evaluated by immunoblotting analysis. Confluent cells were lysated and proteins were migrated on SDS-page electrophoresis gel (8% acrylammide). Bands were transferred on nylon membrane. Following incubation with specific anti-LDL receptor antibody (goat anti-human, Santa-Cruz Biotechnology INC.) and extensive washing with PBS containing 0.05% Tween-20 (PBS-T), membranes were incubated with horseradish peroxidase-conjugated mouse anti-goat IgG for 1 h at 37°C. Membranes were extensively washed with (PBS-T), and bands were visualized by enhanced chemioluminescence detection.

2.8 Apo E adsorption on nanoparticles

The adsorption of Apo E at the surface of these fluorescently labeled NPs was evaluated by immunblotting as previously described.[20] 350 µL of nanoparticles suspension (20mg.mL^{-1}) was incubated in 1.75 mL of Sprague-Dawley rat serum for 20 min at 37°C. Plasma proteins adsorbed onto the nanoparticles were separated from bulk serum by centrifugation (15,000g for 1.5 h at 4°C). The supernatant was discarded, and the pellet was washed by centrifugation (15,000g for 1.5 h at 4°C) to remove the excess of serum. After the centrifugation the NPs were resuspended in 100 µL of a solution containing 2.5% of SDS and 30 mM DTE, and incubated at 50°C for 2 h to detach the proteins from the NPs surface. The solution was then centrifuged (15,000g, 1 h at 4°C) to eliminate the NP. The supernatant was collected and migrated on SDS-page electrophoresis gel (12% acrylammide), the proteins were transferred on a nylon membrane. After extensively washing with PBS-T, Apo E was detected using a specific primary antibody and HRP-conjugated IgG. The bands were visualized by enhanced chemioluminescence detection.

2.9 2D-PAGE electrophoresis

The previously mentioned protein solution was applied to the gel as follows. For isoelectric focusing (IEF), 133 µg of adsorbed plasma protein dissolved in 125 µL of aqueous solubilization solution (7M Urea, 2 M Thiourea, 3% CHAPS, 10 nM DTT and 0.5% IPG Buffer) was loaded onto pH 3-11 nonlinear strips and leave rehydrated for 5 h at room temperature. IEF was carried out for about 40 000 V.h as follows: 50 V for 2 h (stable), 300 V for 1 h (gradient), 1000 V for 2 h (gradient), 5000 V for 4 h (gradient) and 5000 V for 3 h (stable). The gels were incubated for 15 min with equilibration buffer 1 (Tris pH 8.8 50 mM, Urea 6 M, Glycerol 30%, SDS 2% and DTT 10 mM) and with equilibration buffer 2 (Tris pH 8.8 50 mM, Urea 6 M, Glycerol 30%, SDS 2% and iodoacetamide 2.5%) 15 min. The second dimension were applied on 12 % polyarylamide gels at 80 V, 15 mA/gel 25 W for 15 min and 150 V, 40 mA/gel 25 W for around 2 h, per gel until the dye front reached the lower end of the gel. Fluorescence (Sypro Ruby) staining of proteins was performed with the gels and visualized with Typhoon™ 9410 Variable Mode Imager (λex: 488nm, λem: 610nm BP30 filter). The protein spots were identified by matching the gels to the sera reference map and to the gels described by Kim et al.[20]

2.10. Cell culture protocols for NPs translocation

BBB *in vitro* model was prepared as previously described.[24] Briefly, hCMEC/D3 cells were seeded on 4.67 cm^2 diameter 0.45 µm pore size collagen pre-coated transwells at a concentration of

50,000 cells.cm^{-2} using the same medium described in previous paragraph both in apical i.e. upper chamber and basolateral i.e. under chamber compartments. At day 3 the medium was replaced with fresh one. At day 7 permeability experiments were performed.

In order to characterize the model, trans-endothelial electrical resistance (TEER) measurements were performed using EVOM apparatus (World Precision Instruments Inc.) starting from day 0 up to day 7. Transwells without cells were employed as control.

2.11. Permeability studies on cell-covered transwells

[^{14}C]-Sucrose permeability was measured as previously described.[24] After 7 days of culture, sucrose was added to the upper chamber, the lower chamber was sampled after 0, 5, 20 and 60 minutes and the radioactivity that passed through the cell-covered transwells was determined by using β-scintillation counter (Beckman Coulter LS6500). The clearance principle was used to obtain a concentration-independent transport parameter. Cleared volume, obtained as described by M.P. Dehouch et al.[27], was plotted against time and the slopes of the curves were employed to calculate the Permeability Coefficient (Pe) of the model:

$$1/Ps = 1/me - 1/mf$$

$$Pe = Ps/s$$

Where *me* and *mf* are the slopes of the curve corresponding to BBB model and transwell only, respectively and *s* is the surface of the filter (cm^2). The same protocol, but using fluorescence detection, was employed in order to study the permeability of rhodamine B cyanoacetate, the fluorophore employed for NPs labeling.

2.12. Translocation of nanoparticles on cell-covered transwells

The translocation of fluorescently tagged nanoparticles was studied by following fluorescence signal across the cell-covered transwells. A medium containing a solution of NPs (final concentration 30 μg.mL^{-1}) was deposed within the apical chamber, after different elapsed times, the apical and basolateral chambers media were withdrawed and the fluorescence was measured by using a Luminescence Spectrometer LS50B (Perkin Elmer) with excitation λ of 564 nm. Fluorescence signal was then employed to measure a permeability coefficient for the NPs across this human model by using the same formula previously described. NPs passage was evaluated also after longer incubation times: 6 h and 12 h.

To assure the absence of topical effect of the employed nanoparticles on the cellular monolayer, sucrose permeability and TEER measurement were performed after treatment with the particles.

2.13. Nanoparticles identification after passage

To identify the nanoparticles within the receiving chamber, after setting-up of the model, nanoparticles were added within the donor chamber at 30 µg.mL^{-1} and leaved onto the cells for 12 h. The medium within the basolateral chamber was collected and concentrated using a Micon Bioseparation (Microcon) 0.5 mL 30 kDa. The resulting sample is then observed using Transmission Electron Microscopy (Philips EM208). 5 µL of samples were deposed on a copper grid and leave dry at room temperature. The samples were then visualized by TEM operating at 60 kV at a nominal magnification of 20,000 to 90,000. The images were directly recorded with a AMT-40 CCD camera (Hamamatsu). The receptor chamber of a sample not treated with nanoparticles and concentrated in the same way was used as negative control. Moreover, a mere suspension of nanoparticles (30 µg.mL^{-1}) in medium was concentrated in the same way and used as positive control.

3. Results and discussion

Fluorescently labeled NPs have been investigated to finely study their endocytosis, their intracellular localization and finally their transcytosis through hCMEC/D3 cells used as a human BBB model. hCMEC/D3 cells have been investigated according both protocols for internalization and translocation experiments. All the data have been compared with previous results obtained with a rat BBB model from primary cultures.

3.1. Nanoparticles characterization

The purified fluorescent nanoparticles were characterized by DLS and ζ-potential measurements. PEGylated nanoparticles, P(HDCA-*co*-RCA-*co*-MePEGCA) and QD/P(HDCA-*co*-RCA-*co*-MePEGCA) NPs, presented an average diameter in the 100-200 nm range (124 and 171 nm, respectively) with narrow particle size distribution (0.106 and 0.119, respectively) and exhibited a negative ζ-potential (-35 and -16 mV, respectively).[26] The characteristics of these NPs are similar to the fluorescently and radio-labeled NPs used in previous studies with the rat BBB model.[18, 21] The protocols described for the nanoparticles preparations provide stable colloidal suspensions of particles with absence of toxic effects on hCMEC/D3 cells according to previous MTT tests.[23, 26]

3.2. NPs internalization and intracellular localization

During the evaluation of NPs internalization and intracellular localization, the hCMEC/D3 cells were seeded on glass disks or well plates for confocal laser microscopy or flow cytometry analyses, respectively.

3.2.1. NPs uptake in confluent cells

For these uptake experiments, hCMEC/D3 cells have been cultured at confluence (7 days culture) in order to better reproduce *in vivo* endothelial cells conditions and avoiding the influence of mitotic process on nanoparticles up-take (see chap. 3.2.2). Figure 1a, b showed a clearly uptake of fluorescent NPs by cells. The punctuated localization of red fluorescence in cells suggested the presence of NPs into vesicles and an entry mechanism by endocytosis. The covalent linkage of fluorescent dye to polymer matrix allows us to avoid all the artifacts due to dye leakage from the particles in medium and to get highly resolute images. Previous results revealed only 11–14 % of fluorescence loss due to polymer degradation after 8 h incubation of these fluorescent nanoparticles at different concentrations with Fischer rat plasma at 37°C suggesting a very low release in cell culture medium composed of only 10% of serum.[23] Since rhodamine is a substrate of P-gp pump which are expressed from this model line,[28] the presence of the dye within the cells confirms the absence of its leakage from the particles before their cell penetration. Another proof of NPs internalization has been previously published using double fluorescent labeled QD/P(HDCA-co-RCA-co-MePEGCA) NPs.[26] These data have shown a colocalization of the fluorescences from rhodamine and quantum dots inside hCMEC/D3 cells by confocal microscopy evidencing the integrity of the NPs which have been up-taken by the BBB cells.

Flow cytometry analyses were employed to identify and quantify the nanoparticles internalization within hCMEC/D3 cells. Figure 2 showed the normalized amount of NPs internalized within the cells as a function of incubation time. After 24 h at 37°C, a 400% increase on intracellular fluorescence was observed. The NPs internalization started suddenly after NPs interaction with the cells, describing a fast internalization process. To assure that an endocytic mechanism is governing the NPs internalization, the endothelial cells have been treated with fluorescent NPs at 4°C. Figure 2 shows the quasi-total absence of NPs internalization within cells stored at 4°C (the small increase observed would be due to the practical working-time at room temperature). Confocal microscopy experiments confirmed the difference of NPs internalization when the cells were stored at 4 or 37°C (Figure 1). These results evidenced that these NPs are internalized in these cells by an endocytosis

mechanism, as previously described with the rat BBB model.[21] So the entry process of these NPs seems identical in both BBB models.

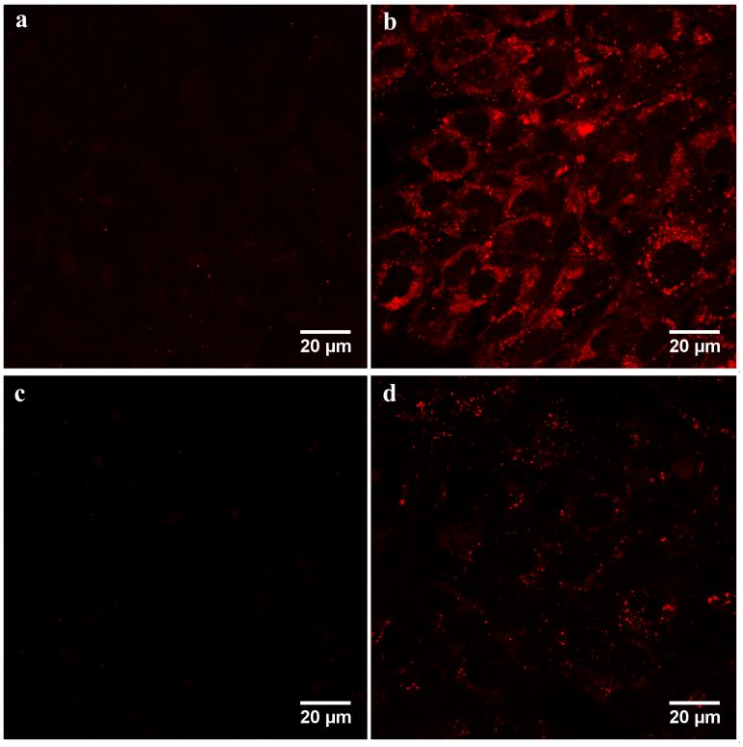

Figure 1. *Confocal microscopy of hCMEC/D3 cells treated with fluorescent P(HDCA-co-RCA-co-MePEGCA) nanoparticles for 20 min at 37°C (a) or 4°C (c) and for 1 h at 37°C (b) or 4°C (d).*

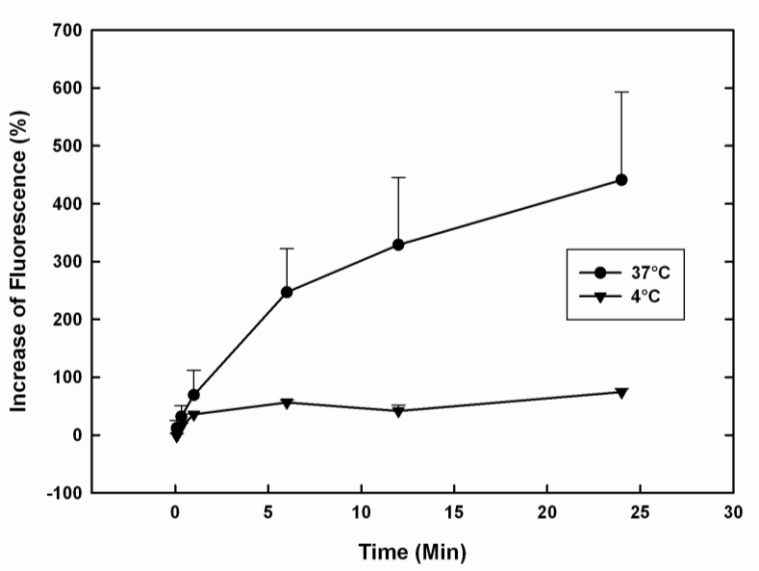

Figure 2*. Flow Cytometry experiments of rhodamine labeled NPs internalization within hCMEC/D3 cells at 37 (●) and 4°C (▼).*

3.2.2. Cell division influence on nanoparticles up-take and intracellular trafficking

Experiments have been performed by confocal laser scanning microscopy using non-confluent cells (Figure 3). Several dividing cells were identified during the visualization of non-confluent cells treated with fluorescent particles underlining the normal activity of cell cycle in presence of nanoparticles. Interestingly a drastic increase of nanoparticles up-take from dividing cells and a specific intracellular trafficking during mitotic division were observed (Figure 3). So far, different contrasting theories have been proposed to describe the progress of endocytosis during mitotic event. However, a recent work by Boucrot et al., demonstrated that during the mitosis the endocytosis process is kept constant while membrane recycling to the surface is strongly reduced in order to supply the cells of necessary materials for cell division.[29] At this reduced recycling we can more likely attribute the increase of the particles amount within the dividing cells.

Moreover, the vesicles containing the particles, placed at the extremity of the cells during the early stage of dividing cycle (Prophase/Metaphase), are trafficked to the midbody area of the dividing cells, where membrane material is required for the cytokinesis, tracing filamentous-like structures more likely highlithing the actin microtubules (Figure 3).[30] These results give clear information on the NPs trafficking once internalized within human brain endothelial cells confirming the endocytosis mechanism.

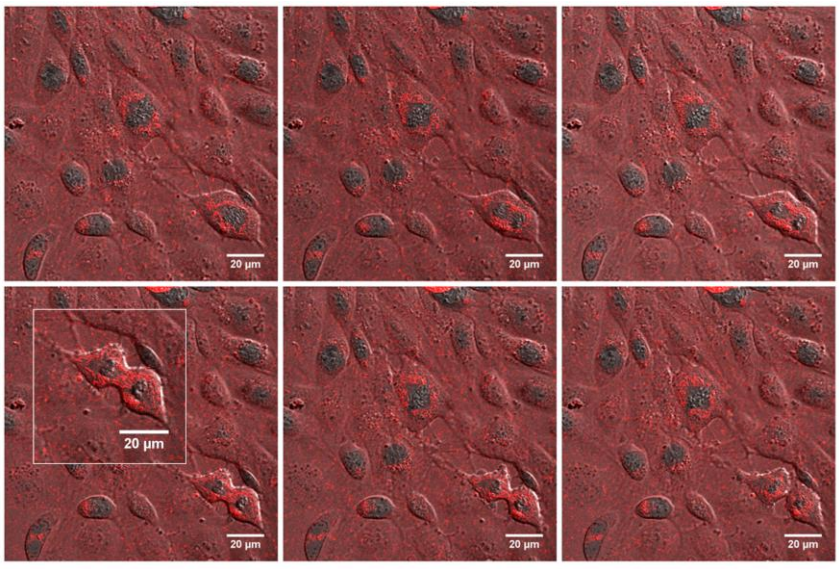

Figure 3. *Sequential contrast images merged with red fluorescence signals of hCMEC/D3 cells treated with fluorescent P(HDCA-co-RCA-co-MePEGCA) nanoparticles 30 µg.mL-1. (time = 0-9 min). (Inlet) Zoom of mitotic cell.*

3.2.3. Intracellular localization of nanoparticles in confluent cells

The intracellular localization of NPs was identified in confluent cells using specific antibodies (Ab) for Golgi apparatus, Endoplasmic Reticulum, Endosomes and Lysosomes. Once reached the confluence (7 days after seeding) cells were treated with fluorescent nanoparticles for different incubation times, fixed, treated with specific Abs and observed by confocal laser scanning microscopy.

No NPs were observed within Golgi apparatus or Endoplasmic Reticulum after all the analyzed incubation times (Figure 4), showing an expected time-independent non-involvement of these two cellular compartments in NPs up-take from cells.

On the contrary a large amount of red signal was observed within endosomal vesicles and, after longer incubation times, within the lysosomes (Figure 4). Interestingly some nanoparticles do not co-localize with these two compartments suggesting a double internalization mechanism or an escape of endosomes/lysosomes for some nanoparticles.

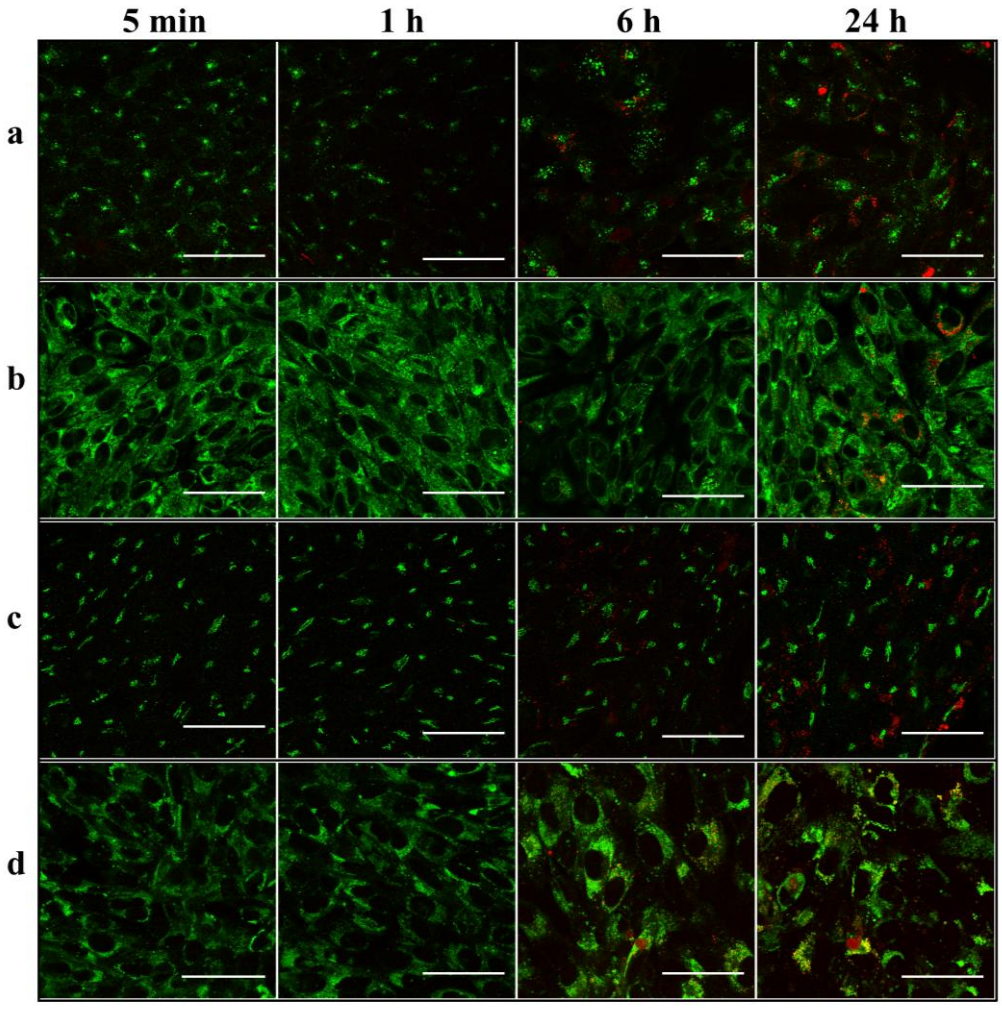

Figure 4. *Confocal microscopy pictures of hCMEC/D3 cells treated with fluorescent P(HDCA-co-RCA-co-MePEGCA) (red signal) nanoparticles for increasing elapsed times. Visualization of different intracellular compartments using specific antibodies (green signal): (a) anti-Early Endosomes, (b) Endoplasmic Reticulum, (c) Golgi apparatus, (d) Late endosomes/Lysosomes. Scale bar = 50 µm.*

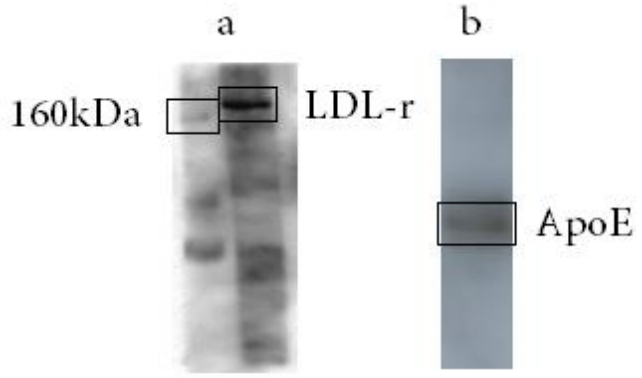

Figure 5. *Expression of LDL-r from hCMEC/D3 cells (a) and adsorption of Apo E at the surface of the Rhodamine labeled nanoparticles (b).*

3.2.4. NPs internalization mechanism

Previous works from our group showed the pivotal role of LDL-receptor on the NPs internalization process within rat brain endothelial cells. Indeed, these PEGylated nanoparticles can "capture" the ApolipoproteinE (Apo E) in (rat or human) serum which is recognized by LDL-r at the surface of brain endothelial cells and internalized.[21] Then, the expression of the receptor in the new human model was checked by WB using a specific HRP-conjugated Ab. The experiments clearly demonstrated the expression of the LDL-r by the hCMEC/D3 cells (Figure 5a). Again, to check that Apo E can adsorb on the Rhodamine tagged NPs as observed on non-labeled NPs used in previous studies, WB was performed in the same conditions using rat serum.[19] The experiments showed the presence of Apo E at the NPs surface once incubated in rat serum (Figure 5b). Moreover, a 2D electrophoresis was performed after NPs incubation in rat serum in order to check the total protein pattern adsorbed at the surface of the nanoparticles (Figure 6). The protein spots were identified by matching the gels to the rat serum 2D PAGE reference map. The same pattern of proteins obtained with non-labeled P(HDCA-*co*-MePEGCA) nanoparticles in rat serum[19] was obtained with these labeled nanoparticles suggesting rhodamine labeling has no influence on protein adsorption at the surface of NPs. It is to note that Apo E from human serum can also adsorb on non-labeled NPs according to previous work[19] suggesting that this adsorption can also occur on labeled NPs when incubated in human serum.

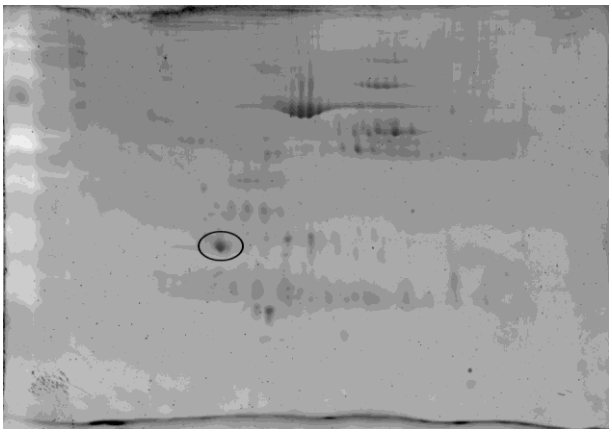

Figure 6. *Sypro ruby stained 2-D page gels of adsorbed proteins on the P(HDCA-co-RCA-co-MePEGCA) nanoparticles after 20 min incubation in rat serum. Indicated spots: Apo E identified by the rat serum 2D PAGE reference map.*[31]

3.3. NPs translocation

Translocation of fluorescent NPs has been performed using hCMEC/D3 cells seeded on transwell system.

3.3.1. Validation of the BBB model for NPs translocation experiments

The BBB model composed of hCMEC/D3 cells cultured on an insert system was first validated by measuring TEER and permeability of small hydrophilic marker as previously described.[24] TEER measurements on the monolayer of hCMEC/D3 cell line confirmed (Figure 7) the resistance values previously described for the employed model.[24] These values at the plateau are close to those observed with primary culture of rat endothelial cells.[18] Moreover this experiment evidenced the stabilization of TEER values after 7 days when the cells reach the confluence.

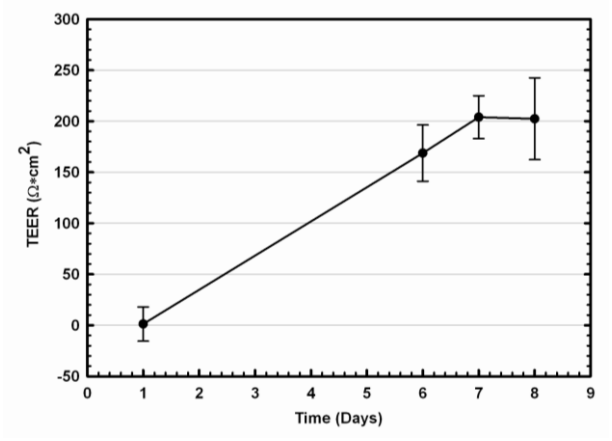

Figure 7. *TEER measurements as function of time on hCMEC/D3 cells cultured on Transwell filters.*

The quality of the monolayer formed by the hCMEC/D3 cells, grown to confluence on semipermeable Transwell filters, was also evaluated by their permeability to sucrose, a hydrophilic molecule routinely employed as paracellular permeability marker. As reported in table 1, the permeability of the model is around 2.5 x 10^{-3} cm.min^{-1}, in the same magnitude of previous works on the model.[24] However the sucrose permeability with this model looks higher compared to value obtained from previously employed rat model[18] as expected when cell line is compared to primary culture.

3.3.2. NPs translocation experiments

The validated *in vitro* BBB model was employed to study the NPs transcytosis. Fluorescence intensity measurements were used to follow and quantify the fluorescent polymer across the model. The same formula employed to calculate the sucrose permeability coefficient (Pe) was applied to measure the NPs permeability coefficient (Tab. 1). As a control the permeability of Rhodamine cyanoacetate was measured. The results showed a low permeability of free Rhodamine likely due to the expression of Multi Drug Resistance protein from the cells as previously reported.[24] Moreover the higher Pe value of Rhodamine tagged NPs, indicate an important ability of these NPs to cross the BBB, clearly evidencing that these particles increased the passage of Rhodamine Cyanoacetate, the marker used to label the particles.

Table 1. *Permeability coefficients of hCMEC/D3 cells (n ≥ 3 except for rhodamine cyanoacetate)*

	Permeability Coefficient (Pe) (x 10^{-3} cm.min^{-1})
^{14}C Sucrose	2.8 ±0.26
^{14}C Sucrose + P(MePEGCA-co-RCA-co-HDCA) NPs	2.65±0.28
Rhodamine Cyanoacetate	0.48
P(MePEGCA-co-RCA-co-HDCA) NPs	1.8 ± 0.50

The co-incubation of sucrose and NPs do not modify the Pe of sucrose evidencing the absence of any toxic effect of NPs on cells such as tight junction opening. Moreover TEER values measured after NPs incubation during 12 h were not modified. These points evidenced the passage of the NPs by a transcellular pathway.

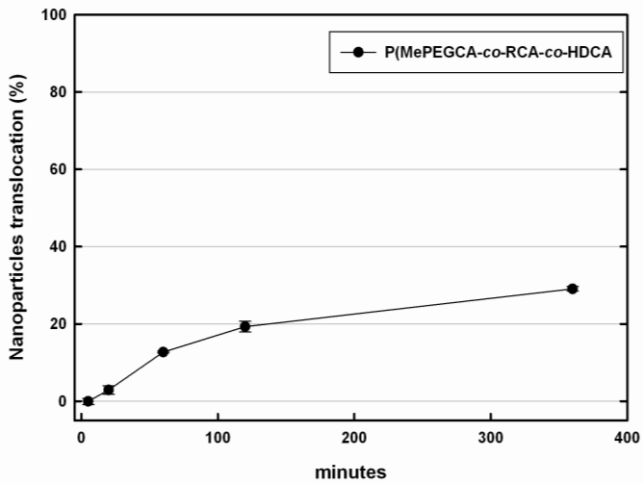

Figure 8. *Translocation kinetic as a function of time of rhodamine labeled P(MePEGCA-co-RCA-co-HDCA) nanoparticles across hCMEC/D3 cells after 7 days in culture.*

The kinetic of nanoparticles transcytosis was also evaluated in terms of percentage evolution as a function of time incubation (Figure 8). Important passage ability for these nanoparticles is observed. Up to 25% of fluorescence is recovered within the basolateral chamber after 6 h of incubation. An interesting difference was observed compared to rat model, where the passage was significantly slower.[18] By comparing this result and the intracellular localization experiment it's interesting to observe that an appreciable amount of particles crosses the BBB model already after 1 h incubation and that at this time point any nanoparticle is observed within the lysosomes, confirming the presence of a receptor mediated transcytosis process able to bypass the lysosomes compartment.

3.3.3. NPs identification after passage

An essential information investigated by only a low amount of works remains the identification of a nanoparticulate system within the basolateral compartment. Indeed, the most of the works are just limited to quantification of the tracker (radiomarker or fluorescence) after passage. In order to evaluate the presence of nanoparticles in the receiving chamber, transmission electron microscopy (TEM) experiments were employed. The receiving medium was filtered and concentrated in order to retain the bigger entities. TEM images showed the presence of spherical objects of around 120 nm within the positive control and within the basolateral chamber of sample treated with NPs (Figures 9 a and b, respectively), whereas the same objects were not observed within the negative control (typical slat crystals were detected, Figure 9c). These results represent a preliminary proof of the passage of intact nanoparticles across this BBB model. Additional figures are given in Supporting Information.

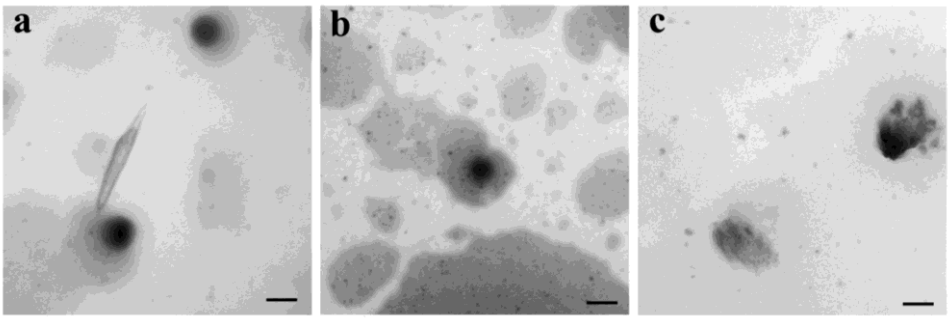

Figure 9. *Representative TEM images of: cell culture medium doped with P(MePEGCA-co-RCA-co-HDCA) nanoparticles (a), basolateral chamber of BBB in vitro model after 12 h treatment with P(MePEGCA-co-RCA-co-HDCA) nanoparticles (b) and basolateral chamber of BBB in vitro model non treated with nanoparticles (c). Scale bars = 100nm.*

4. Conclusions

In this paper the internalization and the transcytosis of polymeric P(HDCA-*co*-RCA-*co*-MePEGCA) nanoparticles within a novel human BBB *in-vitro* model has been studied in details. A recently designed fluorescent polymer has been employed to build the nanoparticles and to assure the absence of fluorescence leakage phenomenon during all the experiments. Once incubated with the hCMEC/D3 cells, fast and strong nanoparticles internalization was observed with an increase of fluorescence up to 400% after 24 h of incubation. The same experiments performed at 4°C showed the absence of NPs internalization indicating an active internalization process.

Our experiments demonstrated an interesting influence of cell division onto the internalization process; indeed an increased up-take and a precise intracellular distribution are observed, and corroborated by theoretical hypothesis, in dividing cells. This highlights the importance of uniformity on the cell culture timetable for all the internalization/transcytosis experiments.

Moreover, the comparison of the results obtained using the hCMEC/D3 model showed a significant variation compared to previous described with primary rat model, especially in terms of internalization and transcytosis kinetics which are significantly faster using this human model. This allows stressing the difficulty of comparison between different cellular models.

A particular attention has been dedicated to the integrity of the particles once crossed the BBB model. A first proof of the integrity of these particles up to 24 h within the hCMEC/D3 cells has been reported in this paper by using TEM microscopy. Further experiments based on following the passage

of double labeled (QD/Rhodamine) NPs will be performed to confirm the presence of intact particles within the basolateral medium.

All the data lead to propose a passage of these NPs through the human BBB model thanks to a receptor mediated endocytosis pathway allowing lysosome escape where an Apo E receptor such as LDL-r could be involved. To confirm this hypothesis, the specific transcytosis mechanism of these polymeric nanoparticles will be more precisely identified by using specific inhibitors for endocytosis mechanism such as sodium azyde, chloropromazine, receptor associated protein and others. The mitosis influence on nanoparticles could be in-depth studied by using cell division synchronising molecules.

5. References

1. Webster TJ. Nanomedicine: What's in a definition? Int J Nanomedicine 2006; 1: 115-6.

2. Farokhzad OC,Langer R. Impact of nanotechnology on drug delivery. ACS Nano 2009; 3: 16-20.

3. Blanco E, Hsiao A, Mann AP, Landry MG, Meric-Bernstam F,Ferrari M. Nanomedicine in cancer therapy: Innovative trends and prospects. Cancer Science 2011; 102: 1247-52.

4. Nicolas J,Couvreur P. Synthesis of poly(alkyl cyanoacrylate)-based colloidal nanomedicines. Wiley Interdiscip Rev Nanomed Nanobiotechnol 2009; 1: 111-27.

5. Fattal E, Youssef M, Couvreur P,Andremont A. Treatment of experimental salmonellosis in mice with ampicillin-bound nanoparticles. Antimicrob Agents Chemother 1989; 33: 1540-3.

6. de Kozak Y, Andrieux K, Villarroya H, Klein C, Thillaye-Goldenberg B, Naud MC, et al. Intraocular injection of tamoxifen-loaded nanoparticles: A new treatment of experimental autoimmune uveoretinitis. Eur J Immunol 2004; 34: 3702-12.

7. Vauthier C, Dubernet C, Fattal E, Pinto-Alphandary H,Couvreur P. Poly(alkylcyanoacrylates) as biodegradable materials for biomedical applications. Adv Drug Deliv Rev 2003; 55: 519-48.

8. Malakoutikhah M, Teixido M,Giralt E. Shuttle-mediated drug delivery to the brain. Angew Chem Int Ed Engl 2011;

9. Hossain S, Akaike T,Chowdhury EH. Current approaches for drug delivery to central nervous system. Curr Drug Deliv 2010; 7: 389-97.

10. Potschka H. Targeting the brain surmounting or bypassing the blood brain barrier. Handbook of Experimental Pharmacology 2010; 197: 411-31.

11. Brambilla D, Le Droumaguet B, Nicolas J, Hashemi SH, Wu LP, Moghimi SM, et al. Nanotechnologies for alzheimer's disease: Diagnosis, therapy, and safety issues. Nanomedicine 2011; 7: 521-40.

12. Brigger I, Morizet J, Aubert G, Chacun H, Terrier-Lacombe MJ, Couvreur P, et al. Poly(ethylene glycol)-coated hexadecylcyanoacrylate nanospheres display a combined effect for brain tumor targeting. J Pharmacol Exp Ther 2002; 303: 928-36.

13. Calvo P, Gouritin B, Chacun H, Desmaele D, D'Angelo J, Noel JP, et al. Long-circulating pegylated polycyanoacrylate nanoparticles as new drug carrier for brain delivery. Pharm Res 2001; 18: 1157-66.

14. Wohlfart S, Khalansky AS, Gelperina S, Maksimenko O, Bernreuther C, Glatzel M, et al. Efficient chemotherapy of rat glioblastoma using doxorubicin-loaded plga nanoparticles with different stabilizers. PLoS One 2011; 6: e19121.

15. Aktas Y, Yemisci M, Andrieux K, Gursoy RN, Alonso MJ, Fernandez-Megia E, et al. Development and brain delivery of chitosan-peg nanoparticles functionalized with the monoclonal antibody ox26. Bioconjug Chem 2005; 16: 1503-11.

16. Vastag M,Keseru GM. Current in vitro and in silico models of blood-brain barrier penetration: A practical view. Curr Opin Drug Discov Devel 2009; 12: 115-24.

17. Calvo P, Gouritin B, Brigger I, Lasmezas C, Deslys J, Williams A, et al. Pegylated polycyanoacrylate nanoparticles as vector for drug delivery in prion diseases. J Neurosci Methods 2001; 111: 151-5.

18. Garcia-Garcia E, Gil S, Andrieux K, Desmaele D, Nicolas V, Taran F, et al. A relevant in vitro rat model for the evaluation of blood-brain barrier translocation of nanoparticles. Cell Mol Life Sci 2005; 62: 1400-8.

19. Kim HR, Andrieux K, Delomenie C, Chacun H, Appel M, Desmaele D, et al. Analysis of plasma protein adsorption onto pegylated nanoparticles by complementary methods: 2-de, ce and protein lab-on-chip system. Electrophoresis 2007; 28: 2252-61.

20. Kim HR, Andrieux K, Gil S, Taverna M, Chacun H, Desmaele D, et al. Translocation of poly(ethylene glycol-co-hexadecyl)cyanoacrylate nanoparticles into rat brain endothelial cells: Role of apolipoproteins in receptor-mediated endocytosis. Biomacromolecules 2007; 8: 793-9.

21. Kim HR, Gil S, Andrieux K, Nicolas V, Appel M, Chacun H, et al. Low-density lipoprotein receptor-mediated endocytosis of pegylated nanoparticles in rat brain endothelial cells. Cell Mol Life Sci 2007; 64: 356-64.

22. Garcia-Garcia E, Andrieux K, Gil S, Kim HR, Le Doan T, Desmaele D, et al. A methodology to study intracellular distribution of nanoparticles in brain endothelial cells. Int J Pharm 2005; 298: 310-4.

23. Brambilla D, Nicolas J, Le Droumaguet B, Andrieux K, Marsaud V, Couraud PO, et al. Design of fluorescently tagged poly(alkyl cyanoacrylate) nanoparticles for human brain endothelial cell imaging. Chem Commun (Camb) 2010; 46: 2602-4.

24. Weksler BB, Subileau EA, Perriere N, Charneau P, Holloway K, Leveque M, et al. Blood-brain barrier-specific properties of a human adult brain endothelial cell line. FASEB J 2005; 19: 1872-4.

25. Xu P, Gullotti E, Tong L, Highley CB, Errabelli DR, Hasan T, et al. Intracellular drug delivery by poly(lactic-co-glycolic acid) nanoparticles, revisited. Mol Pharm 2009; 6: 190-201.

26. Nicolas J, Brambilla D, Carion O, Pons T, Maksimovic I, Larquet E, et al. Quantum dot-loaded pegylated poly(alkyl cyanoacrylate) nanoparticles for in vitro and in vivo imaging. Soft Matter 2011; 7: 6187-93.

27. Dehouck MP, Jolliet-Riant P, Bree F, Fruchart JC, Cecchelli R,Tillement JP. Drug transfer across the blood-brain barrier: Correlation between in vitro and in vivo models. J Neurochem 1992; 58: 1790-7.

28. Neri A, Frosini M, Valoti M, Cacace MG, Teodori E,Sgaragli G. N,n-bis(cyclohexanol)amine aryl esters inhibit p-glycoprotein as transport substrates. Biochemical Pharmacology

29. Boucrot E,Kirchhausen T. Endosomal recycling controls plasma membrane area during mitosis. Proc Natl Acad Sci U S A 2007; 104: 7939-44.

30. Schweitzer JK, Burke EE, Goodson HV,D'Souza-Schorey C. Endocytosis resumes during late mitosis and is required for cytokinesis. J Biol Chem 2005; 280: 41628-35.

31. Haynes P, Miller I, Aebersold R, Gemeiner M, Eberini I, Lovati MR, et al. Proteins of rat serum: I. Establishing a reference two-dimensional electrophoresis map by immunodetection and microbore high performance liquid chromatography-electrospray mass spectrometry. Electrophoresis 1998; 19: 1484-92.

Supporting information

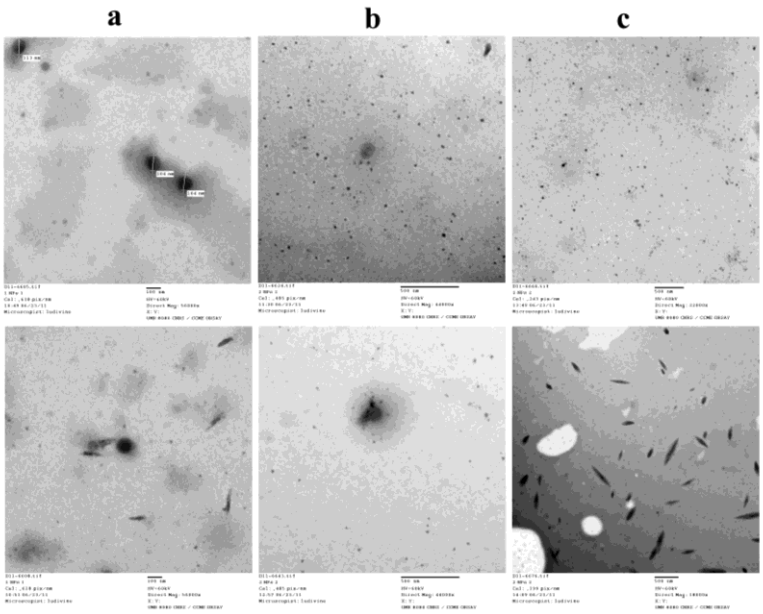

Figure S1. *Representative TEM images of: cell culture medium doped with P(MePEGCA-co-RCA-co-HDCA) nanoparticles (a), basolateral chamber of BBB in vitro model after 12 h treatment with P(MePEGCA-co-RCA-co-HDCA) nanoparticles (b) and basolateral chamber of BBB in vitro model non treated with nanoparticles (c).*

Conclusions et perspectives futures

Dans cette partie, la conception et la caractérisation de nouvelles nanoparticules polymériques fluorescentes ont été décrites. L'internalisation cellulaire de ces particules et leur aptitude à traverser un nouveau modèle humaine de BHE ont été étudiées en détails. L'étape suivante de la première partie du projet porte sur l'utilisation de nanoparticules fonctionnalisées avec des anticorps monoclonaux dirigés contre le récepteur de la transferrine (CD-71) et l'évaluation de leur internalisation et transcystose à travers le modèle de BHE. Les nanoparticules chargées avec des QDs seront utilisées afin d'étudier leur capacité à atteindre le système nerveux central (SNC) *in vivo* and *in vitro*. Par ailleurs, le double marquage (Rhodamine B et QD) sera un avantageux outil pour étudier l'intégrité des particules après avoir traversé la monocouche cellulaire.

Conclusions and future perspectives

During this part of the work the design and the characterization of novel fluorescently-tagged polymeric nanoparticles have been described. The internalization of the particles and their ability to cross a novel human BBB model has been studied in details. The next step for this part of the project will be use of NPs functionalized with anti-tranferrin receptor monoclonal antibody (CD-71) and evaluation of their internalization and transcystosis across the model. QD-loaded NPs will be employed in order to study the ability of the particles to reach the CNS *in vitro* and *in vivo*. Moreover, the double labelling (Rhodammine B and QD) will be a useful tool to study the particles integrity after crossing the cell monolayer.

Chapitre 2 : Interaction de nanoparticules polymériques avec le peptide $A\beta_{1-42}$

Chapter 2: Polymeric nanoparticle interaction with $A\beta_{1-42}$ peptide

Ce deuxième chapitre décrit le développement d'une nouvelle méthodologie permettant l'étude de l'interaction entre des nanoparticules et le peptide amyloïde ($A\beta_{1-42}$) et son application à différents types de nanoparticules. Il est composé de 4 sections sous la forme d'articles :

La première partie est dédiée à la conception d'un protocole d'électrophorèse capillaire couplé avec un détecteur laser (CE-LIF) pour détecter et suivre en fonction du temps l'interaction entre les nanoparticules et le peptide $A\beta_{1-42}$. La méthode a été validée en utilisant d'autres techniques complémentaires déjà utilisées en routine comme la spectroscopie de la Thyoflavine, la résonance plasmonique de surface et la microscopie confocale.

La deuxième section décrit une étude sur l'influence des caractéristiques colloïdales (taille, potentiel zeta etc…) des nanoparticules sur l'interaction avec le peptide amyloïde.

La troisième section concerne l'utilisation de différentes techniques *in vitro* et *in silico* pour identifier le rôle important des chaines de PEG à la surface des nanoparticules dans l'interaction avec le peptide amyloïde.

La dernière section est dédiée au développement de nanoparticules fonctionnalisées avec une molécule ayant une importante affinité pour le peptide amyloïde (sélégiline) et leur capacité d'interaction avec ce dernier en solution.

This chapter describes the development of a novel methodology for the study of the interaction between nanoparticles and the amyloid β peptide ($A\beta_{1-42}$) and its application to different types of nanoparticles. It is composed of 4 sections in the form of articles:

The first one is dedicated to the design of a capillary electrophoresis protocol coupled with fluorescence detector (CE-LIF) to detect and follow, as a function of time, the interaction between nanoparticles and Aβ. The method has been validated by using complementary techniques routinely used such as the Thyoflavine spectroscopy, surface plasmon resonance et confocal laser scanning microscopy.

The second section reports a deeper investigation of the colloidal properties (size, ξ-potential, etc..) of the particles on the interaction with the amyloid peptide.

The third section concerns the employment of different *in vitro* and *in silico* techniques to identify the pivotal role of the PEG chains at the surface of the nanoparticles within the interaction with the amyloid peptide.

The last section describes the synthesis of nanoparticles functionalized with a molecule having a high affinity with the Aβ (selegiline) peptide and their ability to interact in solution.

Section 1

Implications dans le projet NAD

Le but central du projet NAD a été de concevoir des nanoparticules capables de capturer les formes monomériques et oligomériques du peptide $A\beta_{1-42}$, qui sont considérées comme les plus toxiques et l'une des principales causes de la dégénérescence neuronale. Pour étudier la capacité des nanoparticules à interagir avec ce peptide, la méthode de choix *in vitro* est la résonance plasmonique de surface pour laquelle, soit le peptide, soit les particules sont fixées sur la surface d'or de la puce. Cependant, notre but a été de développer une nouvelle technique capable de quantifier cette interaction en gardant le peptide et les nanoparticules en suspension et à des concentrations peptidiques représentant mieux les conditions physiologiques. Pour y parvenir, nous avons choisi l'électrophorèse capillaire couplée avec un détecteur de fluorescence (CE-LIF). Pour la première fois, cette technique a été utilisée pour étudier l'interaction entre des nanoparticules et des macromolécules, et sera utilisée pour l'étude de toutes les nanoparticules développées dans ce projet.

Implications in the NAD project

The main goal of the NAD project was the development of nanoparticles able to sequester both the monomeric and the oligomeric forms of the $A\beta_{1-42}$ peptide, which are considered as the most toxic species and one of the factors triggering the neurodegeneration. In order to study *in vitro* the ability of the particles to interact with the peptide, the foremost employed technique is the surface plasmon resonance in which the peptide or the particles are fixed on the gold chip. Nevertheless, our aim was to develop a versatile method enabling to quantify this interaction in suspension and at low peptidic concentration, better representing the physiological conditions. For this purpose, the selected technique has been the Capillary Electrophoresis coupled with a Fluorescence detector (CE-LIF). For the first time this technique was employed to study the interaction between nanoparticles and macromolecules. The technique will be applied to study all the nanoparticles developed during the project.

A new method based on capillary electrophoresis with laser-induced fluorescence detection (CE-LIF) to monitor interaction between nanoparticles and the amyloid-β peptide

Analytical Chemistry, **2010**, 82 (24), 10083.

Davide Brambilla,[1] Romain Verpillot,[1] Myriam Taverna,[1] Line De Kimpe,[2] Benjamin Le Droumaguet,[1] Julien Nicolas,[1] Mara Canovi,[3] Marco Gobbi,[3] Francesco Mantegazza,[4] Mario Salmona,[3] Valerie Nicolas,[5] Wiep Scheper,[2] Patrick Couvreur[1] and Karine Andrieux[1]

[1] Laboratoire de Physico-Chimie, Pharmacotechnie et Biopharmacie, UMR CNRS 8612, Univ Paris-Sud, Faculté de Pharmacie, 5 rue Jean-Baptiste Clément, F-92296 Chatenay-Malabry, France;

[2] Neurogenetics Laboratory, Academic Medical Center, Amsterdam, The Netherlands;

[3] Istituto di Ricerche Farmacologiche "Mario Negri", Milano, Italy;

[4] Department of Experimental Medicine, University of Milano-Bicocca, Monza, Italy;

[5] Institut d'Innovation Thérapeutique (IFR141 ITFM), Univ Paris-Sud, Faculté de Pharmacie, 5 rue Jean-Baptiste Clément, F-92296 Châtenay-Malabry, France;

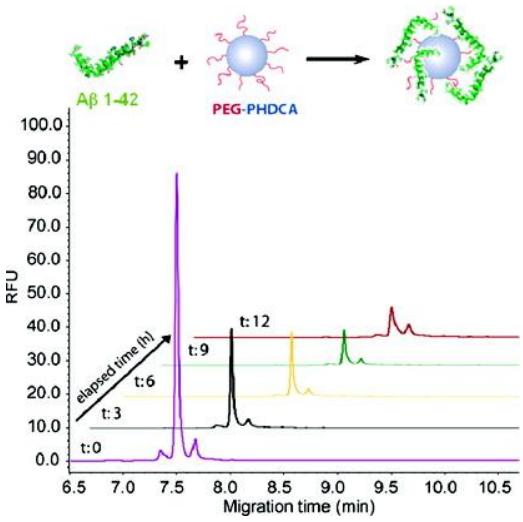

Résumé

Une nouvelle méthode analytique, basée sur l'électrophorèse capillaire couplée à un système de détection par fluorescence (CE-LIF), est proposée pour détecter et suivre de manière efficace l'interaction entre des nanoparticules polymériques et le peptide β-amyloïde ($A\beta_{1-42}$). Ce biomarqueur de la maladie d'Alzheimer serait ainsi détectable à des concentrations proches des conditions physiologiques. Cette méthode a permis de mettre à jour l'interaction entre les nanoparticules (NPs) PEGylées de poly(cyanoacrylate d'alkyle) et la forme monomérique du peptide $A\beta_{1-42}$. Ces résultats ont été confirmés par résonance plasmonique de surface (SPR) et par microscopie confocale à balayage laser (CLSM). Alors que la SPR a montré une interaction entre les NPs et le peptide $A\beta_{1-42}$, la CLSM a permis la visualisation de la formation de large agrégats à fortes concentrations de peptide et de NPs. Tous ces résultats suggèrent que les nanoparticules pourraient se lier au peptide $A\beta_{1-42}$ et influencer sa cinétique d'agrégation. Il est intéressant de noter que les NPs non PEGylées n'influent pas sur la cinétique d'agrégation du peptide ce qui révèle le haut niveau de discrimination de la méthode CE-LIF vis à vis des NPs.

Abstract

A novel analytical method based on capillary electrophoresis with laser-induced fluorescence detection (CE-LIF) was proposed to efficiently detect and monitor the interaction between polymeric nanoparticles and the β-Amyloid peptide ($A\beta_{1-42}$), a biomarker for Alzheimer's Disease (AD), at concentrations close to physiological conditions. The CE-LIF method allowed the interaction between PEGylated poly(alkyl cyanoacrylate) nanoparticles (NPs) and the soluble $A\beta_{1-42}$ peptide monomers to be highlighted. These results were confirmed by surface plasmon resonance (SPR) and confocal laser scanning microscopy (CLSM). Whereas SPR showed an interaction between the NPs and the $A\beta_{1-42}$ peptide, CLSM allowed the formation of large aggregates/assemblies at high NP and peptide concentrations to be visualized. All these results suggested that these nanoparticles could bind the $A\beta_{1-42}$ peptide and influence its aggregation kinetics. Interestingly, the non-PEGylated poly(alkyl cyanoacrylate) NPs did not alter the aggregation kinetics of the $A\beta_{1-42}$ peptide, thus emphasizing the high level of discrimination of the CE-LIF method with respect to NPs.

1. Introduction

The Alzheimer's disease (AD) is a neurodegenerative disorder characterized by a progressive loss of cognitive functions and characteristic pathological changes in the brain. It is the most common elderly dementia, affecting 35 million people worldwide.[1] It is histopathologically characterized by two main hallmarks: (i) the extracellular deposition of amyloid plaques mainly composed of β-amyloid peptides (Aβ) and (ii) intracellular neurofibrillar tangles composed of hyperphosphorylated Tau protein.[2,3] AD is a very complex disease which is likely the result of a multifactorial process strongly influenced by genetic and environmental components, but the mechanisms involved are not yet clearly understood and still under debate.[4,6]

The treatment of AD represents a crucial challenge due to incomplete understanding of the etiology and the lack of diagnostic methods able to discriminate between AD and other neurological diseases. All currently approved therapies, such as the *N*-methyl-D-aspartate (NMDA) receptor antagonist [7-9] and the acetylcholinesterase (AchE) inhibitors,[10-12] are only directed toward the alleviation of AD symptoms and exhibit many side effects.[7]

Among etiopathological hypothesises that have been proposed so far, the neuronal loss due to the toxicity of Aβ peptide aggregates, usually referred to as the "amyloid hypothesis", is one of the most widely-accepted.[13,14] Aβ peptide is produced by neurons through sequential proteolytic cleavage of the amyloid precursor protein (APP) by β- and γ-secretases, forming peptides with a variable number of amino-acids, usually from 39 to 42.[15,16] Among the different species, the Aβ peptide 1-42 ($A\beta_{1-42}$) is believed to be the most representative and the most toxic species in AD physiopathology due to its high tendency to spontaneously self-aggregate.[17,18]

The aggregation kinetics of $A\beta_{1-42}$ peptide involves several steps and leads to the formation of species exhibiting variable sizes: typically small soluble oligomers, higher molar mass oligomers, larger protofibrils and eventually insoluble fibrils. This folding and assembly are governed by remarkably complex processes leading to multiple coexisting physical forms.

Even though it is well-known that the peptide adopts *in vivo* a helical conformation when it is part of the trans-membrane domain of APP,[19] spectroscopic studies have reported a random coil structure in aqueous media.[20] It may aggregate into multiple small oligomers (up to 6 peptides) which coalesce into intermediate assemblies.[21,22] The existence of a transitory conversion from the random coil to a helical structure upon oligomerization has been shown by NMR.[19] A further conformational change has been proposed, leading to soluble *β*-sheet aggregates and then to non-soluble fibrils.[20]

Several therapeutic approaches targeting Aβ peptides are under investigation. Among them, one can find the design of β- and γ-secretase inhibitors[23] and monoamine oxidase inhibitors,[24-27]

together with $A\beta_{1-42}$ passive and active immunization[28-29] and dual inhibitor[30-32] strategies. More recently, the development of small molecules based on methylene blue and curcumin derivatives, which can interfere with the aggregation kinetics, may also represent a promising therapeutic approach.[33,34]

In this context, we are currently developing novel nanoparticulate systems to target and/or to influence the aggregation kinetics of the Aβ peptides. Among suitable nanocarriers, biodegradable PEGylated poly(alkyl cyanoacrylate) nanoparticles (NPs) were selected as a first candidate to investigate this new therapeutic approach due to their biodegradable properties and their well-established use for drug delivery purposes[35] as well as their *in vivo* ability to overpass the blood brain barrier (BBB).[36,37]

To screen the ability of our NPs to efficiently bind $A\beta_{1-42}$, we have developed a new method based on capillary electrophoresis (CE) coupled to laser-induced fluorescence (LIF) detection to analyse fluorescently-labelled Aβ. CE with UV detection has previously been used for the *in vitro* identification of small molecules as potential inhibitors of Aβ aggregation.[38,39] This innovative work, was however limited due to the high concentrations of peptide required for the screening, which were about 5 orders of magnitude higher than those found *in vivo*. More recently, Kato *et al*.[40] reported a CE-LIF method allowing the anti-aggregation features of molecules towards fibrils to be monitored. However, those species are no longer considered to be the main toxic species for AD.[41-43] Consequently, a novel analytical method is required and must be adapted to Aβ monomers and resulting soluble oligomers.

Based on the work of De Lorenzi's research group related to the screening of antifibrillogenic activity of small molecules,[39] we report herein an analytical method able to monitor in real time the binding of soluble $A\beta_{1-42}$ monomers to nanoparticles. Importantly, this is the first time that CE is developed to evaluate nanocarriers as potential therapeutic agents for AD treatment using *in vitro* conditions compatible with clinical application/trials. This analytical method was further associated to confocal laser scanning microscopy (CLSM) experiments which demonstrated a binding effect of the nanoparticles to the amyloid peptide, by influencing their aggregation kinetics. The physiological peptide concentration detectable with this method allowed nanoparticulate systems with potential binding feature to the amyloid peptide to be readily screened and quantitatively evaluated.

2. Experimental Section

2.1. Material and chemicals

Poly[hexadecyl cyanoacrylate-*co*-rhodamine B cyanoacrylate-*co*-methoxypoly(ethylene glycol) cyanoacrylate] P(MePEGCA-*co*-RCA-*co*-HDCA) copolymers,[44] poly[hexadecyl cyanoacrylate-*co*-methoxypoly(ethylene glycol) cyanoacrylate] P(MePEGCA-*co*-HDCA) copolymers[35] and poly(hexadecyl cyanoacrylate) P(HDCA) homopolymers[37] were obtained following previously reported procedures. NaH_2PO_4 (>99%) was purchased from Merck & Co (Fontenay Sous Bois, France), Na_2HPO_4 (>98%) was obtained from Prolabo (Strasbourg, France), thioflavine (99%), ammonium hydroxide (NH_4OH) 28.1% (m/V), Pluronic F-68 (99%), 1,1,1,3,3,3-hexafluoro-2-propanol (HFIP) (99.8%), dimethyl sulfoxide (99.5%), sodium dodecyl sulphate (SDS, 99%), acetic acid (99%), sodium acetate (99%), bovine serum albumin (BSA, 99%) and ethanolamine (99%) were purchased from Sigma-Aldrich (St. Quentin Fallavier, France). Sodium hydroxide (NaOH, 1 M) was obtained from VWR (Fontenay-sous Bois, France). Acetone was purchased at the highest grade from Carlo Erba (Val de Reuil, France). Lyophilized HiLyte Fluor^{TM} 488 labeled $A\beta_{1-42}$ and $A\beta_{1-42}$ peptides were provided by ANASPEC (Le Perray en Yvelines, France). Anti-Aβ antibody 6E10 was from Covance (Princeton, New Jersey).

3. Apparatus

3.1. Capillary electrophoresis

CE was performed on PA 800 instrument (Beckman Coulter, Roissy, France) using uncoated silica capillaries (Phymep, Paris) with an internal diameter of 50 µm and 50 cm total length (40 cm effective length was employed for the separation). All buffers were prepared with deionized water and were filtered through a 0.22 µm membrane (VWR) before use. Before analysis, the capillaries were preconditioned by the following rinsing sequence: 0.1 M NaOH for 5 min, 1 M NaOH for 5 min and then deionised water for 5 min. The in-between-runs rinsing cycles were carried out by pumping sequentially through the capillary: water for 5 min, 50 mM SDS for 2 min (to inhibit the aggregation and subsequent peptide adsorption on the capillary wall),[45] and 0.1 M NaOH for 5 min. The samples were introduced into the capillary by hydrodynamic injection under 3.4 kPa. The capillary was thermostated at 25°C and the samples were maintained at 37°C by the storage sample module of the PA 800 apparatus. The separations were carried out at 16 kV with positive polarity at the inlet using 80 mM phosphate buffer pH 7.4. The electrolyte was renewed after each run. The peptides were detected by a Laser-Induced Fluorescence (LIF) detection system equipped with 3.5 mW argon-ion

laser with a wavelength excitation of 488 nm, the emission being collected through a 520 nm band-pass filter or by Diode-Array Detector (DAD) at 190 nm. Peak areas were estimated using the 32 Karat™ software (Beckman Coulter).

3.2. Confocal Laser Scanning Microscope

Observations were made by sequential acquisition with a Zeiss LSM-510 confocal scanning laser microscope equipped with a 30 mW argon laser and 1 mW helium neon laser, using a Plan-Apochromat 63X objective lens (NA 1.40, oil immersion). Red fluorescence was observed with a long-pass 560 nm emission filter and under a 543 nm laser illumination. Green fluorescence was observed with a band-pass 505 and 550 nm emission filter and under a 488 nm laser illumination. The pinhole diameter was set at 61 µm giving an optical section thickness of 0.6 µm. Stacks of images were collected every 0.3 µm along the z axis. 12 bit numerical images were acquired with LSM 510 software version 3.2.

3.3. SPR apparatus

ProteOn XPR36 (Biorad) apparatus, which has six parallel flow channels that can be used to uniformly immobilize strips of six ligands on the sensor surface, was employed. The fluidic system of Proteon XPR36 can automatically rotate 90° so that up to six different analytes (*e.g.* different nanoparticle preparations, or different concentrations of the same nanoparticle) can be injected simultaneously over all the different immobilized molecules. All the injections were carried out for 3 min at a flow rate of 30 µL.min^{-1} at 30°C in PBST (Phosphate buffer saline + 0.005% Tween20, pH 7.4).

4. Methods

4.1. Nanoparticles preparation

Fluorescent and non-fluorescent nanoparticles were prepared using P(MePEGCA-*co*-RCA-*co*-HDCA), P(MePEGCA-*co*-HDCA) copolymers and P(HDCA) homopolymer according to protocols recently published by our group.[44] The (co)polymer (10 mg) was dissolved in acetone (2 mL) and this solution was added dropwise to an aqueous solution 0.5 % (w/v) of Pluronic F68 (4 mL) under vigorous mechanical stirring. A milky suspension was observed almost instantaneously. Acetone was then evaporated under reduced pressure and nanoparticles were purified by ultracentrifugation (150 000 *g*, 1 h, 4°C, Beckman Coulter, Inc.). The supernatant was discarded and the pellet was

resuspended in the appropriate volume of deionized water to yield a 2.5 $mg.mL^{-1}$ nanoparticle suspension.

4.2. Nanoparticles characterization

The nanoparticle diameter (D_z) was measured by dynamic light scattering (DLS) with a Nano ZS from Malvern (173° scattering angle) at 25°C. DLS measurements were used to monitor the nanoparticles stability as a function of time upon their incubation at 37°C in the buffer employed for capillary electrophoresis experiments. The nanoparticle surface charge was investigated by ζ-potential measurement at 25°C after dilution with 1 mM NaCl solution applying the Smoluchowski equation and using the same apparatus.

4.3. Peptide samples preparation and storage

Lyophilized $A\beta_{1-42}$ and HiLyte Fluor™ labeled $A\beta_{1-42}$ peptide were dissolved in 0.16% (m/V) ammonium hydroxide aqueous solution to reach a concentration of 2 $mg.mL^{-1}$. The fluorescent and non-labeled peptide solutions were then divided into aliquots individually stored at -20°C which were freshly defrosted prior analysis.

The $A\beta_{1-42}$ peptide used for SPR experiments was prepared from a depsi-$A\beta_{1-42}$ peptide synthesized as previously described.[46] This depsi-peptide is much more soluble than the native peptide and has also a much lower propensity to aggregate, thus preventing the spontaneous formation of 'seeds' in solution.[46] The native $A\beta_{1-42}$ peptide was then obtained from the depsi-peptide by a "switching" procedure involving a change in pH.[46-47] The $A\beta_{1-42}$ peptide solution obtained immediately after switching was shown to be free of seed. The $A\beta_{1-42}$ peptide obtained by this procedure is therefore in its original state and, for the sake of simplicity; it will be referred here to as the "monomer".

The peptide concentration required for the different methods described below were not strictly the same as long as different detection thresholds had to be taken into account.

4.4. Capillary electrophoresis experiments

To study the interaction between the monomeric form of the $A\beta_{1-42}$ peptide and the nanoparticles, aliquots of HiLyte Fluor™ labeled $A\beta_{1-42}$ peptide stock solutions were diluted in 20 mM phosphate buffer (NaH_2PO_4) at pH 7.4 containing a 20 µM P(MePEGCA-*co*-RCA-*co*-HDCA) nanoparticle suspension to obtain final peptide concentrations of 5, 1, 0.5 and 0.05 µM. The samples were then incubated at 37°C and analyzed by capillary electrophoresis every 2 h. The same protocol

was followed with P(MePEGCA-*co*-RCA-*co*-HDCA) nanoparticle suspension or $A\beta_{1-42}$ peptide solution.

Similarly, a mixture of non-fluorescent P(MePEGCA-*co*-HDCA) or PHDCA nanoparticle suspensions (20 µM final concentration) and $A\beta_{1-42}$ at 10 µM were analyzed by CE using the DAD detector at 190 nm as control.

These experiments allowed the evolution of % monomer peak as a function of incubation time to be determined. % monomer peak is calculated as the ratio between the absolute peak area of the monomer observed at $t = 0$ and the one observed at each incubation time.

4.5. Surface Plasmon Resonance experiments

$A\beta_{1-42}$ monomers were immobilized in parallel-flow channels of a GLC sensor chip (Biorad) using amine-coupling chemistry. Briefly, after surface activation the peptide solutions (10 µM in acetate buffer pH 4.0) were injected for 5 min at a flow rate of 30 $\mu L.min^{-1}$ and the remaining activated groups were blocked with ethanolamine at pH 8.0. The final immobilization levels were about 2500 Resonance Units (1 RU = 1 pg $protein.mm^{-2}$). Bovine serum albumin (BSA) was immobilized, in a parallel flow channel as a reference protein. Another reference surface was prepared in parallel using the same immobilization procedure but without addition of the peptide (naked surface). Before performing experiments with nanoparticles, we checked that Aβ species immobilized can bind with high affinity to the anti-Aβ antibody 6E10 (see Figure S6c). The suspension of P(MePEGCA-*co*-PHDCA) NPs was diluted at different concentrations (0.3 to 20 µM) and flowed into the machine simultaneously.

4.6. Confocal Laser Scanning Microscopy analysis

The interaction between the polymeric nanoparticles and the $A\beta_{1-42}$ peptide was investigated by confocal laser scanning microscopy (CLSM) using HiLyte Fluor™ labeled $A\beta_{1-42}$ peptide and rhodamine-labelled P(MePEGCA-*co*-RCA-*co*-HDCA) NPs.

The $A\beta_{1-42}$ peptide aliquots were defrost, immediately diluted with 20 mM phosphate buffer and incubated with 20 µM nanoparticle suspension to reach a final peptide concentration of 10, 1 or 0.05 µM. A 10 µL deposit of this final incubation sample on glass coverslips was immediately analyzed by CLSM. The remaining suspensions were incubated at 37°C and, after 12 h, another 10 µL was withdrawn from the suspension and analyzed in the same manner by CLSM.

4.7. Thioflavin T aggregation assay

$A\beta_{1-42}$ was dissolved in hexafluorisopropanol (HFIP) at a final concentration of 1 $mg.mL^{-1}$, sampled and allowed to evaporate. For co-aggregation experiments, the peptide film was first dissolved in DMSO and sonicated in a bath sonicator for 10 min. Subsequently, $A\beta_{1-42}$ was diluted in phosphate-buffer saline (PBS, 20 mM sodium phosphate buffer, pH 7.4, containing 137 mM NaCl) to a final concentration of 50 µM. This mixture was aggregated in the presence or absence of P(MePEGCA-*co*-HDCA) NPs for 24 h at 37ºC. Aggregated $A\beta_{1-42}$ was diluted to a final concentration of 5 µM into 50 mM glycine buffer at pH 7.4 containing 10 µM ThT. Fluorescence was measured in 96 well non-binding plates (Greiner Bio One, Frickenhausen, Germany) using a Fluostar Omega microplate reader at an excitation wavelength of 450 nm and emission at 485 nm.

5. Results and Discussion

The purified fluorescent and non-fluorescent nanoparticles prepared by nanoprecipitation were characterized by DLS and ζ-potential measurements. PEGylated nanoparticles presented an average diameter in the 90-100 nm range with narrow particle size distribution, whereas non-PEGylated counterparts were centered around 160 nm (see Figure S1). Those nanoparticles exhibited a negative ζ-potential (-30 ± 5 mV), which is in a suitable window for biomedical applications. Notably all kinds of nanoparticles showed good colloidal stability in the capillary electrophoresis buffer (*i.e.* phosphate buffer pH 7.4, 20 mM) as assessed by DLS measurement during 72 h (Figure S1).

The CE-LIF method described in this study was developed to investigate the interaction between rhodamine B-labeled nanoparticles and HiLyte Fluor^{TM} labeled $A\beta_{1-42}$. The LIF detection allowed a lower concentration of peptide to be used than with UV detection, in order to better fit with physiological processes and conditions. Indeed, Aβ peptide is found in biological fluids, such as the cerebro-spinal fluid (CSF), at nanomolar concentrations and therefore a sensitive and discriminative analytical method is required.

The CE-LIF analysis of a solution of the fluorescent $A\beta_{1-42}$ showed a single peak migrating at ~7.5 min and mainly constituted by the monomeric form. Interestingly, the electrophoretic profile of the peptide sample stayed constant over time up to 24 h (Figure 1.a), thus demonstrating an excellent stability of the fluorescent peptide in its monomeric form at this concentration in the buffer.

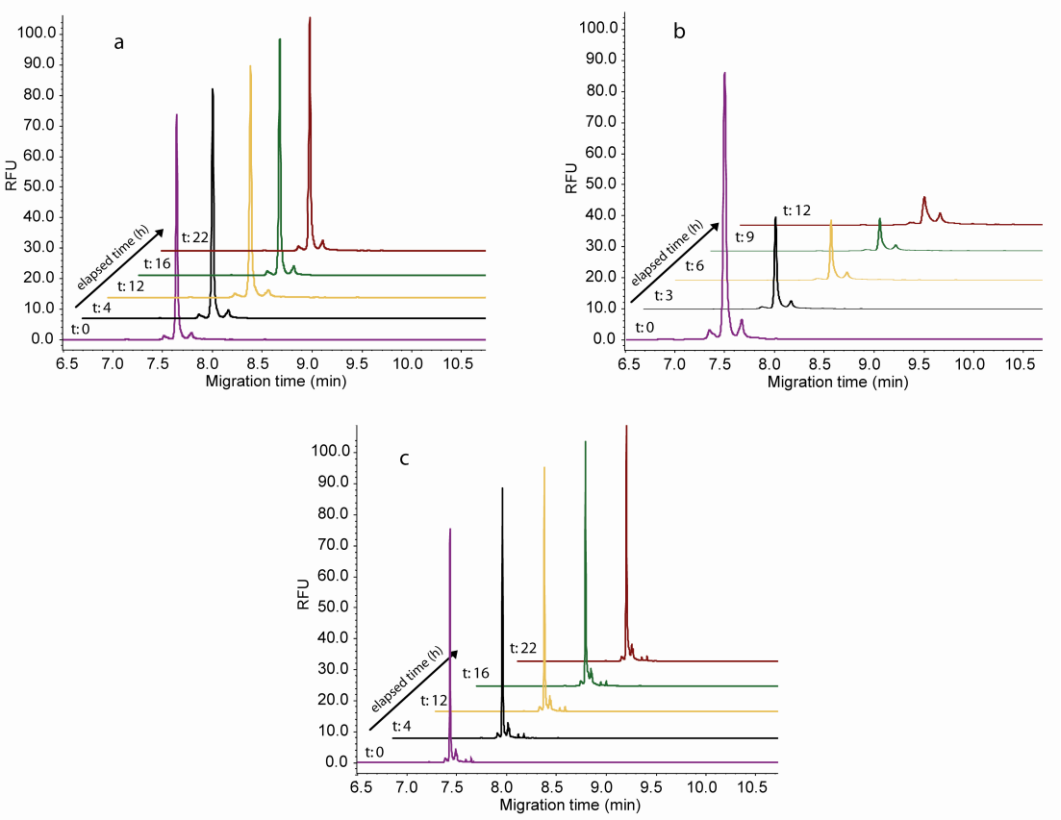

Figure 1. *(a) Evolution of the electrophoretic profile as a function of time at 37°C of a 5 µM Hilyte Fluor™ Aβ$_{1-42}$ solution alone and (b) in the presence of a 20 µM P(MePEGCA-co-RCA-co-HDCA) nanoparticle suspension and (c) in the presence of a 20 µM PHDCA nanoparticle suspension.*

Remarkably, when the same concentration of Aβ$_{1-42}$ peptide solution was incubated with 20 µM of fluorescent P(MePEGCA-*co*-RCA-*co*-HDCA) nanoparticle suspension, a gradual decrease of the monomeric peptide peak was observed (Figure 1b). These results indicate an interaction between the peptide and the nanoparticles. In order to validate this finding, the method was then applied to other NPs with different surface features; namely non-PEGylated poly(hexadecyl cyanoacrylate) (PHDCA) nanoparticles. Interestingly, no variation of the monomer peak was observed over time upon incubation with PHDCA NPs under the same experimental conditions as the PEGylated counterparts (Figure 1c). It is well-known that PEG chains can interplay with protein environment altering their solubility in aqueous media,[48] although the mechanism has not yet been fully elucidated.[49] In our case, it is believed that PEG chains locally modified the peptide solubility and thus triggered its uptake by the nanoparticles. Therefore, these results confirm that the analytical method presented in this study is able to efficiently discriminate nanoparticles with respect to their respective aptitude to bind Aβ$_{1-42}$.

Similar experiments were then performed with non-fluorescent peptide and NPs to confirm the previous findings and check whether the fluorescent tags could have altered the binding behavior observed so far. To this purpose, CE with UV detection was employed for the monitoring and similar results were obtained than with fluorescent $A\beta_{1\text{-}42}$ and rhodamine B-tagged NPs (Figure 2). In addition, multiple spikes exhibiting migration times around 10-11 min appeared after a 6 h incubation time period on the corresponding profile (Figure 2b). These peaks, the intensity and number of which increased as a function of time, were assigned to the association between non-labeled peptide species and the nanoparticles. However, these peaks were not observed with the CE-LIF method likely due to optical features of the LIF detection.

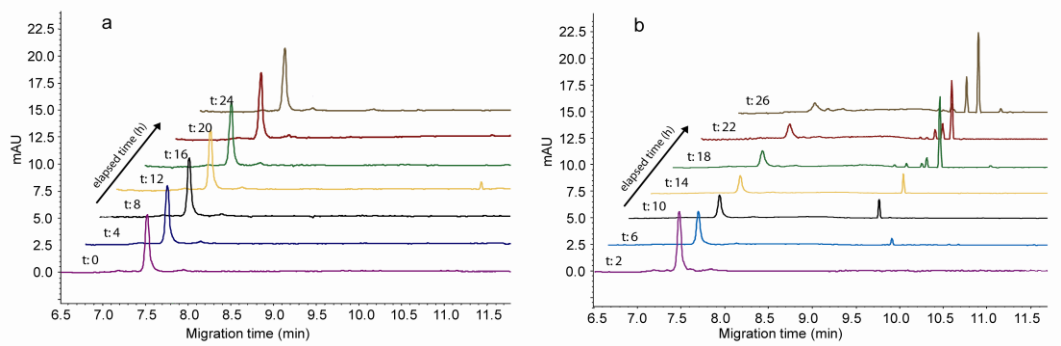

***Figure 2**. Evolution of the electrophoretic profile as a function of time at 37°C of (a) a 10 µM $A\beta_{1\text{-}42}$ solution alone and (b) a 10 µM $A\beta_{1\text{-}42}$ solution incubated with a 20 µM P(MePEGCA-co-HDCA) nanoparticle suspension.*

The CE-LIF method was also used to evaluate the kinetics of disappearance of the monomeric peptide as a function of the concentration ratio between P(MePEGCA-*co*-RCA-*co*-HDCA) NPs and $A\beta_{1\text{-}42}$. As shown in Figure 3, whatever the concentration ratio, there is an uptake of peptide by the NPs (capture varying from 20 to 85%) and this process is strictly dependent on the peptide availability in solution. The higher the initial peptide concentration, the faster and the higher the capture. Assuming in a first approach that the $A\beta_{1\text{-}42}$-NPs interaction was governed by a first-order kinetic, we have estimated the affinity constant, k_d, for this interaction to be 0.55 µM (see Figures S2 and S3). Interestingly, for the highest peptide concentrations, we observed a nonlinear disappearance of the monomeric peak over time suggesting the formation of peptide aggregates at the surface of the nanoparticles. Interestingly in the absence of nanoparticles, the peptide did not spontaneously form any aggregate in the concentration range (0.05-5µM) of this experiment.

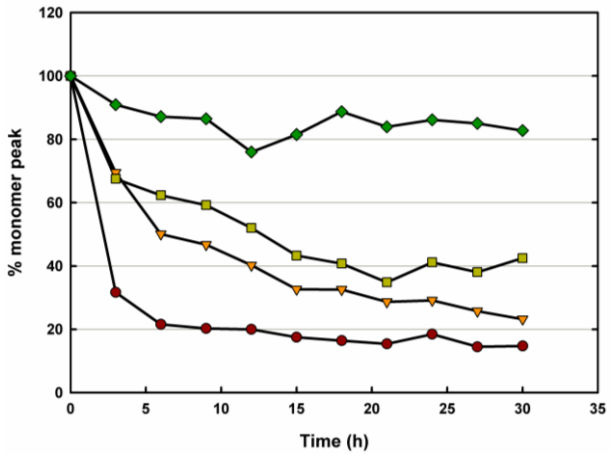

Figure 3. *$A\beta_{1-42}$ monomer peak intensity as a function of time upon incubation of $A\beta_{1-42}$ in the presence of fluorescent P(MePEGCA-co-RCA-co-PHDCA) NPs at 20 µM. The concentration of $A\beta_{1-42}$ was 0.05 µM (♦), 0.5 µM (■), 1 µM (▼) or 5 µM (●)*

To investigate whether the P(MePEGCA-*co*-HDCA) NPs could indeed influence the aggregation kinetics of $A\beta_{1-42}$, we performed a Thioflavin T assay in the absence or in the presence of these NPs. ThT experiments performed at high peptide concentration (50 µM), facilitating its aggregation, confirmed that the P(MePEGCA-*co*-HDCA) NPs strongly increase $A\beta_{1-42}$ aggregation (Figure S4). Therefore, it is reasonable to assume that the aggregation of peptides is initiated by nanoparticle surfaces. This hypothesis is completely supported by previous computational work reported by Auer *et al.*[50] about the catalyzed/acceleration of peptide aggregation by nanoparticles.

CLSM was then employed for two main reasons: (i) to have a direct visualization of the binding process and thus to confirm previous results obtained by CE-LIF and (ii) to have a better insight into the nature of the aggregates that formed at the surface of the NPs. The P(MePEGCA-*co*-RCA-*co*-HDCA) nanoparticle suspension was added to fluorescent $A\beta_{1-42}$ solution at different ratios ($[A\beta]_0$ = 0.05-10 µM) and the resulting samples were observed immediately after mixing (time zero) and after a 12 h incubation time period at 37°C. At time zero, a faint colocalization was observed (Figure S5). After 12 h of incubation, a complete colocalization of green (fluorescent peptide) and red (rhodamine B-labeled nanoparticles) channels was observed (Figure 4) evidencing a strong NP-peptide interaction. Moreover, a proportional decrease of the size of these dual-fluorescent assemblies was noticed as a function of the $[A\beta]_0/[NPs]_0$ ratio (Figure 4). For the lowest peptide concentration, no aggregate was formed (Figure 4e) suggesting the aggregation threshold was not reached.

According to the literature, peptide aggregation is concentration-dependent and the nucleation reaction is believed to be the rate limiting step.[51] It can be therefore hypothesized that, when there is an affinity between the peptide and some nanoparticles, the interaction of the peptide with the nanoparticle surface increases its local concentration, reaching the nucleation threshold which then triggers the aggregation process.

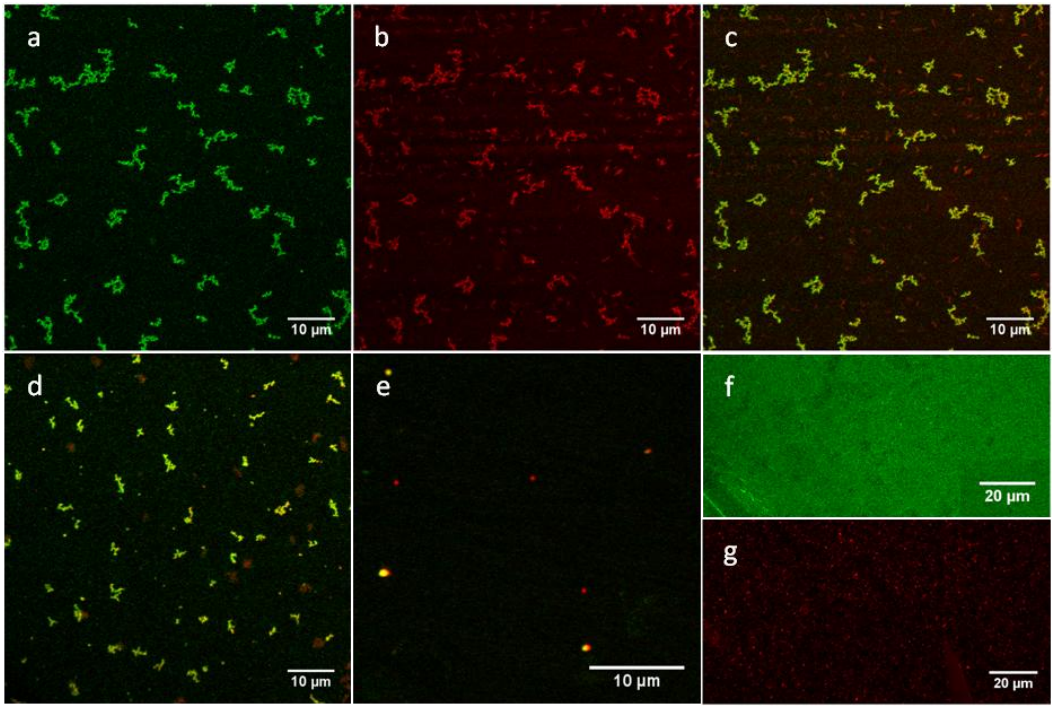

***Figure 4**: Confocal microscopy images showing colocalization of Hilyte Fluor™ $A\beta_{1-42}$ and P(MePEGCA-co-RCA-co-HDCA) nanoparticle suspension after their incubation for 12 h. (a) $A\beta_{1-42}$ peptide (10 µM) (green channel) (b) P(MePEGCA-co-RCA-co-HDCA) nanoparticles (20 µM) (red channel) (c) merge of (a) and (b). Effect of the peptide concentration on the size of the assemblies: (d) solution of Hilyte Fluor™ $A\beta_{1-42}$ (1 µM) and P(MePEGCA-co-RCA-co-HDCA) nanoparticles (20 µM); (e) solution of Hilyte Fluor™ $A\beta_{1-42}$ (50 nM) and P(MePEGCA-co-RCA-co-HDCA) nanoparticles (20 µM). Control experiments: (f) solution of Hilyte Fluor™ $A\beta_{1-42}$ (10 µM) and (g) P(MePEGCA-co-RCA-co-HDCA) nanoparticles (20 µM).*

At highest concentrations, the formation of aggregates and their modulation of size can be explained by a self-aggregation of PEGylated nanoparticles driven by the presence of monomeric and/or peptide oligomers on their surface and is thereby directly proportional to the amount of peptide available in solution. These microscopy observations fully support the CE results regarding the ability of

PEGylated poly(alkyl cyanoacrylate) nanoparticles to bind the $A\beta_{1-42}$ monomer and to promote its aggregation at their surface, leading to large aggregate formation only at the highest concentrations of peptides. Moreover, due to the size of those assemblies, it is possible to envision that once the nucleation process is triggered at the nanoparticle surface, the aggregation takes place, creating also oligomer bridges between NPs.

To our knowledge, this is the first time that interaction between polymeric nanoparticles and $A\beta_{1-42}$ peptide in solution is experimentally monitored, described and quantified. Finally the nanoparticle ability to interact with the $A\beta_{1-42}$ peptide, highlighted by CE and confocal microscopy was evaluated by SPR experiments used as a complementary method. Increasing concentrations (0.3, 3 and 20 μM) of a suspension of P(MePEGCA-*co*-RCA-*co*-HDCA) NPs were flowed over a chip coated with the monomeric $A\beta_{1-42}$ for 3 min. The resulting sensorgrams clearly showed a concentration-dependent interaction between the PEGylated nanoparticles and the peptide immobilized onto the chip (Figure S6a). As a control, the same experiment was performed on a BSA-coated chip and revealed no interaction with the nanoparticles (Figure S6b). This is quite striking as long as BSA is usually considered as a "sticky" protein that binds many other proteins, surfaces and molecules. These SPR results confirmed the interaction between PEGylated NPs and the $A\beta_{1-42}$ peptide.

6. Conclusions

In this work a new method relying on CE-LIF was proposed to evidence the ability of polymeric nanoparticles to bind the $A\beta_{1-42}$ peptide, the main molecular species involved in the pathological process of neurodegeneration in AD.

To this end, we have highlighted an interaction between PEGylated poly(alkyl cyanoacrylate) nanoparticles and $A\beta_{1-42}$. Importantly, combining these results with confocal microscopy and surface plasmon resonance allowed to demonstrate that these nanoparticles could bind $A\beta_{1-42}$ and thus to influence its aggregation kinetics. Further works are under progress in order to elucidate the the role of PEG chains in the binding mechanism with $A\beta_{1-42}$. However, the difference observed between PEGylated and non-PEGylated nanoparticles underlined the utility of the CE-LIF technique.

The proposed method exhibits high sensitivity, rapid analysis and great ability to mimic *in vivo* conditions. In contrast, other techniques such as SPR and Thioflavine T assay required higher concentrations of peptide which do not match with physiological conditions. Therefore, CE-LIF represents a clear advance and could open new routes for the screening of novel nanoparticle-based

drugs for amyloidogenic pathology treatment but also for the detection of β Amyloid peptide from CSF to propose an early diagnosis of AD.

7. Acknowledgments

The research leading to these results has received funding from the European Community's Seventh Framework Programme (FP7/2007-2013) under agreement n°212043. The CNRS and the French Ministry of Research are also warmly acknowledgment for financial support.

8. References

1. Querfurth HW, LaFerla FM. Alzheimer's disease. N. Engl. J. Med. 2010; 362: 329-44.

2. Aguzzi A,O'Connor T. Protein aggregation diseases: Pathogenicity and therapeutic perspectives. Nat. Rev. Drug Discovery 2010; 9: 237-48.

3. Panza F, Solfrizzi V, Frisardi V, Imbimbo BP, Capurso C, D'Introno A, et al. Beyond the neurotransmitter-focused approach in treating alzheimer's disease: Drugs targeting beta-amyloid and tau protein. Aging: Clin. Exp. Res. 2009; 21: 386-406.

4. Aliev G, Smith MA, de la Torre JC,Perry G. Mitochondria as a primary target for vascular hypoperfusion and oxidative stress in alzheimer's disease. Mitochondrion 2004; 4: 649-63.

5. de la Torre JC. Is alzheimer's disease a neurodegenerative or a vascular disorder? Data, dogma, and dialectics. Lancet Neurol. 2004; 3: 184-90.

6. Korolainen MA, Nyman TA, Aittokallio T,Pirttila T. An update on clinical proteomics in alzheimer's research. J. Neurochem. 2010; 112: 1386-414.

7. Kemp JA,McKernan RM. Nmda receptor pathways as drug targets. Nat. Neurosci. 2002; 5 Suppl: 1039-42.

8. Parsons CG, Danysz W,Quack G. Memantine is a clinically well tolerated n-methyl-d-aspartate (nmda) receptor antagonist--a review of preclinical data. Neuropharmacology 1999; 38: 735-67.

9. Reisberg B, Doody R, Stoffler A, Schmitt F, Ferris S,Mobius HJ. Memantine in moderate-to-severe alzheimer's disease. N. Engl. J. Med. 2003; 348: 1333-41.

10. Sugimoto H, Iimura Y, Yamanishi Y,Yamatsu K. Synthesis and structure-activity relationships of acetylcholinesterase inhibitors: 1-benzyl-4-[(5,6-dimethoxy-1-oxoindan-2-yl)methyl]piperidine hydrochloride and related compounds. J. Med. Chem. 1995; 38: 4821-9.

11. Munoz-Torrero D. Acetylcholinesterase inhibitors as disease-modifying therapies for alzheimer's disease. Curr. Med. Chem. 2008; 15: 2433-55.

12. Birks J, Grimley Evans J, Iakovidou V, Tsolaki M,Holt FE. Rivastigmine for alzheimer's disease. Cochrane Database Syst. Rev. 2009; CD001191.

13. Townsend M, Mehta T,Selkoe DJ. Soluble abeta inhibits specific signal transduction cascades common to the insulin receptor pathway. J. Biol. Chem. 2007; 282: 33305-12.

14. Gralle M, Botelho MG,Wouters FS. Neuroprotective secreted amyloid precursor protein acts by disrupting amyloid precursor protein dimers. J. Biol. Chem. 2009; 284: 15016-25.

15. Pierrot N,Octave J-N. Processing of amyloid precursor protein and amyloid peptide neurotoxicity. Curr Alzheimer Res 2008; 5: 92-9.

16. Chow VW, Mattson MP, Wong PC,Gleichmann M. An overview of app processing enzymes and products. NeuroMol. Med. 2009; 12: 1.

17. Garcia-Matas S, de Vera N, Aznar AO, Marimon JM, Adell A, Planas AM, et al. In vitro and in vivo activation of astrocytes by amyloid-beta is potentiated by pro-oxidant agents. J. Alzheimers Dis. 2010; 20: 229-45.

18. Allaman I, Gavillet M, Belanger M, Laroche T, Viertl D, Lashuel HA, et al. Amyloid-beta aggregates cause alterations of astrocytic metabolic phenotype: Impact on neuronal viability. J. Neurosci. 2010; 30: 3326-38.

19. Crescenzi O, Tomaselli S, Guerrini R, Salvadori S, D'Ursi AM, Temussi PA, et al. Solution structure of the alzheimer amyloid beta-peptide (1-42) in an apolar microenvironment. Similarity with a virus fusion domain. Eur. J. Biochem. 2002; 269: 5642-8.

20. Tomaselli S, Esposito V, Vangone P, van Nuland NA, Bonvin AM, Guerrini R, et al. The alpha-to-beta conformational transition of alzheimer's abeta-(1-42) peptide in aqueous media is reversible: A step by step conformational analysis suggests the location of beta conformation seeding. ChemBioChem 2006; 7: 257-67.

21. Kayed R, Head E, Thompson JL, McIntire TM, Milton SC, Cotman CW, et al. Common structure of soluble amyloid oligomers implies common mechanism of pathogenesis. Science 2003; 300: 486-9.

22. Klein WL, Krafft GA,Finch CE. Targeting small a[beta] oligomers: The solution to an alzheimer's disease conundrum? Trends Neurosci. 2001; 24: 219-24.

23. Shao D, Zou C, Luo C, Tang X,Li Y. Synthesis and evaluation of tacrine-e2020 hybrids as acetylcholinesterase inhibitors for the treatment of alzheimer's disease. Bioorg. Med. Chem. Lett. 2004; 14: 4639-42.

24. Sano M, Ernesto C, Thomas RG, Klauber MR, Schafer K, Grundman M, et al. A controlled trial of selegiline, alpha-tocopherol, or both as treatment for alzheimer's disease. The alzheimer's disease cooperative study. N. Engl. J. Med. 1997; 336: 1216-22.

25. Riederer P, Danielczyk W,Grunblatt E. Monoamine oxidase-b inhibition in alzheimer's disease. Neurotoxicology 2004; 25: 271-7.

26. Youdim MBH,Buccafusco JJ. Multi-functional drugs for various cns targets in the treatment of neurodegenerative disorders. Trends in pharmacological sciences 2005; 26: 27-35.

27. Huang W, Chen Y, Shohami E,Weinstock M. Neuroprotective effect of rasagiline, a selective monoamine oxidase-b inhibitor, against closed head injury in the mouse. Eur. J. Pharmacol. 1999; 366: 127-35.

28. Zou J, Yao Z, Zhang G, Wang H, Xu J, Yew DT, et al. Vaccination of alzheimer's model mice with adenovirus vector containing quadrivalent foldable a[beta]1-15 reduces a[beta] burden and behavioral impairment without a[beta]-specific t cell response. J. Neurol.Sci. 2008; 272: 87-98.

29. Dodart JC, Bales KR,Paul SM. Immunotherapy for alzheimer's disease: Will vaccination work? Trends Mol. Med. 2003; 9: 85-7.

30. Bolognesi ML, Andrisano V, Bartolini M, Banzi R,Melchiorre C. Propidium-based polyamine ligands as potent inhibitors of acetylcholinesterase and acetylcholinesterase-induced amyloid-beta aggregation. J. Med. Chem. 2005; 48: 24-7.

31. Camps P, Formosa X, Munoz-Torrero D, Petrignet J, Badia A,Clos MV. Synthesis and pharmacological evaluation of huprine-tacrine heterodimers: Subnanomolar dual binding site acetylcholinesterase inhibitors. J. Med. Chem. 2005; 48: 1701-4.

32. Toda N, Tago K, Marumoto S, Takami K, Ori M, Yamada N, et al. Design, synthesis and structure-activity relationships of dual inhibitors of acetylcholinesterase and serotonin transporter as potential agents for alzheimer's disease. Bioorg. Med. Chem. 2003; 11: 1935-55.

33. Yadav A,Sonker M. Perspectives in designing anti aggregation agents as alzheimer disease drugs. Eur. J. Med. Chem. 2009; 44: 3866-73.

34. Hawkes CA, Deng LH, Shaw JE, Nitz M,McLaurin J. Small molecule beta-amyloid inhibitors that stabilize protofibrillar structures in vitro improve cognition and pathology in a mouse model of alzheimer's disease. Eur. J. Neurosci. 2010; 31: 203-13.

35. Nicolas J,Couvreur P. Synthesis of poly(alkyl cyanoacrylate)-based colloidal nanomedicines. Wiley Interdiscip. Rev.: Nanomed. Nanobiotechnol. 2009; 1: 111-27.

36. Andrieux K,Couvreur P. Polyalkylcyanoacrylate nanoparticles for delivery of drugs across the blood-brain barrier. Wiley Interdiscip. Rev.: Nanomed. Nanobiotechnol. 2009; 1: 463-74.

37. Brigger I, Morizet J, Aubert G, Chacun H, Terrier-Lacombe MJ, Couvreur P, et al. Poly(ethylene glycol)-coated hexadecylcyanoacrylate nanospheres display a combined effect for brain tumor targeting. J Pharmacol Exp Ther 2002; 303: 928-36.

38. Sabella S, Quaglia M, Lanni C, Racchi M, Govoni S, Caccialanza G, et al. Capillary electrophoresis studies on the aggregation process of beta-amyloid 1-42 and 1-40 peptides. Electrophoresis 2004; 25: 3186-94.

39. Colombo R, Carotti A, Catto M, Racchi M, Lanni C, Verga L, et al. Ce can identify small molecules that selectively target soluble oligomers of amyloid beta protein and display antifibrillogenic activity. Electrophoresis 2009; 30: 1418-29.

40. Kato M, Kinoshita H, Enokita M, Hori Y, Hashimoto T, Iwatsubo T, et al. Analytical method for beta-amyloid fibrils using ce-laser induced fluorescence and its application to screening for inhibitors of beta-amyloid protein aggregation. Anal. Chem. 2007; 79: 4887-91.

41. Dahlgren KN, Manelli AM, Stine WB, Jr., Baker LK, Krafft GA,LaDu MJ. Oligomeric and fibrillar species of amyloid-beta peptides differentially affect neuronal viability. J. Biol. Chem. 2002; 277: 32046-53.

42. Cizas P, Budvytyte R, Morkuniene R, Moldovan R, Broccio M, Losche M, et al. Size-dependent neurotoxicity of beta-amyloid oligomers. Arch. Biochem. Biophys. 2010; 496: 84-92.

43. Roychaudhuri R, Yang M, Hoshi MM,Teplow DB. Amyloid beta-protein assembly and alzheimer disease. J. Biol. Chem. 2009; 284: 4749-53.

44. Brambilla D, Nicolas J, Droumaguet BL, Andrieux K, Marsaud V, Couraud P-O, et al. Design of fluorescently tagged poly(alkyl cyanoacrylate) nanoparticles for human brain endothelial cell imaging. Chem. Commun. (Cambridge, U. K.) 2010; 46: 2602-04.

45. Han Y, He C, Cao M, Huang X, Wang Y,Li Z. Facile disassembly of amyloid fibrils using gemini surfactant micelles. Langmuir 2009; 26: 1583-87.

46. Taniguchi A, Sohma Y, Hirayama Y, Mukai H, Kimura T, Hayashi Y, et al. "Click peptide": Ph-triggered in situ production and aggregation of monomer abeta1-42. Chembiochem 2009; 10: 710-5.

47. Balducci C, Beeg M, Stravalaci M, Bastone A, Sclip A, Biasini E, et al. Synthetic amyloid-beta oligomers impair long-term memory independently of cellular prion protein. Proc Natl Acad Sci U S A 2010; 107: 2295-300.

48. Atha DH,Ingham KC. Mechanism of precipitation of proteins by polyethylene glycols. Analysis in terms of excluded volume. J Biol Chem 1981; 256: 12108-17.

49. Shulgin IL,Ruckenstein E. A protein molecule in a mixed solvent: The preferential binding parameter via the kirkwood-buff theory. Biophys J 2006; 90: 704-7.

50. Auer S, Trovato A,Vendruscolo M. A condensation-ordering mechanism in nanoparticle-catalyzed peptide aggregation. PLoS Comput Biol 2009; 5: e1000458.

51. Chiti F,Dobson CM. Protein misfolding, functional amyloid, and human disease. Annu Rev Biochem 2006; 75: 333-66.

Supporting Information

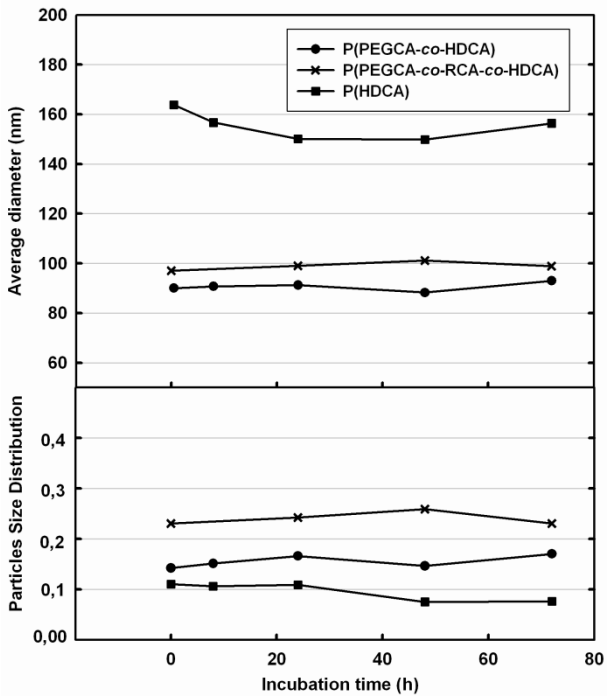

Figure S1: : *Evolution of average diameters and particle size distributions of P(MePEGCA-co-HDCA), P(MePEGCA-co-RCA-co-HDCA) and PHDCA nanoparticles in capillary electrophoresis buffer (NaH_2PO_4/Na_2HPO_4) at 37 °C as a function of time.*

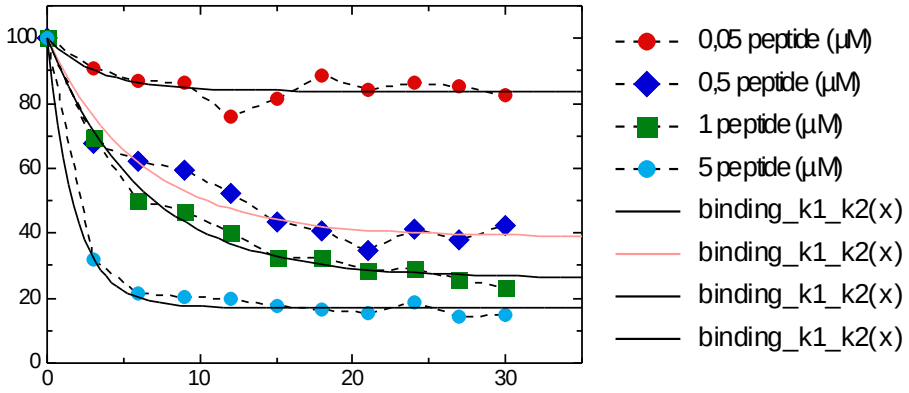

Figure S2*: Fitting of plot describing the $A\beta_{1\text{-}42}$ monomer disappearance as function of time in the presence of P(MePEGCA-co-RCA-co-HDCA) nanoparticles.*

Figure S2 shows the fitting curves employed to quantitatively analyze the binding phenomenon using the following considerations. We assumed that the Aβ-nanoparticles interaction is governed by a first-order kinetics (see supporting material of Bornhop et al.).[203] All the fitting reported in the figure were obtained using eq 1:

$$CE(t) = 100 - Y_{\max} e^{-k_{obs} t} \qquad (1)$$

The free parameter of the fit, k_{obs}, has been extracted for different values of $A\beta_{1\text{-}42}$ concentration. k_{obs} values have been plotted as a function of the peptide concentration (Figure S3).

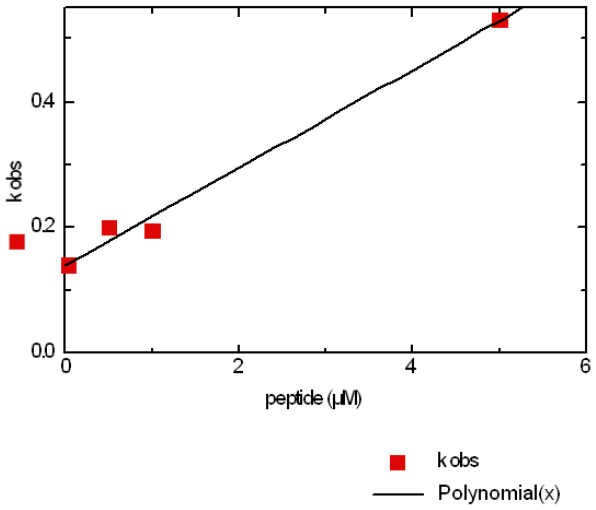

Figure S3*: k_{obs} vs peptide concentration plots deriving from eq 1, which describes the $A\beta_{1\text{-}42}$ monomer disappearance as function of time in the presence of P(MePEGCA-co-RCA-co-HDCA) nanoparticles.*

As shown in Figure S3, the evolution of k_{obs} is linear as a function of the $A\beta_{1\text{-}42}$ concentration (C_{Abeta}) and can be described by eq 2:

$$k_{obs} = k_1 C_{Abeta} + k_2 \qquad (2)$$

Where k_1 represents the slope of the linear fit and k_2 its intercept. According to the equilibrium dissociation constant, $k_d = k_2/k_1$. By a linear fit of k_{obs} vs C_{Abeta} plot, we extracted the values of the free parameters $k_1 = 0.14\ \mu M^{-1}$ and $k_2 = 0.078$. As consequence, the binding constant was estimated to $k_d = 0.55\ \mu M$.

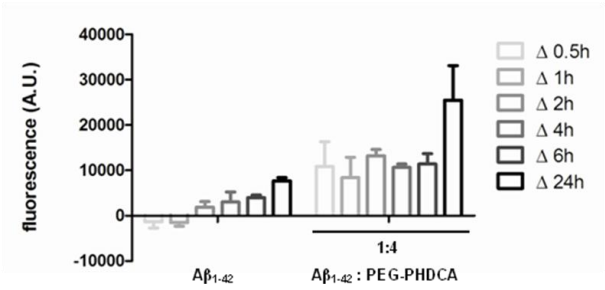

Figure S4. *Aβ$_{1-42}$ (50μM) was incubated in the presence of P(MePEGCA-co-HDCA) NPs for 24h at 37 ºC. At the indicated time points aliquots were taken to analyze the β-sheet content by the ThT assay. Each bar represents the absolute change in fluorescence for the different time slots. The graph represents the mean ± SD (n=3) from one experiment. Results shown are representative of three independent experiments.*

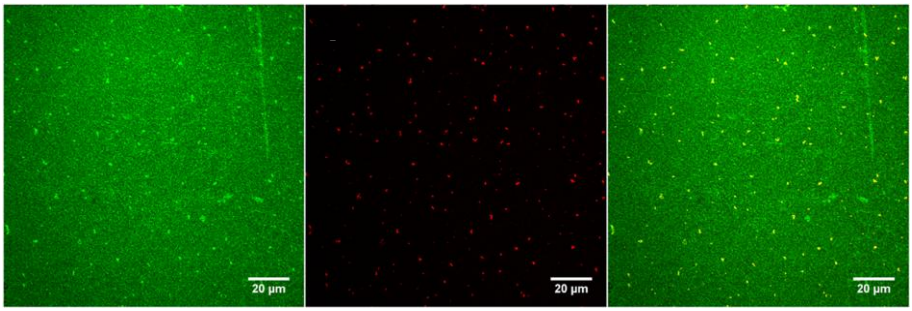

Figure S5. *CLSM images obtained immediately after mixing of P(MePEGCA-co-RCA-co-HDCA) NPs with Hilyte Fluo™ Aβ$_{1-42}$ (10 μM). Visualization of (a) Aβ peptide (10 μM) (green channel), (b) P(MePEGCA-co-RCA-co-HDCA) nanoparticles (20 μM) (red channel) and (c) colocalization (merge of a and b).*

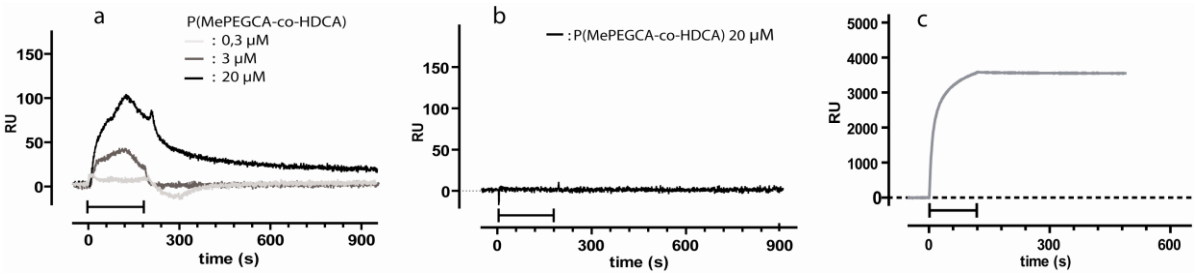

Figure S6. Sensorgrams of (a) P(MePEGCA-co-HDCA) NPs flowed onto a Aβ$_{1-42}$ immobilized gold chip and (b) P(MePEGCA-co-HDCA) NPs flowed onto an BSA immobilized gold chip; (c) Binding of the anti-Aβ antibody 6E10 (100 nM) injected onto chip surface immobilizing Aβ$_{1-42}$ monomers.

1. Bornhop, D. J.; Latham, J. C.; Kussrow, A.; Markov, D. A.; Jones, R. D.; Sorensen, H. S. *Science* 2007, *317*, 1732.

Section 2

Implications dans le projet NAD

Dans cette section du chapitre, est décrite la préparation d'une petite librairie de nanoparticules dans le but d'étudier l'influence des caractérisitiques physicochimiques des nanoparticules telles que la taille, la charge de surface ou la présence de molcules de tensioactif en surface sur l'interaction avec le peptide Aβ. Toutes les particules préparées ont été criblées par Electrophorèse Capillaire. Les résultats obtenus ont démontré que ces différentes caractéritiques des nanoparticules ont un rôle fondamental dans l'interaction avec le peptide.

Implications in the NAD project

In the section of this chapter is described a small library of polymeric nanoparticles which have been prepared in order to study the roles of the physicochemical characteristics such as the size, the surface charge or the presence of surfactant molecules in surface for the interaction with the peptide. The prepared nanoparticles have been screened by Capillary Electrophoresis. The results outlined that these different characteristics of nanoparticles have a fundamental role on the interaction with the peptide.

Colloidal properties of biodegradable nanoparticles influence interaction with amyloid-β peptide

Journal of Biotechnology, *In Press*, doi:10.1016/j.jbiotec.2011.07.020

Davide Brambilla,[¥] Hayfa Souguir,[¥] Julien Nicolas, Nicolas Mackiewicz, Romain Verpillot, Benjamin Le Droumaguet, Myriam Taverna, Patrick Couvreur and Karine Andrieux*

Laboratoire de Physico-Chimie, Pharmacotechnie et Biopharmacie, Univ. Paris-Sud, UMR CNRS 8612, Faculté de Pharmacie, 5 rue Jean-Baptiste Clément, F-92296 Châtenay-Malabry cedex, France.

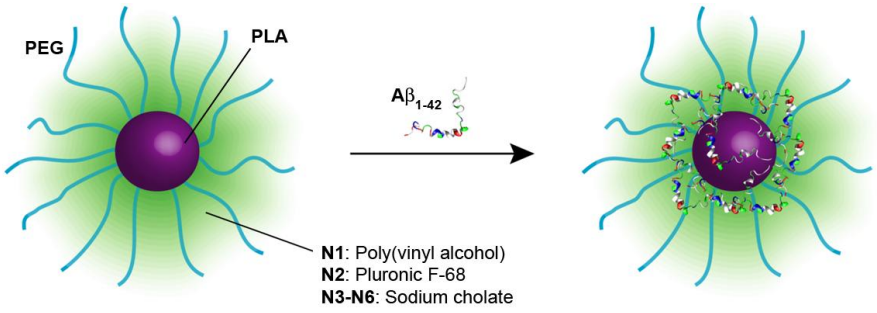

Résumé

La Maladie d'Alzheimer (MA) est une maladie neuro-dégénérative caractérisée par le dépôt extracellulaire de peptides amyloïdes β (Aβ). Durant ces dernières années, des approches prometteuses, basées sur les nanotechnologies, ont émergé pour modifier l'agrégation du peptide Aβ et réduire sa toxicité. Cette étude vise à étudier l'influence des propriétés colloïdales des nanoparticules sur l'interaction avec le peptide Aβ 1-42 ($A\beta_{1-42}$). L'utilisation de la technique CE-LIF a permis de montrer que des NPs biodégradables de poly(éthylène glycol)-*block*-polylactide (PEG-*b*-PLA) pouvaient interagir avec le peptide $A\beta_{1-42}$ conduisant à sa capture très rapidement. De plus, nous avons mis à jour le rôle crucial des propriétés colloïdales des nanovecteurs sur la cinétique de capture. Alors que des nanoparticules stabilisées par du cholate de sodium (donnant une taille de NPs plus petite et une plus forte charge négative de surface) ont donné une cinétique d'adsorption optimale, leur stabilisation par d'autres tensio-actifs ont présenté moins d'interactions. Par contre, la variation de la densité de PEG n'a semblé avoir aucune influence sur l'interaction lorsque le cholate de sodium a été utilisé pour leur préparation. Cette étude entend aider à déterminer les meilleures caractéristiques des nanoparticules pour établir des nouvelles stratégies thérapeutiques contre la MA.

Abstract

Alzheimer's Disease (AD) is a neurodegenerative disorder characterized by the extracellular deposition of amyloid-β peptides (Aβ). During the past few years, promising approaches based on nanotechnologies have emerged to alter Aβ aggregation and its related toxicity. This study aims to investigate the influence of the nanoparticle colloidal properties over the interaction with Aβ peptide 1-42 ($A\beta_{1-42}$). Using capillary electrophoresis with laser-induced fluorescence detection, it was shown that biodegradable poly(ethylene glycol)-*block*-polylactide (PEG-*b*-PLA) nanoparticles were able to interact with $A\beta_{1-42}$ peptide leading to its uptake in rather short time periods. In addition, we highlighted the crucial role of the nanocarrier colloidal properties on the uptake kinetics. Whereas nanoparticles stabilized by sodium cholate (lower size and higher negative surface charge) gave optimum uptake kinetics, nanoparticles stabilized with others surfactants presented lower interactions. In contrast, PEG density seemed to have no influence on the interaction when sodium cholate was used for the preparation. This study intends to give new insights into $A\beta_{1-42}$ peptide interaction with nanoparticulate systems by helping to determine suitable nanoparticle characteristics regarding forthcoming therapeutic strategies against AD.

Keywords

Alzheimer's disease, nanoparticles, surface properties, amyloid-β peptide.

1. Introduction

Alzheimer's Disease (AD) is a neurodegenerative disorder characterized by a progressive loss of cognitive functions and characteristic pathological changes in the brain.[1] It is histopathologically characterized by two main hallmarks: (i) the extracellular deposition of amyloid plaques, mainly composed of amyloid-β peptides (Aβ) and (ii) intracellular neurofibrillar tangles composed of hyperphosphorylated τ protein.[2,3] Among the different species, the Aβ peptide 1-42 ($A\beta_{1-42}$) is believed to be the most representative and the most toxic species in AD physiopathology due to its high tendency to spontaneously self-aggregate.[4] Despite all scientific efforts, efficient pharmacotherapeutic options for the prevention and the treatment of this disease are still lacking.[5]

During the past few years, promising developments in relation to passive and active drug delivery to the brain using nanoparticles have been witnessed.[6] In parallel, remarkable approaches based on nanotechnologies that can alter Aβ aggregation both in the brain and in the peripheral circulation thus aiding experimental AD therapy have emerged.[7] In this view, a novel application of capillary electrophoresis with laser-induced fluorescence detection (CE-LIF) was recently proposed to efficiently detect and monitor interaction between polymeric nanoparticles and $A\beta_{1-42}$ peptide, at concentrations close to physiological conditions (Brambilla et al., 2010). It was demonstrated that PEGylated poly(alkyl cyanoacrylate) nanoparticles could bind the soluble $A\beta_{1-42}$ peptide monomers and influence its aggregation kinetics whereas non-PEGylated counterparts did not lead to detectable interaction, thus suggesting the crucial role of the colloidal properties of the nanoparticles employed. Moreover, other experiments using surface plasmon resonance have evidenced a certain specificity of the interaction between PEGylated NPs and the Aβ peptide as long as no interaction was observed under identical experimental conditions between these NPs and BSA, a major serum protein.[7]

Herein, we wish to go a step further by investigating: (i) whether this interaction could be obtained with another kind of PEGylated, biodegradable nanoparticles and (ii) the influence of the nanoparticle colloidal properties (size, charge and PEG density) over interaction with $A\beta_{1-42}$ peptide (Figure 1). To achieve this goal, we have selected poly(ethylene glycol)-*block*-polylactide (PEG-*b*-PLA) copolymer nanoparticles, which represent a widely-employed class of nanocarriers for biomedical purposes.[8] The colloidal features of the nanoparticles were modulated by playing with the

nature of the surfactant, whereas the density of PEG chains displayed at the nanoparticle surface was finely tuned by using various PEG-*b*-PLA/PLA blend ratios during nanoparticle preparation.

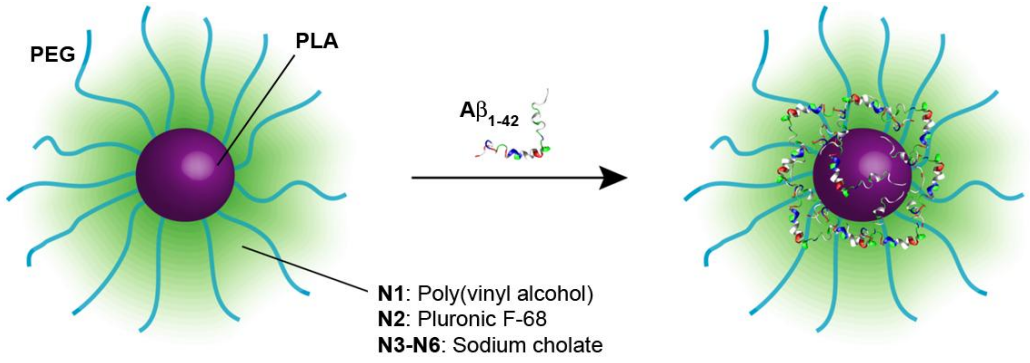

Figure 1. *Schematic representation of poly(ethylene glycol)-block-polylactide (PEG-b-PLA) copolymer nanoparticles prepared with different surfactants and subsequent interaction with* $A\beta_{1\text{-}42}$ *peptide.*

2. Results and Discussion

A small library of PEG-*b*-PLA nanoparticle suspensions (**N1**–**N6**) displaying various colloidal characteristics was prepared by the emulsion/evaporation procedure using three different surfactants and four different PEG contents (Table 1). Two neutral surfactants, poly(vinyl alcohol) and Pluronic F-68, together with sodium cholate as a negatively-charged surfactant, were used in order to cover a broad range of surface charges and properties. The density of PEG chains located at the surface of the particles was tuned by varying the PEG-*b*-PLA/PLA blend ratio upon nanoparticle preparation, as previously described by Gref et al.[9,10]

Table 1. *Preparation of PEGylated, biodegradable nanoparticles with various colloidal properties.*

Nanoparticles	PEG-*b*-PLA[a]:PLA[b]	Surfactant[c]	*S*[d]	PEG distance[e]
	wt./wt.		nm^2	nm
N1	100:0	PVA (30-70 kDa)	0.60	0.78
N2	100:0	Pluronic F-68	0.83	0.91
N3	100:0	Sodium Cholate	1.39	1.18
N4	66:34	Sodium Cholate	2.10	1.45
N5	3:97	Sodium Cholate	46.3	6.81
N6	0:100	Sodium Cholate	0	0

*[a]PLA-b-PEG block copolymers were synthesized by ring opening polymerization. To a solution of methoxypoly(ethylene glycol) (M_n = 2000 g.mol^{-1}, 500 mg, 0.24 mmol) in 5.2 mL of anhydrous toluene, was added D,L-lactide (2.43 g, 16.9 mmol) and Sn(Oct)$_2$ (5.4 µL, 16.5 µmol). The reaction mixture was degassed by bubbling nitrogen for 30 min and then stirred in a pre-heated oil bath at 115°C for 5.5 h. The toluene was removed under reduced pressure and the obtained product was dissolved into a minimum amount of THF and further precipitated twice in water and subsequently freeze-dried overnight to yield a white powder (conversion = 93%, m = 1.7 g, $M_{n,NMR}$ = 12200 g.mol^{-1}, $M_{n,SEC}$ = 12400 g.mol^{-1}; M_w/M_n = 1.12). [b]M_n ~ 23000 g.mol^{-1} (Boehringer-Ingelheim, Germany). [c]Nanoparticle suspensions (**N1**–**N6**) were prepared by the emulsion/evaporation procedure. 10 mg of PLA-b-PEG copolymer were dissolved in 4 mL of dichloromethane (ethyl acetate for **N2**) and added to a 10 mL aqueous solution of surfactant (1 wt.%). The resulting sample was vortexed two times for 1 min at 3200 rpm and ultrasonicated on ice for 1 min at 300 W (40%) using a Vibral-cell sonicator. The organic solvent was evaporated at atmospheric (reduced for **N2**) pressure and room temperature under magnetic stirring. The resulting nanoparticles were purified from free surfactant by ultracentrifugation (21000 g, 20 min, 4 °C) and resuspended in deionized water. [d]The surface (S) available for each PEG chain at the nanoparticle surface (also called ρPEG) is described by $S = (6.M_{n,PEG})/(d.N_A.f.\rho)$, with d the nanoparticle mean diameter, N_A the Avogadro number (6.022 × 10^{23} mol^{-1}), $M_{n,PEG}$ the number-average molar mass of PEG (2000 g.mol^{-1}), f the PEG weight fraction in the PEG-b-PLA/PLA blend and ρ the density of the nanoparticles (1,27 g.cm^{-3}). [e]PEG distance represents the spatial gap between each PEG chain at the surface, calculated as $\sqrt{S}$.*

In all cases, stable nanoparticles with relatively narrow particle size distributions were obtained, exhibiting average diameters in the 70–160 nm range depending on the surfactant used (**N1**–**N6**, Figure 2-a). In addition, zeta-potential (ξ) values were in good agreement with the nature of the surfactant (Figure 2-b). Indeed, PVA conducted to a nearly neutral surface charge (**N1**), Pluronic F-68

gave a slightly negative surface charge of about –15 mV (**N2**), close to literature data,[11] and sodium cholate yielded strongly negative ξ-potential values below –30 mV (**N3**–**N6**). However, by modifying the surface occupied by each PEG chain at the nanoparticle surface from 0 to 46.3 nm^2 (Table 1), no detectable changes in the colloidal characteristic of the nanoparticles were obtained (Figure 2-b).

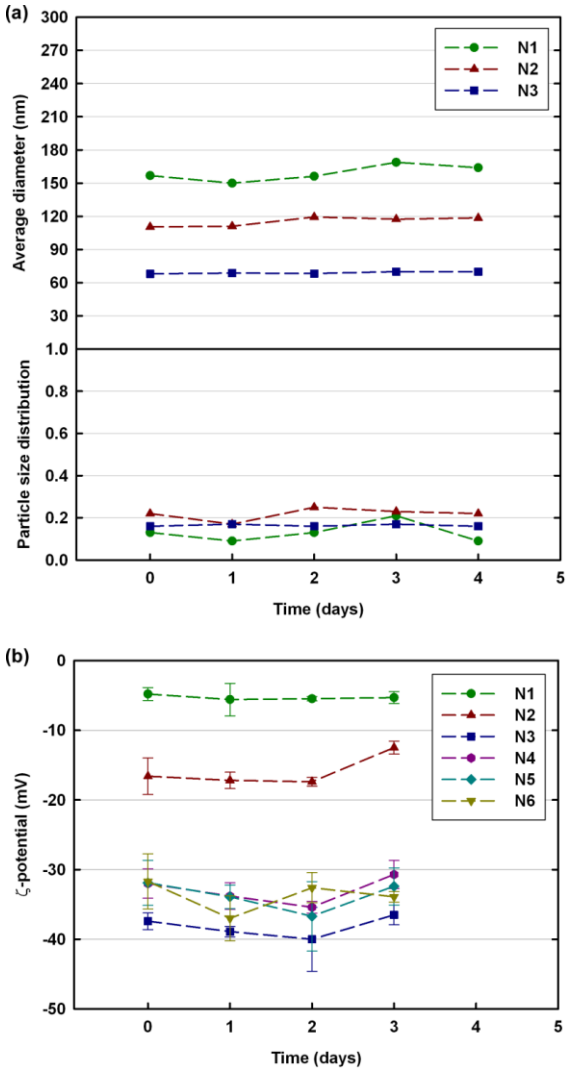

Figure 2. *Evolution of average diameters and particle size distribution in 20 mM NaH_2PO_4 buffer (a) and ζ-potential measured in a 1 mM KCl solution (b) of PLA-b-PEG nanoparticles (**N1–N6**) at 37°C as a function of time. Nanoparticle average diameter was measured by dynamic light scattering (DLS) with a Nano ZS from Malvern (173° scattering angle) at a temperature of 37 °C. The ζ-potential was calculated with the same apparatus.*

The $A\beta_{1-42}$ peptide was incubated with nanoparticles **N1**–**N6** and its uptake by the colloidal nanocarriers was monitored *via* CE-LIF,[7] by following the disappearance of the fluorescently-labeled $A\beta_{1-42}$ peptide monomer peak with time (Figure 3). Importantly, we observed a dramatic influence of the nanoparticle colloidal properties over the uptake kinetics. Whereas sodium cholate-stabilized

nanoparticles (**N3**), which exhibited the lowest mean diameter and the most negative charge, yielded the fastest $A\beta_{1\text{-}42}$ peptide uptake kinetics, nanoparticles stabilized by PVA (**N1**) and Pluronic F-68 (**N2**) exhibited slower kinetics. It is noteworthy that PVA-stabilized nanoparticles with the highest size and the lowest charge led to the slowest uptake kinetic. Interestingly, no significant difference was observed when varying the PEG density displayed at the surface of the sodium cholate-stabilized nanoparticles (**N3**–**N6**). In particular, the high peptide uptake of nanoparticles **N6**, which are non-PEGylated, suggested the major role of the surfactant in comparison with PEG density.

Therefore, it is clear that the colloidal properties of the nanoparticles played an important role during the interaction with the $A\beta_{1\text{-}42}$ peptide and that nanoparticle surface chemistry must be precisely tuned in order to achieve an efficient uptake. However, from our results, it seems that the surface chemistry deriving from the surfactant itself (functional groups, charge, etc) are likely to govern the uptake.

Moreover, the obtained results prompted a role for the nanoparticle average diameter (whereby the lower the average diameter, the higher the surface contact area) in the interaction with amyloid peptide. However, further analyses are under progress in order to establish the precise surface chemistry/interaction and average diameter/interaction relationships and will be the topic of a forthcoming paper.

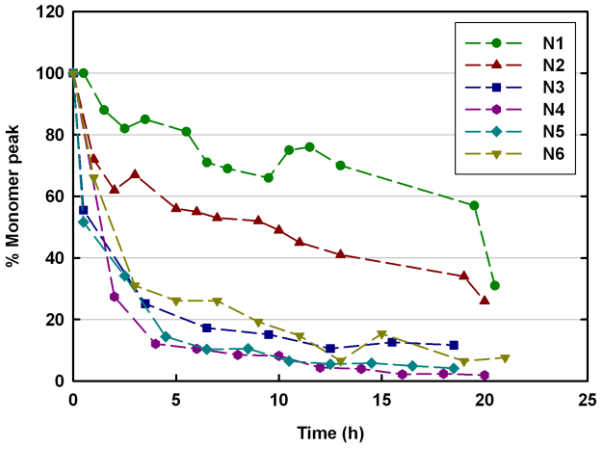

Figure 3. *Corrected areas of the $A\beta_{1\text{-}42}$ monomer peak as a function of time upon incubation in the presence of different surface-coated nanoparticles. The nanoparticles (20 µM) were incubated with the Hilyte Fluor™ labeled $A\beta_{1\text{-}42}$ peptide (5 µM) in phosphate buffer (NaH_2PO_4, 20 mM), stored at 37°C and analyzed every 2 h by CE-LIF as previously described.*

3. Conclusions

We have shown by CE-LIF that well-established, biodegradable PEG-*b*-PLA nanoparticles were able to interact with $A\beta_{1-42}$ peptide leading to its uptake in rather short time periods, thus broadening the range of potential nanodevices for AD treatment. In addition, we highlighted the crucial role of the colloidal properties of the employed nanocarriers on the uptake kinetics, where nanoparticles stabilized by sodium cholate gave optimum uptake kinetics. In contrast, the variation of the PEG density exposed at their surface did not lead to appreciable kinetic differences. This study intends to give new insights into $A\beta_{1-42}$ peptide interaction with nanoparticulate systems by helping to determine suitable nanoparticle characteristics for forthcoming therapeutic strategies against AD.

4. Acknowledgments

We thank the European Community's Seventh Framework Programme (FP7/2007-2013) under grant agreement n^{o} 212043 for funding (DB and BLD). The French ministry of research and CNRS are also warmly acknowledged for financial support.

5. References

1. Querfurth, H.W., LaFerla, F.M. Alzheimer's disease. N Engl J Med 2010, 362, 329.
2. Aguzzi, A., O'Connor, T. Protein aggregation diseases: pathogenicity and therapeutic perspectives. Nat Rev Drug Discov 2010, 9, 237.
3. Panza, F., Solfrizzi, V., Frisardi, V., Imbimbo, B.P., Capurso, C., D'Introno, A., Colacicco, A.M., Seripa, D., Vendemiale, G., Capurso, A., Pilotto, A. Beyond the neurotransmitter-focused approach in treating Alzheimer's disease: drugs targeting beta -amyloid and tau protein. Aging Clin Exp Res, 2009, 21, 386.
5. Wollen, K.A. Alzheimer's Disease: The Pros and Cons of Pharmaceutical, Nutritional, Botanical, and Stimulatory Therapies, with a Discussion of Treatment Strategies from the Perspective of Patients and Practitioners. Altern Med Rev 2010, 15, 223.
4. Findeis, M.A. The role of amyloid [beta] peptide 42 in Alzheimer's disease. Pharmacology & Therapeutics 2007 116, 266.
6. Brambilla, D., Le Droumaguet, B., Nicolas, J., Hashemi, S.H., Wu, L.-P., Moghimi, S.M., Couvreur, P., Andrieux, K. Nanotechnologies for Alzheimer's disease: therapy, diagnosis and safety issues. Nanomedicine: NBM, 2011,7(5), 521.
7. Brambilla, D., Verpillot, R., Taverna, M., De Kimpe, L., Le Droumaguet, B., Nicolas, J., Mantegazza, F., Canovi, M., Gobbi, M., Salmona, M., Nicolas, V., Scheper, W., Couvreur, P., Andrieux, K. Capillary electrophoresis with laser-induced fluorescence detection (CE-LIF) as a new protocol to monitor interaction between nanoparticles and the amyloid-β peptide. Anal Chem 2010, 82, 10083.
8. Benny, O., Fainaru, O., Adini, A., Cassiola, F., Bazinet, L., Adini, I., Pravda, E., Nahmias, Y., Koirala, S., Corfas, G., D'Amato, R.J., Folkman, J. An orally delivered small-molecule formulation with antiangiogenic and anticancer activity. Nat Biotechnol 2008, 26, 799.

9. Gref, R., Minamitake, Y., Peracchia, M.T., Trubetskoy, V., Torchilin, V., Langer, R. Biodegradable Long-Circulating Polymeric Nanospheres. Science 1994, 263, 1600.

10. Gref, R., Luck, M., Quellec, P., Marchand, M., Dellacherie, E., Harnisch, S., Blunk, T., Muller, R.H. 'Stealth' corona-core nanoparticles surface modified by polyethylene glycol (PEG): influences of the corona (PEG chain length and surface density) and of the core composition on phagocytic uptake and plasma protein adsorption. Colloids Surf B Biointerfaces 2000, 18, 301.

11. Pierson, L.-A., Nicolas, J., Lalanne, M., Brambilla, D., Marsaud, V., Nicolas, V., Ball, R., Stanimirovic, D., Couvreur, P., Andrieux, K. Formulation of didanosine prodrugs into PEGylated poly(alkyl cyanoacrylate) nanoparticles and uptake by brain endothelial cells. J Nanoneurosci 2009, 1, 174.

Section 3

Implications dans le projet NAD

Des études d'Electrophorèse Capillaire et de Résonance Plasmonique de Surface nous ont permis d'identifier le rôle majeur joué par les chaines PEG présentent à la surface de nanoparticules pour l'interaction de ces dernières avec le peptide $A\beta_{1-42}$. Pendant cette étude, plusieurs expériences ont été réalisées pour mieux comprendre les mécanismes mis en jeux lors de cette interaction. Des études de modélisation moléculaire, entre autres, ont permis de mettre à jour le probable mécanisme moléculaire potentiel de l'interaction.

Implications in the NAD project

The Capillary Electrophoresis and Surface Plasmon Resonance experiments showed the major role of the PEG chains at the surface of the nanoparticles for their interaction with the $A\beta_{1-42}$ peptide. During this study several experiments have been performed in order to better understand the mechanism of this interaction. Molecular modeling studies, among other ones, outlined the probable molecular mechanism of interaction.

Polyethylene Glycol at the surface of nanocarriers alters Aβ peptide conformation: toward a nanomedicine for Alzheimer's disease

Paper in finalization

Davide Brambilla[1], Romain Verpillot[1],Benjamin Le Droumaguet[1], Myriam Taverna[1], Julien Nicolas[1], Juraj Kóňa[2], S. Hossein Hashemi[3], Barbara Lettiero[3], Line De Kimpe[4], Marco Gobbi[5], Valérie Nicolas[6], Wiep Scheper[4], S. Moein Moghimi[3], Igor Tvaroška[2], Patrick Couvreur[1], Karine Andrieux[1]

[1]Laboratoire de Physico-Chimie, Pharmacotechnie et Biopharmacie, UMR CNRS 8612, Univ Paris-Sud 11, Faculté de Pharmacie, 5 rue Jean-Baptiste Clément, F-92296 Chatenay-Malabry, France;

[2] Institute of Chemistry, Center for Glycomics, Slovak Academy of Sciences, Dúbravska cesta 9, 845 38 Bratislava, Slovakia;

[3]Centre for Pharmaceutical Nanotechnology and Nanotoxicology, Department of Pharmaceutics and Analytical Chemistry, University of Copenhagen, Universitetsparken 2, DK-2100 Copenhagen, Denmark;

[4]Neurogenetics Laboratory, Academic Medical Center, Amsterdam, The Netherlands;

[5]Istituto di Ricerche Farmacologiche "Mario Negri", Milano, Italy;

[6]Institut d'Innovation Thérapeutique (IFR141 ITFM), Univ Paris-Sud, Faculté de Pharmacie, 5 rue Jean-Baptiste Clément, F-92296 Châtenay-Malabry, France.

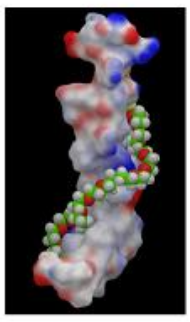

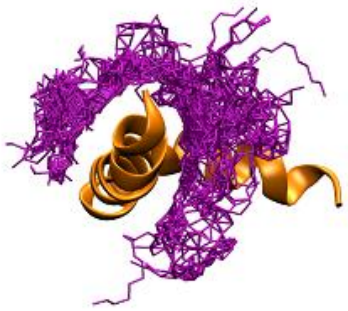

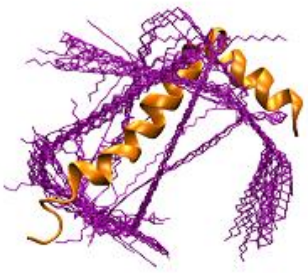

Resumé

Le mécanisme par lequel la couronne de polyéthylène glycol (PEG) à la surface des nanoparticules de poly(cyanoacrylate d'alkyl) (PACA) interagit avec le peptide $A\beta_{1-42}$ a été largement étudié dans le but de concevoir des nanomédicaments efficaces contre la maladie d'Alzheimer. Pour atteindre cet objectif, l'interaction des nanoparticules PACA PEGylées avec différentes formes du peptide $A\beta_{1-42}$ (*c'est à dire* le peptide monomère, les oligomères solubles et les fibriles), correspondants aux différentes étapes de son agrégation, a été étudiée par l'utilisation d'une combinaison de plusieurs techniques : l'électrophorèse capillaire, la résonance plasmonique de surface, l'analyse à la thioflavine T, la microscopie confocale et les expériences *in silico*. L'ensemble des résultats ont montré que les nanoparticules de poly[hexadécyl cyanoacrylate-*co*-méthoxypoly(éthylène glycol) cyanoacrylate] (P(HDCA-*co*-MePEGCA)) interagissent avec la cinétique d'agrégation du peptide *via* la capture de sa ses formes les plus toxiques et ont mis en évidence le rôle clé des chaines de PEG dans cette interaction. Les expériences *in silico* ont démontré que le PEG, largement utilisé pour couvrir les nanovecteurs, pouvait interagir avec les résidus hydrophobes et hydrophiles du peptide et ainsi induire un changement de conformation, ce ce qui déclencherait son agrégation à la surface des nanoparticules. L'activation du complément et l'adsorption de l'Apo E par ces NPs quand le peptide $A\beta_{1-42}$ y a été pré-adsorbé ne sont modifiés. Cela suggère que ces NPs, agissant comme des particules LDL, pourrait capturer le peptide sous ses formes solubles dans le sang et augmenter son élimination du sang et du cerveau grâce à ce qu'on appelle l'« effet sink ». Tous les résultats suggèrent que les NPs de P(HDCA-*co*-MePEGCA) sont un nanomédicament prometteur contre la maladie d'Alzheimer.

Abstract

The mechanism by which the polyethylene glycol (PEG) corona at the surface of poly(alkyl cyanoacrylate) (PACA) nanoparticles interacts with the $A\beta_{1-42}$ peptide has been deeply investigated in order to design suitable and efficient nanomedicines against Alzheimer's disease. To this purpose, the binding of these polymeric PEGylated PACA nanoparticles with different forms of $A\beta_{1-42}$ *i.e.* the monomeric peptide, soluble oligomers and fibrils, corresponding to different steps of its aggregation, has been examined through the combination of different techniques: capillary electrophoresis, surface plasmon resonance, thioflavine T assay, confocal microscopy and *in silico* experiments. The overall results evidenced that poly[hexadecyl cyanoacrylate-*co*-methoxypoly(ethylene glycol) cyanoacrylate] (P(HDCA-*co*-MePEGCA)) NPs interfere with the peptide aggregation kinetic via the uptake of its

most toxic forms and revealed the pivotal role of PEG chains regarding this binding. *In silico* experiments indicated that PEG, widely employed to cloak nanocarriers, can interact with both hydrophobic and hydrophilic residues of the peptide, thus leading to its conformational change widely believed to trigger its aggregation at the nanoparticle surface. Complement activation and Apo E adsorption by these NPs when preadsorbed with $A\beta_{1-42}$ peptide are not modified suggesting that these NPs, acting as LDL-like particles, might capture the peptide soluble forms in blood and increase its clearance from blood and brain thanks to the so called "sink effect". All the results suggest that P(HDCA-*co*-MePEGCA) NPs are a promising nanomedicine against Alzheimer's disease.

Keywords

Polyethylene glycol, nanoparticles, $A\beta_{1-42}$, Alzheimer's disease.

1. Introduction

Alzheimer's disease (AD) is the most common form of senile dementia affecting more than 35 million people worldwide. This neurodegenerative disorder, clinically characterized by a progressive loss of memory and other cognitive abilities, can be distinguished by different physiopathological hallmarks such as neuronal loss, glial proliferation, extracellular amyloid plaques deposition mainly composed of β-amyloid peptide (Aβ) and intracellular neurofibrillar tangles composed of hyperphosphorylated τ-protein.[1] AD is likely the result of a multifactorial process in which genetic and environmental factors are involved. Unfortunately the etiology of the disease is still under debate in the scientific community.[2-4] AD treatment constitutes a major challenge in medicine as all current therapies are just palliative and only oriented to AD symptoms alleviation.

Important evidences pointed out that progressive production, accumulation and aggregation of Aβ peptide, leading to the formation of amyloid plaques, were observed in patient's brain.[5-6] Aβ peptides are produced by numerous cells such as neurons from the proteolysis of Amyloid Precursor Protein (APP). In AD patients, APP is preferentially but "pathologically" cleaved by β- and γ-secretases forming Aβ peptides with varying number of amino-acids ranging from 39 to 42.[7-8] The origin of the Aβ peptide that accumulates in the brain is still unclear,[9] however, once released in the brain, the monomer can cross the blood-brain barrier (BBB) likely due to the lipoprotein receptor related protein (LRP)[10] and apolipoprotein E (Apo E),[11] reaching the bloodstream where it can be efficiently cleared. Other pathways for Aβ peptide elimination, that avoid its accumulation in healthy brain, are also

described in the literature.[12] Under pathological conditions, the clearance of Aβ peptide from the body seems dramatically decreased, thus leading to peptide accumulation in the brain that progressively aggregates in small oligomers, soluble *β*-sheet aggregates, fibrils and finally plaques.[13-16] Among these different species, the Aβ peptide 1-42 ($A\beta_{1-42}$) monomer is considered nowadays as the most toxic isoform due to its higher hydrophobic nature and tendency to aggregate[17-18] while plaques, fibrils and especially soluble $A\beta_{1-42}$ oligomers are known to be responsible of toxic effects on neurons.[19-20] Considering this, great efforts have been so far devoted to the development of new molecules which can interact with Aβ peptide at different steps of its aggregation pathway in order to favour its elimination and to reach the equilibrium between production and clearance or to slow down the fibrillogenesis process.[21]

For many years, nanoparticles (NPs) composed of poly(alkyl cyanoacrylate) (PACA) (co)polymers have been used in various research groups, especially for their biocompatibility and biodegradability properties.[22] Thereby, these NPs have been used as potential carriers for drug targeting and nanomedicine purposes. PACA NPs are actually in phase III clinical trials for an application in the treatment of MDR hepatocarcinoma.[23]

A milestone of these particles has been the synthesis of the PEGylated form of the polymer able to self assemble in stealth nanoparticles.[24] Indeed, the PEG shell drastically increases the blood half-life of the NPs by decreasing the opsonin adsorption and allowing the escape from the immune system. In the same time, the PEG outer shell favours the adsorption of Apo E, another serum (lipo)protein which has a relatively low plasmatic concentration.[24-27] These nanoparticles are finally degraded by serum esterases and eliminated by the liver and the spleen. Due to their relatively long blood circulation time, P(HDCA-*co*-MePEGCA) NPs appear as promising carriers to kidnap the circulating Aβ peptide. Recently, a powerful application using capillary electrophoresis coupled to laser-induced fluorescence detection (CE-LIF) was proposed to efficiently monitor the interactions between nanoparticles and $A\beta_{1-42}$ monomers at concentrations close to physiological conditions.[28] The results suggested that P(HDCA-*co*-MePEGCA) nanoparticles can bind the peptide and that their non-PEGylated counterparts cannot, thus pointing out the essential role of PEG chains at the nanoparticle surface for this interaction.

In the present study, *in vitro* and *in silico* experiments were performed to investigate in details the mechanism by which the interaction between PEGylated nanoparticles and Aβ peptide originates from. For this purpose, the interplay of P(HDCA-*co*-MePEGCA) nanoparticles with $A\beta_{1-42}$ peptide at different steps of aggregation (i.e., monomeric peptide, small and soluble oligomers and fibrils) was studied by complementary analytical methods. Their non-PEGylated counterparts were used as

negative control. The influence of either the nanoparticle core or the PEG outer shell regarding this binding was also carried out using CE-LIF by measuring the uptake of the monomeric peptide by methoxypoly(ethylene glycol-*b*-poly(lactic acid) (MePEG-*b*-PLA) *vs.* poly(lactic acid) (PLA) polymeric NPs and by free methoxypoly(ethylene glycol) (MePEG) having the same molecular weight than the one used to synthesize the polymers. To verify that this interaction originates from PEG chains, molecular modelling experiments were conducted. Finally, the complement activation and the Apo E adsorption by these NPs were studied in presence or absence of $A\beta_{1-42}$ peptide in order to anticipate *in vivo* ability of these NPs to increase peptide clearance in AD patient.

2. Results and discussion

The interaction of $A\beta_{1-42}$ peptide with PEG and NPs with various size, surface charge and composition (Tab. 1) was investigated by complementary techniques *i.e.* CE-LIF/UV, surface plasmon resonance (SPR), thioflavine T assay, confocal laser scanning microscopy (CLSM) and molecular modelling.

Table 1. Physico-Chemical Properties of the Nanoparticles Used in CE-LIF Experiments.

Sample	P(HDCA)	P(MePEGCA-*co*-RCA-*co*-HDCA)	PLA	PLA-PEG
Mean diameter (nm)	160	124	105	110
Polydispersity index	0.14	0.11	0.22	0.21
Zeta-potential (mV)	-26 ± 7	-35 ± 3	-10 ± 4	-15 ± 5
PEG-distance (nm)	-	1.21	-	0.91

2.1. Monitoring of monomeric forms of $A\beta_{1-42}$ by CE-LIF

Previous studies have highlighted the ability of CE-LIF to monitor and quantify the interaction between a fluorescent $A\beta_{1-42}$ peptide and NPs.[28] The kinetic of $A\beta_{1-42}$ capture in aqueous buffer solution containing P(MePEGCA-*co*-HDCA) NPs evidenced that the peptide disappearance is directly

correlated with its local surface adsorption onto NPs, involving the decrease of the concentration of its free form in solution.

Herein, this method has been adapted to the investigation of the kinetic of $A\beta_{1-42}$ disappearance in the buffer containing either free PEG or PEG covalently attached at the surface of two types of polymeric nanoparticles (PACA and PLA). The intensity of the monomeric $A\beta_{1-42}$ peptide peak was followed as a function of time by capillary electrophoresis and corresponding kinetics were compared. The figure 1 shows the $A\beta_{1-42}$ concentration variation (expressed as the % of the initial concentration) plots as a function of incubation time with the different nanoparticles. When alone, the peptide was maintained under its monomeric form, during the CE analysis, (Figure 1a) where no significant change of the monomer peak concentration was observed. Figure 1a, shows the percentage of monomeric $A\beta_{1-42}$ decrease upon incubation with free linear MePEG (MW 2 kDa) as compared to the control (peptide alone), suggesting either a simple affinity between the peptide and PEG or a tendency of the $A\beta_{1-42}$ to aggregate in presence of PEG. Then, the interaction between $A\beta_{1-42}$ and the different NPs was evaluated under the same CE-LIF conditions. The results obtained with the investigated P(MePEGCA-*co*-RCA-*co*-HDCA) or unmodified P(HDCA) NPs and PEG-PLA or unmodified PLA NPs are showed in Figure 1b and Figure 1c, respectively. Whatever the nature of the polymeric core of NPs, higher decreases of the free monomer peak concentration were observed with PEGylated NPs even if the kinetics were different. Figure 1b showed that the incubation of P(MePEGCA-*co*-RCA-*co*-HDCA) NPs with the monomeric peptide induced a dramatic decrease of the peak as a function of time whereas the amount of free monomer in the analysis buffer remained unchanged in presence of P(HDCA) NPs. The peptide uptake by the surface of P(MePEGCA-*co*-RCA-*co*-HDCA) NPs is probably the main reason of this feature with a first rapid stage and then a plateau after 6 h incubation, where only 20% of the initial peptide amount remains in solution. In the case of PLA NPs (Figure 1c), a decrease of the monomer peak was observed for both PEGylated and non-PEGylated nanoparticles. In contrast to PHDCA NPs, PLA NPs were able to bind the peptide monomer according to a kinetic following three phases: 45% of peptide uptake in the first 6 h followed by 30% of binding in the 6 to 12 h incubation period and finally a slow uptake of 5% during the last 4 h of the analysis. PEG-PLA NPs were more efficient than PLA ones to interact with the monomer and exhibited also a "three steps kinetic": a high decrease around 75% of monomer peak in the first 6 h, an intermediate phase (around 10% of uptake in 5/6 h) and a final phase marked by a very slow decrease 12 hours after the beginning of the analysis.

All the tested samples, excepted for P(HDCA) NPs, presented an affinity for the monomeric peptide but with different kinetics (Figure 1). Thus, this result could provide an efficient tool to screen *in vitro*

and predict the potential of NPs to interact with Aβ peptide *in vivo*. Considering that these NPs have different plasmatic circulation times: 0.3 and 30% of injected dose were found in plasma 6 h after intravenous injection for PHDCA and P(MePEGCA-*co*-RCA-*co*-HDCA) NPs respectively,[24] the first 6-7 hours of incubation is the key period to evaluate their respective binding efficacy. During this incubation time, the $A\beta_{1-42}$ monomer uptake was classified as follows: P(MePEGCA-*co*-RCA-*co*-HDCA) NPs > PEG-PLA NPs > PEG alone > PLA NPs, highlighting the pivotal role of PEG on this binding. The faster kinetic of peptide uptake with PEGylated NPs than with free PEG (used at the same concentration than the polymers) can be attributed to multiple interactions of the peptide monomer that take place with numerous PEG chains and, to an increase of local concentration of peptide at the NPs surface. CE experiments also evidenced an increased binding on P(MePEGCA-*co*-RCA-*co*-HDCA) NPs compared to that observed on PEG-PLA NPs even if the PEG density was lower at the surface of the former NPs (Tab. 1). Previous experiments have highlighted that the size, the surface charge and the nature of the surfactant used for nanoparticle preparation can have a strong influence on their affinity for the peptide monomer.[29] In the present study, the lower zeta potential value of P(MePEGCA-*co*-RCA-*co*-HDCA) NPs, due to the presence of rhodamine B labelling,[30] (Tab. 1) could also explain their higher affinity for the peptide. Previous studies, comparing PEG-PLA, PEG-PLGA and PEG-PCL nanoparticles with similar coating surface thickness, demonstrated that these NPs have adsorbed proteins to a different extent demonstrating that the nature of the core plays also an important role regarding the plasma protein adsorption onto the NPs surface.[31-32] In this work, interestingly, PLA NPs had a certain affinity for $A\beta_{1-42}$ peptide in opposition with PHDCA NPs which exhibit a lower zeta potential but a higher mean diameter. This evidences that the PLA core can favour the peptide affinity. However, after PEGylation, PHDCA NPs were more efficient to bind the peptide than NPs composed of a PLA core. Our data suggest that the adsorption of $A\beta_{1-42}$ peptide on PEGylated NPs is principally driven by the PEG interactions that can mask the core effect but it is also influenced by parameters such as the nanoparticulate colloidal features (size and surface charge). Finally among all the investigated NPs, P(MePEGCA-*co*-RCA-*co*-HDCA) ones appear as the most promising nanocarriers for potential treatment in AD pathology due to its high propensity to capture the peptide monomer.

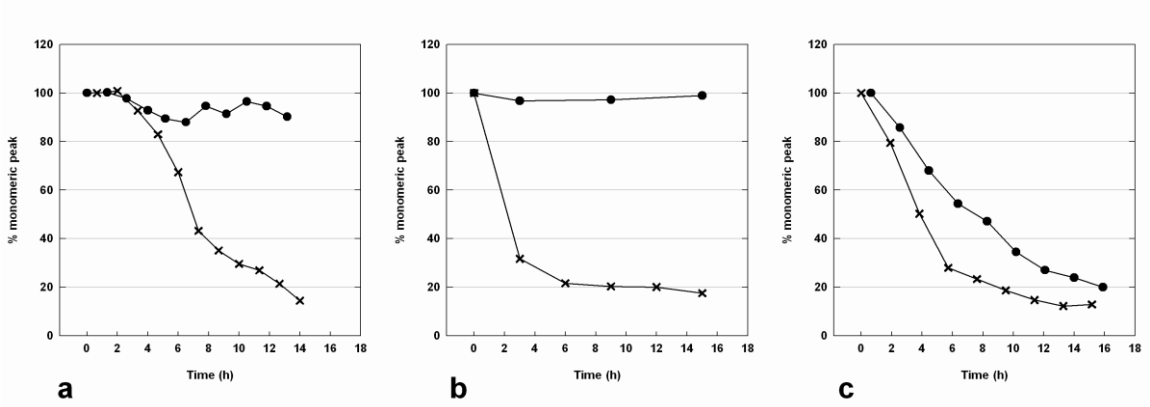

Figure 1. *CE-LIF experiments. Evolution of the monomer peak intensity as a function of time at 37°C of (a) 5 µM Hilyte Fluor™ $A\beta_{1-42}$ solution alone (●) and in the presence of 20 µM of free 2KDa MePEG (✕), (b) 5 µM Hilyte Fluor™ $A\beta_{1-42}$ in the presence of 20 µM P(MePEGCA-co-RCA-co-HDCA) (✕) or PHDCA nanoparticle suspension (●) and (c) 5 µM Hilyte Fluor™ $A\beta_{1-42}$ in presence of PEG-PLA(✕) or PLA (●) nanoparticle suspension.*

2.2. Binding experiments with monomers and fibrils of $A\beta_{1-42}$ by SPR

To further investigate the behaviour of P(MePEGCA-*co*-HDCA) NPs toward the $A\beta_{1-42}$ peptide, the binding properties of PEGylated and non PEGylated PACA NPs with monomers and fibrils of $A\beta_{1-42}$ were evaluated by SPR analyses. The figures 3a and c show good affinities of circulating P(MePEGCA-*co*-HDCA) NPs for both the peptide monomers and fibrils (immobilized on the chip), respectively at concentrations greater than 3 µM. On the contrary, no binding was observed between PHDCA NPs and the peptide under both isoforms even at higher NPs concentrations (20 µM, Figure 3b and d). Moreover, control experiments with BSA immobilized on the chip revealed the absence of signal upon injection of NPs suspension at the highest concentration (20 µM, data not shown).

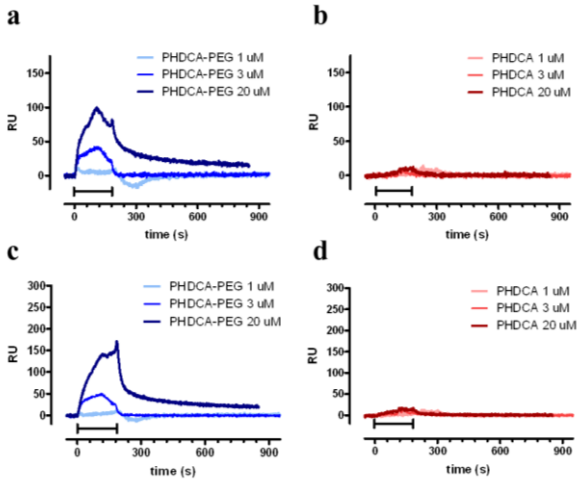

Figure 2. *Surface Plasmon Resonance experiments. Sensorgrams of (a, c) P(MePEGCA-co-HDCA) NPs and (b, d) PHDCA NPs suspensions at 1, 3 and 20 µM flowed onto a* $A\beta_{1\text{-}42}$ *monomers (a, b) or fibrils (c, d) immobilized gold chip.*

A second set of SPR experiments (Figure S1) allowed the determination of k_d values of 234 and 99 µM for the affinity between P(MePEGCA-*co*-HDCA) NPs and $A\beta_{1\text{-}42}$ monomer or fibrils, respectively. Moreover the fluorescent P(MePEGCA-*co*-RCA-*co*-HDCA) NPs in which rhodamine B is covalently linked to the copolymer used for the CE-LIF experiments were also evaluated by SPR analyses revealing lower k_d values: 161 and 51 µM for the monomer and fibrils, respectively. All these results indicate a higher affinity of PEGylated NPs for the aggregated forms of the peptide such as fibrils. In addition, the k_d values determined by SPR for the peptide monomer are higher than the ones calculated from previous CE-LIF experiments (0.55 µM),[28] likely due to the intrinsic differences between the two techniques due to the fixation of the peptide in SPR experiments.

2.3. Binding experiments with $A\beta_{1\text{-}42}$ by thioflavine T assay and CLSM

To confirm these results, a thioflavin T (ThT) assay was performed to detect the $A\beta_{1\text{-}42}$ aggregation (through *β*-sheet formation pathway). $A\beta_{1\text{-}42}$ peptide was incubated with or without P(MePEGCA-*co*-HDCA) and P(HDCA) NPs. The peptide/NP molar ratio was tuned from 1/0 to 1/4 and the fluorescence intensity, arising from thioflavin T but in direct correlation with the Aβ peptide *β*-sheet amount in the sample, was measured at different incubation times (from 0.5 to 24 h) (Figure 3). ThT experiments were performed at higher peptide concentration (50 µM) than for CE experiments using monomer solution in order to favor the peptide aggregation. This aggregation can be observed in the control experiment containing the peptide alone through an increase of the fluorescence intensity

(due to the increase of *β*-sheets structures) as a function of time (Figure 3, ratio 1/0). After the incubation with NPs, and whatever the $A\beta_{1-42}$/NPs molar ratio employed, PHDCA NPs had no effect on peptide aggregation kinetics (Figure 3, molar ratios $A\beta_{1-42}$/NPs = 1/2 and 1/4) whereas P(MePEGCA-*co*-HDCA) NPs strongly increased *β*-sheet amount and formation rate (Figure 3, $A\beta_{1-42}$/NPs = 1/2 and 1/4). These results suggest a higher and quicker peptide aggregation in the presence of PEGylated NPs and this phenomenon increases when the $A\beta_{1-42}$/NP molar ratio drops down.

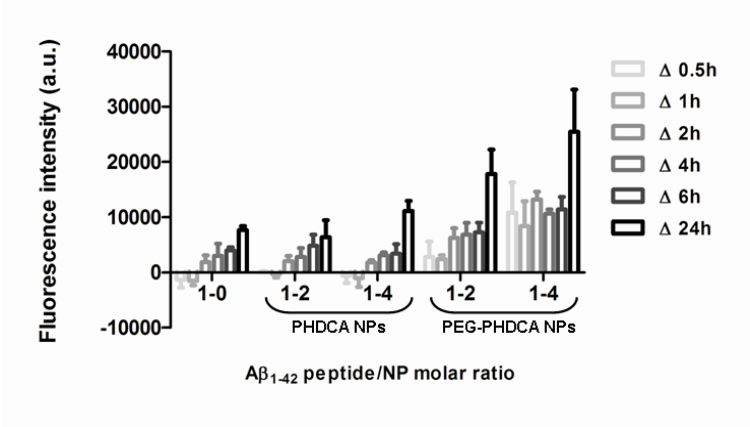

Figure 3. *ThT assay. $A\beta_{1-42}$ (50 µM) was incubated in the presence of P(MePEGCA-co-HDCA) or PHDCA NPs at different peptide/NP molar ratios for 24 h at 37ºC. At the indicated time points aliquots were taken to analyze the β-sheet content by the ThT assay. Each bar represents the absolute change in fluorescence for the different time slots. The graph represents the mean ± SD (n=3) from one experiment. Results shown are representative of three independent experiments.*

Previous experiments by confocal microscopy have also evidenced the ability of the peptide to adsorb and aggregate at the surface of PEGylated NPs when high peptide (10 µM) and NPs (20 µM) concentrations are used.[28] In this study, CLSM experiments were performed under the same conditions on non-PEGylated NPs, evidencing neither interaction between PHDCA NPs and the peptide nor peptide aggregation (Figure S2). Therefore, it is reasonable to assume that the peptide aggregation, which was observed with both techniques, was initiated or increased after the capture of the peptide by the PEGylated outer shell of the NPs and this occurred only on these surfaces.

2.4. NPs influence on $A\beta_{1-42}$ aggregation by CE

In order to have a better insight on the influence of PEGylated NPs on the peptide aggregation, a CE protocol was developed. Prior to the analysis in presence of NPs, thioflavin T analysis was employed to confirm the formation of *β*-sheet in solution during the CE protocol. An aggregating

solution (50 µM) of non-labelled $A\beta_{1-42}$, obtained by adapting a protocol previously described,[33] was doped with thioflavin and the sample was analyzed by CE-LIF as a function of incubation time at 37°C. The fluorescence detector allowed observing the formation and accumulation of fluorescent species in the sample (retention time ~ 11 min, with glycine/NaOH containing buffer) as a function of time, thus confirming the formation of typical amyloid soluble oligomers (Figure S3).

Then, NPs were added to the aggregating solution of $A\beta_{1-42}$ peptide and the formation/disappearance of every amyloid monomer and soluble oligomers were closely followed and quantified by CE coupled to UV detection. Mere peptide solution was employed as the control experiment. The analysis of this control showed a reduction of monomeric forms concomitant with an increase of oligomeric form as a function of incubation time, well in accordance with the peptide aggregation (Figure 4a). Interestingly, when NPs are added to the sample, three main differences were observed when compared to the peptide alone: (*i*) a faster decrease of the monomer peak, (*ii*) a decrease of oligomer species present at the beginning of the experiments and (*iii*) the formation "spike-shape" peaks probably due to bigger aggregates formation in complex with the NPs (Figure 4b).

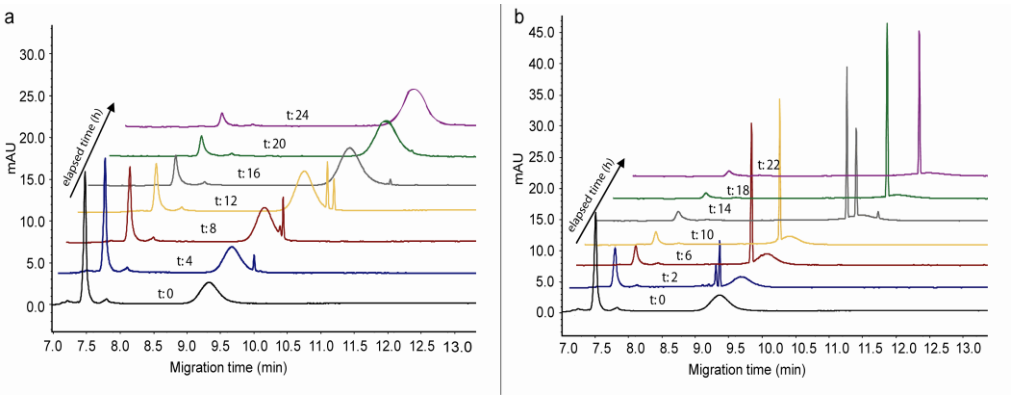

Figure 4. *CE-UV experiments. Evolution of the oligomer peak intensity as a function of time at 37°C of a 50 µM $A\beta_{1-42}$ solution alone (a) and in the presence of a 20 µM P(MePEGCA-co-HDCA) nanoparticles (b).*

The results indicate an ability of the PEGylated NPs to capture the peptide monomer and soluble oligomers in solution. The NPs seem to inhibit the formation of new soluble peptide oligomers: 75% of the pre-existing soluble oligomers were no more detectable in the solution after 28 h of incubation whereas, in absence of NPs, an 80% increase of peptide oligomers quantity was observed after 28 h (Figure 5).

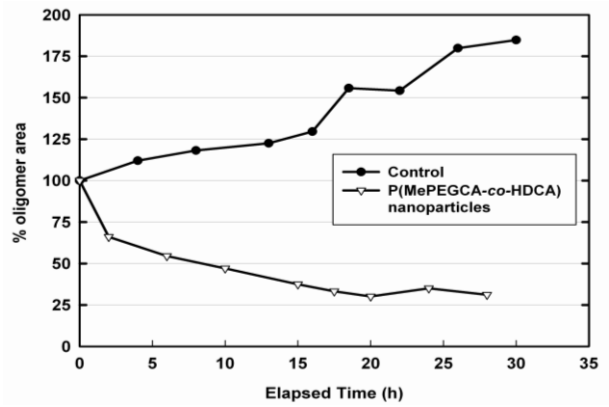

Figure 5. *Quantification of oligomer peak as function of time at 37°C of 50 µM $A\beta_{1-42}$ solution alone and in the presence of 20 µM P(MePEGCA-co-HDCA) nanoparticle suspension.*

These results confirm the interaction between the NPs and the peptide and, more importantly, underline the ability of these particles to inhibit the oligomers formation in solution.

2.5. Molecular modelling experiments

In order to study the nature of the interactions between the PEG chains and the $A\beta_{1-42}$ monomer and their consequences on the conformation of the peptide, molecular modelling experiments have been performed (Figure 6 and 7). As a comparison, the dynamics of the polyethylene (PE) chain, which is exclusively hydrophobic, was also docked in the presence of the peptide.

The docking calculations were performed (*i*) to build a starting geometry of the model nanoparticle-peptide complexes; (*ii*) to analyze interactions between the polymeric PEG (or PE) unit and amino-acid residues of the peptide. The structural analysis of docked poses of the PEG chain at $A\beta_{1-42}$ indicated that the polymeric fragment was capable to bind to the peptide in a non-specific manner (Figure 6a). It wound around the helix (1-25) of the peptide, preferably to the sequence between the His13 and Gly25 residues. In Figure 6b, 50 poses of the docked PEG chain with the best docking score are visualized. As can be seen from the Figure, the PEG was preferably wound around the helix (1-25) (yellow) and interacted partially with the helix (26-42) (blue) at the turn between the helices. It interacted by the glycol oxygens either with polar (or basic) side chains of His13, Lys28, Lys16, Gln15 (hydrogen bonds) or with hydrophobic chains of Phe19, Phe20 (π-stack interactions), and Val24, Ile31, Leu34, Met35 (van der Waals interactions). To evaluate the role of PEG oxygen atoms on binding with the peptide, the alkyl PE chain was also docked to the peptide (Figure 6c) for a comparison. The alkyl chain was not capable to wind around the helix (1-25) (yellow), and interacted

only with terminal parts of both helices (1-25) and (26-42). The very weak binding of the alkyl chain to the peptide was also supported by a docking score, which was in a range (-1.51) - (+0.98) kcal.mol^{-1} going from the best pose to the 50th pose of the ligand. For a comparison, the docking score of the PEG chain ranged from (-3.68) – (-0.24) kcal.mol^{-1}. This clearly indicates the importance of the glycol oxygen atoms of the PEG chain for the interactions of the $A\beta_{1-42}$ peptide to the PEG chains onto the nanoparticles.

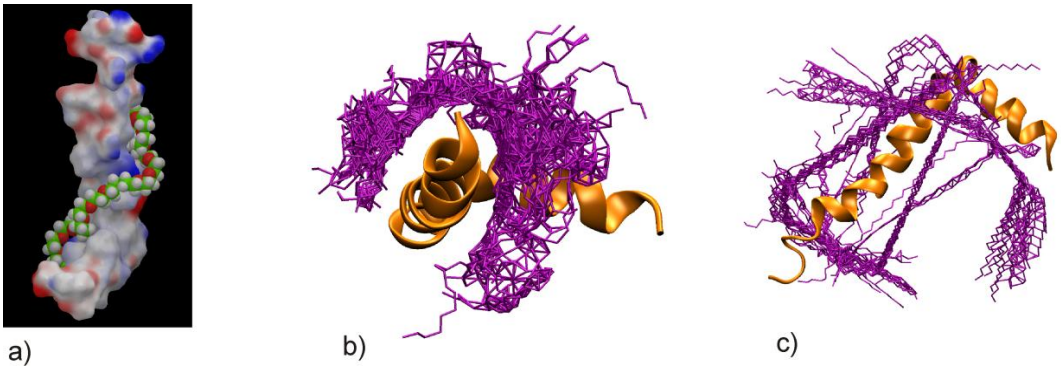

Figure 6. *Docking experiments. (a) The PEG chain (vdw) docked to $A\beta_{1-42}$ (surfaces). The chain interacts with both hydrophobic as well as hydrophilic residues of the peptide and forms a spiral structure. (b) The best 50 poses of the PEG chain (purple) docked to $A\beta_{1-42}$ (orange). (c) The alkyl PE chain (purple) docked to $A\beta_{1-42}$ (orange).*

The molecular dynamics simulations were realized to (*i*) verify a permanent interaction between the PEG chain and $A\beta_{1-42}$ as well as (*ii*) analyze conformational changes of the peptide induced by interactions with the PEG chain. The starting geometry of $A\beta_{1-42}$ taken from the crystal structure is characterized by two α-helical regions (sequences 15-25 and 31-39) connected by a flexible link. During the simulation with the PEG chain, these helices were partially disrupted and then again partially restored into shorter sequences (19-22 and 31-34) (Figure 7a). In opposite, in the presence of the hydrophobic PE chain, the region of the α-helix (15-25) was maintained in its initial conformation (Figure 7b). The other α-helix (31-39) was disrupted at the beginning of the simulation and again restored at the end. It seems that in the presence of the hydrophobic PE chain, the peptide maintains more its helical character and is more resistant to conformational changes because the helical structures of the peptide are transformed into smaller helical fragments separated by turns and coils. The most intensive conformational changes of $A\beta_{1-42}$ in the presence of the PEG chain are evident from the calculated root-mean-square deviation (RMSD) of the Cα carbons of the backbone of $A\beta_{1-42}$ during the simulations (Figure S4). The RMSD for the system with the PEG chain is higher

compared to that with the PE chain. Conformational changes of $A\beta_{1-42}$ produce the conversion of the starting L-like shape structure of the peptide to V-like, U-like shapes or even more complex conformations. The main feature of the conformational interconversion of $A\beta_{1-42}$ is a permanent interaction with the PEG chain. The permanent interaction of the peptide with the polymeric chain was also observed for the system with PE chain; however, this interaction slowed down conformational changes and stabilized the peptide in its α-helical conformation. Both PEG and PE chains showed high flexibility during the simulations changing their shapes from several linear conformations wound around $A\beta_{1-42}$ into partially packed structures of different shapes resided inside the U-like or more complex shapes of $A\beta_{1-42}$.

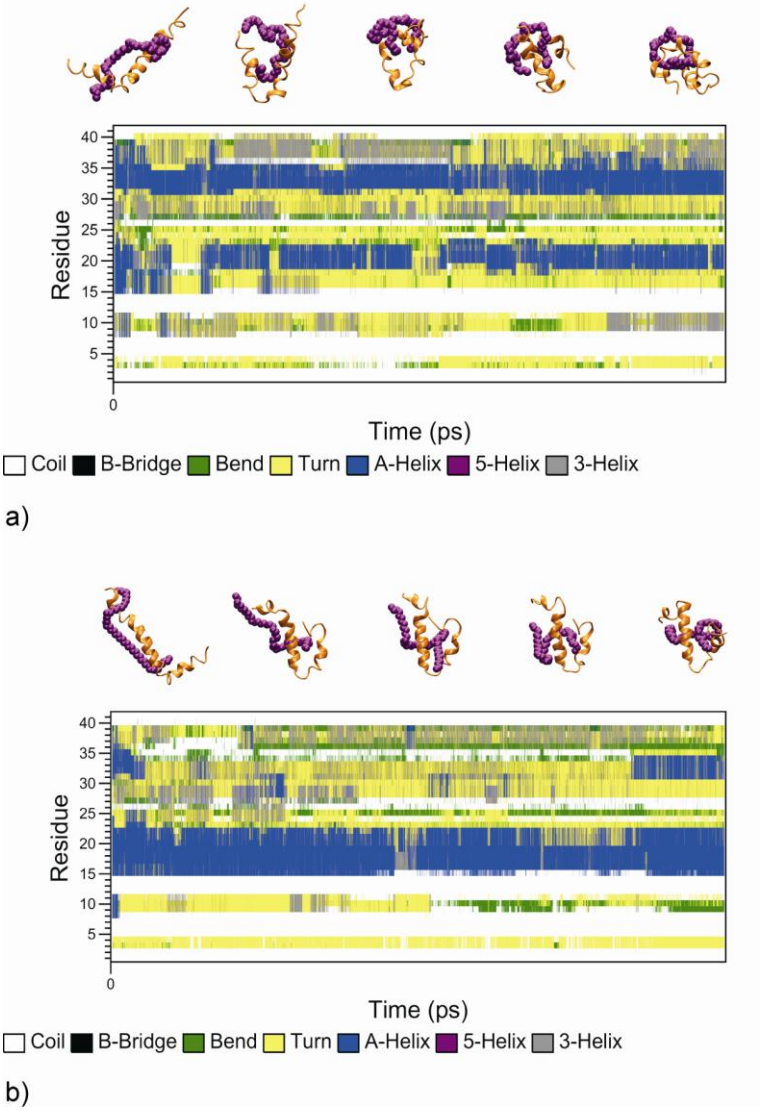

Figure 7. *Molecular dynamic simulation experiments. Changes of the secondary structure of $A\beta_{1-42}$ for the complexes (a) PEG - $A\beta_{1-42}$ and (b) PE - $A\beta_{1-42}$ during 20 ns of simulation.*

These molecular modelling experiments elucidate the interaction mechanism between PEG shell of nanoparticles and $A\beta_{1-42}$ monomer and explain the conformation change of adsorbed peptide at NP surface.

2.6. Complement activation of the selected particles

Complement activation is one of the mechanisms involved in the clearance of NPs *in vivo*. The role of Aβ peptide adsorbed at the surface of NPs is an important issue to consider as it could modify the complement activation and thus lead to a modification of NP elimination. Complement activation experiments, performed by incubation of P(MePEGCA-*co*-HDCA) NPs in human serum have been investigated with or without a $A\beta_{1-42}$ peptide pre-adsorption step onto NPs. The dosages of complement activation products, C4d, Bb, C5a and SC5b-9, did not reveal any difference between incubations of both NPs preparations (Figure 8). In any case, only a little complement activation was observed in comparison with positive controls (aggregated IgG and Zymosan), as what is generally expected from PEGylated NPs. Therefore this result suggests that these nanoparticles will be eliminated *in vivo* according to the same kinetic than the one observed in normal blood. Previous studies have demonstrated that the biodegradation of P(MePEGCA-*co*-HDCA) NPs after IV injection to healthy rats and the elimination of degradation products by kidneys happens with a mean blood-elimination rate constant of 3.94×10^{-2} min^{-1}.[25]

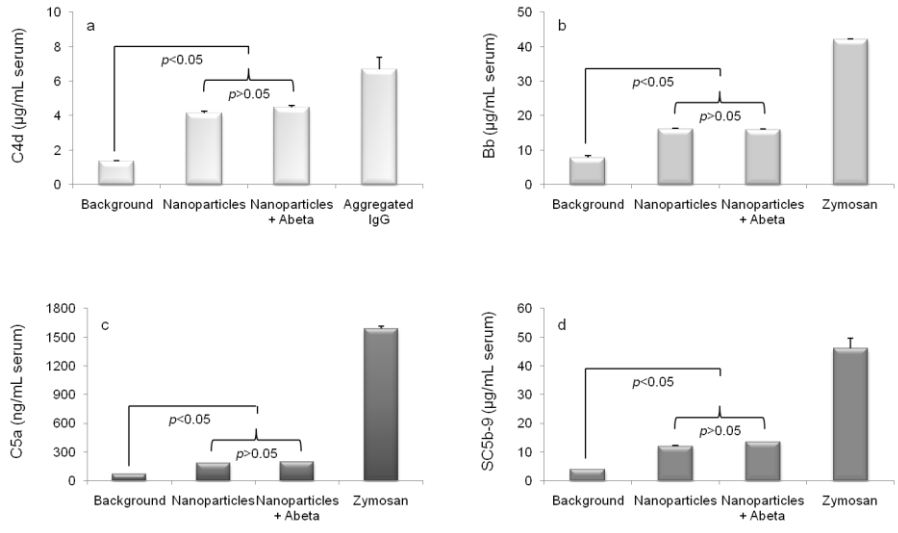

Figure 8. *Complement activation. Quantification of complement activation products, (a) C4d, (b) Bb, (c) C5a and (d) SC5b-9, in healthy human serum after incubation of P(MePEGCA-co- HDCA) nanoparticles with or without $A\beta_{1-42}$ peptide preadsorption step. Background and positive control (Aggregated IgG or Zymosan) are presented for each product.*

2.7. Apo E adsorption on NPs in presence of $A\beta_{1-42}$ peptide

Another point to anticipate NP behaviour after IV injection to AD patient concerns the competition between amyloid peptide and serum proteins for binding to NPs surface. Previous experiments using 2D-PAGE analysis and Western blotting evidenced the adsorption of Apo E at the surface of P(MePEGCA-*co*-HDCA) NPs after 20 min incubation of NPs in rat serum (Kim et al. 2007 biomacromolecules). Because Apo E is known to interact with the $A\beta_{1-42}$ peptide *in vivo*, its adsorption on NPs if conserved in presence of $A\beta_{1-42}$ peptide in blood could increase the peptide affinity for NPs. In this work, the same Western blotting experiment has been performed by incubating NPs in rat serum supplemented with $A\beta_{1-42}$ peptide (Figure 9). The results showed the presence of Apo E at the surface of NPs even in presence of $A\beta_{1-42}$ peptide suggesting that the binding of Aβ peptide does not suppress the adsorption of serum proteins like Apo E at the surface of these NPs. Therefore, we can hypothesize that our NPs could act as LDL-like particles which can increase *in vivo* the clearance of Aβ peptide from the biological fluids by capturing its soluble forms. Taking into consideration a recent study that evidenced the crucial role of blood peptide clearance in the decreasing of the peptide toxicity in the brain (the so-called "*sink effect*"),[9] this feature could prevent from the β-amyloid aggregation process and from its subsequent toxic effects on neuronal cells.[34-35] In this context, these PEGylated NPs, which probably act toward the amyloid peptide through this "sink effect" mechanism, appear as a suitable and promising nanomedicine for AD treatment.

Figure 9. *Western blot image using anti-Apo E antibody of the adsorbed plasma proteins after 20 min incubation of P(MePEGCA-co- HDCA) nanoparticles in rat serum supplemented (b) or not (a) with* $A\beta_{1-42}$ *peptide. The antibody recognizes specifically rat Apo E.*

3. Conclusions

Herein, we have demonstrated that PEGylated NPs and especially P(MePEGCA-*co*-HDCA) NPs have a good affinity for different $A\beta_{1-42}$ peptide isoforms such as monomers, oligomers and fibrils corresponding to different steps of the peptide oligomerization process.

CE and Thioflavin spectroscopy analyses showed the ability of these particles to interact with the peptide aggregation kinetic by reducing the formation of soluble oligomers which are the most toxic forms of Aβ. SPR experiments evidenced a higher affinity constant of these NPs for fibrils than for monomers. Interestingly all the experiments showed the pivotal role of the PEG chains at the surface of the particles for this interaction.

Targeted *in silico* experiments showed that the PEG chains likely interact with both hydrophobic and hydrophilic residues of the peptide and form a spiral-like 3D structure. The simulation confirmed a permanent, even if non-specific, interaction of the peptide with the PEG chain, leading to its conformational change. These results proposed an interaction mechanism between the PEG chains and the $A\beta_{1-42}$ peptide that explains the conformation change of the peptide (bound at the surface of the NPs) observed during Thioflavine T assay and confocal microscopy experiments. Even if the nature of the nanoparticulate system is a parameter to take into consideration, PEG chains, especially when organized at the NP surface, appear to be critical feature to ensure an efficient capture of the free amyloid peptide in solution. We can speculate that the increased affinity between PEGylated NPs and amyloid peptide, compared to molecular PEG can be related to an increase of local peptide concentration at the surface of the nanoparticles acting as aggregation initiator.

To anticipate the potential of P(MePEGCA-*co*-HDCA) NPs *in vivo, in vitro* complement activation and Apo E adsorption experiments provide similar features after adsorption of Aβ peptide at their surface. Then, it can be hypothesized that after intravenous injection, long circulating P(MePEGCA-*co*-HDCA) NPs, which can mimic LDL particles, would be able to capture Aβ peptide soluble forms in blood prior to their degradation and elimination, allowing an increase of the peptide clearance in the bloodstream and thus in the brain through a "*sink effect*" (Scheme 1).

In vivo experiments will be undertaken to confirm the ability of P(MePEGCA-*co*-HDCA) NPs to undergo this so-called "sink effect" and in order to extrapolate if (P(HDCA-*co*-MePEGCA)) nanoparticles can be a promising candidate for Alzheimer's disease treatment.

4. Experimental section

4.1. Materials

PLA homopolymer and PLA-*b*-PEG block copolymers were synthesized by ring opening polymerization.[36] To a solution of methoxypoly(ethylene glycol) (M_n = 2000 g.mol^{-1}, 500 mg, 0.24 mmol) in 5.2 mL of anhydrous toluene, was added D,L-lactide (2.43 g, 16.9 mmol) and $Sn(Oct)_2$ (5.4 µL, 16.5 µmol). The reaction mixture was degassed by bubbling nitrogen for 30 min and then stirred in a pre-heated oil bath at 115°C for 5.5 h. The toluene was removed under reduced pressure and the obtained product was dissolved into a minimum amount of THF and further precipitated twice in water and subsequently freeze-dried overnight to yield a white powder (conversion = 93%, *m* = 1.7 g, $M_{n,NMR}$ = 12200 g.mol^{-1}, $M_{n,SEC}$ = 12400 g.mol^{-1}; M_w/M_n = 1.12). Poly[hexadecyl cyanoacrylate-*co*-rhodamine B cyanoacrylate-*co*-methoxypoly(ethylene glycol) cyanoacrylate] P(MePEGCA-*co*-RCA-*co*-HDCA) copolymers, poly[hexadecyl cyanoacrylate-*co*-methoxypoly(ethylene glycol) cyanoacrylate] P(MePEGCA-*co*-HDCA) copolymers, poly(hexadecyl cyanoacrylate-*co*-rhodamine cyanoacrilate) P(HDCA-*co*-RCA) and poly(hexadecyl cyanoacrylate) P(HDCA) homopolymers were obtained following previously reported procedures.[30]

NaH_2PO_4 (>99%) was purchased from Merck & Co (Fontenay Sous Bois, France), Na_2HPO_4 (>98%) was obtained from Prolabo (Strasbourg, France), thioflavine (99%), ammonium hydroxide (NH_4OH) 28.1% (m/V), Pluronic F-68 (99%), 1,1,1,3,3,3-hexafluoro-2-propanol (HFIP) (99.8%), dimethyl sulfoxide (99.5%), sodium dodecyl sulphate (SDS, 99%), acetic acid (99%), sodium acetate (99%), bovine serum albumin (BSA, 99%) and ethanolamine (99%) were purchased from Sigma-Aldrich (St. Quentin Fallavier, France). Sodium hydroxide (NaOH, 1 M) was obtained from VWR (Fontenay-sous Bois, France). Goat polyclonal anti-Rat ApoE (R-20) and mouse anti-goat-HRP antibodies were purchased from Santa-Cruz Biotechnology INC. Anti-Aβ antibody 6E10 was from Covance (Princeton, New Jersey). Acetone was purchased at the highest grade from Carlo Erba (Val de Reuil, France).

4.2. Nanoparticle preparation

Fluorescent and non-fluorescent PACA nanoparticles were prepared using P(MePEGCA-*co*-RCA-*co*-HDCA), P(MePEGCA-*co*-HDCA) copolymers, P(HDCA-*co*-RCA) and P(HDCA) homopolymer according to protocols recently published by our group.[37]

The (co)polymer (10 mg) was dissolved in acetone (2 mL) and this solution was added dropwise to an aqueous solution 0.5 % (w/v) of Pluronic F68 (4 mL) under vigorous mechanical stirring. A milky suspension was observed almost instantaneously. Acetone was then evaporated under reduced pressure

and nanoparticles were purified by ultracentrifugation (150,000 *g*, 1 h, 4°C, Beckman Coulter, Inc.). The supernatant was discarded and the pellet was resuspended in the appropriate volume of deionized water to yield a 2.5 $mg.mL^{-1}$ nanoparticle suspension.

PLA and PLA-PEG nanoparticles were prepared as follow: 10 mg of polymers powder was dissolved in 4 mL of Dichloromethane and added to 10 mL of an aqueous solution 1% (w/v) of Pluronic F68. The resulting sample was physically mixed for 1 min and sonicated with a sonicator probe for 10 min (300 W). The organic solvent is then evaporated at room pressure and temperature under magnetic stirring and nanoparticles were purified by ultracentrifugation 20,000 g 20 min at 4°C. The supernatant was discarded and the pellet was resuspended in the appropriate volume of deionized water to yield a 2.5 $mg.mL^{-1}$ nanoparticle suspension.

4.3. Nanoparticle characterization

The nanoparticle diameter (D_z) was measured by dynamic light scattering (DLS) with a Nano ZS from Malvern (173° scattering angle) at 25°C. The nanoparticle stability as a function of time using DLS measurements has been verified during their incubation at 37°C in the buffer employed for capillary electrophoresis experiments. The nanoparticle surface charge was investigated by ζ-potential measurement at 25°C after dilution with 1 mM NaCl solution applying the Smoluchowski equation and using the same apparatus. The PEG chains density at the surface of PLA and PACA nanoparticles were obtained by previous paper. [29, 31] All the values are presented in the table 1.

4.4. Capillary electrophoresis experiments

CE was performed on PA 800 instrument (Beckman Coulter, Roissy, France) using uncoated silica capillaries (Phymep, Paris) with an internal diameter of 50 µm and 50 cm total length (40 cm effective length was employed for the separation). All buffers were prepared with deionized water and were filtered through a 0.22 µm membrane (VWR) before use. Before analysis, the capillaries were preconditioned by the following rinsing sequence: 0.1 M NaOH for 5 min, 1 M NaOH for 5 min and then deionised water for 5 min. The in-between-runs rinsing cycles were carried out by pumping sequentially through the capillary: water for 5 min, 50 mM SDS for 2 min (to inhibit the aggregation and subsequent peptide adsorption on the capillary wall),[38] and 0.1 M NaOH for 5 min. The samples were introduced into the capillary by hydrodynamic injection under 3.4 kPa. The capillary was thermostated at 25°C and the samples were maintained at 37°C by the storage sample module of the PA 800 apparatus. The separations were carried out at 16 kV with positive polarity at the inlet using 80 mM phosphate buffer (NaH_2PO_4/Na_2HPO_4) pH 7.4. The electrolyte was renewed after each run.

The peptides were detected by a Laser-Induced Fluorescence (LIF) detection system equipped with 3.5 mW argon-ion laser with a wavelength excitation of 488 nm, the emission being collected through a 520 nm band-pass filter or by Diode-Array Detector (DAD) at 190 nm. Peak areas were estimated using the 32 Karat™ software (Beckman Coulter).

Lyophilized $A\beta_{1-42}$ and HiLyte Fluor™ labeled $A\beta_{1-42}$ peptide (ANASPEC, Le Perray en Yvelines, France) were dissolved in 0.16% (m/V) ammonium hydroxide aqueous solution to reach a concentration of 0.5 and 2 $mg.mL^{-1}$ respectively. The fluorescent and non-labeled peptide solutions were then divided into aliquots individually stored at -20°C which were freshly defrosted prior analysis.

To evaluate the interaction between the monomeric form of the $A\beta_{1-42}$ peptide and the nanoparticles, HiLyte Fluor™ labeled $A\beta_{1-42}$ peptide stock solution were diluted in 20 mM phosphate buffer (NaH_2PO_4) at pH 7.4 containing a 20 µM PEG solution or P(MePEGCA-*co*-RCA-*co*-HDCA), PHDCA, PEG-PLA or PLA nanoparticle suspension to obtain final peptide concentrations of 5 µM. The samples were then incubated at 37°C and analyzed by capillary electrophoresis several time as a function of time. The same protocol was followed with $A\beta_{1-42}$ peptide solution alone as a control.

A protocol to study the influence of Polymeric NPs to the peptide aggregation kinetic was developed. An aggregating peptide solution was obtained as previously described.[33] Monomeric peptide was solubilized with final concentration of 50 µM in phosphate buffer 20 mM (NaH_2PO_4), freeze dried and centrifuged 6,000 g for 20 min at room temperature. To assure the aggregating behavior of the solution, ThT was employed. Under CE-LIF detection conditions, the anisotropic effect allowed a fluorescence emission from ThT when these molecules are exclusively linked to *β*-sheet structures. According the studies of Kato et al,[39] only the soluble oligomeric forms of the $A\beta_{1-42}$ peptide contain *β*-sheet structure are susceptible to interact with ThT which are subsequently detected with CE-LIF method. An alkaline buffer (pH 9.5; 0.2 M) of glycine/NaOH containg 10 µM of ThT were prepared, stored in the dark at 4 °C and then used as migration buffer. The samples were incubated at 4 °C and subsequent separations were performed at 16 kV. The monomer form was not detected under these conditions.

To study the influence of Polymeric NPs on this peptide aggregation kinetic, the same protocol to have an aggregating solution was followed. The obtained solution was analyzed by capillary electrophoresis with DAD detector in 20mM phosphate buffer (NaH_2PO_4) pH 7.4 in presence of 20 µM polymeric P(MePEGCA-*co*-HDCA) nanoparticles. Control experiments were performed without adding nanoparticles to the aggregating peptide solution.

These experiments allowed the quantification of the evolution of monomer or oligomer peak as a function of incubation time to be determined. % monomer or oligomer peaks were calculated as the ratio between the absolute peak area of the monomer or oligomer observed at t = 0 and the one observed at each incubation time.

4.5. Surface Plasmon Resonance experiments

The $A\beta_{1-42}$ peptide used for SPR experiments was prepared from a depsi-$A\beta_{1-42}$ peptide synthesized as previously described.[40] This depsi-peptide is much more soluble than the native peptide and has also a much lower propensity to aggregate, thus preventing the spontaneous formation of 'seeds' in solution.[40] The native $A\beta_{1-42}$ peptide was then obtained from the depsi-peptide by a "switching" procedure involving a change in pH.[40] The $A\beta_{1-42}$ peptide solution obtained immediately after switching was shown to be free of seed. The $A\beta_{1-42}$ peptide obtained by this procedure is therefore in its original state and, for the sake of simplicity; it will be referred here to as the "monomer". Further characterizations, carried out by Gobbi's group, indicated that the Aβ "monomer" used for the present study gave no ThT signal and was unstructured as observed by circular dichroism.[41]

For binding studies was used the ProteOn XPR36 (Biorad) apparatus, which has six parallel flow channels that can be used to uniformly immobilize strips of six ligands on the sensor surface. $A\beta_{1-42}$ monomers and fibrils were immobilized in parallel-flow channels of a GLC sensor chip (Biorad) using amine-coupling chemistry. Briefly, after surface activation the peptide solutions (10 µM in acetate buffer pH 4.0) were injected for 5 min at a flow rate of 30 $\mu L.min^{-1}$, and the remaining activated groups were blocked with ethanolamine, pH 8.0. The final immobilization levels were similar, about 2500 and 3000 Resonance Units (1 RU = 1 pg protein/mm^2) for fibrils and monomers, respectively. Bovine serum albumin (BSA) was immobilized too, in a parallel flow channel, as a reference protein. Another reference surface was prepared in parallel using the same immobilization procedure but without addition of the peptide (naked surface). Before performing experiments with nanoparticles, we previously checked that Aβ species immobilized were binding with high affinity the anti-Aβ antibody 6E10 (data not shown). PHDCA and (P(HDCA-*co*-MePEGCA)) NPs were then injected at different concentrations (0.3 to 20 µM), and flowed onto the chip surfaces for 3 min at a flow rate of 30 µL/min at 30°C in PBST (Phosphate buffer saline + 0.005% Tween 20, pH 7.4). A second set of experiments (2000 RU both for fibrils and monomers) were performed using (P(HDCA-*co*-MePEGCA)) and P(MePEGCA-*co*-RCA-*co*-HDCA) with increased contact time (10 min) to evaluate the influence of fluorescent dye on the interaction and to calculate the affinity constants.

4.6. Thioflavin T aggregation assay

$A\beta_{1-42}$ was dissolved in hexafluorisopropanol (HFIP) at a final concentration of 1 $mg.mL^{-1}$, sampled and allowed to evaporate. For co-aggregation experiments, the peptide film was first dissolved in DMSO and sonicated in a bath sonicator for 10 min. Subsequently, $A\beta_{1-42}$ was diluted in phosphate-buffer saline (PBS, 20 mM sodium phosphate buffer, pH 7.4, containing 137 mM NaCl) to a final concentration of 50 µM. This mixture was aggregated in the presence or absence of P(HDCA) or P(MePEGCA-*co*-HDCA) NPs for 24 h at 37ºC. At each point of analysis (0.5, 1, 2, 4, 6, 24 h), aggregated $A\beta_{1-42}$ was diluted to a final concentration of 5 µM into 50 mM glycine buffer at pH 7.4 containing 10 µM ThT. Fluorescence was measured in 96 well non-binding plates (Greiner Bio One, Frickenhausen, Germany) using a Fluostar Omega microplate reader at an excitation wavelength of 450 nm and emission at 485 nm.

4.7. Confocal Laser Scanning Microscopy experiments

Observations were made by sequential acquisition with a Zeiss LSM-510 confocal scanning laser microscope equipped with a 30 mW argon laser and 1 mW helium neon laser, using a Plan-Apochromat 63X objective lens (NA 1.40, oil immersion). Red fluorescence was observed with a long-pass 560 nm emission filter and under a 543 nm laser illumination. Green fluorescence was observed with a band-pass 505 and 550 nm emission filter and under a 488 nm laser illumination. The pinhole diameter was set at 61 µm giving an optical section thickness of 0.6 µm. Stacks of images were collected every 0.3 µm along the z axis. 12 bit numerical images were acquired with LSM 510 software version 3.2.

The interaction between the polymeric nanoparticles and the $A\beta_{1-42}$ peptide was investigated by confocal laser scanning microscopy (CLSM) using HiLyte Fluor™ labeled $A\beta_{1-42}$ peptide and rhodamine-labelled P(MePEGCA-*co*-RCA-*co*-HDCA) and P(HDCA-co-RCA) NPs. The $A\beta_{1-42}$ peptide aliquots were defrost, immediately diluted with 20 mM phosphate buffer and incubated with 20 µM nanoparticle suspension to reach a final peptide concentration of 10 µM. After 12 h of incubation at 37°C, a 10 µL deposit of the sample on glass coverslips was analyzed by CLSM.

4.8. Molecular modeling experiments

For the docking calculations we used a polymeric chain with the 16 PEG (polyethylene glycol) units (it is the maximum length of the PEG chain allowable for the flexible docking calculations, i.e. a maximum 50 rotatable bonds) and 24 PE (polyethylene) units as ligands and a solution structures (PDB ID: 1IYT)[14] of the $A\beta_{1-42}$ peptide as a receptor. For the docking calculations default values of

parameters were used by means of the GLIDE[42-43] program of the Schrödinger package.[44] The receptor box for the docking conformational search was centered at the receptor with a size of 50×50×50 Å using partial atomic charges for the receptor and ligand from the OPLS2005 force field.[45-46] The grid maps were created with no Van der Waals radius and charge scaling for the atoms of the receptor. Flexible docking in standard (SP) and extra (XP) precision was used for the PEG and PE ligands. The potential for nonpolar parts of the ligands was softened by scaling the Van der Waals radii by a factor of 1.0 for atoms of the ligands with partial atomic charges less than specified cutoff of 0.15. The 5000 poses were kept per ligand for the initial docking stage with scoring window of 100 kcal mol-1 for keeping initial poses; and the best 400 poses were kept per ligand for energy minimization. The ligand poses with RMS deviations less than 0.5 Å and maximum atomic displacement less than 1.3 Å were discarded as duplicates. For 50 ligand poses with the best docking score post-docking minimizations were performed. Subsequent structural analyses were done using the MAESTRO viewer of the Schrödinger package.[47]

For molecular dynamics simulations, the $A\beta_{1-42}$-PEG (or PE) systems were solvated by more than 4800 TIP3P[48] water molecules in a box (82 × 68 × 96 Å) using the LEAP [49] program of the Amber 10 program package.[50] The $A\beta_{1-42}$ peptide was treated with the standard AMBER 99 force field with the "Stony Brook" (SB) modification to ff99 backbone torsions, and for the PEG and PE chains the parameters were derived from the GAFF force field. The ionization states of the ionizing residues of $A\beta_{1-42}$ were predicted by the PropKa program,[51-52] considering an *in vivo* pH of 7. Terminal and side-chain ionizing groups (amino and carboxyl) of $A\beta_{1-42}$ were treated in their ionized configurations (as -NH3+ or $–COO^-$) in all MD simulations. The Berendsen algorithm[53] for the temperature and pressure coupling, with coupling constants of τ_t = 1.0 ps and τ_p = 1.0 ps, were used at a constant temperature (300 K) and pressure (101.325 kPa) employing the PMEMD module. Periodic boundary conditions were used together with the particle-mesh Ewald (PME)[50] method for treating long-range electrostatics. A time step of 1.0 fs, with the SHAKE algorithm[54] to constrain bonds involving hydrogens, was used along simulations with a 10 Å nonbonded cut-off, and the nonbonded pairlist was updated every 20 time steps. The simulations, preceded by initial minimizations (300 steps) were carried out over 20 ns and coordinates were saved for analysis every 1 ps. The MD trajectories were analyzed by the VMD package[55] and the DSSP program.[56]

4.9. Complement activation analyses

First P(HDCA-*co*-MePEGCA) nanoparticles (64 µg) were incubated with the $A\beta_{1-42}$ peptide (4.9 µg) in a total volume of 1 mL saline for 24 h at 37 °C. Aβ -bound nanoparticles were pelleted by

centrifugation at 100,000 *g* for 1h at 4°C. After removing the supernatant the pellet was washed with deionized water and concentrated by centrifugation. Finally, the pellet was re-suspended in an appropriated volume of physiological saline and used immediately for complement activation testing. (P(HDCA-*co*-MePEGCA))-containing sample without Aβ peptide was used as control and it was processed as above where Aβ peptide was replaced with an equal volume of deionized water.

Blood was drawn from healthy volunteers according to approved local protocols (Moghimi's group, University of Copenhagen). Blood was allowed to clot at room temperature and serum was prepared, aliquoted and stored at – 80 °C. Serum samples were thawed and kept at 4 °C before incubation with test reagents.

To measure complement activation *in vitro*, we compared Aβ bound (P(HDCA-*co*-MePEGCA))- and unbound (P(HDCA-*co*-MePEGCA))-induced rise of serum complement activation products Bb, C4d, C5a and SC5b-9 using respective Quidel's ELISA kits according to the manufacturer's protocols, as described previously.[57-59] The reaction was started by adding the required amount of Aβ bound (P(HDCA-*co*-MePEGCA)) or unbound (P(HDCA-*co*-MePEGCA)) to undiluted serum (NPs : serum volume ratio, 1:4) in Eppendorf tubes (in triplicate) in a shaking water bath at 37 °C for 30 min. The final concentration of (P(HDCA-*co*-MePEGCA)) was 0.4 mg/mL of serum. Reactions were terminated by 20-fold dilution with "sample diluents" provided with assay kit supplemented with 25 mM EDTA for Bb, C4d and SC5b-9 detection, whereas a 200-fold dilution was made prior to C5a measurement. Control serum incubations contained saline (the same volume as nanoparticles) for assessing background levels of complement activation products. Zymosan (1 mg/mL, final concentration) and heat aggregated-IgG (5 mg/mL, final concentration) were used as positive controls for alternative and calcium-sensitive pathways, respectively. The level of the complement activation products was then measured by the respective ELISA kits and compared with control incubations in the absence of nanoparticles. For quantification of complement activation products, standards curves were constructed using the assigned concentration of each respective standard supplied by the manufacturer and validated. The slope, intercept and correlation coefficient of the derived best- fit line for Bb, C4d, C5a and SC5b-9 standard curves were within the manufacturer's specified range. The efficacy of Aβ bound (P(HDCA-*co*-MePEGCA)) and unbound (P(HDCA-*co*-MePEGCA)) was established by comparison with baseline levels using paired t-test, correlations between two variables were analyzed by linear regression. The result of a typical experiment from one blood donor is presented.

4.10. Apo E adsorption on the NPs

A total of 350 µl of P(MePEGCA-*co*-HDCA) nanoparticle suspension (20 $mg.mL^{-1}$) was incubated in 1.75 mL of Sprague-Dawley rat serum (Charles River Laboratories) for 20 min at 37°C with or without $A\beta_{1-42}$. Plasma proteins adsorbed onto the nanoparticles were separated from bulk serum by centrifugation at 15,000g for 1.5 h at 4 °C. The supernatant serum was discarded, and the pellet was extensively washed with water by centrifugation (15,000g for 1.5 h at 4 °C) to remove the excess serum. After the centrifugation the plasma protein adsorbed nanoparticles were resuspended in 100 µL of solution containing 2.5 % sodium dodecyl sulfate (SDS) and 30 mM 1,4-dithioerythritol (DTE). The suspension were incubated at 50 °C for 2 h to detach the adsorbed proteins from the nanoparticles.[60] After centrifugation at 15,000g for 1 h at 4 °C, Bradford assay was applied to quantify the amount proteins in the final supernatant. A total of 40 µg of proteins was migrated on a 12 % SDS polyacrylamide gel and electrophoretically transferred to a nitrocellulose membrane. Blots were blocked with BSA 5 % (w/v) in tris buffer saline. Then the blots were extensively washed and incubated with an apolipoprotein specific antibody overnight at 4 °C, followed by a peroxidise-conjugated anti-goat IgG as a secondary antibody. The immunoreactive bands were visualized by an enhanced chemoluminescence system (Amersham Bioscience).

5. Acknowledgements

The research leading to these results has received funding from the European Community's Seventh Framework Programme (FP7/2007-2013) under agreement n°212043. The CNRS and the French Ministry of Research are also warmly acknowledged for financial support. J.K. and I.T. also acknowledge financial support from the Scientific Grant Agency of the Ministry of Education of Slovak Republic and Slovak Academy of Sciences (the project VEGA-02/0176/09).

6. References

1. Querfurth HW and LaFerla FM. Alzheimer's disease. *N Engl J Med* 2010; 362: 329-344.
2. Aliev G, Smith MA, de la Torre JC and Perry G. Mitochondria as a primary target for vascular hypoperfusion and oxidative stress in Alzheimer's disease. *Mitochondrion* 2004; 4: 649-663.
3. de la Torre JC. Is Alzheimer's disease a neurodegenerative or a vascular disorder? Data, dogma, and dialectics. *Lancet Neurol* 2004; 3: 184-190.
4. Korolainen MA, Nyman TA, Aittokallio T and Pirttila T. An update on clinical proteomics in Alzheimer's research. *J Neurochem* 2010; 112: 1386-1414.
5. Townsend M, Mehta T and Selkoe DJ. Soluble Abeta inhibits specific signal transduction cascades common to the insulin receptor pathway. *J Biol Chem* 2007; 282: 33305-33312.
6. Gralle M, Botelho MG and Wouters FS. Neuroprotective secreted amyloid precursor protein acts by disrupting amyloid precursor protein dimers. *J Biol Chem* 2009; 284: 15016-15025.
7. Pierrot N. and Octave J. Processing of amyloid precursor protein and amyloid peptide neurotoxicity. *Curr Alzheimer Res* 2008; 5: 92-99.

8. Chow VW, Mattson MP, Wong PC and Gleichmann M. An Overview of APP Processing Enzymes and Products. *Neuromolecular Med* 2009;

9. Sutcliffe JG, Hedlund PB, Thomas EA, Bloom FE and Hilbush BS. Peripheral reduction of beta-amyloid is sufficient to reduce brain beta-amyloid: implications for Alzheimer's disease. *J Neurosci Res* 2011; 89: 808-814.

10. Sagare A, Deane R, Bell RD, Johnson B, Hamm K, Pendu R, Marky A, Lenting PJ, Wu Z, Zarcone T, Goate A, Mayo K, Perlmutter D, Coma M, Zhong Z and Zlokovic BV. Clearance of amyloid-beta by circulating lipoprotein receptors. *Nat Med* 2007; 13: 1029-1031.

11. Zlokovic BV. Clearing amyloid through the blood-brain barrier. *J Neurochem* 2004; 89: 807-811.

12. Bates KA, Verdile G, Li QX, Ames D, Hudson P, Masters CL and Martins RN. Clearance mechanisms of Alzheimer's amyloid-beta peptide: implications for therapeutic design and diagnostic tests. *Mol Psychiatry* 2009; 14: 469-486.

13. Tomaselli S, Esposito V, Vangone P, van Nuland NA, Bonvin AM, Guerrini R, Tancredi T, Temussi PA and Picone D. The alpha-to-beta conformational transition of Alzheimer's Abeta-(1-42) peptide in aqueous media is reversible: a step by step conformational analysis suggests the location of beta conformation seeding. *ChemBioChem* 2006; 7: 257-267.

14. Crescenzi O, Tomaselli S, Guerrini R, Salvadori S, D'Ursi AM, Temussi PA and Picone D. Solution structure of the Alzheimer amyloid beta-peptide (1-42) in an apolar microenvironment. Similarity with a virus fusion domain. *Eur. J. Biochem.* 2002; 269: 5642-5648.

15. Kayed R, Head E, Thompson JL, McIntire TM, Milton SC, Cotman CW and Glabe CG. Common structure of soluble amyloid oligomers implies common mechanism of pathogenesis. *Science* 2003; 300: 486-489.

16. Klein WL, Krafft GA and Finch CE. Targeting small A[beta] oligomers: the solution to an Alzheimer's disease conundrum? *Trends Neurosci.* 2001; 24: 219-224.

17. Allaman I, Gavillet M, Belanger M, Laroche T, Viertl D, Lashuel HA and Magistretti PJ. Amyloid-beta aggregates cause alterations of astrocytic metabolic phenotype: impact on neuronal viability. *J. Neurosci.* 2010; 30: 3326-3338.

18. Garcia-Matas S, de Vera N, Aznar AO, Marimon JM, Adell A, Planas AM, Cristofol R and Sanfeliu C. In vitro and in vivo activation of astrocytes by amyloid-beta is potentiated by pro-oxidant agents. *J. Alzheimers Dis.* 2010; 20: 229-245.

19. Maezawa I, Zimin PI, Wulff H and Jin LW. Amyloid-beta protein oligomer at low nanomolar concentrations activates microglia and induces microglial neurotoxicity. *J Biol Chem* 2011; 286: 3693-3706.

20. Cizas P, Budvytyte R, Morkuniene R, Moldovan R, Broccio M, Losche M, Niaura G, Valincius G and Borutaite V. Size-dependent neurotoxicity of beta-amyloid oligomers. *Arch Biochem Biophys* 2010; 496: 84-92.

21. Viet MH, Ngo ST, Lam NS and Li MS. Inhibition of aggregation of amyloid peptides by Beta-sheet breaker peptides and their binding affinity. *J Phys Chem B* 2011; 115: 7433-7446.

22. Vauthier C, Dubernet C, Fattal E, Pinto-Alphandary H and Couvreur P. Poly(alkylcyanoacrylates) as biodegradable materials for biomedical applications. *Adv Drug Deliv Rev* 2003; 55: 519-548.

23. Bioalliance. *Unpublished results from BioAlliance Pharma*

24. Peracchia MT, Fattal E, Desmaele D, Besnard M, Noel JP, Gomis JM, Appel M, d'Angelo J and Couvreur P. Stealth PEGylated polycyanoacrylate nanoparticles for intravenous administration and splenic targeting. *J Control Release* 1999; 60: 121-128.

25. Brigger I, Morizet J, Aubert G, Chacun H, Terrier-Lacombe MJ, Couvreur P and Vassal G. Poly(ethylene glycol)-coated hexadecylcyanoacrylate nanospheres display a combined effect for brain tumor targeting. *J Pharmacol Exp Ther* 2002; 303: 928-936.

26. Kim HR, Andrieux K, Gil S, Taverna M, Chacun H, Desmaele D, Taran F, Georgin D and Couvreur P. Translocation of poly(ethylene glycol-co-hexadecyl)cyanoacrylate nanoparticles into rat brain endothelial cells: role of apolipoproteins in receptor-mediated endocytosis. *Biomacromolecules* 2007; 8: 793-799.

27. Peracchia MT, Harnisch S, Pinto-Alphandary H, Gulik A, Dedieu JC, Desmaele D, d'Angelo J, Muller RH and Couvreur P. Visualization of in vitro protein-rejecting properties of PEGylated stealth polycyanoacrylate nanoparticles. *Biomaterials* 1999; 20: 1269-1275.

28. Brambilla D, Verpillot R, Taverna M, De Kimpe L, Le Droumaguet B, Nicolas J, Canovi M, Gobbi M, Mantegazza F, Salmona M, Nicolas V, Scheper W, Couvreur P and Andrieux K. New method based on capillary electrophoresis with laser-induced fluorescence detection (CE-LIF) to monitor interaction between nanoparticles and the amyloid-beta peptide. *Anal Chem* 2010; 82: 10083-10089.

29. Brambilla D, Souguir H, Nicolas J, Mackiewicz N, Verpillot R, Le Droumaguet B, Taverna M, Couvreur P and Andrieux K. Colloidal properties of biodegradable nanoparticles influence interaction with amyloid-[beta] peptide. *Journal of Biotechnology* In Press, Uncorrected Proof:

30. Brambilla D, Nicolas J, Le Droumaguet B, Andrieux K, Marsaud V, Couraud PO and Couvreur P. Design of fluorescently tagged poly(alkyl cyanoacrylate) nanoparticles for human brain endothelial cell imaging. *Chem Commun (Camb)* 2010; 46: 2602-2604.

31. Gref R, Luck M, Quellec P, Marchand M, Dellacherie E, Harnisch S, Blunk T and Muller RH. 'Stealth' corona-core nanoparticles surface modified by polyethylene glycol (PEG): influences of the corona (PEG chain length and surface density) and of the core composition on phagocytic uptake and plasma protein adsorption. *Colloids Surf B Biointerfaces* 2000; 18: 301-313.

32. Gref R, Minamitake Y, Peracchia MT, Trubetskoy V, Torchilin V and Langer R. Biodegradable long-circulating polymeric nanospheres. *Science* 1994; 263: 1600-1603.

33. Sabella S, Quaglia M, Lanni C, Racchi M, Govoni S, Caccialanza G, Calligaro A, Bellotti V and De Lorenzi E. Capillary electrophoresis studies on the aggregation process of beta-amyloid 1-42 and 1-40 peptides. *Electrophoresis* 2004; 25: 3186-3194.

34. Matsuoka Y, Saito M, LaFrancois J, Gaynor K, Olm V, Wang L, Casey E, Lu Y, Shiratori C, Lemere C and Duff K. Novel therapeutic approach for the treatment of Alzheimer's disease by peripheral administration of agents with an affinity to beta-amyloid. *J Neurosci* 2003; 23: 29-33.

35. Re F, Airoldi C, Zona C, Masserini M, La Ferla B, Quattrocchi N and Nicotra F. Beta amyloid aggregation inhibitors: small molecules as candidate drugs for therapy of Alzheimer's disease. *Curr Med Chem* 2010; 17: 2990-3006.

36. Brambilla D, Souguir H, Nicolas J, Mackiewicz N, Verpillot R, Le Droumaguet B, Taverna M, Couvreur P and Andrieux K. Colloidal properties of biodegradable nanoparticles influence interaction with amyloid-beta peptide. *Journal of Biotechnology* Submitted:

37. Brambilla D, Nicolas J, Droumaguet BL, Andrieux K, Marsaud V, Couraud P-O and Couvreur P. Design of fluorescently tagged poly(alkyl cyanoacrylate) nanoparticles for human brain endothelial cell imaging. *Chem. Commun. (Cambridge, U. K.)* 2010; 46: 2602-2604.

38. Han Y, He C, Cao M, Huang X, Wang Y and Li Z. Facile Disassembly of Amyloid Fibrils Using Gemini Surfactant Micelles. *Langmuir* 2009; 26: 1583-1587.

39. Kato M, Kinoshita H, Enokita M, Hori Y, Hashimoto T, Iwatsubo T and Toyo'oka T. Analytical method for beta-amyloid fibrils using CE-laser induced fluorescence and its application to screening for inhibitors of beta-amyloid protein aggregation. *Anal Chem* 2007; 79: 4887-4891.

40. Taniguchi A, Sohma Y, Hirayama Y, Mukai H et al. "Click Peptide": pH-Triggered in Situ Production and Aggregation of Monomer Aβ1–42. *Chembiochem* 2009; 10: 710-715.

41. Beeg M, Stravalaci M, Bastone A, Salmona M and Gobbi M. A modified protocol to prepare seed-free starting solutions of amyloid-beta (Abeta) and Abeta from the corresponding depsipeptides. *Anal Biochem* 2011; 411: 297-299.

42. Friesner RA, Murphy RB, Repasky MP, Frye LL, Greenwood JR, Halgren TA, Sanschagrin PC and Mainz DT. Extra precision glide: docking and scoring incorporating a model of hydrophobic enclosure for protein-ligand complexes. *J Med Chem* 2006; 49: 6177-6196.

43. Friesner RA, Banks JL, Murphy RB, Halgren TA, Klicic JJ, Mainz DT, Repasky MP, Knoll EH, Shelley M, Perry JK, Shaw DE, Francis P and Shenkin PS. Glide: a new approach for rapid, accurate docking and scoring. 1. Method and assessment of docking accuracy. *J Med Chem* 2004; 47: 1739-1749.

44. Glide. *Schrodinger, LLC: New York* 2009; Version 5.5

45. Jorgensen WL, Maxwell DS and Tirado-Rives J. Development and Testing of the OPLS All-Atom Force Field on Conformational Energetics and Properties of Organic Liquids. *Journal of the American Chemical Society* 1996; 118: 11225-11236.

46. Kaminski GA, Friesner RA, Tirado-Rives J and Jorgensen WL. Evaluation and Reparametrization of the OPLS-AA Force Field for Proteins via Comparison with Accurate Quantum Chemical Calculations on Peptides†. *The Journal of Physical Chemistry B* 2001; 105: 6474-6487.

47. MAESTRO. *Schrodinger, LLC: New York* 2009; Version 9.0:

48. Jorgensen WL, Chandrasekhar J, Madura JD, Impey RW and Klein ML. Comparison of Simple Potential Functions for Simulating Liquid Water. *Journal of Chemical Physics* 1983; 79: 926-935.

49. Schafmeister WS, Ross WS and Romanovski V. LEAP, C.E.A.F. *University of California, San Francisco* 1995;

50. Case DA, Darden TA, Cheatham III TE, Simmerling CL, Wang J, Duke RE, Luo R, Crowley M, Walker RC, Zhang W, Merz KM, Wang B, Hayik S, Roitberg A, Seabra G, Kolossvary I, Wong KF, Paesani F, Vanicek J, Wu X, Brozell SR, Steinbrecher T, Gohlke H, Yang L, Tan C, Mongan J, Hornak V, Cui G, Mathews DH, Seetin MG, Sagui C, Babin V and Kollman PA. University of California, San Francisco. 2008;

51. Bas DC, Rogers DM and Jensen JH. *Proteins-Structure Function and Bioinformatics* 2008; 73: 765-783.

52. Li H, Robertson AD and Jensen JH. *Proteins-Structure Function and Bioinformatics* 2005; 61 704-721.

53. Berendsen HJC, Postma JPM, Vangunsteren WF, Dinola A and Haak JR. Molecular-Dynamics with Coupling to an External Bath. *Journal of Chemical Physics* 1984; 81: 3684-3690.

54. Ryckaert JP, Ciccotti G and Berendsen HJC. *J. Comput. Phys.* 1977; 23: 327-341.

55. Humphrey W, Dalke A and Schulten K. VMD: visual molecular dynamics. *J Mol Graph* 1996; 14: 33-38, 27-38.

56. Kabsch W and Sander C. Dictionary of protein secondary structure: pattern recognition of hydrogen-bonded and geometrical features. *Biopolymers* 1983; 22: 2577-2637.

57. Moghimi SM, Hamad I, Andresen TL, Jorgensen K and Szebeni J. Methylation of the phosphate oxygen moiety of phospholipid-methoxy(polyethylene glycol) conjugate prevents PEGylated liposome-mediated complement activation and anaphylatoxin production. *FASEB J* 2006; 20: 2591-2593.

58. Hamad I, Hunter AC, Szebeni J and Moghimi SM. Poly(ethylene glycol)s generate complement activation products in human serum through increased alternative pathway turnover and a MASP-2-dependent process. *Mol Immunol* 2008; 46: 225-232.

59. Moghimi SM, Hamad I, Al-Hanbali O, Hunter AC, Rutt KJ and Andresen TL. Distinct Polymer Architecture Mediates Switching of Complement Activation Pathways at the Nanosphere-Serum Interface: Implications for Stealth Nanoparticle Engineering. *Acs Nano* 2010; 4: 6629-6638.

60. Allemann E, Gravel P, Leroux JC, Balant L and Gurny R. Kinetics of blood component adsorption on poly(D,L-lactic acid) nanoparticles: evidence of complement C3 component involvement. *J Biomed Mater Res* 1997; 37: 229-234.

Supporting information

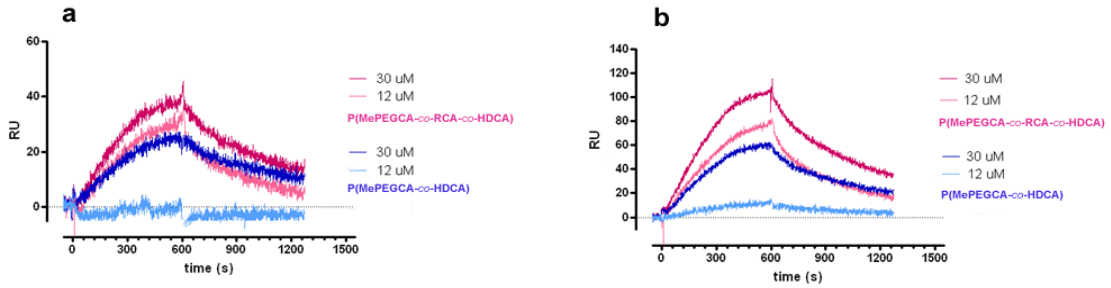

Figure S1. *Surface plasmon resonance experiments. Sensorgrams of P(MePEGCA-co-HDCA) NPs and of P(MePEGCA-co-RCA-co-HDCA) NPs suspensions at 12 and 30 μM flowed onto a* $A\beta_{1\text{-}42}$ *monomers (a) or fibrils (b) immobilized gold chip.*

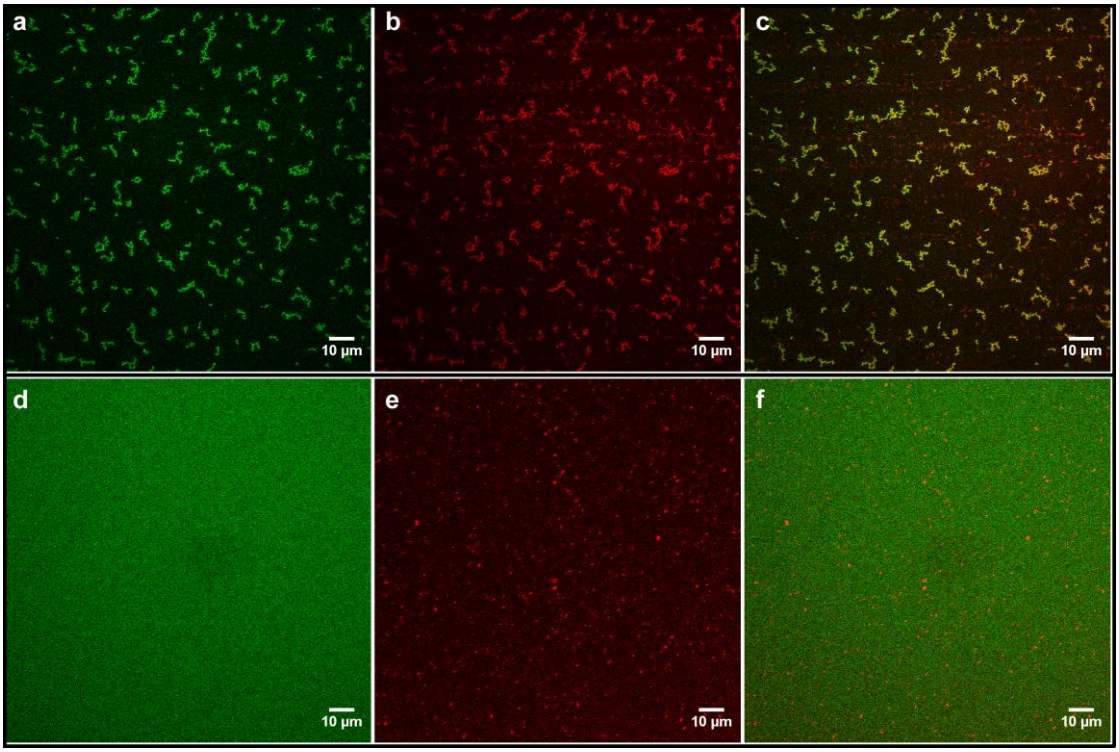

Figure S2. *Confocal microscopy images. Colocalization of Hilyte Fluo*^{TM} $A\beta_{1\text{-}42}$ *and P(MePEGCA-co-RCA-co-HDCA)* and PHDCA nanoparticles suspension after 12h incubation at 37°C. (a) Aβ peptide (10 μM) (green channel), (b) P(MePEGCA-co-RCA-co-HDCA) nanoparticles (20 μM) (red channel), (c) merge of a and b, (d) Aβ peptide (10 μM) (green channel), (e) P(HDCA-co-RCA) nanoparticles (20 μM) (red channel), (f) merge of d and e. *Results from Brambilla et al., 2010.*

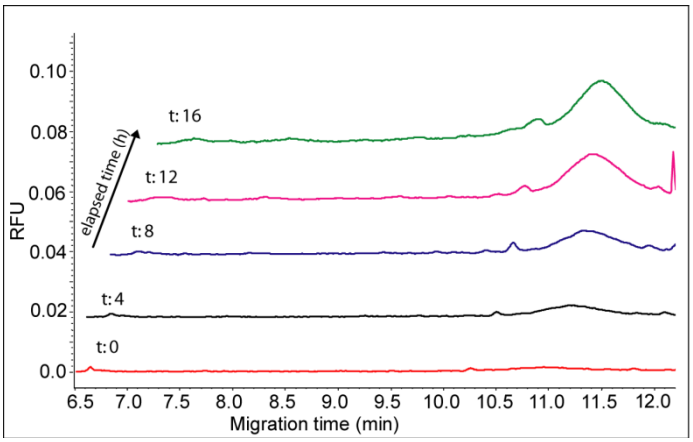

Figure S3. *CE-LIF experiments. Aggregating $A\beta_{1\text{-}42}$ peptide (50 µM) added of Thioflavin (10 µM) analyzed as a function of elapsed time.*

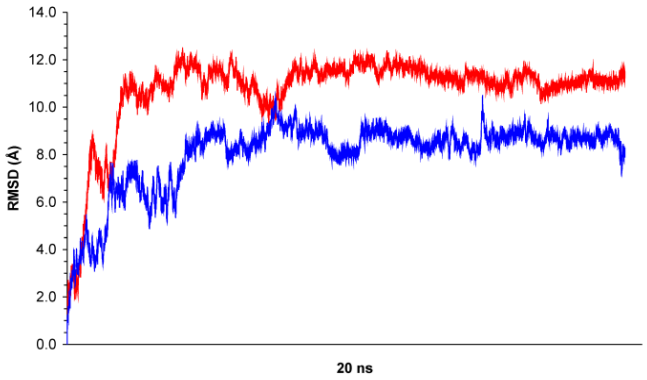

Figure S4. *Root-mean-square deviation (RMSD) of the Cα carbons of the $A\beta_{1\text{-}42}$ backbone between the crystal structure (PDB ID: 1IYT) and the solution structure with the PEG (red) and PE (blue) chains.*

Section 4

Implications dans le projet NAD

Récemment, plusieurs polyphénols comme la Thioflavine T, la Curcumine et le Rouge Congo ont démontré une bonne affinité pour le peptide $A\beta_{1-42}$. Aussi, nous avons porté notre attention sur la Sélégiline, une molécule aromatique utilisée pour ralentir la progression de la maladie de Parkinson et montrant également une certaine affinité pour le peptide $A\beta_{1-42}$. Cette étude porte donc sur la synthèse de nanoparticules recouvertes de chaines PEG à l'extrémité desquelles la Sélégiline a été couplée par chimie « click » et leur utilisation pour la capture du peptide Aβ dans les fluides biologiques. Pour étudier cette interaction, la technique CE-LIF a été utilisée. Les résultats ont montré une réorganisation significative de surface des nanoparticules limitant l'interaction de la sélégiline avec le peptide.

Implications in the NAD project

Recently, several polyphenols such as Thioflavin T, Curcumine and Congo red, have shown the ability to target with a good affinity the $A\beta_{1-42}$ peptide. Thus, we focused our attention on Selegiline, an aromatic molecule that is employed to slow down the progression of Parkinson's disease, but also exhibited a certain affinity for the $A\beta_{1-42}$ peptide. In this study, we presented the synthesis of selegiline-functionalized nanoparticles as devices for Aβ capturing in biological fluids. Selegiline has been attached by the so called click-chemistry at the extremity of the PEG chains that surround the nanoparticles. CE-LIF protocol was employed to study the ability of these nanoparticles to interact with the peptide. The results evidenced a significant nanoparticles surface reorganization limiting the interation of the selegiline with the peptide.

Selegiline-Functionalized, PEGylated poly (alkyl cyanoacrylate) Nanoparticles: Investigation of Interaction with Amyloid-β Peptide

International Journal of Pharmaceutics, Volume 416, (2), 2011, 453-460

Benjamin Le Droumaguet,[1,¥] Hayfa Souguir,[1,¥] Davide Brambilla,[1] Romain Verpillot,[1] Julien Nicolas,[1] Myriam Taverna,[1] Patrick Couvreur [1]and Karine Andrieux[1]

[1]Laboratoire de Physico-Chimie, Pharmacotechnie et Biopharmacie, Univ. Paris-Sud, UMR CNRS 8612, Faculté de Pharmacie, 5 rue Jean-Baptiste Clément, 92296 Châtenay-Malabry, France.

[¥]both authors contributed equally to this work.

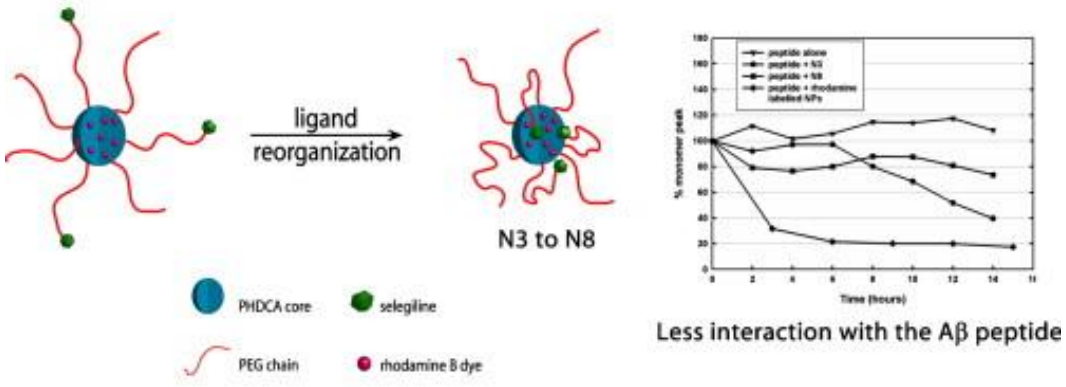

Résumé

La maladie d'Alzheimer (MA) est une affection neuro-dégénérative pour laquelle la recherche de nouveaux traitements est très compétitive. Puisque la fibrillogénèse du peptide amyloïde 1-42 ($A\beta_{1-42}$) est considérée comme une cause majeure de la dégénérescence neuronale, un intérêt particulier a été porté sur les molécules aromatiques permettant de cibler ce peptide. Ce papier décrit la synthèse de nanoparticules fluorescentes de poly-(cyanoacrylate d'alkyle) fonctionnalisées avec la sélégiline et leur évaluation pour le ciblage du peptide $A\beta_{1-42}$. La stratégie de synthèse utilisée s'appuie sur la conception de copolymères amphiphiles à base de cyanoacétates par la méthode tandem de Knoevenagel-addition de Michael, suivie par leur auto-assemblage en solution aqueuse. Les différents cyanoacetates utilisés sont: (i) le cyanoacétate hexadécyle pour former le noyau hydrophobe de la NP, (ii) la rhodamine B cyanoacétate apportant les propriétés fluorescentes, (iii) le méthoxypoly-(éthylène glycol) cyanoacétate (MePEGCA) pour les propriétés furtives et (iv) la sélégiline-poly (éthylène glycol) cyanoacétate (SelPEGCA) pour obtenir la fonctionnalité désirée. Deux copolymères amphiphiles différents ont été synthétisés, un copolymère containant la sélégiline, P(MePEGCA-*co*-SelPEGCA-*co*-HDCA), et un autre marqué à la rhodamine, P(MePEGCA-*co*-RCA-*co*-HDCA). Ces copolymères ont été mélangés avec différents ratios pour ajuster la quantité de sélégiline présente à la surface des NPs.

Les formulations optimales contenant les différents copolymères amphiphiles ont été déterminées par l'étude des caractéristiques colloïdales des NPs. De façon intéressante, il a été démontré que le potentiel zêta des nanoparticules fonctionnalisées avec la sélégiline est considérablement diminué, soulignant une modification significative de la charge de surface des nanoparticules. L'électrophorèse capillaire a ensuite été utilisée pour tester la capacité des NPs à interagir avec le peptide $A\beta_{1-42}$. En comparaison avec les NPs non fonctionnalisées, aucune augmentation de l'interaction avce la forme monomérique du peptide n'a été observée, soulignant ainsi le manque de disponibilité du ligand à la surface des nanoparticules. Pour expliquer ce résultat, un mécanisme, principalement basé sur l'enterrement du ligand hydrophobe, sélégiline, dans le coeur des nanoparticules, a été proposé.

Abstract

Alzheimer's disease (AD) is a neurodegenerative disorder for which the research of new treatments is highly challenging. Since the fibrillogenesis of amyloid-β peptide 1-42 ($A\beta_{1-42}$) peptide is considered as a major cause of neuronal degeneration, specific interest has been focused on aromatic

molecules for targeting this peptide. In this paper, the synthesis of selegiline-functionalized and fluorescent poly(alkyl cyanoacrylate) nanoparticles (NPs) and their evaluation for the targeting of the $A\beta_{1-42}$ peptide are reported. The synthetic strategy relied on the design of amphiphilic copolymers by tandem Knoevenagel-Michael addition of cyanoacetate derivatives, followed by their self-assembly in aqueous solutions to give the corresponding NPs. Different cyanoacetates were used: (i) hexadecyl cyanoacetate (HDCA) to form the hydrophobic core of the NPs; (ii) rhodamine B cyanoacetate (RCA) for fluorescent purposes; (iii) methoxypoly(ethylene glycol) cyanoacetate (MePEGCA) for stealth properties and (iv) selegiline-poly(ethylene glycol) cyanoacetate (SelPEGCA) to obtain the desired functionality. Two different amphiphilic copolymers were synthesized, a selegiline-containing copolymer, P(MePEGCA-*co*-SelPEGCA-*co*-HDCA), and a rhodamine-labelled counterpart, P(MePEGCA-*co*-RCA-*co*-HDCA), further blended at variable ratios to tune the amount of selegiline moieties displayed at the surface of the NPs.

Optimal formulations involving the different amphiphilic copolymers were determined by the study of the NP colloidal characteristics. Interestingly, it was shown that the zeta potential value of the selegiline-functionalized nanoparticles dramatically decreased, thus emphasizing a significant modification in the surface charge of the nanoparticles. Capillary electrophoresis has then been used to test the ability of the selegiline-functionalized NPs to interact with the $A\beta_{1-42}$ peptide. In comparison with non functionalized NPs, no increase of the interaction between these functionalized NPs and the monomeric form of the $A\beta_{1-42}$ peptide was observed, thus highlighting the lack of availability of the ligand at the surface of the nanoparticles. A mechanism explaining this result has been proposed and was mainly based on the burial of the hydrophobic selegiline ligand within the nanoparticles core.

Keywords

Alzheimer's Disease, Selegiline, Amyloid-β peptide, Poly(alkyl cyanoacrylate) nanoparticles, Functionalization.

1. Introduction

Alzheimer's disease (AD) is a severe neurodegenerative illness affecting more and more aging population over the world. AD represents the most common cause of dementia and is characterized by a progressive, but irreversible deterioration of cognitive functions and a loss of memory.[1] Although the mechanisms leading to these dysfunctions are still unclear and under debate,[2-4] the disease is physiologically characterized by two main pathological features. These hallmarks are: the intracellular accumulation of the hyperphosphorylated tau protein in the neurons and (ii) the progressive production

and aggregation of β-amyloid peptide (Aβ),[5,6] the latter being considered as the main cause of AD.[7] Neurons produce Aβ peptides with a variable number of amino-acids and the Aβ peptide 1-42 ($A\beta_{1-42}$) is believed to be the most representative and the most toxic species in AD physiopathology due to its high tendency to spontaneously self-aggregate.[8,9]

In the last decades, the pharmaceutical companies have only attempted to combat clinical manifestations of AD. In particular, acetylcholinesterase (AchE) inhibitors [10-12] and *N*-methyl-D-aspartate (NMDA) receptor antagonists[13-15] have been widely used but without significant success. Unfortunately, no efficient treatment aiming at the eradication of AD has been proposed so far.

Recently, different studies promoted the utilization of small aromatic molecules for targeting the $A\beta_{1-42}$ peptide, such as curcumine[16-18] and its derivatives,[19] Thioflavine T,[20] Congo red[21-23] and their analogues such as Chrysamine G[22,24,25] and X34.[26,27] These molecules have shown a certain efficiency to hinder, or even to stop, the oligomerization of the $A\beta_{1-42}$ peptide and thus the production of oligomers and/or fibrils, which are commonly considered as the toxic species for neuronal cells. These ligands have also been extensively used as tracers of the presence of senile plaques in the brain due to their fluorescent properties. Moreover, they can be modified with radiolabeled elements for diagnostic purposes.[28-32] Unfortunately, these compounds do not overpass the blood-brain barrier (BBB). To circumvent this crucial problem, researchers have developed three main strategies: (i) the chemical modification of ligands to make them able to cross the BBB (ii) their encapsulation into nanoparticles (NPs) and (iii) their ligation to NPs.[19,33]

Among the pool of efficient ligands discovered so far, we have focused our attention on selegiline, an aromatic molecule that has been employed to slow down the progression of the Parkinson's disease,[34] but that has been more importantly used as monoamine oxidase-B inhibitor for the treatment of AD.[35-37] Selegiline also exhibited a certain affinity for the $A\beta_{1-42}$ peptide.[38] In this study, we presented the synthesis of selegiline-functionalized and fluorescent poly(alkyl cyanoacrylate) nanoparticles for $A\beta_{1-42}$ peptide targeting and anti-fibrillogenesis purposes. By capturing monomeric peptide at the surface of these nanoparticles, we aim to inhibit its fibrillogenesis. The synthesis strategy relied on the dual modification of poly[methoxypoly(ethylene glycol) cyanoacrylate)-*co*-poly(hexadecyl cyanoacrylate)] (P(MePEGCA-*co*-HDCA)) copolymers[39,40] to introduce: (i) selegiline moieties at the extremity of PEG chains and (ii) rhodamine B probes within the copolymer structure. The P(MePEGCA-*co*-HDCA) copolymer scaffold has been selected due to its successful ability to cross the BBB.[41-43] Moreover, we took advantage of a recent study that demonstrated the efficient derivatization of such copolymers with azido-functional groups allowing subsequent reaction with alkyne-containing ligands through copper-catalyzed azide-alkyne

cycloaddition (CuAAC).[44] Functionalization was undertaken with selegiline by CuAAC *via* its native alkyne group. NPs were obtained from the self-assembly of different ratios of selegiline-functionalized and rhodamine B-tagged copolymers in order to tune the amount of selegiline moieties displayed at their surface (Figure 1). The resulting functionalized nanoparticles, obtained by the nanoprecipitation technique, were characterized by dynamic light scattering (DLS) and zeta potential (ζ) measurements. Finally, we used capillary electrophoresis (CE) to monitor the interaction of the selegiline-functionalized NPs with the $A\beta_{1\text{-}42}$ peptide.[45]

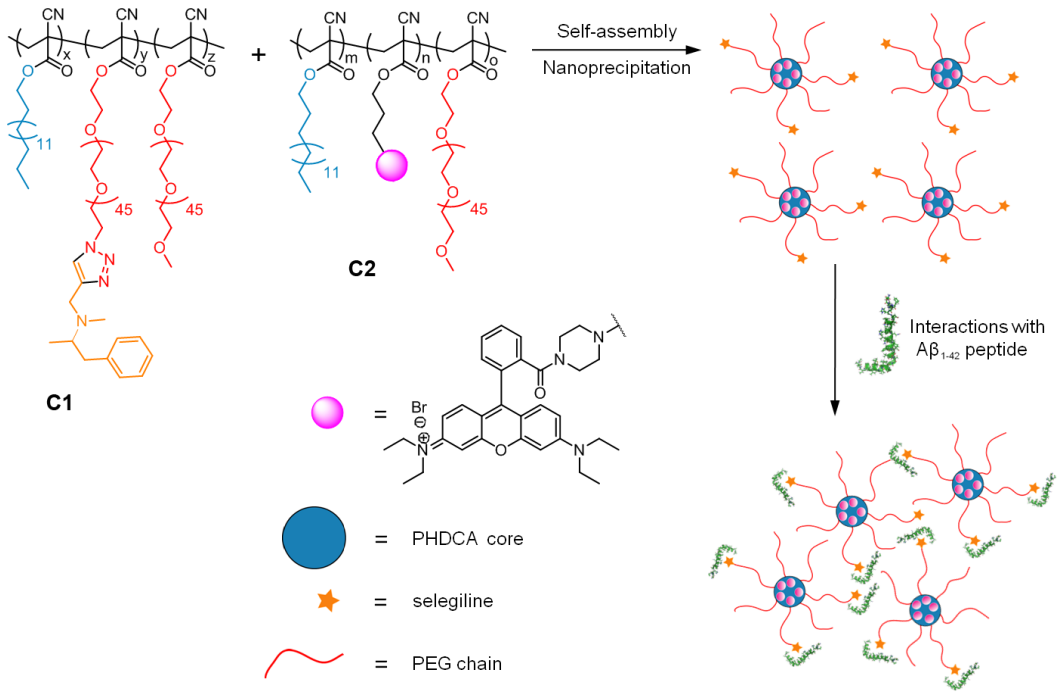

Figure 1. *General approach for the synthesis of selegiline-functionalized, PEGylated poly(alkyl cyanoacrylate) nanoparticles and their possible interaction with the HiLyte Fluor™ 488 labelled amyloid-β 1-42 ($A\beta_{1\text{-}42}$) peptide.*

2. Materials and Methods

2.1. Materials

Azidopoly(ethylene glycol) cyanoacetate (N_3PEGCA, M_n = 2 kDa), methoxypoly(ethylene glycol) cyanoacetate (MePEGCA, M_n = 2 kDa) and hexadecyl cyanoacetate (HDCA) were obtained from already published synthetic procedures.[44] Poly[hexadecyl cyanoacrylate-*co*-rhodamine B cyanoacrylate-*co*-methoxypoly(ethylene glycol) cyanoacrylate] (P(HDCA-*co*-RCA-*co*-MePEGCA), C1) copolymer containing 5% rhodamine cyanoacetate (with respect to HDCA monomer) and poly[hexadecyl cyanoacrylate-*co*-azidopoly(ethylene glycol) cyanoacrylate] P(HDCA-*co*-N_3PEGCA)

copolymers were obtained by tandem Knoevenagel-Michael addition of cyanoacetate.[44,46] NaH_2PO_4 (>99%) was purchased from Merck & Co (Fontenay-sous-Bois, France). Na_2HPO_4 (>98%) was obtained from Prolabo (Strasbourg, France). Pluronic F-68 (99%), sodium carbonate (Na_2CO_3, BioUltra, minimum 99.5%) and sodium dodecyl sulfate (SDS, 99%), R-(−)-Deprenyl hydrochloride (selegiline, ≥98%), *N*-dicyclohexylcarbodiimide (DCC, Fluka, ≥99% GC), 4-dimethylaminopyridine (DMAP, 99%), formaldehyde solution (37 wt. % in water, contains 10-15% methanol as stabilizer), pyrrolidine (99% GC, T), copper sulphate pentahydrate ($CuSO_4 \cdot 5H_2O$, ≥98%), (+)-sodium L-ascorbate (crystalline, 98%), ethylene-diaminetetraacetic acid tetrasodium salt hydrate (EDTA, practical grade ~95%) were purchased from Sigma-Aldrich (St. Quentin Fallavier, France). Sodium hydroxide (NaOH) solution (1 M) was obtained from VWR (Fontenay-sous Bois, France). All solvents were purchased at the highest grade from Carlo Erba (Val de Reuil, France). Deuterated chloroform ($CDCl_3$, ≥99.8 atom% D) and dimethyl sulfoxide (DMSO-d_6, ≥99.8 atom% D) were obtained from Sigma Aldrich and used as received.

Lyophilized HiLyte Fluor™ 488 labelled amyloid-β 1-42 ($A\beta_{1-42}$) peptide was provided by ANASPEC (Le Perray en Yvelines, France). Spectra/Por dialysis bags (2 kDa molecular weight cut off) were purchased from Spectrum Laboratories Inc. and used after washing in deionized water for 1 h.

2.2. Analytical techniques

2.2.1. ^{1}H NMR Spectroscopy

All ^{1}H NMR spectra were performed in deuterated solvents ($CDCl_3$ or d_6-DMSO) at ambient temperature on a Bruker Avance 300 MHz spectrometer.

2.2.2. Mean average diameter and zeta potential measurements

Nanoparticles average diameter (D_z) was measured by dynamic light scattering (DLS) with a Nano ZS from Malvern (173° scattering angle) at a temperature of 25 °C. Colloidal stability was evaluated as a function of time in different buffers (cell culture medium, phosphate buffer saline) at 25°C. The zeta potential (ζ) was calculated with the same apparatus from the electrophoretic mobility (u) using the Smoluchowsky relationship $\zeta = \eta.u/\varepsilon.f(\kappa a)$, where it is assumed that $\kappa.a >> 1$, where η is the solution viscosity, ε is the dielectric constant of the medium, and κ and a are the Debye-Hückel parameter and the particle radius, respectively, $f(\kappa a)$ is the Henry's function and its value is 1.5 (Smoluchowski approximation) when the electrophoretic determinations of zeta potential are made in aqueous media and moderate electrolyte concentration. ζ-potential measurements of nanoparticle dilute aqueous solutions were carried out at 25 °C in 10^{-3} M KCl.

2.2.3. Capillary electrophoresis

Capillary electrophoresis (CE) was performed on a PA 800 instrument (Beckman Coulter, Roissy, France) using uncoated silica capillaries (Phymep, Paris) with an internal diameter of 50 µm and 50 cm total length (40 cm effective length was employed for the separation). All buffers were prepared with deionized water and were filtered through a 0.22 µm membrane (VWR) before use. Prior analysis, the capillaries were preconditioned by the following rinsing sequence: 0.1 M NaOH for 5 min, 1 M NaOH for 5 min and then deionised water for 5 min. The in-between runs rinsing cycles were carried out by pumping sequentially through the capillary: water for 5 min, 50 mM SDS for 2 min, to inhibit the aggregation and subsequent peptide adsorption on the capillary wall, and 0.1 M NaOH for 5 min. The samples were introduced into the capillary by hydrodynamic injection under 3.4 kPa. The capillary was thermostated at 25°C and the samples were maintained at 37°C by the storage sample module of the PA 800 apparatus. The separations were carried out at 16 kV with positive polarity at the inlet using 80 mM phosphate buffer pH 7.4. The running electrolyte was renewed after each run. The fluorescent peptide was detected by a laser-induced fluorescence (LIF) detection system equipped with 3.5 mW argon-ion laser with a wavelength excitation of 488 nm, the emission being collected through a 520 nm band-pass filter. Peak areas were estimated using the 32 Karat™ software (Beckman Coulter). The results are expressed as the evolution of percentage of monomer peak area as a function of time.[45]

2.3. Synthesis of P(MePEGCA-*co*-SelPEGCA-*co*-HDCA) copolymers

2.3.1. Neutral form of selegiline

Selegiline•HCl (100 mg, 0.45 mmol) was dispersed in a 1 M Na_2CO_3 solution (5 mL, 5 mmol). The solution was vigorously stirred for 1 h and transferred into a separation funnel. Neutralized selegiline was extracted with diethylether (3 × 15 mL). The joined organic fractions were dried over $MgSO_4$, filtered off and the solvent was removed under reduced pressure to give the desired product as a colourless oil in a quantitative yield. ^{1}H NMR (d_6-DMSO, 298 K) δ (ppm): 0.87 (d, 3H, J = 6.6 Hz), 2.27 (s, 3H), 2.90 (td, 2H, J = 4.1 and 12.6 Hz), 3.10 (t, 1H, J = 2.5 Hz), 3.35 (t, 2H, J = 2.45 Hz), 7.13-7.20 (m, 3H), 7.22-7.30 (m, 2H).

2.3.2. Selegiline-poly(ethylene glycol) (SelPEG)

Selegiline-poly(ethylene glycol) was obtained by click chemistry.[47] In a 10 mL round bottom flask, azidopoly(ethylene glycol) (200 mg, 0.1 mmol) and neutralized selegiline (37.5 mg, 0.2 mmol) were dissolved in 2 mL of a 1:1 ^{t}BuOH/deionized water mixture. The solution was bubbled for 10 min with nitrogen at room temperature. Then, $CuSO_4 \bullet 5H_2O$ (2.5 mg, 0.01 mmol) and (+)-sodium L-ascorbate (4.0 mg, 0.02 mmol) were dissolved in 1 mL of deionized water and the resulting solution was immediately added to the reaction mixture, followed by nitrogen bubbling for another 20 min and finally stirred overnight at room temperature under nitrogen atmosphere. ^{t}BuOH was then removed under reduced pressure and the aqueous solution was diluted with 1 mL of a 1M EDTA aqueous solution and extensively dialyzed against deionized water using a 2 kDa dialysis bags. After dialysis, water was removed under reduced pressure and the product, dissolved in DCM, was dried over $MgSO_4$. After removal of the solvent, the pure product was obtained as a slightly brown powder with 75% yield. ^{1}H NMR (298 K, $CDCl_3$) δ (ppm): 1.13 (d, 3H, *J* = 5.5 Hz), 2.55 (br s, 3H), 3.35-3.94 (m, 188H), 4.20 (s, 2H), 4.57 (t, 2H, *J* = 5.1 Hz), 7.19-7.35 (m, 5H), 8.06 (s, 1H).

2.3.3. Synthesis of selegiline-poly(ethylene glycol) cyanoacetate (SelPEGCA)

In a 10 mL round bottom flask containing the selegiline-poly(ethylene glycol) (150 mg, 68 μmol) and cyanoacetic acid (11.5 mg, 136 μmol), were added 2 mL of DCM and 1 mL of ethylacetate. The resulting solution was cooled down with ice and placed under nitrogen atmosphere. DCC (21 mg, 102 μmol) and a catalytic amount of DMAP were dissolved in 1 mL of DCM and added dropwise. The reaction mixture was stirred at room temperature overnight under nitrogen atmosphere. After filtration to discard the insoluble dicyclohexylurea (DCU), the solvents were removed under reduced pressure and the resulting residue was dissolved in a minimum of DCM and precipitated in cold diethyl ether to give the pure product as a slightly brown powder with 86% yield. ^{1}H NMR (298 K, $CDCl_3$) δ (ppm): 1.15 (d, 3H, *J* = 5.5 Hz), 2.52 (br s, 3H), 3.52 (s, 2H), 3.35-3.94 (m, 188H), 4.19 (s, 2H), 4.35 (t, 2H, *J* = 4.7 Hz), 4.59 (t, 2H, *J* = 5.1 Hz), 7.19-7.35 (m, 5H), 8.06 (s, 1H).

2.3.4. Synthesis of selegiline-functionalized copolymer

The procedure for the synthesis of 10% selegiline-functionalized copolymer (P(MePEGCA-*co*-SelPEGCA-*co*-HDCA)) is as follows. In a 10 mL round bottom flask were introduced HDCA (120 mg, 0.38 mmol), MePEGCA (180 mg, 0.864 mmol) and SelPEGCA (22 mg, 0.096 mmol) in 2 mL of DCM and 1 mL of EtOH. To this solution were consecutively added dropwise formalin (0.2 mL, 4.43 mmol) and pyrrolidine (10 μL, 0.122 mmol). The reaction was stirred overnight under nitrogen

atmosphere. The solvents were removed under reduced pressure and the residue was redissolved in DCM. The organic phase was washed with 3 portions of deionized water, once with 1 M HCl solution, once with brine and finally dried over $MgSO_4$. The solvent was removed under reduced pressure to afford the resulting copolymer as a slightly brown sticky solid (92% yield). ^{1}H NMR (298 K, $CDCl_3$, 300 MHz) δ (ppm): 0.81 (t, 12H, *J* = 6.6 Hz), 0.96-1.41 (m, 104H), 1.66 (m, 8H), 2.25-2.77 (br m, 8H), 3.30 (s, 2.7H), 3.33-3.84 (m, 188H), 4.19 (br s, 10H), 4.59 (t, 0.2H, *J* = 5.2 Hz), 7.11-7.29 (m, 0.5H), 8.04 (s, 0.1H).

2.4. Nanoparticles preparation

A typical procedure for the preparation of selegiline-functionalized nanoparticles (Table 1, **N6**) is as follows. 5 mg of 10% selegiline-functionalized P(MePEGCA-*co*-SelPEGCA-*co*-HDCA) copolymer and 5 mg of P(MePEGCA-*co*-RCA-*co*-HDCA) copolymer were dissolved in 2 mL of acetone. This solution was added dropwise to an aqueous solution of 0.5 % (w/v) of Pluronic F-68 (4 mL) under vigorous stirring. Nanoparticle suspension formed immediately. Acetone was then removed under reduced pressure and the nanoparticles were purified by ultracentrifugation (150 000 *g*, 1 h, 4 °C, Beckman Coulter, Inc.). The supernatant was discarded and the pellet was resuspended in the appropriate volume of deionized water to yield a 2.5 $mg.mL^{-1}$ nanoparticle suspension. The colloidal characteristics of the nanoparticles were then analyzed by DLS and zeta potential measurement.

2.5. Peptide samples preparation and storage

Lyophilized HiLyte Fluor™ 488 labelled $A\beta_{1-42}$ peptide was dissolved in 0.16% (w/v) of ammonium hydroxide aqueous solution to reach a concentration of 0.5 $mg.mL^{-1}$. The peptide solution was then divided into aliquots, individually stored at –20 °C freshly thawed prior analysis.

2.6. Nanoparticles interaction with monomeric $A\beta_{1-42}$

To study the interaction between the monomeric form of the fluorescent $A\beta_{1-42}$ peptide and the selegiline-functionalized nanoparticles, aliquots of HiLyte Fluor™ 488 labelled $A\beta_{1-42}$ peptide stock solutions were diluted in 20 mM phosphate buffer (NaH_2PO_4) pH 7.4 containing 20 µM of P(MePEGCA-*co*-RCA-*co*-HDCA) nanoparticles **N3** or **N8** to obtain a final peptide concentration of 5 µM. The samples were then incubated at 37°C and analyzed by CE approximately every 2 h using LIF detection.[45]

3. Results and discussion

As previously mentioned, the "amyloid hypothesis" (*i.e.* the hypothesis that the amyloid fibrils formed by oligomerization of Aβ peptides and especially of the $A\beta_{1-42}$ peptide are the major causes of the neuronal degeneration), is so far considered by researchers as the most probable cause of AD. Consequently, more and more research groups have focused their efforts on the inhibition of this fibrillogenesis with suitable compounds/ligands. Among these ligands, selegiline has been chosen due of its terminal alkyne functionality that allowed for further covalent linkage on azide-containing copolymers/nanoparticles *via* CuAAC reaction. The synthesis of selegiline-functionalized poly(alkyl cyanoacrylate) nanoparticles was therefore undertaken.

3.1. Synthesis and characterization of selegiline-functionalized copolymers

Prior functionalization of PEGCA with selegiline, its hydrochloric salt was turned into its neutral form using Na_2CO_3 in order to avoid any alteration of the copper catalyst involved in the CuAAC. Indeed, some preliminary studies (data not shown) yielded no coupling when selegiline, hydrochloric salt was used under standard click conditions. Neutral selegiline was obtained quantitatively as confirmed by ^{1}H NMR spectroscopy that displayed all protons accounting for the molecule (see experimental part).

We took advantage of a recent study which demonstrated the covalent linkage of model ligands, either at the surface of azido-functionalized nanoparticles or directly to the corresponding copolymer.[44] However, in the present study, a slightly different approach was used whereby a functionalized poly(ethylene glycol) cyanoacetate was first prepared prior synthesis of the corresponding copolymer. Selegiline-poly(ethylene glycol) cyanoacetate (SelPEGCA) was copolymerized with HDCA and MePEGCA in the presence of ethanol, formalin and pyrrolidin to give the selegiline-functionalized P(MePEGCA-*co*-SelPEGCA-*co*-HDCA) copolymer. It was characterized by ^{1}H NMR spectroscopy which confirmed the presence of selegiline moieties within the copolymer structure, *via* its aromatic protons (see experimental part).

3.2. Formation and characterization of selegiline-functionalized nanoparticles

The ability of the selegiline-functionalized poly(alkyl cyanoacrylate) copolymers to form nanoparticles by self-assembly was assessed and the suspensions of nanoparticles were then characterized by DLS and zeta potential measurements as stability studies.

P(MePEGCA-*co*-SelPEGCA-*co*-HDCA) nanoparticles **N1** and **N2** containing respectively 10 or 50% SelPEGCA (with respect to the overall PEGCA content of the copolymer) were prepared by

the nanoprecipitation technique. Their characterization revealed that nanoparticles **N2** obtained by including 50% SelPEGCA exhibited a poor colloidal stability. Indeed, several minutes after their formation, the average diameter dramatically increased from approximately 150 to 200 nm, together with an increase of the particle size distribution (PSD) from less than 0.2 to 0.4. The nanoparticles **N1** synthesized with only 10% SelPEGCA displayed a mean average diameter of around 100 nm (PSD ~0.2). But, within 2 days, their size also increased significantly together with an increase of their particle size distribution above 0.3. Even after some efforts to change the nanoprecipitation parameters (such as the organic phase/aqueous phase ratio or the percentage of Pluronic F-68 surfactant added to the aqueous solution), the poor P(MePEGCA-*co*-SelPEGCA-*co*-HDCA) nanoparticle stability remained unchanged. Therefore, a co-nanoprecipitation approach with P(MePEGCA-*co*-SelPEGCA-*co*-HDCA) (**C1**) and P(MePEGCA-*co*-RCA-*co*-HDCA) (**C2**) copolymers was investigated. Indeed, P(MePEGCA-*co*-RCA-*co*-HDCA) copolymer **C2** exhibited a great colloidal stability over time and a rather low zeta potential value (around –40.6 ± 0.3 mV).[46] Variable blends of these two copolymers **C1** and **C2** were tested (see Table 1).

Table 1. *Composition and initial colloidal properties of selegiline-functionalized Poly(alkyl cyanoacrylate) nanoparticles.*

Expt.	P(MePEGCA-*co*-SelPEGCA-*co*-HDCA) copolymer **C1**[a]	P(MePEGCA-*co*-RCA-*co*-HDCA) copolymer **C2**	SelPEGCA[b]	Average particle diameter[d] (D_z)	Particle size distribution[c,d]	Zeta potential[d] (?)
	wt.%	wt.%	mol.%	nm		mV
1 (N8)	90	10	9%	93	0.16	9
2 (N7)	70	30	7%	92	0.13	7.9
3 (N6)	50	50	5%	96	0.16	–2.4
4 (N5)	10	90	1%	104	0.18	–12.9
5 (N4)	5	95	0.5%	110	0.14	–11.1
6 (N3)	2	98	0.2%	113	0.18	–14.9

[a]copolymer containing 10% SelPEGCA with respect to PEGCA overall content. [b]with respect to PEGCA overall content. [c]given by the DLS apparatus. [d]values measured immediately after purification of the nanoparticles.

These new formulations of selegiline-functionalized nanoparticles **N3** to **N8**, incorporating from 0.2 to 9% selegiline PEGCA, respectively, were characterized by DLS and zeta potential measurement (Table 1). These nanoparticles displayed average diameters in the 90–120 nm range with narrow particle size distribution (PSD < 0.2), together with zeta potential values varying from 10 to –15 mV. It was observed that the more selegiline-functionalized copolymer incorporated in the formulation, the higher the zeta potential. This demonstrated the presence of the selegiline ligands at the surface of the nanoparticles, rendering their surface more positively charged than the non-functionalized ones. The NPs were then subjected to DLS measurements over a period of 8 days in deionized water at 25°C (Figure 2). It was shown that the mean average diameter remained rather stable (the variation observed for **N6** at day 7 should not be considered relevant).

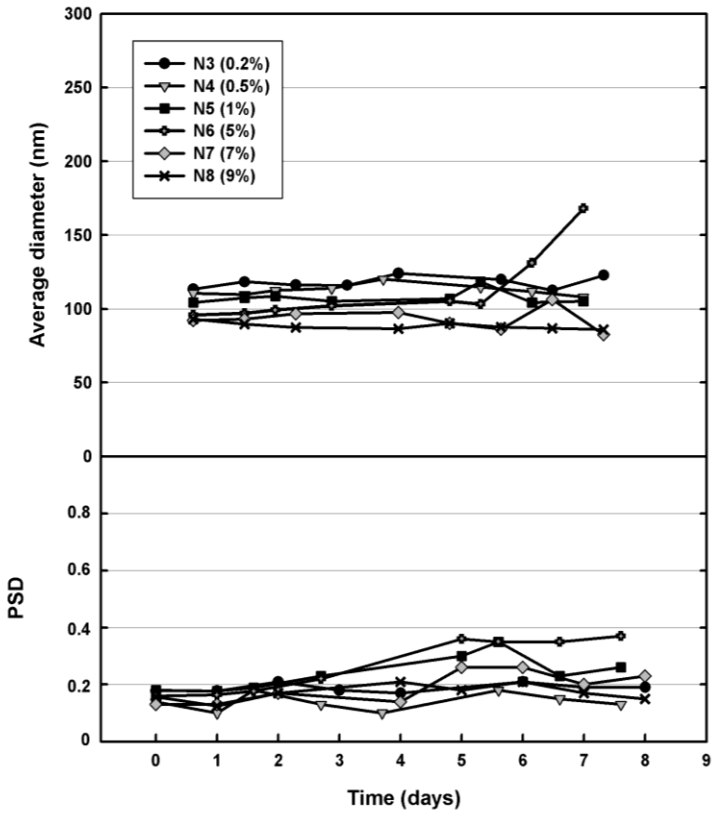

Figure 2. *Evolution with time of the average diameter and of the particle size distribution (PSD) in deionized water at 25°C of the selegiline-functionalized nanoparticles as a function of the selegiline content within the copolymer mixture: ●, N3 (0.2%); □, N4 (0.5 %); ■, N5 (1 %); +, N6 (5 %); ◊, N7 (7 %); x, N8 (9 %).*

However, as shown in Figure 3, the zeta potential values of nanoparticles **N3** to **N8** dramatically decreased within 1 or 2 days, whereas it remained rather constant for rhodamine B-labelled P(MePEGCA-*co*-RCA-*co*-HDCA) NPs as previously published.[46] Indeed, an average drop of

~15 mV was observed, indicating a change in the physico-chemical properties at the surface of the nanoparticles. Following this marked decrease, the zeta potential remained stable, close to values usually observed for P(MePEGCA-*co*-RCA-*co*-HDCA) nanoparticles.[46]

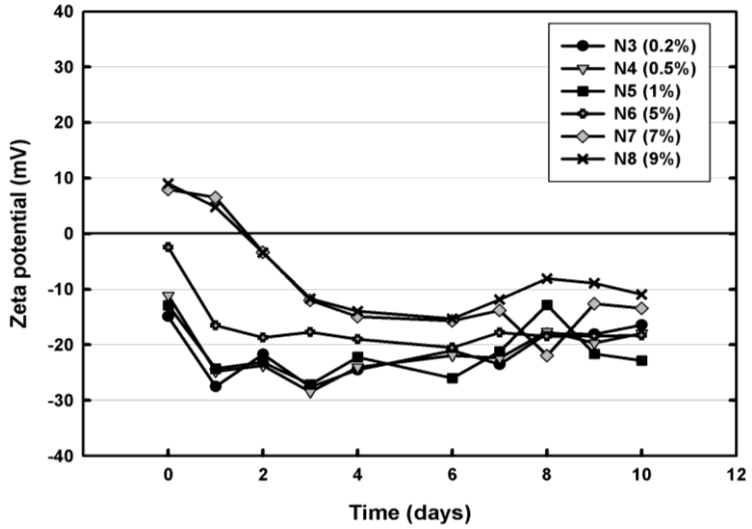

Figure 3. *Evolution with time of the ζ-potential values in deionized water at 25°C of selegiline-functionalized nanoparticles as a function of the selegiline content within t*

◊, N7 (7 %); x, N8 (9 %).

The stability of these NPs was also assessed in phosphate buffer saline (pH 7.4) used in CE analysis and in cell culture medium. As observed in Figure 4, the average diameter of the nanoparticles remained rather stable up to one week with a particle size distribution below 0.3 in both buffers. The decrease in zeta potential was observed in both media, still confirming the surface charge evolution of the nanoparticles with time (data not shown). However, this good stability of the average diameter for nanoparticles **N3** to **N8** in phosphate buffer allowed further studies of their interactions with the $A\beta_{1-42}$ peptide by CE.

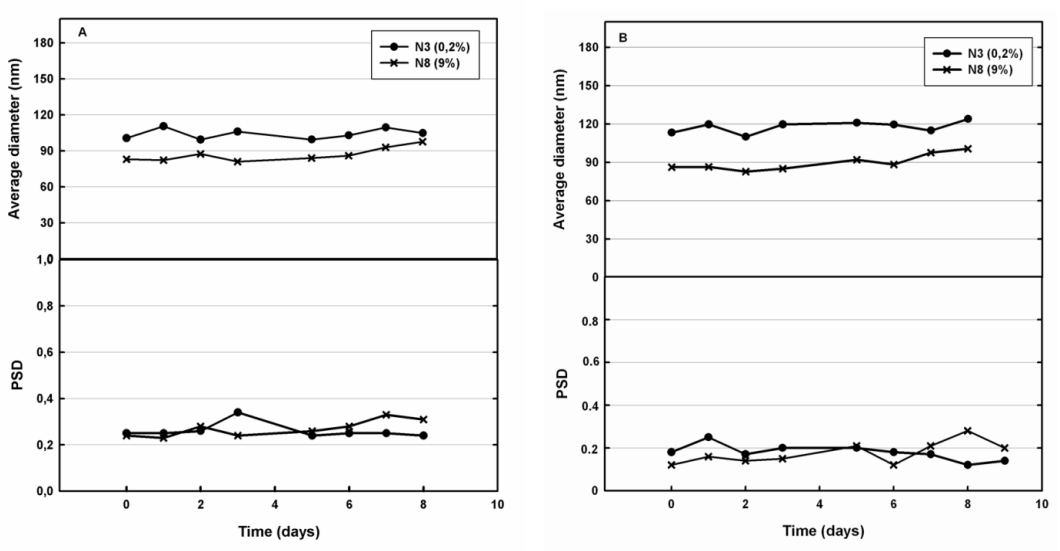

Figure 4*. Evolution of the average diameter and of the particle size distribution of selegiline-functionalized nanoparticles* ***N3*** *(●, 0.2% SelPEGCA) and* ***N8*** *(x , 9% SelPEGCA) at 25°C in (A) cell culture medium and in (B) phosphate buffer saline pH 7.4 as a function of time.*

3.3. Interaction of the nanoparticles with the $A\beta_{1-42}$ peptide

CE is an analytical technique that has been recently used for the screening and identification of efficient ligands towards their inhibition properties against $A\beta_{1-42}$ peptide aggregation.[48-50] Thereby, we recently developed an innovative protocol based on capillary electrophoresis coupled to laser-induced fluorescence (CE-LIF) detection to monitor the interactions of P(MePEGCA-*co*-RCA-*co*-HDCA) nanoparticles with the $A\beta_{1-42}$ peptide.[45] Interestingly, it was demonstrated that the P(MePEGCA-*co*-RCA-*co*-HDCA) nanoparticles were able to bind the $A\beta_{1-42}$ peptide under its so-called "monomeric" form. We claimed that this protocol could be relevant to screen NPs for $A\beta_{1-42}$ targeting and to discover suitable candidates.

Herein, we investigated the interaction of such a functionalization of a similar polymeric scaffold with selegiline, with the $A\beta_{1-42}$ peptide using CE coupled to LIF detection. Samples of fluorescently-tagged $A\beta_{1-42}$ peptide incubated with nanoparticles **N3** and **N8** were analyzed every 2 h using a LIF detection system that allowed monitoring the relative concentration of the peptide. P(MePEGCA-*co*-RCA-*co*-HDCA) nanoparticles dramatically decrease the area under the curve (AUC) of the $A\beta_{1-42}$ peptide monomeric peak (from 100 to 20% after 6 hours) whereas this value remained unchanged in the absence of any polymeric nanocarrier (control experiment, AUC ~100 % after 14 hours) as observed in Figure 5. These data combined with other results have been related to the adsorption of the peptide at the surface of P(MePEGCA-*co*-RCA-*co*-HDCA) nanoparticles.[45] Regarding Aβ peptide affinity, the role of PEG and rhodamine are still unclear but are under

investigation.

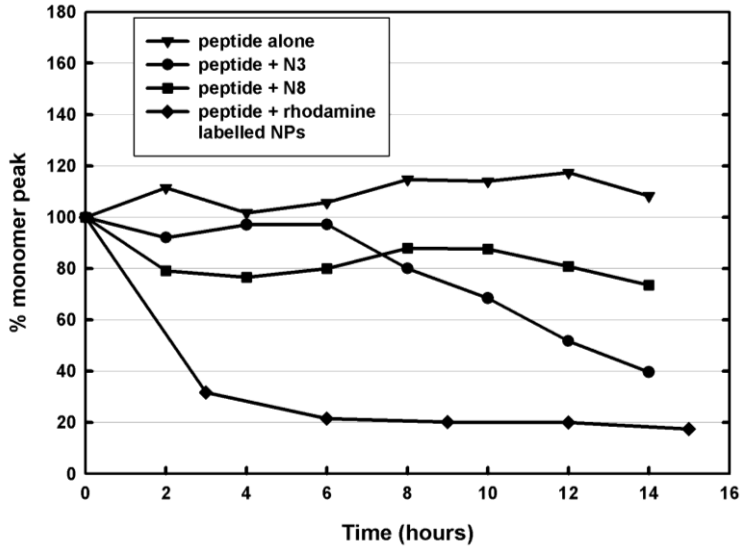

Figure 5. *Comparative evolution of area under curve of HiLyte Fluor™ 488 labelled Aβ$_{1-42}$ peptide monomeric peak alone (blank, ▼), and in presence of non-functionalized (♦) or selegiline-functionalized nanoparticles* ***N3*** *(●) and* ***N8*** *(■).*

However, under identical experimental conditions, no important decrease of the Aβ$_{1-42}$ peptide monomer peak was observed in the case of selegiline-functionalized nanoparticles (**N3** and **N8**) when compared to their non-functionalized counterparts (Figure 5). The effect was even lower, which confirmed an important evolution of the positioning of the ligand at the surface of the P(MePEGCA-*co*-SelPEGCA-*co*-HDCA) nanoparticles. This inefficiency of selegiline-functionalized nanoparticles towards binding to the Aβ$_{1-42}$ peptide clearly demonstrated that the ligand was not well exposed and probably inaccessible for efficient interaction with Aβ$_{1-42}$ peptide which thus confirmed the hypothesis postulated earlier in this study.

Indeed, taken together with previous zeta potential measurements, these data indicate that, after a certain time, selegiline ligands which were initially exposed at the surface of the nanoparticles became not accessible anymore, likely due to rearrangement of the SelPEG chains. The hydrophobic nature of selegiline and/or possible hydrophobic interaction between selegiline moieties could conduct to PEG loops with selegiline extremities, either buried in the hydrophobic PHDCA core and/or stuck to each other by hydrophobic interactions (Figure 6). This would conduct to a drastic change in the linear PEG density at the surface of the NPs, which is believed to be an important parameter regarding their binding to the Aβ$_{1-42}$ peptide.[45] This may certainly explain why selegiline-functionalized NPs exhibited less binding activity towards Aβ$_{1-42}$ peptide than non-functionalized, PEGylated NPs. In addition, the higher the selegiline amount in the NPs, the lower the binding efficiency towards the Aβ$_{1-}$

$_{42}$ peptide which is in good agreement with the expected decrease of the linear PEG chain density (in contrast to PEG loops) at the surface of the NPs for higher selegiline content (Figure 6). The activity of nanoparticles **N8** is negligible if one considers the dramatic decrease of the Aβ monomer peak (within 3 h) in the case of non-functionalized NPs. This weak activity is probably more related to remaining MePEG chains at the surface of the NPs than to selegiline-PEG chains. We believe that if there were some specific interactions in-between the peptide and the exposed ligand, the variation of the peptide monomer peak would have been more intense.

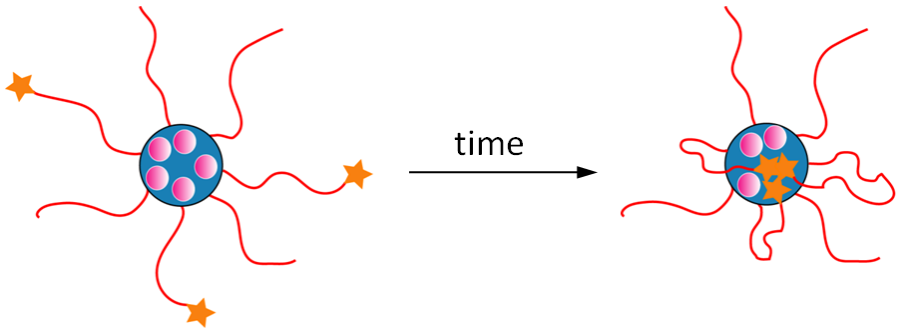

Figure 6. *Schematic representation describing the rearrengment of the seligiline ligands at the surface of the seligiline-functionalized nanoparticles* ***N3*** *to* ***N8****.*

4. Conclusion

This study investigated the potential binding activity of polymeric selegiline-functionalized, PEGylated poly(alkyl cyanoacrylate) nanoparticles to the $A\beta_{1-42}$ peptide, a biomarker of the Alzheimer's disease. Whereas a poor colloidal stability was obtained with the pure selegiline-functionalized copolymer, best stability conditions were obtained after simultaneous nanoprecipitation of this polymer with the rhodamine-labelled, PEGylated poly(alkyl cyanoacrylate) copolymer species in variable ratios. It allowed the amount of selegiline moieties initially displayed at the surface of the NPs to be finely tuned. Although the size of the selegiline-functionalized NPs remained constant with time, the value of the zeta potential drastically decreased. This was confirmed by capillary electrophoresis which showed a lower interaction of selegiline decorated nanoparticles towards $A\beta_{1-42}$ comparatively to the non-functionalized nanoparticles. A possible explanation was proposed and relied on a rearrangement of functionalized selegiline chains at the surface of the NPs leading to their complete inaccessibility towards $A\beta_{1-42}$. More importantly, this study points out the importance of the hydrophobicity/hydrophilicity of the selected ligand displayed at the surface of polymeric NPs.

5. Acknowledgments

The research leading to these results has received funding from the European Community's Seventh Framework Programme (FP7/2007-2013) under agreement n°212043. The CNRS and the French Ministry of Research are also warmly acknowledgment for financial support.

6. References

1. Querfurth HW,LaFerla FM. Alzheimer's disease. N. Engl. J. Med. 2010; 362: 329-44.

2. Aliev G, Smith MA, de la Torre JC,Perry G. Mitochondria as a primary target for vascular hypoperfusion and oxidative stress in alzheimer's disease. Mitochondrion 2004; 4: 649-63.

3. de la Torre JC. Is alzheimer's disease a neurodegenerative or a vascular disorder? Data, dogma, and dialectics. Lancet Neurol. 2004; 3: 184-90.

4. Korolainen MA, Nyman TA, Aittokallio T,Pirttila T. An update on clinical proteomics in alzheimer's research. J. Neurochem. 2010; 112: 1386-414.

5. Aguzzi A,O'Connor T. Protein aggregation diseases: Pathogenicity and therapeutic perspectives. Nat. Rev. Drug Discovery 2010; 9: 237-48.

6. Panza F, Solfrizzi V, Frisardi V, Imbimbo BP, Capurso C, D'Introno A, et al. Beyond the neurotransmitter-focused approach in treating alzheimer's disease: Drugs targeting beta-amyloid and tau protein. Aging: Clin. Exp. Res. 2009; 21: 386-406.

7. Gralle M, Botelho MG,Wouters FS. Neuroprotective secreted amyloid precursor protein acts by disrupting amyloid precursor protein dimers. J. Biol. Chem. 2009; 284: 15016-25.

8. Chow V, Mattson M, Wong P,Gleichmann M. An overview of app processing enzymes and products. NeuroMol. Med. 2010; 12: 1-12.

9. García-Matas S, de Vera N, Aznar AO, Marimon JM, Adell A, Planas AM, et al. In vitro and in vivo activation of astrocytes by amyloid-β is potentiated by pro-oxidant agents. J. Alzheimer's Dis. 2010; 20: 229-45.

10. Sugimoto H, Iimura Y, Yamanishi Y,Yamatsu K. Synthesis and structure-activity relationships of acetylcholinesterase inhibitors: 1-benzyl-4-[(5,6-dimethoxy-1-oxoindan-2-yl)methyl]piperidine hydrochloride and related compounds. J. Med. Chem. 1995; 38: 4821-9.

11. Munoz-Torrero D. Acetylcholinesterase inhibitors as disease-modifying therapies for alzheimer's disease. Curr. Med. Chem. 2008; 15: 2433-55.

12. Birks J, Grimley Evans J, Iakovidou V, Tsolaki M,Holt FE. Rivastigmine for alzheimer's disease. Cochrane Database Syst Rev 2009; CD001191.

13. Kemp JA,McKernan RM. Nmda receptor pathways as drug targets. Nat. Neurosci. 2002; 5 Suppl: 1039-42.

14. Parsons CG, Danysz W,Quack G. Memantine is a clinically well tolerated n-methyl-d-aspartate (nmda) receptor antagonist--a review of preclinical data. Neuropharmacology 1999; 38: 735-67.

15. Reisberg B, Doody R, Stoffler A, Schmitt F, Ferris S,Mobius HJ. Memantine in moderate-to-severe alzheimer's disease. N. Engl. J. Med. 2003; 348: 1333-41.

16. Lim GP, Chu T, Yang F, Beech W, Frautschy SA,Cole GM. The curry spice curcumin reduces oxidative damage and amyloid pathology in an alzheimer transgenic mouse. J. Neurosci. 2001; 21: 8370-77.

17. Ono K, Hasegawa K, Naiki H,Yamada M. Curcumin has potent anti-amyloidogenic effects for alzheimer's β-amyloid fibrils in vitro. J. Neurosci. Res. 2004; 75: 742-50.

18. Garcia-Alloza M, Borrelli LA, Rozkalne A, Hyman BT,Bacskai BJ. Curcumin labels amyloid pathology in vivo, disrupts existing plaques, and partially restores distorted neurites in an alzheimer mouse model. J. Neurochem. 2007; 102: 1095-104.

19. Narlawar R, Pickhardt M, Leuchtenberger S, Baumann K, Krause S, Dyrks T, et al. Curcumin-derived pyrazoles and isoxazoles: Swiss army knives or blunt tools for alzheimer's disease? ChemMedChem 2008; 3: 165-72.

20. Xie Y, Deng S, Chen Z, Yan S,Landry DW. Identification of small-molecule inhibitors of the ab-abad interaction. Bioorg. Medicinal Chem. Lett. 2006; 16: 4657-60.

21. Lorenzo A,Yankner BA. Beta-amyloid neurotoxicity requires fibril formation and is inhibited by congo red. Proc. Natl. Acad. Sci. U. S. A. 1994; 91: 12243-47.

22. Virginia MYL. Amyloid binding ligands as alzheimer's disease therapies. Neurobiol. Aging 2002; 23: 1039-42.

23. Carter DB,Chou KC. A model for structure-dependent binding of congo red to alzheimer β-amyloid fibrils. Neurobiol. Aging 1998; 19: 37-40.

24. Lee VMY. Amyloid binding ligands as alzheimer's disease therapies. Neurobiol. Aging 2002; 23: 1039-42.

25. Klunk WE, Debnath ML, Koros AMC,Pettegrew JW. Chrysamine-g, a lipophilic analogue of congo red, inhibits ab-induced toxicity in pc12 cells. Life Sci. 1998; 63: 1807-14.

26. Christopher DL, Carolyn JJ, Virginia F, Marie-Christine P, David HH, Scot S, et al. Visualization of fibrillar amyloid deposits in living, transgenic caenorhabditis elegans animals using the sensitive amyloid dye, x-34. NeuroMol. Med. 2001; 22: 217-26.

27. Styren SD, Hamilton RL, Styren GC,Klunk WE. X-34, a fluorescent derivative of congo red: A novel histochemical stain for alzheimer's disease pathology. J. Histochem. Cytochem. 2000; 48: 1223-32.

28. Dezutter NA, de Groot TJ, Busson RH, Janssen GA,Verbruggen AM. Preparation of ^{99m}tc-n_2s_2 conjugates of chrysamine g, potential probes for the beta-amyloid protein of alzheimer's disease. J. Labelled Compd. Radiopharm. 1999; 42: 309-24.

29. J. Mol. Neurosci.Wang Y, Klunk W, Huang G-F, Debnath M, Holt D,Mathis C. Synthesis and evaluation of 2-(3′-lodo-4′-aminophenyl)-6-hydroxybenzothiazole for in vivo quantitation of amyloid deposits in alzheimer's disease. J. Mol. Neurosci. 2002; 19: 11-16.

30. Nordberg A. Pet imaging of amyloid in alzheimer's disease. Lancet Neurol. 2004; 3: 519-27.

31. Wang Y, Klunk W, Debnath M, Huang G-F, Holt D, Shao L, et al. Development of a pet/spect agent for amyloid imaging in alzheimer's disease. J. Mol. Neurosci. 2004; 24: 55-62.

32. Dezutter NA, Dom RJ, de Groot TJ, Bormans GM,Verbruggen AM. ^{99m}tc-mama-chrysamine g, a probe for beta-amyloid protein of alzheimer's disease. Eur. J. Nucl. Med. Mol. Imaging 1999; 26: 1392-99.

33. Sun M, Gao Y, Guo C, Cao F, Song Z, Xi Y, et al. Enhancement of transport of curcumin to brain in mice by poly(n-butylcyanoacrylate) nanoparticle. J. Nanopart. Res. 2010; 1-12.

34. Tetrud J,Langston J. The effect of deprenyl (selegiline) on the natural history of parkinson's disease. Science 1989; 245: 519-22.

35. Wilcock GK, Birks J, Whitehead A,Evans SJG. The effect of selegiline in the treatment of people with alzheimer's disease: A meta-analysis of published trials. Int. J. Geriatr. Psych. 2002; 17: 175-83.

36. Tom T. Monoamine oxidase-b inhibitors in the treatment of alzheimers disease. Neurobiol. Aging 2000; 21: 343-48.

37. Sano M, Ernesto C, Thomas RG, Klauber MR, Schafer K, Grundman M, et al. A controlled trial of selegiline, alpha-tocopherol, or both as treatment for alzheimer's disease. N. Engl. J. Med. 1997; 336: 1216-22.

38. Re F, Airoldi C, Zona C, Masserini M, Ferla BL, Quattrocchi N, et al. Beta amyloid aggregation inhibitors: Small molecules as candidate drugs for therapy of alzheimers disease. Curr. Med. Chem. 2010; 17: 2990-3006.

39. Peracchia MT, Fattal E, Desmaële D, Besnard M, Noël JP, Gomis JM, et al. Stealth® pegylated polycyanoacrylate nanoparticles for intravenous administration and splenic targeting. J. Controlled Release 1999; 60: 121-28.

40. Nicolas J,Couvreur P. Synthesis of poly(alkyl cyanoacrylate)-based colloidal nanomedicines. Wiley Interdiscip. Rev.: Nanomed. Nanobiotechnol. 2009; 1: 111-27.

41. Calvo P, Gouritin B, Chacun H, Desmaële D, D'Angelo J, Noel J-P, et al. Long-circulating pegylated polycyanoacrylate nanoparticles as new drug carrier for brain delivery. Pharm. Res. 2001; 18: 1157-66.

42. Garcia-Garcia E, Andrieux K, Gil S,Couvreur P. Colloidal carriers and blood-brain barrier (bbb) translocation: A way to deliver drugs to the brain? Int. J. Pharm. 2005; 298: 274-92.

43. Garcia-Garcia E, Gil S, Andrieux K, Desmaële D, Nicolas V, Taran F, et al. A relevant in vitro rat model for the evaluation of blood-brain barrier translocation of nanoparticles. Cell. Mol. Life Sci. 2005; 62: 1400-08.

44. Nicolas J, Bensaid F, Desmaele D, Grogna M, Detrembleur C, Andrieux K, et al. Synthesis of highly functionalized poly(alkyl cyanoacrylate) nanoparticles by means of click chemistry. Macromolecules 2008; 41: 8418-28.

45. Brambilla D, Verpillot R, Taverna M, De Kimpe L, Le Droumaguet B, Nicolas J, et al. Capillary electrophoresis with laser-induced fluorescence detection (ce-lif) as a new protocol to monitor interaction between nanoparticles and the amyloid-β peptide. Anal. Chem. 2010; 82: 10083-89.

46. Brambilla D, Nicolas J, Le Droumaguet B, Andrieux K, Marsaud V, Couraud P-O, et al. Design of fluorescently tagged poly(alkyl cyanoacrylate) nanoparticles for human brain endothelial cell imaging. Chem. Commun. 2010; 46: 2602-04.

47. Kolb HC, Finn MG,Sharpless KB. Click chemistry: Diverse chemical function from a few good reactions. Angew. Chem., Int. Ed. 2001; 40: 2004-21.

48. Colombo R, Carotti A, Catto M, Racchi M, Lanni C, Verga L, et al. Ce can identify small molecules that selectively target soluble oligomers of amyloid β protein and display antifibrillogenic activity. Electrophoresis 2009; 30: 1418-29.

49. Kato M, Kinoshita H, Enokita M, Hori Y, Hashimoto T, Iwatsubo T, et al. Analytical method for β-amyloid fibrils using ce-laser induced fluorescence and its application to screening for inhibitors of β-amyloid protein aggregation. Anal. Chem. 2007; 79: 4887-91.

50. Sabella S, Quaglia M, Lanni C, Racchi M, Govoni S, Caccialanza G, et al. Capillary electrophoresis studies on the aggregation process of β-amyloid 1-42 and 1-40 peptides. Electrophoresis 2004; 25: 3186-94.

Conclusions et perspectives futures

Dans cette deuxième partie du projet, un nouveau protocole permettant de suivre et de quantifier l'interaction des nanoparticules de polymères et le peptide Aβ1-42 a été décrit. Des techniques d'analyse de routine ont été utilisés afin de valider l'approche choisie et plusieurs types de nanoparticules ont été conçues et criblés. Des résultats convergents ont suggèré le rôle central du PEG à la surface des nanoparticules dans l'interaction avec le peptide et les résultats d'expériences in silico éclaircissent la base moléculaire de cette interaction. Un premier exemple de nanoparticule fonctionnalisée avec une molécule ayant une grande affinité pour le peptide Aβ a été réalisé et caractérisé.

L'étape suivante sera l'évaluation de la capacité à capturer le peptide Aβ par des nanoparticules fonctionnalisées avec des molécules, ayant une grande affinité pour ce dernier. Notre attention se portera particulièrement sur un anticorps monoclonal dirigé contre le peptide et synthétisé par un partenaire du consortium Européen. Enfin, les meilleures particules seront sélectionnées et utilisées pour des expériences in vivo.

Conclusions and future perspectives

In this second part of the work we have described the development of a novel protocol to follow and quantify the interaction between polymeric nanoparticles and the $A\beta_{1\text{-}42}$. Routinely employed techniques have been used to validate our method and several types of particles have been designed and screened. Convergent results suggested a pivotal role of PEG at the surface of the nanocarriers in the interaction with the peptide and in silico experiments clarify the molecular basis of this interplay. A first example of nanoparticle functionalized with a molecule with high affinity for the Aβ peptide have been performed and characterized.

The next step will be the evaluation of the ability to kidnap the peptide by nanoparticles functionalized with other molecules with high affinity for the peptide and, in particular, a monoclonal antibody directed against the peptide and synthesized by a partner of the European consortium. Finally, the best particles will be selected and employed for *in vivo* experiments.

Discussion générale

General discussion

Several hypotheses for the etiology of Alzheimer's disease have been proposed so far. The neuronal loss due to the toxicity of Amyloid β peptide aggregates, usually refereed as the "amyloid hypothesis", remains one of the most widely accepted.[1-2] Aβ peptide is produced through sequential proteolytic cleavages of the amyloid precursor protein (APP) by β- and γ-secretases, forming peptides with a variable length, usually from 39 to 42 amino acids.[3] Among the different species, the Aβ peptide 1-42 ($A\beta_{1-42}$) is believed to play a pivotal role in AD physiopathology due to its high tendency to spontaneously self-aggregate.[4-5]

Yet, a main limitation for the development of active drugs against AD, and other brain-related diseases, is due to the presence of the Blood-Brain Barrier (BBB), a physiological "wall" which keeps the brain environment homeostasis by powerfully selecting the molecule access to the CNS. Hence, the aim of this work was the development of multifunctional polymeric nanoparticles able to (*i*) cross the Blood-Brain Barrier (BBB) in an appreciable amount via cellular transcytosis and (*ii*) to kidnap the $A\beta_{1-42}$ peptide from biological fluids *i.e.* blood and Cerebrospinal Fluid (CSF) to quench its toxicity (Scheme 1).

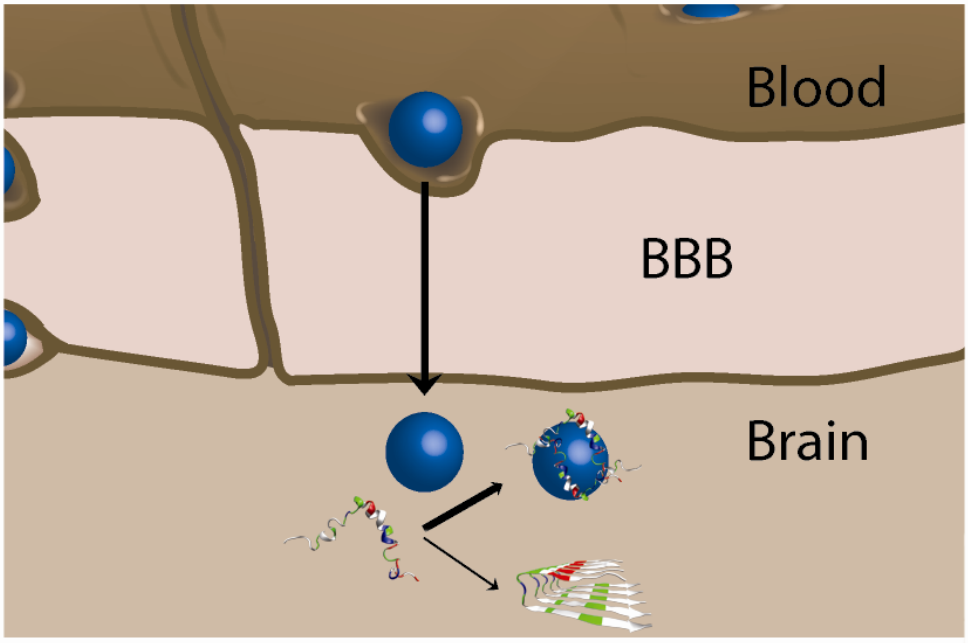

Scheme 1. *The desired multifunctional nanoparticles able to cross the Blood-Brain Barrier and to kidnap with high affinity the* $A\beta_{1-42}$ *peptide monomers to reduce its aggregation and toxicity.*

1. Nanoparticles design

1.1 Rhodamine B tagged nanoparticles

Poly(alkyl cyanoacrylate) nanoparticles were chosen as a well-established technology for colloidal nanomedicine developed in our laboratory for several years.[6] Previous works on these nanoparticles provided significant achievements in multiple pathologies such as cancer, severe infections and metabolic diseases, well-reviewed in recent literature.[7-8]

It has been recently demonstrated that after intravenous administration, a small fraction of the injected PEGylated nanoparticles composed of amphiphilic poly[hexadecyl cyanoacrylate-*co*-methoxypoly(ethylene glycol) cyanoacrylate] (P(HDCA-*co*-MePEGCA)) copolymer were able to cross the BBB, as opposed to their non-PEGylated counterparts, thus opening the door to drug delivery into the Central Nervous System (CNS).[9-10]

Fluorescence was chosen as tracking tool during the *in vitro* and *in vivo* experiments in this work. So far, the elected strategy to prepare fluorescent nanoparticles was to encapsulate a lipophilic dye during the self-assembly process of the corresponding amphiphilic copolymer. However, to circumvent the drawbacks due to dye leakage or burst release during the imaging studies our strategy was to incorporate the dye during the synthesis of an amphiphilic PEGylated PACA copolymer (Figure 1a).

Different copolymers were synthesized by tuning the initial amount and the nature of the dye (Rhodamine B and Dansyl). The resulting structures have been thoroughly characterized by means of complementary techniques. Stable and well-defined nanoparticles with a 100 nm average diameter and narrow particle size distribution were formed by self-assembly in aqueous medium (Figure 1b), ξ-potential measurements showed a partial surface organization of the dye. Fluorescent properties of the materials were then thoroughly studied by fluorescence spectroscopy and a linear evolution of the fluorescence intensity *vs* concentration was observed up to rather high concentrations, a useful property for future nanoparticle quantification in biologic media (Figure 1c).

1.2. Quantum Dots loaded nanoparticles design

The unique optical properties offered by Quantum dots (QD) make them as a useful tool for bio-imaging studies. A great deal of work has focused on QD surface modification for enhanced water-solubility, (bio)conjugation and other applications in biological field.[11-12] We decided to encapsulate different types of QDs into PEGylated PACA nanoparticles and to create double-tagged entities by using the previously described dye-labeled copolymer nanoparticles, for *in vitro* and *in vivo* imaging purposes.

By varying the nature of the QDs, a small library of nanoparticles was obtained. All the preparations resulted in a stable suspension of nanoparticles with an average diameter of 160 nm with a narrow particle size distribution (Figure 1b). Transmission Electron Microscopy, used after sucrose gradient

purification, showed the presence of QDs within the core of well defined particles with a certain distribution at the periphery of the polymeric matrix (Figure 1d). A pretty good encapsulation yield, from 11 to 35%, was obtained. "Barcode" nanoparticles were also prepared by a concomitant encapsulation of two different types of QDs and, interestingly, Fluorescence Micro-Spectroscopy showed that the initial stoichiometry (*i.e.* the initial ratio between the two populations of QDs) was maintained individually in each nanoparticle. These latter results showed the flexibility of our approach and propose it as a versatile fluorescent nanoparticulate platform useful for biomedical applications.

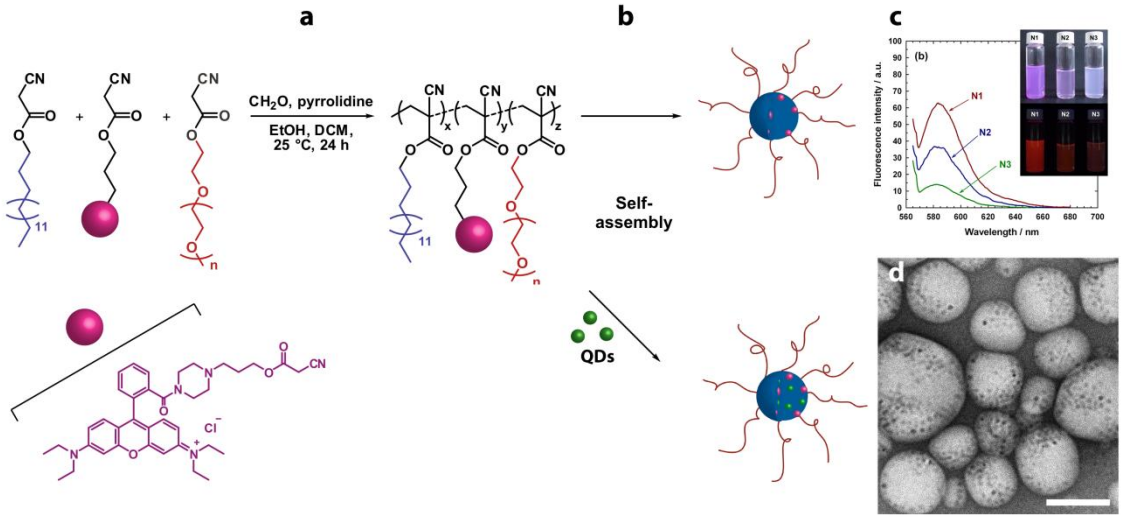

Figure 1. *Scheme of the synthesis route to Rhodamine labeled (P(HDCA-co-RCA-co-MePEGCA) copolymer (a), self-assembling in nanoparticles both empty and loaded with Quantum Dots (b), Fluorescence emission of Rhodamine tagged particles in water (c) and Transmission Electron Microscopy of Quantum Dots loaded nanospheres with negative staining (d). scale bar = 100nm.*

2. Nanoparticles and cells

2.1. Internalization of NPs within hCMEC/D3 cells

The above mentioned nanoparticles were employed for *in vitro* imaging studies on the hCMEC/D3 brain cell line, a recently developed human BBB model.[13] Prior to imaging studies, the cytotoxicity of the empty rhodamine labeled nanoparticles (P(HDCA-*co*-RCA-*co*-MePEGCA)) and QDs loaded counterpart was evaluated showing no significant cytotoxic effect.

Confocal Laser Scanning Microscopy (CLSM) was then employed for imaging studies. Nomarsky contrast image showed a typical fibroblast shape for the cells with no morphological alteration, thus supporting the absence of cytotoxicity, and fluorescence images showed intense and fine fluorescence spots accumulated within the cells and especially around the nuclei. Under identical experimental

conditions and acquisition settings, a lower amount of rhodamine dye covalently linked to the nanoparticles resulted in a decrease of fluorescent intensity. Nevertheless, by increasing the detector gain and the laser power, intense fluorescence spots appeared around cell nuclei. Therefore, tuning the amount of fluorescent dye attached to the nanoparticles together with adjusting acquisition settings allowed great flexibility regarding *in vitro* imaging. In the same way, QD-loaded nanoparticles are internalized within the cells and accumulate around the nuclei. Considering that poly(alkyl cyanoacrylate) nanoparticles are enzymatically biodegraded via hydrolysis of the ester functions, it was important to assess that the fluorescence signal arising from CLSM images was assigned to QDs still encapsulated into PACA nanoparticles and not to free QDs that would have precociously leaked out of PACA nanocarriers. Therefore, green-emitting QDs were encapsulated into rhodamine B-tagged nanoparticles in order to separately visualize fluorescent signals coming from the two dyes. After a 24 h incubation period, an almost perfect co-localization of both signals was obtained leading us to speculate that fluorescence signals can be safely assigned to the presence of encapsulated QDs into intact poly(alkyl cyanoacrylate) nanoparticles within the cells.

By Flow cytometry analyses a fluorescence increase of 400% after 24h incubation of rhodamine tagged nanoparticles with cells was quantified; the NPs internalization starts suddenly after NPs interaction with the cells, describing a fast internalization process. Moreover, the absence of internalization at 4°C suggests that an active endocytosis mechanism governs the NPs internalization (Figure 2a).

Several dividing cells were identified during the visualization on non-confluent cells treated with fluorescent particles and, interestingly, a drastic increase of nanoparticles uptake was observed in those cells. The cause of this difference might likely be that during the mitosis the endocytosis process is kept constant while membrane recycling to the surface is strongly reduced to supply the cells of necessary materials for cell division.[14] At this reduced recycling we can more likely attribute the increase of the particles amount within the dividing cells.

Moreover, a specific intracellular trafficking during mitotic division was observed: the particles, placed at the extremity of the cells during the early stage of dividing cycle (Prophase/Metaphase), are trafficked to the midbody area of the dividing cells, where membrane material is needed for the cytokinesis, tracing filamentous-like structures more likely highlighting the actin microtubules.[15] These results underline the ability of these particles to provide extremely precise details on intracellular mechanisms and give clear information on their trafficking once internalized within human brain endothelial cells (Figure 2b).

To identify the intracellular localization of these NPs, once reached the confluence cells were treated with fluorescent nanoparticles for different incubation times, the main cellular regions were visualized with specific antibodies and observed with CLSM. No NPs were observed within Golgi apparatus or Endoplasmic Reticulum after all the analyzed incubation times, showing an expected time-independent non-involvement of these two cellular compartments in NPs uptake from cells.
On the contrary a large amount of red signal was observed within endosomal vesicles and, after longer incubation times, within the lysosomes. Interestingly some nanoparticles do not co-localize with these two compartments suggesting a double internalization mechanism or an escape from endosomes/lysosomes for a nanoparticles part.

Previous works from our group showed the pivotal role of LDL-receptor on the NPs internalization process within rat brain endothelial cells. Indeed, these PEGylated nanoparticles can "capture" the Apolipoprotein E (Apo E) in serum which is recognized by LDL-r at the surface of brain endothelial cells and internalized.[16] Hence, the expression of the receptor in this human model and the adsorption of ApoE from Rhodamine tagged particles were confirmed by Western Blot. The internalization of NPs into the human brain endothelial cells via Apo E adsorption and recognition of LDL-r expressed at the surface of the cells remain a probable hypothesis. Further experiments are needed to confirm this mechanism.

2.2. Translocation of nanoparticles in human BBB *in vitro* model

For translocation experiments, the BBB *in vitro* model was prepared by seeding hCMEC/D3 cells on 0.45µm pore size collagen pre-coated transwells. After 7 days of culture, permeability experiments were performed. TEER and ^{14}C-Sucrose permeability measurements were employed to characterize the cellular monolayer and results confirm the values previously described for this model.[13]
The NPs passage across the model was studied by adding the fluorescently-tagged particles within the apical medium and by recovering the fluorescent signal within the basolateral compartment at increasing time points. An interesting difference was observed compared to rat model, where the passage was significantly slower.[17] By comparing transcytosis results and the intracellular localization experiment it's interesting to observe that an appreciable amount of particles crosses the BBB model already after 1h incubation and that at this time point any nanoparticle is observed within the lysosomes, confirming the presence of a receptor mediated transcytosis process able to bypass the lysosomes compartment.

Since numerous *in vitro* and *in vivo* studies have investigated the passage of labeled or drug loaded NPs through the BBB by measuring the label amount or directly the drug effect in animal brain but few ones have demonstrated the localization of intact NPs inside brain parenchyma, a particular attention was dedicated to the identification of intact nanoparticles within the basolateral compartment. The receiving medium was filtered and concentrated in order to retain the bigger entities and observed with TEM. The images, showed the presence of spherical objects of around 120 nm within the basolateral chamber of sample treated with NPs, whereas the same objects were not observed within a sample non-treated with nanoparticles suggesting the passage of intact particles across the BBB. Further other experimental approaches are now running to clearly confirm the hypothesis.

2.3. Visualisation of nanoparticles *in vivo*

A preliminary *in vivo* visualization of the QD-loaded NPs was obtained by loading Cd-free near-infrared (NIR) QDs within the polymeric nanoparticles. Nanoparticles were administrated by retro-orbital injection in nude mice and imaged noninvasively by fluorescence optical imaging after 24h. NIR QD-loaded nanoparticles were easily visualized in *in vivo* conditions, and a big amount of the fluorescence was identified within the liver (Figure 2c). A liver accumulation was not surprising, even somewhat expected, at a time interval as long as 24h post-injection.[10] However, the result represents the proof of concept of the usefulness of these particles as *in vivo* imaging system for the future purpose of designing NPs for diagnosis of AD. Indeed, specific polymers with increased ability to reach the CNS are now under construction in the project.

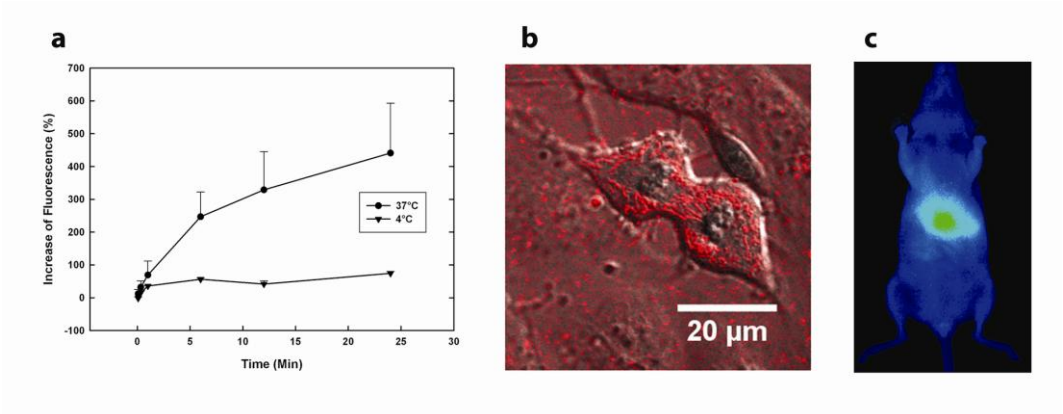

Figure 2. *Quantification of Rhodamine labeled nanoparticles internalization within hCEMC/D3 cells at 37 and 4°C as a function of time (a), nanoparticles within a mitotic hCEMC/D3 cell displaying a characteristic intracellular trafficking (b) and in vivo visualization of NIR-QDs loaded nanoparticles (c).*

3. Nanoparticles and $A\beta_{1-42}$ peptide

The aggregation kinetics of $A\beta_{1-42}$ peptide involves several steps and leads to the formation of species exhibiting variable sizes: typically small soluble oligomers, higher molar mass oligomers, larger protofibrils and eventually insoluble fibrils. This folding and assembly are governed by remarkably complex processes leading to multiple coexisting physical forms. Recently, the development of small molecules based on methylene blue, curcumin and derivatives and others, which can interfere with the aggregation kinetics, were proposed as a promising therapeutic approach.[18] Other few works devoted their attention to the influence of nanoparticulate systems on the Aβ peptide aggregation and toxicity.[19-21] In this context we are currently developing novel biodegradable nanoparticulate systems to target and/or influence the aggregation kinetics of the $A\beta_{1-42}$ peptide and to reduce its toxicity.

3.1. A method to monitor nanoparticles and $A\beta_{1-42}$ interaction

Up to now, two main techniques were employed to study the interaction and the aggregation influence of molecules/nanoparticles on the Aβ peptide. Surface Plasmon Resonance is based on the fixation of the peptide (or the molecules/nanoparticles) on a gold chip and the flowing of the counterpart over the chip. The interaction between the two species is evaluated as a modification of the refractive index on the sensor surface. Its main limitation is the "fixed nature" of one of the species, limiting a space-free interaction.[21-22] Thioflavine spectroscopy is based on its enhanced fluorescent and red-shifting once inserted within *β*-sheets formed during the aggregation process of the amyloid β peptides. It allows the study of the aggregation kinetics in presence of anti-aggregating candidates.[21] In this case the main limitation is the relatively high peptide concentration required. Additionally to these techniques is worth to mention others such as Isotermal Titration Calorimetry, *in silico* studies, Nuclear Magnetic Resonance and Circular Dichroism.[23] However, the poor stability of the peptide and the high concentration needed for these techniques strongly limit their applicability at physiological conditions.

To screen the ability of nanoparticles to efficiently bind $A\beta_{1-42}$, we decided to develop a protocol based on Capillary Electrophoresis coupled to Laser Induced Fluorescence (CE-LIF) able to analyse very low concentrations of peptide close of physiological conditions (nM range). The previously described Rhodamine B-tagged nanoparticles were used as model to validate the protocol. Briefly, the monomeric fluorescent Hilyte Fluor labeled $A\beta_{1-42}$ peptide was mixed with the nanoparticles and incubated at 37°C. The samples were then analyzed by capillary electrophoresis

after increasing elapsed times. The CE-LIF analysis of a solution of the fluorescent peptide alone, showed a single peak mainly constituted by the monomeric form, stable as a function of time. Remarkably, when the same concentration of $A\beta_{1\text{-}42}$ peptide solution was incubated with fluorescent P(HDCA-*co*-RCA-*co*-MePEGCA) nanoparticle suspension, a gradual decrease of the monomeric peptide peak was observed and could be interpreted as the capture of the peptide by the particles (Figure 3a).

To validate this finding, equivalent amount of Antibody anti-$A\beta_{1\text{-}42}$ were incubated with the fluorescent peptide and analyzed as a function of time by CE-LIF. The results clearly indicate that the rapid capture of the monomeric peptide was observed as a reduction of monomeric peak and the formation of a bigger molecular weight species (Ab-Aβ complexes) validating our translation of the technique to the $A\beta_{1\text{-}42}$ peptide (Figure3b).

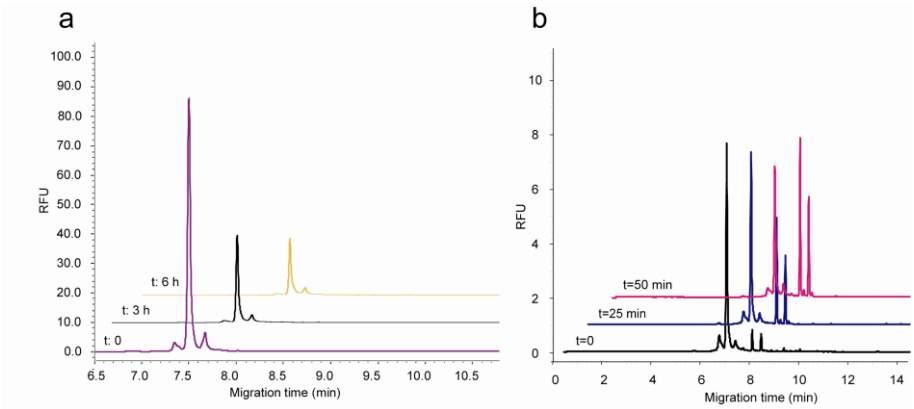

Figure 3. *Free $A\beta_{1\text{-}42}$ monomeric form depletion as a function of time in presence of PEGylated nanoparticles (a), free $A\beta_{1\text{-}42}$ monomeric form depletion in presence of Anti Aβ antibody and formation of Ab-$A\beta_{1\text{-}42}$ complex as a function of time (b).*

Moreover, CLSM observations were employed: red emitting nanoparticles were incubated with green emitting $A\beta_{1\text{-}42}$ peptide at different ratios and analyzed by confocal microscopy after different elapsed times. At time zero, a faint colocalization was observed; after 12h, a complete colocalization was observed evidencing a strong NPs-peptide interaction and validating the CE-LIF results. This experiment also showed an aggregation of the peptide at the surface of the NPs leading to the formation of mixed peptide/NP aggregates. Moreover, the CE-LIF method was also used to evaluate the kinetics of disappearance of the monomeric peptide as a function of the concentration ratio between nanoparticles and peptide. Whatever the concentration ratio, there is an uptake of peptide by the NPs and this process is strictly dependent on the peptide availability in solution. The

higher is the initial peptide concentration, the faster and the higher is the capture. Assuming in a first approach that the $A\beta_{1-42}$-NPs interaction was governed by a first-order kinetic, we have estimated the affinity constant, kd, for this interaction to be 0.55 μM. Interestingly, for the highest peptide concentrations, we observed a nonlinear disappearance of the monomeric peak over time suggesting the formation of peptide aggregates at the surface of the nanoparticles.

By CLSM a proportional decrease of the size of these dual-fluorescent assemblies was noticed as a function of the [Aβ]/[NPs] ratio. For the lowest peptide concentration, no aggregate was formed (Figure 4e) suggesting the aggregation threshold was not reached. According to the literature, peptide aggregation is concentration-dependent and the nucleation reaction is believed to be the rate limiting step.[19] It can be therefore hypothesized that, when there is an affinity between the peptide and some nanoparticles, the interaction of the peptide with the nanoparticle surface increases its local concentration, reaching the nucleation threshold which then triggers the aggregation process.

This technique highlighted the importance of the colloidal properties of the nanoparticles such as the surface charge or the size of the nanoparticles on the interaction with the Amyloid peptide.

3.2. Influence of PEG on $A\beta_{1-42}$-NPs interaction

Interestingly, when non-PEGylated P(HDCA) nanoparticles were employed, no variation of the monomeric peak was observed over time by CE-LIF. To ascertain a role to the PEG chains, nanoparticles of a different polymeric core (PLA) were used. Also in this case, the PEGylated PLA nanoparticles showed an increased ability to interact with the peptide compared to the non PEGylated counterpart confirming the results obtained with the PACA nanoparticles.

To better understand the role of PEG chains onto the nanoparticles surface, other more routinely employed techniques such as Surface Plasmon Resonance (SPR), Confocal Microscopy and Thioflavine spectroscopy were performed. Interestingly, all the techniques outlined an ability to capture the peptide only with PEGylated PACA nanoparticles, confirming the CE-LIF results.

It is well know that PEG chains can interplay with protein environment altering their solubility in aqueous media, however, the mechanism has not yet been fully elucidated. To get better inside on this interaction, molecular modeling was employed. Docking calculations showed that PEG chains wound around the 1-25 helix of the peptide through hydrogen bonds, π-stack and Van der Walls interactions forming an unspecific but permanent binding. A pivotal role of PEG oxygen atoms on binding was obtained by docking the alkyl PE chain to the peptide that was not capable to wind around the helix and did not showed a permanent binding. Moreover, molecular dynamic simulations showed that PEG promotes permanent conformational changes of $A\beta_{1-42}$ from starting L-like shape structure to V-like,

U-like shapes or even more complex conformations. The main feature of the conformational interconversion of $A\beta_{1-42}$ is a permanent interaction with the PEG chain.

To take a step forward, the ability of the PEGylated PACA nanoparticles to influence the aggregation kinetics of $A\beta_{1-42}$ was studied by CE-UV protocol. NPs were added to the aggregating solution of $A\beta_{1-42}$ peptide and the formation/disappearance of every amyloid isoforms (monomer and soluble oligomer) was closely followed and quantified by CE coupled to UV detection. The results indicate an ability of the PEGylated NPs to capture the peptide monomer and soluble oligomers in solution. Additionally, the NPs seem to inhibit the formation of new soluble peptide oligomers: most of the pre-existing soluble oligomers were no more detectable in the solution after 28 h of incubation whereas, in absence of NPs, an 80% increase of peptide oligomers quantity was observed after 28 h. These results confirm the interaction between the NPs and the peptide, also in soluble oligomeric form and, more importantly, underline the ability of these nanoparticles to inhibit the formation of new oligomers. Noteworthy, oligomers are now considered as the most toxic species of the peptide, underlining the interest of these particles. The high blood half-life of these PEGylated polymeric nanoparticles, elect them as a potential therapeutic agent through the so called "sink effect": during the last years the hypothesis of the existence of an osmotic equilibrium of Aβ peptide between the blood and brain compartments has taken importance and credit in the scientific community.[24] Hence, a particle able to kidnap the peptide within the blood flow might move the equilibrium and promote the brain-to-blood transfer of peptide reducing its concentration and toxicity in CNS (Scheme 2).

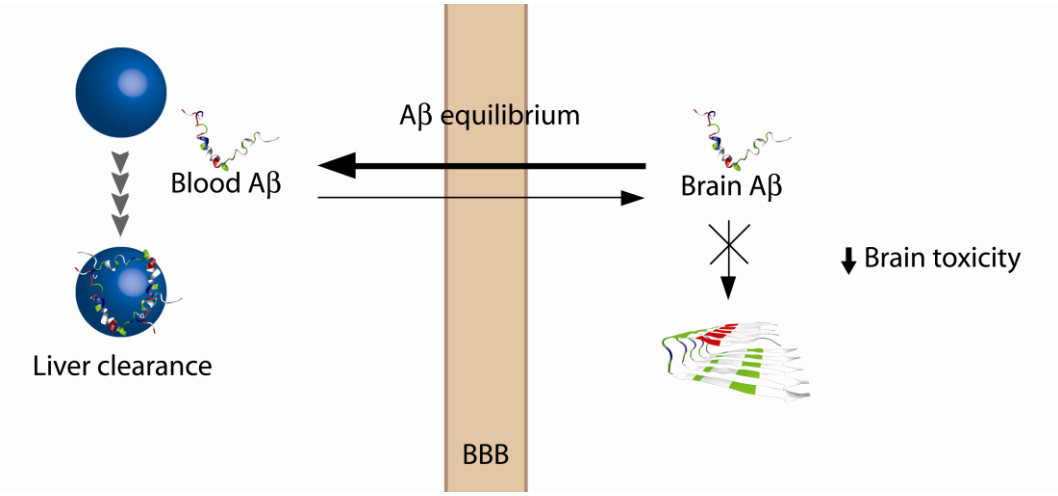

Scheme 2. *Aβ peptide "sink effect" across the BBB: the reduction of peptide within the blood might move the equilibrium from the brain to the blood and reduce the aggregation and related toxicity of the peptide in the brain.*

3.3. Functionalization of NPs for increasing interaction with $A\beta_{1-42}$ peptide.

Although PEGylated nanoparticles showed interesting properties regarding the capture of soluble peptide, a great deal of work has been focused on the functionalization of PEGylated PACA nanoparticles with molecules presenting an endogenous high affinity for the peptide. Recently, different studies proposed the utilization of small polyphenols for targeting the $A\beta_{1-42}$ peptide, such as curcumine and its derivatives, Thioflavine T, Congo red and their analogues such as Chrysamine G and X34.[25-29] These molecules have shown a certain efficiency to hinder, or even to stop, the oligomerization of the $A\beta_{1-42}$ peptide and thus the production of oligomers and/or fibrils. Among the pool of efficient ligands discovered so far, we have focused our attention on Selegiline, an aromatic molecule that has been employed to slow down the progression of the Parkinson's disease, but also exhibited a certain affinity for the $A\beta_{1-42}$ peptide.[30] We synthesized selegiline-functionalized and fluorescent poly(alkyl cyanoacrylate) nanoparticles for $A\beta_{1-42}$ peptide kidnapping and anti-fibrillogenesis purposes.

Functionalization was undertaken with selegiline by copper-catalyzed azide-alkyne cycloaddition (CuAAC) *via* its native alkyne group. Stable NPs suspensions with mean diameter of 100 nm and low PDI values, were obtained from the self-assembly of different ratios of selegiline-functionalized and rhodamine B-tagged copolymers in order to tune the amount of selegiline moieties displayed at their surface. The ability of these particles to interact with the peptide was studied by CE-LIF. Unfortunately, no important decrease of $A\beta_{1-42}$ peptide monomer peak was observed in the presence of selegiline functionalized nanoparticles when compared to non-funtionalized counterparts. This lower effect on kidnapping the peptide has been related to an important evolution of the positioning of the ligand at the surface of the nanoparticles confirmed by ξ-potential measurements; selegiline ligands which were initially exposed at the surface of the nanoparticles became not accessible anymore, likely due to rearrangement of the SelPEG chains.

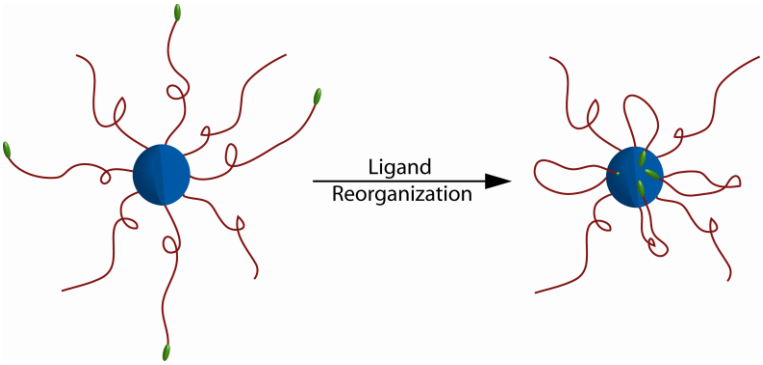

Figure 4. *Cartoon of the hypothesized mechanism of a hydrophobic ligand reorganization onto the nanoparticles surface.*

The hydrophobic nature of selegiline and/or possible hydrophobic interaction between selegiline moieties could conduct to PEG loops with selegiline extremities, either buried in the hydrophobic PHDCA core and/or stuck to each other by hydrophobic interactions (Figure 4).

To overcome this problem and to have particles with the highest possible affinity for the peptide, other nanoparticles functionalized with curcumine derivatives and especially with humanized monoclonal antibody anti-$A\beta_{1-42}$ are now in production.

4. References

1. Townsend M, Mehta T and Selkoe DJ. Soluble Abeta inhibits specific signal transduction cascades common to the insulin receptor pathway. *J Biol Chem* 2007; 282: 33305-33312.

2. Gralle M, Botelho MG and Wouters FS. Neuroprotective secreted amyloid precursor protein acts by disrupting amyloid precursor protein dimers. *J Biol Chem* 2009; 284: 15016-15025.

3. Octave JN and Pierrot N. [Alzheimer's disease: cellular and molecular aspects]. *Bull Acad Natl Med* 2008; 192: 323-331; discussion 331-322.

4. Garcia-Matas S, de Vera N, Aznar AO, Marimon JM, Adell A, Planas AM, Cristofol R and Sanfeliu C. In vitro and in vivo activation of astrocytes by amyloid-beta is potentiated by pro-oxidant agents. *J Alzheimers Dis* 2010; 20: 229-245.

5. Allaman I, Gavillet M, Belanger M, Laroche T, Viertl D, Lashuel HA and Magistretti PJ. Amyloid-beta aggregates cause alterations of astrocytic metabolic phenotype: impact on neuronal viability. *J Neurosci* 2010; 30: 3326-3338.

6. Nicolas J and Couvreur P. Synthesis of poly(alkyl cyanoacrylate)-based colloidal nanomedicines. *Wiley Interdiscip Rev Nanomed Nanobiotechnol* 2009; 1: 111-127.

7. Fattal E, Youssef M, Couvreur P and Andremont A. Treatment of experimental salmonellosis in mice with ampicillin-bound nanoparticles. *Antimicrob Agents Chemother* 1989; 33: 1540-1543.

8. Vauthier C, Dubernet C, Fattal E, Pinto-Alphandary H and Couvreur P. Poly(alkylcyanoacrylates) as biodegradable materials for biomedical applications. *Adv Drug Deliv Rev* 2003; 55: 519-548.

9. Garcia-Garcia E, Andrieux K, Gil S, Kim HR, Le Doan T, Desmaele D, d'Angelo J, Taran F, Georgin D and Couvreur P. A methodology to study intracellular distribution of nanoparticles in brain endothelial cells. *Int J Pharm* 2005; 298: 310-314.

10. Calvo P, Gouritin B, Chacun H, Desmaele D, D'Angelo J, Noel JP, Georgin D, Fattal E, Andreux JP and Couvreur P. Long-circulating PEGylated polycyanoacrylate nanoparticles as new drug carrier for brain delivery. *Pharm Res* 2001; 18: 1157-1166.

11. Medintz IL, Uyeda HT, Goldman ER and Mattoussi H. Quantum dot bioconjugates for imaging, labelling and sensing. *Nat Mater* 2005; 4: 435-446.

12. Michalet X, Pinaud FF, Bentolila LA, Tsay JM, Doose S, Li JJ, Sundaresan G, Wu AM, Gambhir SS and Weiss S. Quantum dots for live cells, in vivo imaging, and diagnostics. *Science* 2005; 307: 538-544.

13. Weksler BB, Subileau EA, Perriere N, Charneau P, Holloway K, Leveque M, Tricoire-Leignel H, Nicotra A, Bourdoulous S, Turowski P, Male DK, Roux F, Greenwood J, Romero IA and Couraud PO. Blood-brain barrier-specific properties of a human adult brain endothelial cell line. *FASEB J* 2005; 19: 1872-1874.

14. Boucrot E and Kirchhausen T. Endosomal recycling controls plasma membrane area during mitosis. *Proc Natl Acad Sci U S A* 2007; 104: 7939-7944.

15. Schweitzer JK, Burke EE, Goodson HV and D'Souza-Schorey C. Endocytosis resumes during late mitosis and is required for cytokinesis. *J Biol Chem* 2005; 280: 41628-41635.

16. Kim HR, Gil S, Andrieux K, Nicolas V, Appel M, Chacun H, Desmaele D, Taran F, Georgin D and Couvreur P. Low-density lipoprotein receptor-mediated endocytosis of PEGylated nanoparticles in rat brain endothelial cells. *Cell Mol Life Sci* 2007; 64: 356-364.

17. Garcia-Garcia E, Gil S, Andrieux K, Desmaele D, Nicolas V, Taran F, Georgin D, Andreux JP, Roux F and Couvreur P. A relevant in vitro rat model for the evaluation of blood-brain barrier translocation of nanoparticles. *Cell Mol Life Sci* 2005; 62: 1400-1408.

18. Yadav A and Sonker M. Perspectives in designing anti aggregation agents as Alzheimer disease drugs. *Eur J Med Chem* 2009; 44: 3866-3873.

19. Auer S, Trovato A and Vendruscolo M. A Condensation-Ordering Mechanism in Nanoparticle-Catalyzed Peptide Aggregation. *PloS Comput Biol* 2009;

20. Cabaleiro-Lago C, Quinlan-Pluck F, Lynch I, Dawson K and Linse S. Dual Effect of Amino Modified Polystyrene Nanoparticles on Amyloid Protein Fibrillation. *ACS Chem Neurosci* 2010; 1: 279-287.

21. Cabaleiro-Lago C, Quinlan-Pluck F, Lynch I, Lindman S, Minogue AM, Thulin E, Walsh DM, Dawson KA and Linse S. Inhibition of amyloid beta protein fibrillation by polymeric nanoparticles. *J Am Chem Soc* 2008; 130: 15437-15443.

22. Canovi M, Markoutsa E, Lazar AN, Pampalakis G, Clemente C, Re F, Sesana S, Masserini M, Salmona M, Duyckaerts C, Flores O, Gobbi M and Antimisiaris SG. The binding affinity of anti-Abeta1-42 MAb-decorated nanoliposomes to Abeta1-42 peptides in vitro and to amyloid deposits in post-mortem tissue. *Biomaterials* 2011; 32: 5489-5497.

23. Airoldi C, Colombo L, Manzoni C, Sironi E, Natalello A, Doglia SM, Forloni G, Tagliavini F, Del Favero E, Cantu L, Nicotra F and Salmona M. Tetracycline prevents Abeta oligomer toxicity through an atypical supramolecular interaction. *Org Biomol Chem* 2011; 9: 463-472.

24. Sutcliffe JG, Hedlund PB, Thomas EA, Bloom FE and Hilbush BS. Peripheral reduction of beta-amyloid is sufficient to reduce brain beta-amyloid: implications for Alzheimer's disease. *J Neurosci Res* 2011; 89: 808-814.

25. Carter DB and Chou KC. A Model for Structure-Dependent Binding of Congo Red to Alzheimer β-Amyloid Fibrils. *Neurobiol. Aging* 1998; 19: 37-40.

26. Christopher DL, Carolyn JJ, Virginia F, Marie-Christine P, David HH, Scot S, Chester AM and William EK. Visualization of fibrillar amyloid deposits in living, transgenic Caenorhabditis elegans animals using the sensitive amyloid dye, X-34. *NeuroMol. Med.* 2001; 22: 217-226.

27. Garcia-Alloza M, Borrelli LA, Rozkalne A, Hyman BT and Bacskai BJ. Curcumin labels amyloid pathology in vivo, disrupts existing plaques, and partially restores distorted neurites in an Alzheimer mouse model. *J. Neurochem.* 2007; 102: 1095-1104.

28. Klunk WE, Debnath ML, Koros AMC and Pettegrew JW. Chrysamine-G, a lipophilic analogue of congo red, inhibits Ab-induced toxicity in PC12 cells. *Life Sci.* 1998; 63: 1807-1814.

29. Narlawar R, Pickhardt M, Leuchtenberger S, Baumann K, Krause S, Dyrks T, Weggen S, Mandelkow E and Schmidt B. Curcumin-Derived Pyrazoles and Isoxazoles: Swiss Army Knives or Blunt Tools for Alzheimer's Disease? *ChemMedChem* 2008; 3: 165-172.

30. Re F, Airoldi C, Zona C, Masserini M, La Ferla B, Quattrocchi N and Nicotra F. Beta amyloid aggregation inhibitors: small molecules as candidate drugs for therapy of Alzheimer's disease. *Curr Med Chem* 2010; 17: 2990-3006.

Conclusion générale et perspectives futures

General conclusion and future perspectives

This work has been performed within a large European project (NAD) aiming to the development of an original nanoparticulate system for the diagnostic and the treatment of Alzheimer's disease. A consistent part of the results have been obtained thanks to fruitful collaborations with numerous partners within the European consortium.

In this view, we have designed a novel fluorescently-tagged PEGylated polymer able to self-assemble in biodegradable nanoparticles. The chemical and physic-chemical properties of these nanoparticles were studied in details leading to their employment for internalization and transcytosis studies using an innovative *in vitro* Blood-Brain Barrier (BBB) human model. Preliminary bio-imaging *in vivo* results were also obtained using Quantum Dot-loaded nanoparticles. These achievements represent important advances and lay down the foundations of the screening of polymeric nanoparticles ability to cross the BBB.

In addition, we challenged to develop a nanoparticulate system acting as "Aβ kidnapper" once in biological fluids. As first step, an original methodology based on capillary electrophoresis allowed us to study the "in solution" interaction of nanoparticules and the $A\beta_{1-42}$ peptide close to physiological conditions. The protocol has been successfully employed with different types of nanoparticles leading to the discovery of an interesting interplay of PEG, a macromolecule largely employed in drug delivery, and the amyloidogenic peptide. The creation of a first example of polymeric nanoparticles functionalized with molecules with endogenous high affinity for the peptide (i.e. Selegiline), has been described and discussed. Other functionalization strategies (i.e. with a monoclonal antibody anti Aβ are still under progress). This work opens the route to the development of a nanoparticulate approach for AD.

The main goals for the remaining two years of our group in the framework of the NAD project are: (*i*) the design and evaluation of fluorescent nanoparticles functionalized with an antibody against the transferrin receptor able to better cross the BBB *in vitro* and *in vivo*, using QDs and radiolabelling as tracking strategy and (*ii*) the study of non-functionalized PEGylated nanoparticles and functionalized nanoparticles (with curcumine and antibody anti-$A\beta_{1-42}$) directed towards the capture of the peptide *in vitro* and *in vivo*.

Finally, the best multifuntionalized nanoparticles both able to cross the BBB and to efficiently "capture" the peptide from biological fluids will be selected and tested *in vivo* against AD models.

Abbreviations

2D-PAGE	Two-dimensional polyacrylamide gel electrophoresis
Ab	Antibody
AChE	Acetylcholinesterase
AD	Alzheimer's Disease
ADDLs	Aβ -Derived Diffusible Ligands
Ag	Antigen
Apo E	Apolipoprotein E
APP	Amyloid Precursor Protein
APS	Ammonium Persulfate
Aβ	Amyloid β
BBB	Blood-Brain Barrier
bFGF	Basic Fibroblast Growth Factor
BSA	Bovine Serum Albumin
CE	Capillary Electrophoresis
CHP	Chlolesterol-Bearing Pullulan
CLSM	Confocal Laser Scanning Microscopy
CNS	Central Nervous System
CSF	Cerebrospinal Fluid
CuAAC	Copper-Catalyzed Azide-Alkyne Cycloaddition
DAD	Diode Array Detector
DCC	N-Dicyclohexylcarbodiimide
DCM	Dichloromethane
DCU	Dicyclohexylurea
DLS	Dynamic Light Scattering
DMAP	4-Dimethylaminopyridine
DMSO	Dimethyl Sulfoxide
DTE	1,4-Dithioerythritol
EDTA	Ethylene-Diaminetetraacetic Acid Tetrasodium Salt Hydrate
ELISA	Enzyme-Linked Immunosorbent Assay
ESI-MS	Electrospray Ionization Mass Spectrometry

EtOAc	Ethyl Acetate
EtOH	Ethanol
FDA	Food And Drug Administratio
ICP-MS	Inductively Coupled Plasma Mass Spectrometry
LDL	Low Density Lipoprotein
LIF	Laser Induced Fluorescence
MDR	Multi Drug Resistance
MePEG	Methoxy Polyethylene Glycol
MRI	Magnetic Resonance Imaging
NAD	Nanoparticles For Alzheimer's Disease
NIR	Near Infrared
NMR	Nuclear Magnetic Resonance
NP	Nanoparticle
PACA	Poly(Alkyl Cyanoacrylate)
PBS	Phosphate Buffer Saline
PDI	Polydispersity Index
PE	Polyethylene
PEG-b-PLA	Poly(Éthylène Glycol)-Block-Polylactide
PFA	Paraformaldehyde
PGMA	Poly(Glycidyl Methacrylate)
PLGA	Poly(Lactide-Co-Glycolide)
PMMA	Poly(Methyl Methacrylate)
PnBCA	Poly(N-Butyl Cyanoacrylate)
poly(MePEGCA-co-HDCA)	poly[hexadecyl cyanoacrylate-co-rhodamine B cyanoacrylate-co-methoxypoly(ethylene glycol) cyanoacrylate]
PS	Polystyrene
PSD	Particle Size Distribution
PVA	Poly(Vinyl Alcohol)
QD	Quantum Dot
RCA	Rhodamine Cyanoacetate
RMSD	Root-Mean-Square Deviation
SDS	Sodium Dodecyl Sulphate
Sel	Selegiline

SPR	Surface Plasmon Resonance
TEER	Trans-Endothelial Electrical Resistance
TEM	Transmission Electron Microscopy
TEMED	Tetramethylethylenediamine
THF	Tetrahydrofuran,
ThT	Thioflavin T
WB	Western Blot

Abréviations

BHE	Barrière Hématoencéphalique
SNC	Système Nerveux Central

Aknowledgments

At the end of this Work I would like to address a sincere thank to Professor Moein Moghimi, Professor Claus-Michael Lehr and Professor Charles Duyckaerts who kindly offered time and energies to review this manuscript..

A special thank is addressed to the UMR-CNRS 8612 group and to his Director Elias Fattal who offered me the chance to carry on this work in a friendly and dynamic environment and for his useful and frank advices.

A big thank is addressed to my PhD co-director Patrick Couvreur who warmly accepted me in his group, to have infused me energy and motivation, for his countless scientific advices and for his contagious enthusiasm and optimism.

All this PhD work would not have been possible without my PhD co-directors Karine and Julien. Both of you taught me a massive dose of scientific and personal things. Thanks for your support for every single experiment, for overcome every single obstacle, and to have promoted, sustained and guided my personal suggestions.

Huge thanks to Benjamin who shared with me every working day of these three years, for all the scientific and personal support, for all the funny moments spent together inside and outside the office; to Nicolas for all the help he offered me during the last two years, for the enjoyable moments spent together watching films, eating, skiing, running (rarely)....; to Lucien for his special advices from the real first beginning of my French stage; to Simon, Glenna and Saidy for the funny moments spent together; to Romain to have sheared with me all the week-ends in the lab! You really gladdened my stay in France!

A special thanks to the master students who worked with me during these three years: Hayfa, Sophie, Valentina, Daunia, Celine, Maria-Laura, Dario and Alessandra; I hope to don't have been too bad; to the "Italian (or half) gang": Chiara, Silvia, Giovanni, Simona, Donato, Raquel, Sabrina, Angelo, Martina, Davide, Evelia, Laura…; to Romain C. and the new arrived Mr Delplace to Laura from Saragoza, Andrey, Trung, Manuela, Samia, Violeta, Nicolas T, Herve H and W...

To all the persons from the NAD project: Marco, Cristiano, Greetje, Francesca, Silvia, Elisa, Moustas… with a special thank to Line for the funny moments at each NAD meeting since Patrass and for the help with "The peptide"!

A special thank to « La Belette qui Tète » for the low cost beer and to the Aβ peptide to have ruined several of my nights!

Finally, thanks to my parents and my brother for the support during all these years and to my "Other Half" Vale.

ABSTRACT

The proof of concept of an original nanotechnology-based theranostic approach for Alzheimer's disease has been explored. Novel fluorescently tagged nanoparticles have been designed and employed for internalization and transcytosis studies across a recently developed human *in vitro* blood-brain barrier model. A small library of polymeric nanoparticles have been designed and their ability to capture the Amyloid β_{1-42} peptide, considered one of the causes of the Alzheimer's disease, has been investigated and quantified using an *on purpose* designed method.

KEYWORDS:

Poly(alkyl cyanocrylate) nanoparticles, Alzheimer's disease, blood-brain barrier, β-amyloid peptide.

RÉSUMÉ

La preuve de concept d'une approche theranostique pour la Maladie de Alzheimer basée sur les nanotechnologies a été explorée. Des nouvelles nanoparticules polymeriques fluorescentes on été conçus, et leur internalisation et aptitude à traverser un nouveau modèle *in vitro* de barrière hémato-encéphalique humaine on été étudiées en détails. Une petite librairie de nanoparticules polymerique a été préparés, et leur capacité de capturer le peptide β-Amyloïde$_{1-42}$, considéré comme une des principales causes de la dégénérescence neuronale, a été évaluées et quantifiées en utilisant une méthode expressément conçus.

MOTS-CLES :

Nanoparticules de poly(cyanoacrylate d'alkyle, maladie d'Alzheimer, barrière hémato-encéphalique, peptide β-Amyloïde.

PÔLE : PHARMACOTECHNIE ET PHYSICO-CHIMIE

LABORATOIRE DE RATTACHEMENT
Laboratoire de Physico-chimie, Pharmacotechnie, et Biopharmacie
UMR CNRS 8612 – UNIVERSITÉ PARIS-SUD XI

UFR «FACULTÉ DE PHARMACIE DE CHATENAY-MALABRY »
5, rue Jean Baptiste Clément
92296 CHÂTENAY-MALABRY Cedex